Dissertation

submitted to the

Combined Faculties for the Natural Sciences and for Mathematics

of the Ruperto-Carola University of Heidelberg, Germany

for the degree of

Doctor of Natural Sciences

Presented by

Lic. Biotechnology Joan Castells Ballester

born in Valencia, Spain

oral examination: 18.11.2019

Study of protein *O*-mannosylation in the context of endoplasmic reticulum protein homeostasis

Referees:

Prof. Dr. Sabine Strahl

Dr. Sebastian Schuck

Al pare, la mare i Pau

“For changing lines, I’ve got no time tonight.”

J.Frusciante

TABLE OF CONTENTS

ABBREVIATIONS

Abs	absorbance
APS	ammonium persulfate
Asn	asparagine
ATP	adenosine triphosphate
CDG	congenital disorder of glycosylation
CMAC	7-amino-4-chloromethylcoumarin
COP	coat complex protein
CWI	cell wall integrity
d.o.	drop out
DAmP	decreased abundance by mRNA Perturbation
ddH_2O	bidest. water
DEPC	diethyl pyrocarbonate
DMSO	dimethyl sulfoxide
DNA	deoxyribonucleic acid
Dol-P	dolichol phosphate
Dol-PP	dolichyl pyrophosphate
DTT	dithiothreitol
EDTA	ethylenediaminetetraacetic acid
ER	endoplasmic reticulum
ERAD	endoplasmic reticulum associated degradation
ERCQ	endoplasmic reticulum quality control
EtOH	ethanol
FW	forward
GDP	guanosine diphosphate
GFP	green fluorescent protein
GlcNAc	n-acetylglucosamine
GPI	glycosylfosfatidylinositol
HRP	horseradish peroxidase
KDa	Kilo dalton

LB	lysogeny broth
LLO	lipid-linked oligosaccharide
Man	mannose
MIR	mannosyltransferase - inositol trisphosphate receptor - ryanodine receptor
mRNA	messenger ribonucleic acid
MW	molecular weight
NP-40	nonyl phenoxypolyethoxylethanol
OD	optical density
ORF	open reading frame
OST	oligosaccharyltransferase
PAA	polyacrylamide
PAGE	polyacrylamide gel electrophoresis
PCR	polymerase chain reaction
PEG	polyethylene glycol
PMSF	phenylmethylsulfonyl fluoride
PMT	protein mannosyltransferase
REV	reverse
RIP	RNA immunoprecipitation
RNA	ribonucleic acid
Rnase A	bovine pancreatic ribonuclease A
RNasin	ribonuclease inhibitor
RNP	ribonucleoprotein
RPKM	reads per kilobase per million
RPM	reads per million
RT	room temperature
RT-PCR	real-time polymerase chain reaction
SD	synthetic defined
SDS	sodium dodecyl sulfate
Ser	serine
SF	soluble fraction
sfGFP	super-folder green fluorescent protein
SGA	synthetic genetic array

SP	signal peptide
SRP	signal recognition particle
TBE	tris/borate/EDTA
TBS	tris-buffered saline
TCA	trichloroacetic acid
TCE	total cell extract
TE	tris-EDTA
TEMED	tetramethylethylenediamine
tFT	tandem Fluorescent timer
Thr	threonine
Tm	melting temperature
TM	total membranes
TMD	transmembrane domain
Tris	tris(hydroxymethyl)-aminomethane
tRNA	transfer ribonucleic acid
UDP	uridine diphosphate
UDP	uridine diphosphate
UPOM	unfolded protein *O*-mannosylation
UPR	unfolded protein response
UPRE	unfolded protein responsive element
UTR	untranslated region
WT	wild type
YNB	yeast nitrogen base
YPD	yeast extract/peptone/dextrose

ABSTRACT

Protein *O*-mannosylation is an essential, conserved and abundant post-translational modification in the eukaryotic secretory pathway. Protein *O*-mannosylation is initiated at the endoplasmic reticulum (ER) by the covalent addition of single mannoses to serine and threonine residues of target polypeptides. This reaction is catalyzed by members of the evolutionarily conserved protein mannosyltransferase family (PMT). In the model organism *Saccaromyces Cerevisiae*, among its different biological roles, protein *O*-mannosylation has been described to target both unfolded and irreversibly misfolded proteins. The recently named unfolded protein *O*-mannosylation (UPOM) pathway is hypothesized to function as a fail-safe mechanism to prevent ineffective folding attempts for polypeptides that did not achieve the native conformation within certain time window. However, although UPOM has been described to target multiple misfolded model proteins, the mechanism by which the PMT machinery discriminates misfolded polypeptides is unknown. In fact, the question of whether UPOM is a physiologically relevant mechanism contributing to maintain homeostasis in the ER remains unanswered.

In this current work, it is shown: I) The relevance of the Pmt1-Pmt2 complex as necessary to maintain ER homeostasis being integrated in the unfolded protein response (UPR). II) Aiming to unravel the UPOM machinery, the genes *PGI1* (phosphoglucose isomerase) and *BFR1* (Brefeldin A resistance) were found as necessary for efficient UPOM. On one hand, the characterization of *PGI1* highlighted a direct link between *O*-mannosylation, cytosolic sugar metabolism, and ER stress. On the other hand, the RNA binding protein (RBP) Bfr1 was found to modulate the translational state of PMT mRNAs among many other ORFs, mainly coding for proteins localizing to the secretory pathway, suggesting a role as a local translational control factor. III) Aiming to address the physiological relevance of UPOM in the ER protein quality control system, the impact of *O*-mannosylation on the stability of a subset of PMT target proteins was investigated. Both, protein stabilization and de-stabilization effects were presented. The prevalence of either effect was largely dependent on the nature of the *O*-mannosylation substrate. In line with this, Pmt1 is shown to be necessary for the degradation of the beta-1,6 synthase Kre6 when mislocalized in the vacuole.

ZUSAMMENFASSUNG

Die Protein-*O*-Mannosylierung ist eine essentielle, konservierte und häufig auftretende, post-translationale Modifikation im eukaryotischen sekretorischen Transportweg. Die Protein-*O*-Mannosylierung beginnt im Endoplasmischen Retikulum (ER) durch die kovalente Bindung einer einzelnen Mannose an Serin- oder Threoninreste von Zielpolypeptiden. Katalysiert wird diese Reaktion von der evolutionär konservierten Protein-*O*-Mannosyltransferase (PMT) Familie. Im Modellorganismus, der Bäckerhefe *Saccaromyces Cerevisiae*, spielt die Protein-*O*-Mannosylierung vielfältige, wichtige biologische Rollen und es konnte gezeigt werden, dass sowohl ungefaltete als auch irreversibel fehlgefaltete Proteine modifiziert werden. Vor kurzem wurde die sogenannte Ungefaltete Protein-*O*-Mannosylierung (UPOM) eingeführt, von welcher vermutet wird, dass Sie als fehlerfreier Mechanismus zur Vermeidung unnützer Faltungszyklen von Polypeptiden dient, welche nicht innerhalb eines festen Zeitfensters korrekt gefaltet werden. Obwohl die Protein-*O*-Mannosylierung für mehrere fehlgefaltete Modellproteine beschrieben wurde, ist der Mechanismus, durch welchen die PMTs diese erkennen, noch unverstanden. Genauso unbeantwortet ist die Frage ob die UPOM als physiologisch relevanter Prozess zur Homöostase des ER beiträgt.

Diese Arbeit zeigt erstens: Die Notwendigkeit des Pmt1-Pmt2-Komplexes für die Intergration der ER Homöostase in die ungefaltete Proteinantwort (UPR). Zweitens: Die Gene *PGI1* (phosphoglucose isomerase) und *BFR1* (Brefeldin A resistance) wurden als notwendige Gene der UPOM Maschinerie identifiziert. Einerseits, konnte durch die Untersuchung von *PGI1* eine direkte Verbindung von Protein-*O*-Mannosylierung zum zytosolischen Zuckermetabolismus und ER Stress Signalwegen hergestellt werden. Andererseits, wurde das RNA-Bindeprotein Bfr1 als Modulator des translationalen Stadiums von PMT mRNAs aus den einzelnen offenen Leserahmen, welche hauptsächlich für Proteine des sekretorischen Wegs kodieren, identifiziert. Dies legt für Bfr1 eine Rolle als lokaler Translationskontrollfaktor nahe. Drittens, wurde der Einflusses der UPOM auf das ER Qualitätskontrollsystem anhand von Stabilitätsuntersuchung von PMT Zielproteinen physiologisch untersucht. Sowohl protein-stabilisierende als auch -destabilisierende Effekte konnten festgestellt werden. Der vorherrschende Effekt hing dabei größtenteils von der Natur des Zielproteins ab. Übereinstimmend mit diesen Beobachtungen konnte hier gezeigt werden, dass Pmt1 notwendig für den Abbau der fälschlich vakuolar lokalisierten beta-1,6 synthase Kre6 ist.

PUBLISHED DATA AND CONTRIBUTION BY CO-WORKERS

This section summarizes published data, contributions of co-workers and experiments performed in collaboration with other groups shown in this current work. Yet, this information can be found in the corresponding description of methods as well as at the indicated figure legends.

The majority of data presented in 4.3 (Monitoring the role of protein *O*-mannosylation in protein dynamics) has been published in a research article (Castells-Ballester *et al.*, 2018) under CC-BY license. This includes Figures 4.32, 4.33, 4.34, 4.35, 4.36, App. 10, Table 1 and App. Data 1. For this current work, figures have been reprinted and redesigned when necessary according to my criteria.

Dr. Daniela Bausewein performed the experiments shown in Figures 4.12B lower panel and 4.15. Patrick Neubert performed the computational analyses and designed Figures 4.33 and App.10 and additionally designed Figures 4.32A and 4.36A. Dr. Ewa Zatorska performed the experiments described in Table 1 and Figure App-2, and designed Figures 4.34A, 4.35A, and 4.36B. The lab technician Anke Metschies helped with single experimental steps when I was hindered to do so. The bachelor student Sven Klassa performed the spotting assay showed in figure 4.18A under my supervision, which was included in the bachelor thesis: "*Phosphoglucose isomerase 1 function in the frame of protein O-mannosylation and ER homeostasis"*, submitted to the Ruprecht-Karls-University (Heidelberg faculty of Biosciences) in 2017. The bachelor student Karen Schriever performed the microscopy experiment shown in Figure App. 3A under my supervision, which was included in the bachelor thesis: "Assessing a possible role of unfolded protein *O*-mannosylation as a complementary Endoplasmic Reticulum quality control mechanism in *Saccharomyces cerevisiae"*, submitted to the Ruprecht-Karls-University (Heidelberg faculty of Biosciences) in 2015.

The ribosome profiling experiment (Figure 4.27) was performed by Ilgin Cotan in the frame of a collaboration with the group of Prof. Bern Bukau and Dr. Gunter Kramer (Zentrum für Molekulare Biologie, Heidelberg, Germany).

The ER-GFP screening was performed by Lihi Gal in the frame of a collaboration with the group of Prof. Maya Schuldiner (Weizmann Institute of Science, Rehovot, Israel).

1 INTRODUCTION

Homeostasis is commonly referred to as the process by which physical and chemical conditions within the internal environment of the body are maintained within tolerable ranges even when the external environment changes. It was first used as a term in physiology by Walter Bradford Cannon in 1926 (Cannon, 1926) and since then it has been applied to describe the equilibrium existing not only at the organismal level but in all physiological systems.

The different components of the cell are no exception and have developed multiple mechanisms to maintain homeostatic conditions within organelles, contributing thus to optimize the cell's physiological functions. Within the cell, the endoplasmic reticulum (ER) is a central cellular hub for the production of secretory proteins. Approximately one-third of the human proteome including both soluble and membrane proteins is translated, translocated and sorted to the ER (reviewed in X. Chen *et al.*, 2010). Protein homeostasis in the ER is achieved by the interplay between different mechanisms that ensure both, correct protein folding and maturation, including the addition of post-translational modifications, and minimize the impact of adverse conditions either caused internally or as a consequence of the cellular environment. Adverse conditions impacting negatively on ER protein homeostasis are commonly referred to as ER stress. ER stress pictures an altered physiological scenario in which the cell is challenged to activate multiple responses at many layers in an attempt to restore protein homeostasis (reviewed in C. Xu *et al.*, 2005). In this current work protein *O*-mannosylation is explored as one of the many tools used by the cell to maintain protein homeostasis in terms of the interplay with other ER stress cellular responses, the different factors that orchestrate it, and its potential physiological role in affecting protein stability.

1.1 Protein glycosylation

The covalent addition of carbohydrates to proteins is not only decisive for the protein's molecular function but establishes a fundamental process concomitant with the existence of all living organisms. First discovered in the 60s (Johansen *et al.*, 1961), protein glycosylation is found as the most abundant and heterogeneous post-translational protein modification across life domains.

Protein glycosylation has been linked to countless aspects of the protein function. These include structural function, contribution to protein stability, determinant for cell-cell and cell-matrix interaction, cell recognition by microorganisms and antibodies and the modulation of the interaction of peptides with their cognate ligands or receptors (reviewed in Varki, 1993). One relevant facet of protein glycosylation is the existence of congenital disorders of glycosylation (CDGs) in humans, inherited systemic diseases that appear linked to the malfunction of different steps of the protein glycosylation pathways. While impairment of protein glycosylation results in embryonic lethality, CDGs appear associated with mutations affecting the glycosylation pathways at different steps of the glycoprotein synthesis and/or maturation. CDGs are diverse and generally classified according to the gene affected in each case and they normally have in common systemic symptoms caused by abnormal development of the brain and defects of the nerve-, liver-, stomach-, and intestinal systems (reviewed in Varki, 1993; Grunewald *et al.*, 2002; Lehle *et al.*, 2006).

The vast complexity of protein glycosylation is reflected by the fact that carbohydrate-protein linkages have been described for most of the functional groups occurring on peptide chains and multiple commonly occurring sugars, establishing an enormous number of possible functional combinations of linear and branched oligosaccharides of distinct length and composition (reviewed in Spiro, 2002). Protein glycosylation is generally classified according to the type of glycopeptide linkage in *N*-glycosylation, *O*-glycosylation, *C*-mannosylation, phophoglycosylation and glycosylfosfatidylinositol (GPI linkage) (reviewed in Spiro, 2002; Lehle *et al.*, 2006). The different types of protein glycosylation largely diverge in prevalence across and within biological kingdoms (reviewed in Dell *et al.*, 2010). In general, glycans present in higher eukaryotes are richer in diversity and complexity than what found in unicellular organisms (Zielinska *et al.*, 2012), representing another layer of

specialization of the cell and expanding the versatility of the organism's proteome (reviewed in Lis & Sharon, 1993; Spiro, 2002; Dell *et al.*, 2010). In baker's yeast, with the exception of glypiation, protein *N*-glycosylation, and protein *O*-mannosylation as the only type of *O*-glycosylation are present. This, together with the high degree of conservation of the biosynthetic pathways of *O*-and *N*-glycans has qualified *Saccharomyces cerevisiae* as a suitable model organism to study protein glycosylation, not only in terms of the molecular mechanism of the glycoprotein biosynthesis and the function of glycans but also to the characterization of different CDG subtypes (reviewed in Lehle *et al.*, 2006). With the focus of this current work put on protein *O*-glycosylation, it is worth to mention that it is precisely the finding and characterization of the protein *O*-mannosylation machinery in yeast (Strahl-Bolsinger *et al.*, 1993, Lussier *et al.*, 1995) what set the basis for the discovery of the conserved pathways in higher eukaryotes (Jurado *et al.*, 1999; Willer *et al.*, 2002; Beltran-Valero de Bernabe *et al.*, 2002).

1.2 Protein glycosylation in *Saccharomyces cerevisiae*

Protein *N*-glycosylation, *O*-mannosylation and the formation of the GPI anchor (with regard to the sugar added to the GPI precursor) are initiated at the ER by the covalent transfer of the core sugar structures from the sugar donor dolichol phosphate (Dol-P) and dolichylpyrophosphate (Dol-PP) to synthesized polypeptides. Dolichol belongs to the family of poly-isoprenoid lipids comprised of a linear structure of fifteen core isoprene units in yeast (Adair & Cafmeyer, 1987). The Dol-P and Dol-PP-linked sugars are synthesized at the cytosolic side of the ER and flipped into the lumen by a yet unknown mechanism to serve as a platform providing sugars for each glycosylation pathway.

One of the yeast compartments primarily found to accumulate glycoproteins is the cell wall, where they comprise approximately 30-50 % of its mass (reviewed in Klis *et al.*, 2006). For some extensively modified glycoproteins, glycans contribute up to 95% of their total molecular mass (Ballou, 1990). Based on prediction it has been initially estimated that 20-50% of the yeast proteome could undergo glycosylation (Apweiler *et al.*, 1999). Discovery-based glycoproteomic studies have been able to identify and map about 270 *N*-glycoproteins (Zielinska *et al.*, 2012), and 512 *O*-mannoproteins (Neubert *et al.*, 2016). The glycoproteins identified in these two studies represent 20-30% of the yeast secretome and this number is still expected to increase as long as glycoproteomic approaches increase in resolution.

1.2.1 Protein *N*-glycosylation

Biosynthesis of *N*-glycoproteins is initiated at the cytosolic side of the ER membrane by the formation of an initial lipid-linked oligosaccharide (LLO). Noteworthy, these steps are shared by all eukaryotes as well as the core structure of the glycan transferred to synthesized proteins. Dolichylpyrophosphate core oligosaccharide is assembled by the coordinated function of enzymes of the ER-glycosyltransferase ALG family. In the cytosol, sugar substrates used for the first steps of the lipid-linked oligosaccharide are derived from the primary metabolism as the nucleotide activated sugars UDP-GlcNAc and GDP-Man. The Alg7 transfers an initial *N*-acetylglucosamine phosphate residue. A second *N*-acetylglucosamine is added by the Alg13-Alg14 complex (Rine *et al.*, 1983; Bickel *et al.*, 2005). The sugar chain is subsequently elongated by the addition of five mannose residues in a stepwise manner by Alg1, Alg2, and Alg11, resulting in the formation of $Man_5GlcNAc_2$-P-P-Dol (Couto *et al.*, 1984; Cipollo *et al.*, 2001; O'Reilly *et al.*, 2006; Kampf *et al.*, 2009), which flips into the ER lumen by a yet unknown mechanism for further processing. In the ER lumen, four mannose and three glucose residues are transferred in a stepwise manner by the glycosyltransferases Alg3, Alg9, Alg12 and Alg6, Alg8 and Alg10 (Stagljar *et al.*, 1994; Aebi *et al.*, 1996; Reiss *et al.*, 1996; Burda & Aebi, 1998; Burda *et al.*, 1999; Frank & Aebi, 2005), resulting in the final LLO. ER luminal glycosyltransferases use Dol-P-Mannose and Dol-P-Glucose as substrate donors, which are assembled in the cytosol from GDP-mannose and UPD-glucose in a reaction catalyzed by Dpm1 (See 1.2.2) and Alg5 (Heesen *et al.*, 1994), respectively, and translocated across the membrane similar to the LLO precursor. The final LLO is used as a sugar donor by the oligosaccharyltransferase (OST) complex, which transfers the core *N*-glycan to Asn residue of the sequon Asn-X-Ser/Thr of synthesized polypeptides, being X any amino acid except proline (Aebi, 2013). Recent studies showed a preference for Asn-X-Thr sites over Asn-X-Ser (Zielinska *et al.*, 2012).

The OST complex in yeast is a heteroligomeric protein complex comprised of eight transmembrane proteins: The four essential subunits Stt3, Ost1, Ost2 and Wbp1 assemble with Ost4, Ost5 and either Ost3 or Ost6, resulting in two different OST complex isoforms that have different polypeptide substrate specificity (Schwarz *et al.*, 2005; Kelleher & Gilmore, 2006; Spirig *et al.*, 2005; Schulz & Aebi, 2009). Based on phylogenetic and structural studies it is assumed that the Stt3 subunit carries the catalytic active site (Izquierdo *et al.*, 2009;

Hese *et al.*, 2009; Nasab *et al.*, 2008; Bai *et al.*, 2018). However, the specific function of other members of the OST complex is not yet understood.

One important feature of the OST complex is that it is found associated to the translocon complex (Shibatani *et al.*, 2005) and structural studies in yeast and bacteria suggest that *N*-glycosylation might precede or compete with folding of target polypeptides (Lizak *et al.*, 2011; Bai *et al.*, 2018).

Once correctly folded (see 1.3), the resulting glycoprotein is packaged into trafficking vesicles to the Golgi apparatus, where the glycans undergo further processing. For heavily glycosylated proteins like invertase, up to 200 mannose residues are added on the core *N*-glycans during the journey of the glycoprotein throughout the Golgi (Ballou, 1990). Elongation steps at the Golgi also work in a step-wise manner by the interplay of different mannosyltranferases: Och1 initiates an α-1,6-polymannose chain, which is elongated and branched by the coordinated function of members of the MNN9, MNN10, KTR, and MNN1 mannosyltranferase families. Some of the *N*-glycan branches also receive a phosphomannose (reviewed in Aebi, 2013; Dean, 1999).

In yeast, the function of *N*-glycans has been linked to key biological processes such as cell wall biogenesis (Lesage & Bussey, 2006), intracellular transport (Nagai *et al.*, 1997) or protein folding and quality control (McCracken & Brodsky, 1996). Quality control of *N*-glycoproteins is one of the most studied aspects of *N*-glycosylation in yeast and likely the most relevant for this current work due to the potential similarities with *O*-mannosylation. The function of *N*-glycans in protein quality control is developed in 1.3.1.

1.2.2 Protein *O*-mannosylation

Protein *O*-mannosylation is a vital protein post-translational modification firstly discovered in the late 60s with the analysis of the glycan composition of the yeast cell wall (Sentandreu & Northcote, 1968). The sugar donor for *O*-mannosylation is Dol-P-Man, which in analogy to other lipid-based sugar donor precursors is synthesized at the cytosolic side of the ER membrane (Babczinski & Tanner, 1973). Dol-P-Man is generated from Dol-P by the addition of a single mannose residue from GDP-Man derived from the primary metabolism. This reaction is catalyzed by dolichol phosphate mannose synthase (Dpm1) (Haselbeck, 1989), an essential mannosyltranferase that in yeast functions as a single ER transmembrane protein (Orlean *et*

al., 1988). Once assembled, Dol-P-Man flips across the ER membrane by a yet unknown mechanism and serves as a crossroad between *O*-mannosylation, *N*-glycosylation, and glypiation, providing single mannoses as a substrate for the different glycosylation machinery in the ER lumen (Rush & Waechter, 1995; reviewed in Schenk *et al.*, 2001).

O-mannosylation is initiated at the luminal side of the ER, where members of the protein mannosyltransferase (PMT) family catalyze the transfer of single mannoses in α- anomeric configuration to the hydroxyl group of Ser or Thr residues of target polypeptides *via* α- mannosidic linkage (Bause & Lehle, 1979).

Knowledge on *O*-mannosylation *in vivo* substrates was for long restricted to cell wall and plasma membrane proteins and found only on regions enriched with high Ser and Thr content (Cappellaro *et al.*, 1991; M. H. Chen *et al.*, 1995; Mrsa *et al.*, 1999; Shimoi *et al.*, 1998; Ecker *et al.*, 2003). Based on this assumption, about 20% of proteins targeted to the ER by a signal peptide were predicted to be *O*-mannosylated (Gonzalez *et al.*, 2012). A different picture is provided by *in vitro* acceptor peptides, where also modest Ser/Thr stretches were shown to be *O*-mannosylated (Weston *et al.*, 1993; Strahl lab, unpublished). However, a recent proteomic study from our group showed that the prevalence of *O*-mannosylation in the secretory pathway is broader than initially excepted (Neubert *et al.*, 2016). 293 secretory proteins were found to be *O*-mannosylated in more than 2000 unique glycosites. This proteomic study also provided evidence of structural features of *O*-mannosylation protein targets: preference for unstructured regions and β-strands, preference for Thr over Ser sites and depletion of *O*-mannosylation in proximity to *N*-glycosylation sites. Nevertheless, the existence of a defined target sequon in analogy to *N*-glycosylation has been so far elusive.

Among the *O*-mannosylation targets, there is significant enrichment of cell wall and plasma membrane proteins, but also proteins in the ER and Golgi. These *O*-mannoproteins fulfill diverse functions in glycosylation, trafficking, and protein quality control, indicating that the function of *O*-glycans in yeast is not solely structural as initially thought and might contribute to multiple key processes in the secretory pathway. This hypothesis is further supported by genomic and transcriptomic studies of the cell response upon defects in *O*-mannosylation where crosstalk between *O*-mannosylation and processes such as *N*-glycosylation, formation, and remodeling of the GPI anchor, the unfolded protein response, the mating response, and the cell wall integrity pathway have been presented (Arroyo *et al.*, 2011; Zatorska *et al.*, 2017).

The protein mannosyltransferase (PMT) family

1.2.2.1

Topologically, PMTs are large polytopic integral ER membrane proteins comprised of eleven transmembrane domains, ten hydrophilic loops, a cytosolic *N*-terminal and a luminal C-terminal domain (Figure 1.1,Bai *et al.*, 2019)

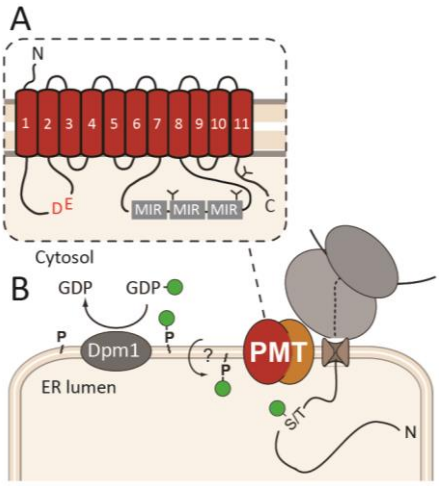

Figure 1.1. (**A**) **Topology of Pmt1** according to Bai *et al.*, 2019. The conserved D-E catalytic site in loop 1 and three MIR domains in loop 7 are indicated. Pmt1 has three *N*-glycosylation sites (Y). (**B**) **Protein *O*-mannosylation in the ER**. Dol-P-man is assembled in the cytosol by Dmp1 and flips across the ER membrane. Members of the PMT family catalyze the transfer of single mannose residues from the sugar donor Dol-P-Man to Ser/Thr residues of target polypeptides. – D, -E; aspartic and Glutamic acid.

Among the hydrophilic loops that face the ER lumen, the loop 1 contains a conserved aspartic and glutamic acid motif that is required for substrate binding and catalytic activity, suggesting that is part of the catalytic active site (Lommel *et al.*, 2011). In the significantly larger loop 7, three MIR (Mannosyltransferase - Inositol trisphosphate receptor - Ryanodine receptor) motives are also required for PMT activity although they do not interfere with the engagement of PMTs with target substrates (Figure 1.1; Girrbach *et al.*, 2000; Lommel *et al.*, 2011).

The PMT family includes at least 6 isoforms in yeast named *PMT1-6* (Immervoll *et al.*, 1995; Lussier *et al.*, 1995; Strahl-Bolsinger & Scheinost, 1999), thought to be originated by genomic duplication during evolution. PMTs are conserved in fungi, animals and some bacteria and archaea (Lommel & Strahl, 2009). So far, no PMT-like protein has been identified in plants. Phylogenetic analyses of the PMT family have classified the different PMT isoforms into three subfamilies: PMT1, PMT2, and PMT4 (Figure 1.2; Girrbach *et al.*, 2000; Willer *et al.*, 2002). The PMT1 subfamily includes Pmt1 and Pmt5; the PMT2 subfamily Pmt2, Pmt5 and Pmt6; and Pmt4 is the only member of the PMT4 subfamily. Redundancy within the different PMT subfamilies is present in some fungi like *Candida albicans* (Lommel & Strahl, 2009) whereas only one member per subfamily exists in other yeast species and filamentous fungi

(Goto, 2007; Olson *et al.*, 2007; Kriangkripipat & Momany, 2009). The PMT1 subfamily is so far fungi-specific whereas in animals only unique members of the PMT2 (POMT2) and PMT4 (POMT1) subfamilies are present (Jurado *et al.*, 1999; Willer *et al.*, 2002; Lommel & Strahl, 2009).

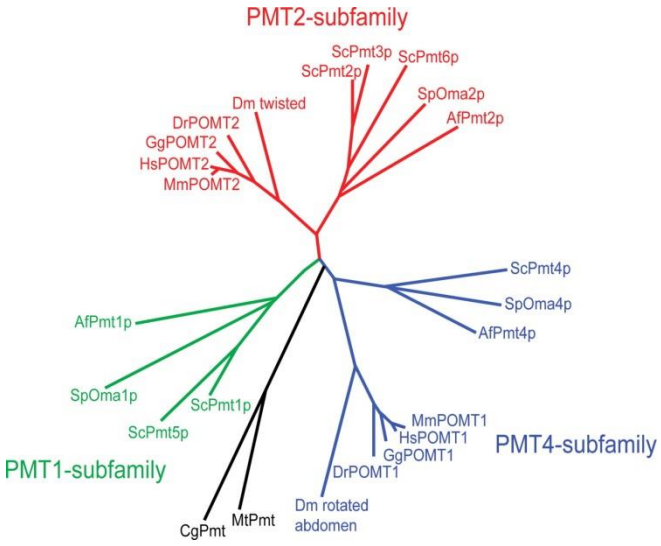

Figure 1.2. Phylogeny within the PMT family. ClustalW-based analysis of PMT protein sequences (J. D. Thompson *et al.*, 1994). Af, *A. fumigatus*; Cg, *C. glutamicum*; Dm, *D. melanogaster*; Dr, *Danio rerio*; Gg, *Gallus gallus*; Hs, *Homo sapiens*; Mm, *Mus musculus*; Mt*, M. tuberculosis;* Sc, *S. cerevisiae*; Sp, *S. pombe*. Taken from (Lommel & Strahl, 2009).

PMTs work forming protein complexes that include members from different PMT subfamilies and/or within the same family. In yeast members of the PMT1 subfamily (Pmt1 and Pmt5) form heteromeric complexes with members of the PMT2 subfamily (Pmt2 and Pmt3) whereas Pmt4 is shown to form homomeric complexes.

Preferentially the Pmt1-Pmt2 and Pmt3-Pmt5 complexes coexist with the Pmt4-Pmt4 complex. However, upon the deletion of their cognate partners, Pmt1-Pmt3 and Pmt2-Pmt5 interactions have been demonstrated (Girrbach & Strahl, 2003). The formation of these complexes has been shown to be necessary for full *in vitro* activity (Tanner *et al.*, 1995) and there is no direct evidence of functional PMT monomers.

Similar to the OST complex, there is evidence of *O*-mannosylation working co-translationally at least to some extent: First, radioactively labeled mannose is found in the polysome fraction of the cell (Larriba *et al.*, 1976); and second, direct interaction with the Sec61 translocon has been proven both *in vivo* and *in vitro* (Loibl *et al.*, 2014). This, however, cannot be generally extended to all scenarios since when translocation has been already completed, prolonged and inefficient folding of proteins seems to be a trigger for the so-called unfolded protein *O*-mannosylation (see 1.4.2; C. Xu *et al.*, 2013).

As mentioned above, *O*-mannosylation is a vital process. Combined deletion of *PMT1*, *PMT2* and *PMT4* results in cell death, however single deletion of any member of the PMT family does not show phenotypes besides the formation of cell clumps likely linked to defects in the cell wall composition. Combination of several deletions is also viable although results in a thermosensitive phenotype (*pmt1pmt4*, *pmt2pmt3*, *pmt1pmt2pmt3*, *pmt1pmt3pmt4*) or growth only upon osmotic stabilization (*pmt2pmt3*, *pmt2pmt4*, *pmt1pmt2pmt3*) (Immervoll *et al.*, 1995; Gentzsch & Tanner, 1996). The Pmt3-5 complex is thought to have overlapping functions with the Pmt1-Pmt2 complex (Girrbach & Strahl, 2003), however a clear effect of its deletion on *O*-mannosylated proteins analyzed *in vivo* has been milder, only present in combination with deletion of Pmt1/Pmt2 or even not observable at all (Gentzsch & Tanner, 1997; Proszynski et al., 2004; Petkova et al., 2012). No physical interaction with other Pmts has been shown for Pmt6 (Girrbach & Strahl, 2003). Taken together this led to the assumption that Pmt3, Pmt5, and Pmt6 are minor contributors to the overall *O*-mannose glycoproteome. In line with this, there is no phenotype associated with *pmt356*Δ, which is indistinguishable from wild type at least under the conditions tested (M. Loibl, unpublished data). Still, dissection of the *O*-mannose glycoproteome into each PMT member's contribution remains to be addressed.

1.3 The ER quality control of secretory proteins

Rapidly after synthesis, proteins undergo a folding process in which polypeptides adopt a 3D-dimensional structure necessary to perform their function. The functional structure of a protein is referred to as the native conformation, and it is achieved by the interplay of the thermodynamic context and local folding factors that work independently in the cytosol, the ER and mitochondria (reviewed in Hartl & Martin, 1995).

In the ER a set of members of the Hsp70 chaperone family (Kar2 and Lhs1) and Hsp40 co-chaperones (Jem1 and Scj1), the nucleotide-exchange factor Sil1, lectin-like proteins such as Cne1 and thiol oxidoreductases (Eps1, Eug1, Mpd1, Mpd2, and Pdi1) assist folding of polypeptides (reviewed in Thibault & Ng, 2012) while and after they are translocated into the lumen (Whitley *et al.*, 1996; reviewed in Fedorov & Baldwin, 1997; and Kowarik *et al.*, 2002). All these factors bind or interact with newly synthesized proteins keeping them soluble, preventing aggregation, ensuring the formation of correct disulfide bonds and stabilizing otherwise unstable structures that would result in incorrect folding. This process requires high

fidelity since incorrect folding results in most cases in loss of protein function, linked to severe diseases such as Alzheimer's or Parkinson's disease (reviewed in Selkoe, 2003). The diverse mechanisms in charge of assisting and monitoring protein folding as well as removing those secretory proteins that irreversibly fail to achieve the native conformation are referred to as ER protein quality control (ERQC) mechanisms.

1.3.1 The endoplasmic reticulum associated degradation (ERAD) pathway

ERAD refers to a molecular pathway occurring in the ER that monitors the correct folding of secretory proteins and targets them to proteasomal degradation when misfolding defects are detected (reviewed in (Ismail & Ng, 2006; Thibault & Ng, 2012). The initial step of ERAD is the recognition and discrimination among different classes of proteins based on their folding state: First, proteins within the folding cycle are protected from premature degradation (Zhang *et al.*, 2017); second, properly folded proteins are normally packaged into coat complex protein II (COPII) vesicles to the Golgi based on sequence-based export signals or kept in the ER when they bear ER retention signals (reviewed in Dancourt & Barlowe, 2010); finally, misfolded proteins are prevented from further trafficking and eventually degraded. In the third case, after recognition misfolded proteins are targeted to the ER membrane where retro-translocation in the cytosol occurs through a still unknown membrane channel with the aid of the Cdc48p AAA-ATPase complex. At the cytosolic side of the ER membrane, E2 ubiquitin-conjugating enzymes and E3 ligases mark misfolded proteins with ubiquitin, which determines the final degradation by the 26S proteasome (reviewed in Thibault & Ng, 2012).

In yeast, two main protein complexes define the ERAD system and are named based on the E3 ligase integrated into each complex: Hrd1 and Doa10. Each complex acts on different classes of misfolded protein grouped according to the topological domain of the protein that presents the misfolded region. Soluble proteins and transmembrane proteins presenting luminal misfolded regions are targeted to the so-called ERAD-L, associated with the function of the Hrd1 complex. Hrd1 is also responsible for the disposal of membrane proteins with aberrant transmembrane domains as part of the ERAD-M pathway. Finally, membrane proteins presenting lesions in their cytosolic domains are targeted to the ERAD-C pathway, represented by the Doa10 complex (Carvalho *et al.*, 2010).

The biochemical reconstitution of both ERAD complexes showed a large overlapping in components as well as some unique features (Gauss *et al.*, 2006; Denic *et al.*, 2006; Carvalho *et al.*, 2006). As part of the complex, the Doa10 E3 ligase interacts with the E2 dimer Ubc7/Cue1 and Cdc48 and its cofactors Npl1 and Ufd1 which get recruited by the bridging factor Ubx2. The Hrd1 complex also includes Cdc48-Npl1-Ufd1 but is in general much more diverse. Hrd3, Der1, Usa1, and Yos9 (see below) define the core components assembled with Hrd1 for ERAD-L. On the other hand, for ERAD-M only Hrd1 and Hrd3 seem to be required. The molecular basis of the substrate recognition is clearer for the Hrd1 complex. As developed in 1.4.1, the lectin Yos9 is responsible for the recognition of aberrant *N*-glycoproteins (Cormier *et al.*, 2005) and it interacts with Kar2 and Hrd3, also capable of binding misfolded proteins (S. I. Nishikawa *et al.*, 2001; Gauss *et al.*, 2006; Denic *et al.*, 2006) likely constituting the luminal core that monitors folding and recognizes misfolded proteins. How the Doa10 complex selects ERAD-C substrates is still unknown.

1.3.2 Post-ER quality control

ER Quality control mechanisms are able to distinguish those proteins that are correctly folded and should generally move on the secretory pathway from those that did not complete the folding cycle yet, retaining them in the ER and potentially sending them for degradation. What are the determinants to make the decision are not entirely clear, although the prolonged engagement with chaperones or the presence of yet hydrophobic segments seem to favor ER retention and eventual degradation, whereas the display of folded ER export signals favors trafficking to the Golgi apparatus *via* COPII vesicles (reviewed in M. C. S. Lee *et al.*, 2004; Dancourt & Barlowe, 2010). Although way less characterized, there are exceptions to these rules since some misfolded proteins are able to escape the ER quality control mechanisms towards the Golgi apparatus (Vashist *et al.*, 2001; Kincaid & Cooper, 2007; reviewed in Dancourt & Barlowe, 2009; Wang & Ng, 2010) and in some cases be diverted to the vacuole for degradation (Spear & Ng, 2003; Coughlan *et al.*, 2004). Vacuolar degradation has been also described for protein aggregates that reach the vacuole by the autophagy pathway (S. I. Nishikawa *et al.*, 2001; Ishida & Nagata, 2009). This alternative pathway to remove aberrant proteins is referred to as post-ER quality control and is suggested to assist the ER quality control mechanisms when these get saturated (Spear & Ng, 2003). However, the mechanisms underlying the sorting of misfolded proteins

for vacuolar turnover and its occasional prevalence over ERAD is not characterized in detail yet.

1.3.3 The unfolded protein response (UPR)

In the context of ER protein homeostasis, the different protein quality control mechanisms coordinate each other to ensure precise and efficient protein production.
Generally, ER stress causes an unbalance between the folding requirements and the capacity of the ER quality control mechanisms, thereby resulting in the accumulation of misfolded proteins. In this scenario, eukaryotic cells have evolved a compensatory mechanism to adapt the protein folding capacity of the ER to an increasing demand for folding factors named the unfolded protein response (UPR). Adaptation to stress is achieved by transcriptional upregulation of ER-chaperones, glycosyltransferases, genes involved in lipid biosynthesis and the ERAD machinery (Travers *et al.*, 2000). In metazoans, the UPR also drives selective mRNA degradation and translational attenuation (Harding *et al.*, 1999; Hollien & Weissman, 2006). In yeast, the activation of the UPR is solely driven by the type I transmembrane protein Ire1, which is the only member of the UPR conserved in all eukaryotes. Upon sensing of ER stress, Ire1 oligomerizes on its *N*-terminal luminal domain and undergoes trans-autophosphorylation through its cytosolic kinase domain (Kimata *et al.*, 2007; Korennykh *et al.*, 2009; Pincus *et al.*, 2010). Upon activation, the cytosolic ribonuclease domain of Ire1 cleaves the intron of HAC1 mRNA in an unconventional splicing reaction (Cox *et al.*, 1993; Mori *et al.*, 1993; Cox & Walter, 1996). HAC1 mRNA exons are then ligated by a tRNA ligase and final mRNA is translated into a bZIP transcription factor that upregulates the expression quality control-related genes (Sidrauski *et al.*, 1996; Travers *et al.*, 2000).
Oligomerization of Ire1 in high-order clusters has been shown to be necessary for full RNase activity (Korennykh *et al.*, 2009; Li *et al.*, 2010). The first step of Ire1 oligomerization is thought to be the formation of dimers that assemble into high-order oligomers by the nucleotide-binding domain of the kinase (K. P. K. Lee *et al.*, 2008; Korennykh *et al.*, 2009). Phosphorylation seems to directly affect Ire1 deactivation (Rubio *et al.*, 2011), which is important since the maintenance of the UPR for prolonged time compromises cell viability (Chawla *et al.*, 2011).
Ire1's sensing of unfolded proteins was though for a long time to rely on the binding of the Hsp70 chaperone Kar2 which dissociates in the presence of unfolded proteins, facilitating

Ire1 oligomerization and activation (Dorner *et al.*, 1992; Kohno *et al.*, 1993; Shamu *et al.*, 1994). More recently, a second mechanism based on the crystal structure of the luminal domain of Ire1 proposed that Ire1 has the capacity to bind unfolded peptides by the formation of a ligand-binding groove (Credle *et al.*, 2005). Further studies have shown that the luminal domain of Ire1 is actually dispensable for Ire1 activation (Oikawa *et al.*, 2007) and direct evidence of interaction with unfolded proteins *in vivo* and *in vitro* have been shown (Kimata *et al.*, 2007). Similar to Kar2, Ire1 interacts preferentially with regions containing basic and hydrophobic residues. This is the case of CPY*, a misfolded protein model shown to interact with Ire1 even when Ire1 carries mutations that prevent oligomerization (Gardner & Walter, 2011; Promlek *et al.*, 2011).

Today it is accepted that direct interaction with unfolded proteins is the main driving force for Ire1 oligomerization and activation. Kar2 association to Ire1 is however thought to stabilize inactive Ire1 monomers, preventing hypersensitivity to modest stress levels and buffering its function (Kimata *et al.*, 2004; Pincus *et al.*, 2010).

In general, conditions that result in the stabilization of high-order Ire1 oligomers are thought to contribute to Ire1 activation. This is the case of altered lipid composition of the ER membrane (Promlek *et al.*, 2011), suggested to decrease membrane protein diffusion. Also, ligand binding to Ire1's cytosolic domain has been shown to activate the UPR by stabilization of Ire1 dimers (Wiseman *et al.*, 2010).

1.4 Protein quality control meets protein glycosylation

1.4.1 Quality control of *N*-glycoproteins

After the transfer of the core *N*-glycan to the target protein in the ER lumen, glucosidases Gls1 and Gls2 trim terminal glucose residues of the A- branch of the glycan as a checkpoint for protein degradation (Hammond *et al.*, 1994; Hitt & Wolf, 2004). This step has been well characterized in mammals and referees as the calnexin cycle, where trimming of terminal glucoses works as a determinant for prolonged cycles of folding and are terminated by re-glucosylation (Trombetta & Helenius, 2000; Solda *et al.*, 2007). In baker's yeast, however, the role of calnexin is yet not well understood (McCracken & Brodsky, 1996).

In *S. cerevisiae* after folding of the glycoprotein is accomplished, subsequent trimming of a terminal mannose from B- and C-branches of the core *N*-glycan by the mannosidases Mns1

and Htm1 define a protein degradation signal recognized by the lectin Yos9 (Jakob *et al.*, 1998; Quan *et al.*, 2008). Discriminating between the signal for protein degradation on terminal mannoses from those that are displayed during the synthesis of the core glycan is likely accomplished by the interplay of other folding factors such as Kar2 and Pdi1. This assumption is based on the fact that α-1,6-linked mannose is not solely recruiting Htm1 and also unfolded segments on the protein need to be exposed (Clerc *et al.*, 2009; Gauss *et al.*, 2011). In terms of protein quality control, the different reactions that precede Htm1 recruitment define a time frame in which the polypeptide undergoes folding. In this context, the resulting structure of the core *N*-glycan functions as a timer thought to determine when the folding cycle of proteins must cease, and the defective protein must undergo ERAD.

1.4.2 The so-called unfolded protein *O*-mannosylation (UPOM)

In the last two decades, protein *O*-mannosylation has been suggested to play a role in folding or quality control of secretory proteins in an increasing number of studies. The branch of *O*-mannosylation that targets misfolded proteins during or as part of their quality control has been recently named unfolded protein *O*-mannosylation (UPOM) (C. Xu *et al.*, 2013).

The term UPOM is based on the analysis of misfolded model proteins, either artificial recombinant constructs or truncations of endogenous proteins that are not targets of this modification in their native state. The first study reporting this phenomenon was published in 2001 by the Römisch group using a mutated version of the yeast pheromone precursor pre pro-alpha-factor Δgpαf (Harty *et al.*, 2001). Δgpαf lacks *N*-glycosylation acceptor sites of the native pre pro-alpha-factor (Mayinger & Meyer, 1993) and is consequently misfolded and targeted for ERAD (McCracken & Brodsky, 1996). Harty and colleagues showed that Δgpαf is *O*-mannosylated by Pmt2 after synthesis *in vitro* and *in vivo*. Based on *in vitro* experiments using yeast microsomes they determined that this type of *O*-mannosylation is a slow process, suggesting that it might occur post-translationally as a result of prolonged exposure of the substrate to PMTs (Harty *et al.*, 2001). Following this first study, several misfolded protein models of diverse nature and topology have been shown to receive *O*-mannosylation by the Pmt1-Pmt2 complex (Vashist *et al.*, 2001; Coughlan *et al.*, 2004; Nakatsukasa *et al.*, 2004; Hirayama *et al.*, 2008; S. Y. Li *et al.*, 2012; Rubenstein *et al.*, 2012; C. Xu *et al.*, 2013). However, the molecular basis of this modification is far from being clear.

For some model protein UPOM was shown to reduce their engagement with the ER chaperone Kar2 (Nakatsukasa *et al.*, 2004; C. Xu *et al.*, 2013), suggesting that *O*-mannosylation might work as a fail-safe mechanism to relieve the workload for ER chaperones and irreversibly mark either irreversibly misfolded proteins (Nakatsukasa *et al.*, 2004) or proteins that fold very inefficiently (C. Xu *et al.*, 2013).

Of particular relevance is the case of ER-GFP, the latest discovered UPOM target to date. GFP was long known to fold poorly when targeted to the ER of either yeast or mammalian cells (Jain *et al.*, 2001; D. G. Huang & Shusta, 2006). Xu and colleagues found out that ER-GFP becomes a target of the Pmt1-Pmt2 complex as a consequence of its poor folding kinetics in the oxidative environment of the ER (Aronson *et al.*, 2011; C. Xu *et al.*, 2013). In contrast, the kinetically engineered version of GFP, sfGFP or as referred to in this and the current work, ER-GFP_{fast}, is able to skip *O*-mannosylation. When genetically deleting *PMT1* and/or *PMT2*, ER-GFP becomes folding competent, suggesting that UPOM prevents futile folding (and worthless investment of resources) of slow folding proteins that could otherwise overwhelm the ER folding capacity. Thus, UPOM targets ER-GFP depending on its folding state and provides a time window in which proteins are able to fold before being irreversibly excluded from the folding cycle. This hypothesis seems to be conceptually similar to what shown for the quality control of *N*-glycoproteins, where trimming of terminal mannoses from the core *N*-glycan by Htm1 recruits ERAD components for effective degradation (Gauss *et al.*, 2011; see 1.4.1).

On the contrary, UPOM does appear to be directly coupled to any specific degradation pathway and the final fate of proteins that undergo UPOM is diverse. On one hand, UPOM is shown to be a determinant for ERAD of several misfolded protein models. This is the case of KHN, the ER-targeted simian virus 5 haemagglutinin neuraminidase (KHN) (Vashist *et al.*, 2001), a pro-region-deleted derivative of *Rhizopus niveus* aspartic proteinase-I (Δpro) (Nakatsukasa *et al.*, 2004) or the A-chain of Shiga-like toxin (S. Li *et al.*, 2012). One common feature of the ERAD targets that receive *O*-mannosylation for their degradation is their capacity to form aggregates in the absence of Pmt1 or Pmt2. It is accepted that the addition of *O*-glycans to these misfolded protein models increases their solubility and therefore facilitates their recognition and extraction from the ER by the ERAD pathway (S. Nishikawa *et al.*, 2001; Vashist *et al.*, 2001; Nakatsukasa *et al.*, 2004). The effect of *O*-mannosylation promoting ERAD of misfolded proteins is, however, not a common feature of all

O-mannosylated ERAD substrates. Some misfolded models receive *O*-mannosylation presumably during their quality control without their degradation efficiency being affected when *O*-mannosylation is compromised. This is the case for models such as the before mentioned *N*-glycosylation mutant of the pre pro-alpha-factor (Harty *et al.*, 2001; Nakatsukasa *et al.*, 2004) or the ER membrane protein Sec62 appended with the Deg1 degron (Rubenstein *et al.*, 2012) or ER-GFP (C. Xu *et al.*, 2013). On the other hand, the deletion of Pmt1 or Pmt2 has been reported to influence the *O*-mannosylation of different misfolded versions of the GPI-anchored protein Gas1, redirecting them from ERAD to post-ER degradation at the vacuole (Hirayama *et al.*, 2008).

1.4.3 The impact of *O*-glycans on protein stability

Besides its role in contributing to the degradation of some misfolded protein models, *O*-mannosylation is also known to play an opposing role in maintaining the stability of *bona fide* proteins. Abrogating *O*-mannosylation by both the Pmt1-Pmt2, and the Pmt4-Pmt4 complex impacts on the maturation and severely reduces the stability of the plasma membrane sensors of the cell wall integrity: Wsc1, Wsc2, Mid2, and Mtl1 (Lommel et al., 2004; De La Torre Ruiz et al., 2012). This, in turn, results in impaired sensing of cell wall defects and activation of the cell wall integrity pathway. A similar effect is observed in the human pathogen *Candida albicans* for Sec20, an ER membrane protein that functions as a tSNARE component in retrograde vesicle traffic and displays maturation defects and decreased stability upon perturbation of *O*-mannosylation (Ernst et al., 2004). Another example is Axl2, a glycoprotein necessary for yeast axial budding shown to require Pmt4-dependent *O*-mannosylation for correct maturation. In the absence of *PMT4*, Axl2 is shown to be unstable and incorrectly localized to the vacuole (Roemer *et al.*, 1996; Sanders *et al.*, 1999).

1.4.4 State of the art: the many gaps in UPOM

One of the many aspects that remain elusive is how the Pmt1-Pmt2 complex targets misfolded proteins. During UPOM, the Pmt1-Pmt2 complex is able to select and discriminate proteins bearing unfolded segments from those that are properly folded. It is plausible that

such a mechanism could involve additional factors recruiting potential UPOM targets to the Pmt1-Pmt2 complex. Analysis of Pmt1 and Pmt2 interactome by mass spectrometry (Goder & Melero, 2011) yielded potential candidates to fulfill this function such as members of the p24 family, the oxidoreductases Ero1 and Pdi1 and even the central E3 ligase of ERAD Hrd1. Additional clues on potential interactors between the Pmt1-Pmt2 complex and misfolded proteins are provided by the sequence of PMTs itself. PMTs include three MIR motifs that share homology with SDF2-type proteins (stromal cell-derived factor 2), poorly characterized ER proteins present in mammals and plants that are known to interact with Hsp40 ER chaperones (Meunier *et al.*, 2002). Therefore, in analogy to SDF2, PMTs might interact *via* loop7 with members of the Hsp40 chaperone family to recruit substrates for UPOM.

In contrast, in the case of ER-GFP UPOM seems to respond to a timing mechanism in which prevalence in the folding cycle works as a determinant for recruitment to the Pmt1-Pmt2 complex (C. Xu *et al.*, 2013). In a scenario where the Pmt1-Pmt2 complex works as a timer, additional factors are not strictly needed since only abnormally prolonged exposure of unfolded moieties would be sufficient to trigger UPOM. By extension, also other more drastically misfolded models that have been described could enter and exit the folding cycle based on the Pmt1-Pmt2 timing mechanism.

Besides potential interactors, another aspect that remains to be answered is how UPOM is regulated. Previous high throughput studies have shown that *O*-mannosylation is integrated in the UPR (Travers *et al.*, 2000; Promlek *et al.*, 2011) and therefore it is likely that proteins involved in the ER stress response are tightly linked to UPOM. That is the case of *HAC1* and the described lethality when deleted together with major PMTs (Arroyo *et al.*, 2011). Likewise, upon treatment with the *N*-glycosylation inhibitor tunicamycin, many proteins receive *O*-glycans (Harty *et al.*, 2001), indicating that ER stress favors UPOM of proteins that would not receive *O*-glycans otherwise**.** Is it then valid to assume that UPOM is only physiologically relevant upon ER stress when UPR is meant to restore ER homeostasis? Although it is not trivial to answer these questions, large scale analysis of both the transcriptome and the sensitivity to the PMT-specific inhibitor R3A-5a have shown signaling pathways such as cell wall integrity (CWI) pathway, filamentous growth or the mating cascade to be activated to compensate PMT loss or reduction in activity (Arroyo *et al.*, 2011; Zatorska *et al.*, 2017). Even though these studies did not discriminate UPOM from *O*-mannosylation in general, they set the basis to speculate about PMTs contributing to the

ER quality control not only in the context of the ER stress. It is, therefore, a major purpose of this study to unravel which components function next to the Pmt1-Pmt2 complex in the so-called UPOM, both being part of the molecular mechanism and orchestrating it perhaps as part of a regulon.

To date, the existence of proteins that receive *O*-mannosylation during ER protein quality control is restricted to misfolded protein models, where damage is artificially introduced to trigger the activation of the different mechanisms that cope with the stress generated. The question of whether *O*-mannosylation targets endogenous proteins and facilitates their turnover, being or not, part of a quality control mechanism remains unanswered. One limitation that arises when studying *O*-mannosylation in the context of protein quality control is the presence of opposing effects in protein stability (detailed in 1.4.2 and 1.4.3). Besides the potential role of this modification facilitating protein turnover, *O*-mannosylation is necessary for maturation of secretory proteins and deletion of the corresponding PMTs is shown to cause protein destabilization (Sanders *et al.*, 1999; Lommel *et al.*, 2004). Moreover, the effect of the high degree of redundancy and substrate specificity among the different *O*-mannosyl transferases limits the study of protein stability to specific physiological processes and down to individual proteins. Therefore, it is a goal of the current work to obtain a broader view of the consequences of *O*-mannosylation defects in protein stability by taking advantage of more systematic approaches.

2 MATERIALS

2.1 Microorganisms

2.1.1 *Escherichia coli* strains

Strain	Genotype	Reference
DH5α	[F^- ϕ80*lac*ZΔM15 Δ(*lac*ZYA-*arg*F)U169] *rec*A1 *end*A1 *hsd*R17(r_K^-, m_K^+) *pho*A *sup*E44 λ^- *thi*-1 *gyr*A96 *rel*A1	(Bethesda Laboratories, 1986)
XL1-Blue	*recA1 endA1 gyrA96 thi-1 hsdR17 supE44 relA1 lac* [F´ *proAB lacI*^{q}*Z*Δ*M15* Tn*10* (Tet^r)]	(Bullock *et al.*, 1987)

2.1.2 *Saccharomyces cerevisiae* strains

Yeast strains directly derived from genetic libraries appear underlined.

Strain	Genotype	Reference
BY4741	*MATa met15-Δ0 his3-Δ1 leu2-Δ0 ura3-Δ0*	(Brachmann *et al.*, 1998)
SEY6210	*MATα lys2-801 his3-Δ200 leu2-3,112 trp1-Δ901 ura3-52 suc2-Δ9*	(Robinson *et al.*, 1988)
MLY213	BY4741 except *pmt1*Δ	M. Loibl (unpublished)
MLY214	BY4741 except *pmt2*Δ	M. Loibl (unpublished)
MLY216	BY4741 except *pmt4*Δ	M. Loibl (unpublished)
MLY231	BY4741 except *pmt356*Δ	M. Loibl (unpublished)
MLY235	BY4741 except *pmt1356*Δ	M. Loibl (unpublished)
MLY241	BY4741 except *pmt4356*Δ	M. Loibl (unpublished)
JCY001	BY4741 except ade8::4xUPRE-GFP	This study
JCY002	MLY213 except ade8::4xUPRE-GFP	This study
JCY003	MLY214 except ade8::4xUPRE-GFP	This study

JCY004	MLY216 except ade8::4xUPRE-GFP	This study
JCY005	MLY231 except ade8::4xUPRE-GFP	This study
JCY006	MLY235 except ade8::4xUPRE-GFP	This study
JCY007	MLY241 except ade8::4xUPRE-GFP	This study
YMS721	*MATa his3Δ1 leu2Δ0 met15Δ0 ura3Δ0 can1Δ::STE2pr-spHIS5 lyp1::STE3pr-LEU2*	(Papic *et al.*, 2013)
JEY05	YMS721 *ho*Δ:: *ER-GFPf-URA3*	Jakob Engel (unpublished)
JEY06	YMS721 *ho*Δ:: *ER-GFP-URA3*	Jakob Engel (unpublished)
JCY010	JEY06 except *pmt1*Δ::KanMX4	This study
JCY011	JEY06 except *pmt2*Δ::KanMX4	This study
JCY012	JEY06 except *pmt4*Δ::KanMX4	This study
*pep4*Δ	BY4741 except *pep4Δ::KanMX4*	Euroscarf
*spf1*Δ	BY4741 except *spf1Δ::KanMX4*	Euroscarf
*pmt1*Δ	BY4741 except *pmt1Δ::KanMX4*	Euroscarf
*pmt2*Δ	BY4741 except *pmt2Δ::KanMX4*	Euroscarf
*ost3*Δ	BY4741 except *pmt2Δ::KanMX4*	Euroscarf
*bfr1*Δ	BY4741 except *bfr1Δ::KanMX4*	Euroscarf
*pop2*Δ	BY4741 except *pop2Δ::KanMX4*	Euroscarf
psa1-DAmP ER-GFP	JEY06 except *psa1Δ::psa1-DAmP*	This study
pgi1-DAmP ER-GFP	JEY06 except *pgi1Δ::pgi1-DAmP*	This study
*bfr1*Δ ER-GFP	JEY06 except *bfr1*Δ::*KanMX4*	This study
*spf1*Δ ER-GFP	JEY06 except *spf1*Δ::*KanMX4*	This study
JCY015	BY4741 except *psa1Δ::psa1-DAmP*	This study
JCY014	BY4741 except *pgi1Δ::pgi1-DAmP*	This study
JCY016	JEY06 except *bfr1*Δ::*KanMX4*	This study
JCY017	BY4741 except *bfr1Δ::BFR1-3xHA*	This study
JCY033	MLY214 except *pgi1Δ::pgi1-DAmP*	This study
MLY014	SEY6210 except *PMT2-GAGA-HA$_3$-kanMX6*	M. Loibl (unpublished)
MLY098	MLY74 except *klTRP1*-P$_{GAL1}$-*UBI4*-R-*PMT2*	M. Loibl (unpublished)
JCY034	MLY098 except *bfr1*Δ::URA3	This study

MLY201	BY4741 except *pmt1Δ*::*KANMX6*	M. Loibl (unpublished)
MLY202	BY4741 except *pmt2Δ*::*KANMX6*	M. Loibl (unpublished)
MLY204	BY4741 except *pmt4Δ*::*KANMX6*	M. Loibl (unpublished)
YMaM330	MATα *can1Δ::STE2pr-SpHIS5 lyp1Δ::STE3pr-LEU2 his3Δ1 leu2Δ0*::*GAL1pr-I-SCEI-natNT2 ura3Δ0*	(Khmelinskii *et al.*, 2014)
WT Kre6-tFT	YMaM330 except *KRE6::mCherry-sfGFP*	(Khmelinskii *et al.*, 2014)
EZY91	WT Kre6-tFT except *pmt1Δ*::*KANMX6*	This study (Castells-Ballester *et al.*, 2018)
WT Vrg4-tFT	YMaM330 except *VRG4::mCherry-sfGFP*	(Khmelinskii *et al.*, 2014)
EYZ96	WT Vrg4-tFT except *pmt1Δ*::*KANMX6*	This study (Castells-Ballester *et al.*, 2018)
WT Axl2-tFT	YMaM330 except *AXL2::mCherry-sfGFP*	(Khmelinskii *et al.*, 2014)
EZY107	WT Axl2-tFT except *pmt4*Δ	This study (Castells-Ballester *et al.*, 2018)
WT YNL058C-tFT	YMaM330 except *YNL058C::mCherry-sfGFP*	(Khmelinskii *et al.*, 2014)
EZY106	WT YNL058C-tFT except *pmt2*Δ	This study (Castells-Ballester *et al.*, 2018)
WT Mnn11-tFT	YMaM330 except *MNN11::mCherry-sfGFP*	(Khmelinskii *et al.*, 2014)
EZY109	WT Mnn11-tFT except *pmt4*Δ	This study (Castells-Ballester *et al.*, 2018)
MGY69	*AXL2::HA*	(Sanders *et al.*, 1999)
MGY72	*AXL2::HA* except *pmt4*Δ	(Sanders *et al.*, 1999)

2.1.3 *Sacharomyces cerevisiae* genetic libraries

Name	Description	Purpose	Reference
Yeast deletion library	BY4741-based Single gene replacement with *KanMX6*	ER-GFP screen. Automated crossing with JEY06	(Giaever *et al.*, 2002)
DAmP library	BY4741-based 3'UTR disruption by *KanMX6* insertion	ER-GFP screen. Automated crossing with JEY06	(Breslow *et al.*, 2008)
Euroscarf	BY4741-based Single gene replacement with *KanMX6*	Hsp150-based re-screen	Euroscarf (Frankfurt, Germany)
tFT library	YMaM330-based *N*-terminal fusions of tFT	tFT screen Automated crossing with MLY201, MLY202, and MLY204.	(Khmelinskii *et al.*, 2014)

2.2 Plasmids

Name	Description	Purpose	Reference
pPN001	Ori, bla, URA3 UPRE-GFP from pDEP017 via *NotI*/*KpnI* in pIS112	Integration of *ade8::4xUPRE-GFP*	P. Neubert (unpublished)
pPN014	Ori, CEN, P_{TDH3}-ER-GFP-3xFLAG-HDEL	ER-GFP-3xFLAG purification	P.Neubert (unpublished)
pWX204	ori, CEN, P_{TDH3}-$Kar2_{SS}$-ER-GFP_f-HDEL, *URA3*	ER-GFP_f expression	(C. Xu *et al.*, 2013)
pWX206	ori, CEN, P_{TDH3}-$Kar2_{SS}$-ER -GFP-HDEL, *URA3*	ER-GFP expression	(C. Xu *et al.*, 2013)
pJC07	ori, CEN, P_{TDH3}-$Kar2_{SS}$-ER -GFP_f, *URA3* HDEL removal by subcloning and reinsertion in pWX204 via BamHI-XbaI	ER-GFP expression	This study

pJC08	ori, CEN, P_{TDH3}-$Kar2_{SS}$-ER -GFP, *URA3* HDEL removal by subcloning and reinsertion in pWX206 via BamHI-XbaI	ER-GFP expression	This study
pJC01	ori, bla, 2µ, *PMT2, LEU2* *PMT2* fragment from pVG76 (Girrbach & Strahl, 2003) subcloned into pRS425 via SalI/PstI	Template for pJC09	This study
pJC02	ori, bla, 2µ, *PMT2, HIS3* *PMT2-3xHA* fragment from pEZ43 subcloned into pRS423 via SalI/SmaI	Template for pJC10	This study
pRS41N	ori, CEN, *natNT2*	Backbone for pJC09/10	(Taxis & Knop, 2006)
pJC09	ori, CEN, *natNT2* *PMT2* fragment from pJC01 subcloned into pRS41N via *ApaI*/*SpeI*	Expression of PMT2	This study
pJC10	ori, CEN, *natNT2* *PMT2-3xHA* fragment from pJC02 subcloned into pRS41N via *ApaI*/*SpeI*	Expression of *PMT2-3xHA*	This study
pRS415	ori, bla, *LEU2*	Backbone for pJC16	(Christianson *et al.*, 1992)
pJC16	ori, CEN, P_{TDH3}-$Kar2_{SS}$-ER -GFP-HDEL, *LEU2* P_{TDH3}-$Kar2_{SS}$-ER -GFP-HDEL subcloned from pWX206 into pRS416 via NotI/SalI	ER-GFP expression	This study
pUG6	ori, bla, *kanMX4*	template for loxP-*kanMX4*-loxP cassette	(Güldener *et al.*, 1996)
pJH24	ori, bla, 2µ, *URA3*, *kanMX6*	template for *C*-terminal 3xHA tagging	Hutzler (2008)

2.3 Oligonucleotides

All oligonucleotides were purchased from Sigma-Aldrich Chemie (Munich, Germany) in dry form and dissolved in ddH_2O to a final concentration of 100 µM. Stock solutions were diluted to a final 10 pmol/µl working concentration.

2.3.1 RT-PCR oligonucleotides

All oligonucleotides described in this list have T_m between 60 and 61 °C.

Name	Description	Sequence (5'-3')
2262	*ACT1* FW	CCACCATGTTCCCAGGTATTGC
2263	*ACT1* REV	GATAGAACCACCAATCCAGACGGAG
2244	*TAF10* FW	ATATTCCAGGATCAGGTCTTCCGTAGC
2245	*TAF10* REV	GTAGTCTTCTCATTCTGTTGATGTTGTTGTTG
2246	*TFC1* FW	GCTGGCACTCATATCTTATCGTTTCACAATG
2247	*TFC1* TEV	GAACCTGCTGTCAATACCGCCTGGAG
2230	*PMT1* FW	AAATCGCAGTGGTTGTCTGGTTGG
2231	*PMT1* REV	TAGTGGCGGCAGGTTGAGATTC
2232	*PMT2* FW	GTACTGTTTCGACGCCGGTTTG
2233	*PMT2* REV	AGTGCCATGAATCCGGCGTATAG
2236	*PMT4* FW	AGTTGGCCCGGTAGTTTAAGTGG
2237	*PMT4* REV	TGACTTGGAACCACCACCCAATG
2264	$HAC1^u$ FW	TGAACAAGAACACTAGCCCCA
2272	$HAC1^u$ REV	ACTCCCCCATCAGAGAACCAC
2266	$HAC1^s$ FW	AATTTGTTTGATGCGGTGGCCTC
2267	$HAC1^s$ REV	CCTGACTGCGCTTCTGGATTACG
2290	*KAR2* FW	ACCGCCATTGCTGAAGACTTTG
2291	*KAR2* REV	AGAACCATCAGCACCTCCGTAC
2872	*PGI1* FW	GGAATATCAACTCTTTCGACCAATGG
2873	*PGI1* REV	GTTGGTAGAAGCATCGTGGGTAGAA

2892	*PSA1* FW	GCAACTCCACCATCAAGAACCA
2893	*PSA1* REV	ACAGTGACACCTTCCAAACGAC
2930	*BFR1* FW	TACAAGAAGAAGAACCAACAGAAGAACACT
2931	*BFR1* REV	TTCGGCCAAAGTAGCAATTAGTGTT

2.3.2 Other oligonucleotides

Sequences homologous to the indicated ORFs within oligos used for genomic modifications appear underlined.

Name	Description	Sequence (5'-3')
2283	Genotype 4xUPRE-GFP strains *ADE8* 5' FW	AGCAGCGCCTAACTACGACC
2284	Genotype 4xUPRE-GFP strains *ADE8* 5' REV	CTTGTTTGTCGTTATGGTTGGCCT
2285	Genotype 4xUPRE-GFP strains *URA3* FW	TAGAAGACGTTCAACTGTCGAGACC
2286	Genotype 4xUPRE-GFP strains *URA3* REV	CCATTTGGGCCTTCTGCTTCC
2287	Genotype 4xUPRE-GFP strains GFP FW	CTTCTGCTTGTTGTTGCTGCTGT
2288	Genotype 4xUPRE-GFP strains GFP REV	GAGAAAGCAAGGCACAACGCA
2722	Genotype *KANMX6* genomic insertions REV	CTGCAGCGAGGAGCCGTAAT
2804	Genotype *bfr1*Δ Upstream 5'	GTAATTCGCATTTTATCTCGAACAT
2805	Genotype *bfr1*Δ coding	GTCTTTTGTCGTAAACACCTTGAGT
2810	*BFR1* knockout via pUG6 as template for *KanMX6* substitution FW	CCTCCTTTTATCAACGTAATAGCATATTTTCTA ACAACACAGCCATTGCCCAGCTGAAGCTTCGT ACGC

2811	*BFR1* knockout via pUG6 as template for *KanMX6* substitution REV	AATTAAGTAATGAAGAAAGATCAGGAGAAAA ATTTTTTTCTACTTCAGGTGCATAGGCCACTA GTGGATCTG
2822	HDEL removal from pWXB204/206 to generate pJC07/08 FW	AAGGATCCAAGAGTAGTCTCAAGGGAA
2823	HDEL removal from pWXB204/206 to generate pJC07/08 REV	CGATCTAGAAAGCTTATTTGTATAGTTCATCC ATGCCATGTGT
2840	Genotype *bfr1*Δ coding FW	ATGTCCTCCCAACAACACAAGTTCAA
2841	Genotype *bfr1*Δ coding REV	TTTCAGACTCTTCCTGTTCTTTCAATC
2872	Genotype *pgi1-DAmP* FW	GGAATATCAACTCTTTCGACCAATGG
2873	Genotype *pgi1-DAmP* REV	GTTGGTAGAAGCATCGTGGGTAGAA
2874	Genotype *pgi1-DAmP* 3’	TATGTCCTTCGCGCACTGATTC
2892	Genotype *psa1-DAmP* FW	GCAACTCCACCATCAAGAACCA
2893	Genotype *psa1-DAmP* REV	ACAGTGACACCTTCCAAACGAC
2894	Genotype *psa1-DAmP* 3’	CTCAGGCTACCACCAATAACACAG
2885	*BFR1* 3xHA genomic tag *via* pJH24 template FW	AAGAAAAAAGATTGAAAGAACAGGAAGAGT CTGAAAAAGATAAAGAAAATGGAGCAGGGG CGGGTGCATACCCATACGATGTTCCTGACTAT GC
2886	*BFR1* 3xHA genomic tag *via* pJH24 template FW	TCAACCAAAGAAAAATTAAGTAATGAAGAAA GATCAGGAGAAAAATTTTTCCCTCACTAAAG GGAACAAAAGCT
3102	*BFR1* knockout via pRS416 as template for *URA3* substitution FW	CCTCCTTTTATCAACGTAATAGCATATTTTCTA ACAACACAGCCATTGCCACCACAGCTTTTCAA TTCAATTCATCATTT
3103	*BFR1* knockout via pRS416 as template for *URA3* substitution REV	AATTAAGTAATGAAGAAAGATCAGGAGAAAA ATTTTTTTCTACTTCAGGTAACAACACTCAACC CTATCTCGGTCTAT

2.4 Antibodies

2.4.1 Primary antibodies

Name	Description	Reference
αPmt1	Rabbit, 1:2,500	(Strahl-Bolsinger & Tanner, 1991)
αPmt2	Rabbit, 1:2,500	(Gentzsch *et al.*, 1995)
αPmt4	Rabbit, 1:250	(Girrbach & Strahl, 2003)
αHsp150	Rabbit, 1:5,000	(Russo *et al.*, 1992)
αSec61	Rabbit, 1:2,500	(Stirling *et al.*, 1992)
αHA	Mouse, 1:10,000, 16B12	#MMS-101R; Covance (Princeton, NJ, USA)
αGas1	Rabbit, 1:2,500	(Popolo *et al.*, 1988)
αWbp1	Rabbit, 1:2,500	(te Heesen *et al.*, 1993)
αKar2	Rabbit, 1:500	Strahl lab
αOst3	Rabbit 1:1,000	Gift from M.Aebi
αG6PDH	Rabbit, 1:5,000	# A9521; Sigma-Aldrich Chemie (Munich, Germany)
αGFP	Rabbit; 1:5,000	#13970; Abcam, Cambridge, UK
αGFP	Rabbit; 1:2,500	#A6455; Thermo Fisher Scientific (Waltham, MA, USA)
αRpl5	Rabbit 1:7,000	Gift from E. Hurt
αPgk1	Mouse, 1:10,000	#A6457; Mobitec (Gottingen, Germany)

2.4.2 Secondary antibodies

Name	Description	Reference
$\alpha mouse^{HRP}$	Rabbit, 1:10,000, HRP conjugate	#A9044, Sigma-Aldrich
$\alpha rabbit^{HRP}$	Goat, 1:10,000, HRP conjugate	#12-348, Sigma-Aldrich

2.5 Databases, web Services and Software

2.5.1 Databases

NCBI	http://www.ncbi.nlm.nih.gov/
Uniprot	https://www.uniprot.org/
SGD	http://www.yeastgenome.org/
YEASTRACT	(Teixeira *et al.*, 2018) http://www.yeastract.com/
YETFASCO 1.02	(de Boer & Hughes, 2012) http://yetfasco.ccbr.utoronto.ca/
SPELL	https://spell.yeastgenome.org
DAVID	https://david.ncifcrf.gov/

2.5.2 Web services

ExPASy	http://expasy.org/
TOPCONS	http://topcons.cbr.su.se/ (Bernsel *et al.*, 2009)

2.5.3 Software

DNA sequence analysis	ApE – A plasmid Editor (by M. Wayne Davis)
Image processing	Adobe: Illustrator CS5, Photoshop CS4
Image analysis	ImageJ (Schneider *et al.*, 2012)
Western blot quantification	Image Studio Lite
RT-PCR analysis	Rotor-Gene Q series software (Qiagen; Venlo, Netherlands)

2.6 Services

Oligonucleotide synthesis	Sigma-Aldrich (Steinheim, Germany)
DNA sequencing	eurofins mwg|operon (Hamburg, Germany)
Flow cytometry	Flow Cytometry & FACS Core Facility, ZMBH (Heidelberg University; Germany)

3 METHODS

3.1 Microbiology

3.1.1 Cultivation of *Escherichia coli*

Bacterial cultures were grown overnight at 37 °C in liquid LB medium with shaking at 200 rpm or on LB plates containing 2% (w/v) agar. For selection, the medium was supplemented with 100 µg/mL ampicillin.

For long-term storage, bacterial cells were grown in liquid LB medium supplemented with 100 µg/mL ampicillin overnight at 37 °C. Cultures were supplemented with 20 % (v/v) glycerol, frozen in liquid nitrogen and stored at -80 °C.

LB medium:

1 % (w/v)	Tryptone
1 % (w/v)	NaCl
0.5 % (w/v)	Yeast extract

3.1.2 Cultivation of *Saccharomyces cerevisiae*

Yeast cultures were routinely grown overnight in YPD/SD liquid medium with 200 rpm shaking or until complete growth on plates containing 2% (w/v) agar at 30 °C. The cell density of liquid cultures was determined as the optical density at 600 nm (OD_{600}) using the spectrophotometer Ultrospec™ 3100 pro (GE Healthcare, Munich, Germany).

For general procedures yeast cells were grown to saturation in the corresponding medium, reinoculated in fresh medium, grown from 5h to 12h and harvested at mid-log phase (YPD: OD_{600} 0.5 - 1.5; SD: OD_{600} 0.4 - 1) by centrifugation (5 min at 3,000 g_{av}).

For short term storage yeast cells were kept as a saturated liquid culture and/or on agar plates with the corresponding medium at 4 °C up to 3 or 6 weeks, respectively. For long term storage yeast cells were grown overnight to saturation, supplemented with 20 % (v/v) glycerol, frozen in liquid nitrogen and stored at -80 °C.

For auxotrophic selection, the corresponding amino acids were excluded from SD medium. For antibiotic-based selection, liquid cultures or agar-containing plates were supplemented

with either 400 µg/mL Geneticin (#11811-031, Invitrogen; Waltham, MA, USA) or 100 mg/L nourseothricin (#96736 -11-7, ClonNAT; Werner BioAgents, Jena-Cospeda, Germany).

YPD medium		d.o. medium	
1 % (w/v)	yeast extract	0.67 % (w/v)	YNB
2 % (w/v)	peptone	0.134 % (w/v)	d.o. mix (-Ade/-His /Leu/Lys/Trp/Ura) (-His /Leu/Lys/Trp/Ura)
2 % (w/v)	glucose	0.002 % (w/v)	His/Trp/Ura/Ade
		0.01 % (w/v)	Leu
		0.003 % (w/v)	Lys
		2 % (w/v)	Glucose

3.1.3 Spotting assay

Cells were routinary grown to mid-log phase in the corresponding medium at 30 °C with 200 rpm shaking, harvested by centrifugation 3 min at 3,000 g_{av} and resuspended in 1 ml ddH_2O. 3 µL of initial concentration and of five serial tenfold dilutions were spotted on solid medium and grown in standard conditions. Solid medium plates containing chemicals when necessary were freshly prepared before the experiment.

3.2 Molecular Biology

3.2.1 Isolation of plasmid DNA from *E. coli*

For plasmid verification, plasmid DNA was isolated from bacterial cultures by the Easy Prep protocol. In brief, 3 mL of overnight culture were pelleted by 1 min centrifugation at 20,000 g_{av}. The cells were resuspended in 40 µL of Easy Prep buffer and heated for 2 min at 95 °C. Next, the samples were chilled on ice for 2 min and centrifuged for 15 min at 20,000 g_{av}. 2 to 4 µL of obtained supernatant were used for plasmid verification by the corresponding restriction endonuclease reaction.

Easy Prep buffer:

10 mM	Tris-HCl pH 8.0
1 mM	EDTA pH 8.0
15 % (w/v)	Sucrose
0.2 % (w/v)	Lysozyme (#L6876, Sigma-Aldrich Chemie; Munich, Germany)
0.02 % (w/v)	RNase A (#A3832, AppliChem; Omaha, NE, USA)
0.01 % (w/v)	BSA (#A5611, Sigma-Aldrich Chemie; Munich, Germany)

For either transformation or further cloning procedures, plasmid DNA was isolated with the GeneJET Miniprep Kit (#K0702, Thermo Fisher Scientific; Waltham, MA, USA) or NucleoBond® Xtra Midi (#740410, Macherey-Nagel; Düren, Germany) according to the manufacturer's indications.

3.2.2 Isolation of genomic DNA from *S. cerevisiae* for PCR-based applications

Genomic DNA was retrieved from yeast cells following the method described in Looke *et al.*, 2011. In brief, a toothpick-tip amount of yeast cells scratched from the agar plate was resuspended in 100 µL of lysis solution, vigorously vortexed and incubated at 70 °C for 5 min. 300 µL of ethanol was added and samples were vortexed and centrifuged 3 min at 15,000 g_{av}. Pellets were washed with 0.5 mL of 70 % ethanol, centrifuged 3 min at 15,000 g_{av} and resuspended in 100 µL of TE buffer. Samples were incubated at RT for 5 min and centrifuged 1 min at 15,000 g_{av} to remove cell debris. The supernatant containing genomic DNA was transferred to a fresh tube and stored at 4 °C for short-term or -20 °C for long-term, respectively.

Lysis solution:

200 mM	LiOAc
1 % (w/v)	SDS

TE buffer:

10 mM	Tris-HCl pH 8.0
1 mM	EDTA pH 8.0

3.2.3 Isolation of total RNA from *S. cerevisiae*

Cells were grown to mid-log phase in the corresponding selective medium at 30 °C with 200 rpm shacking. Ice-cold NaN_3 was added to a final concentration of 100 - 200 mM and 5 OD_{600}

units were harvested by centrifugation 5 min at 3,000 $g_{av.}$ Total RNA was isolated using the Universal RNA Purification Kit (ROBOKLON GMBH, Berlin, Germany) according to the manufacturer's indications.
For spheroplast generation prior to cell lysis, lyticase (#L2524 Sigma-Aldrich Chemie; Munich, Germany) was added to the corresponding buffer. When indicated during the protocol, RNase-free DNase (#M6101, Promega; Madison, WI, USA) was added to the RNA binding columns and incubated at RT for 10 min. For representative sets of samples, total RNA integrity was checked by agarose gel electrophoresis.

3.2.4 cDNA synthesis

First-strand cDNA was prepared from 2 µg of total RNA template in 20 ml final volume by oligo(dT)18 amplification using the First Strand cDNA Kit (#K1622, Thermo Fisher Scientific, Bonn, Germany), and following the recommendations of the manufacturer.

3.2.5 Determination of nucleic acid concentrations

DNA and RNA concentrations were measured at 260 nm using the NanoDrop 2000 (Peqlab, Erlangen, Germany).

3.2.6 Agarose gel electrophoresis

DNA or total RNA were analyzed on 1 % agarose (#16500500, Thermo Fisher Scientific; Waltham, MA, USA) gels prepared in TBE buffer and containing ~0.2 µg/mL of ethidium bromide. The gel was run in TBE buffer at 8 V/cm until the desired separation was reached. When necessary, samples were mixed with DNA or RNA loading dye (#R0611, Thermo Fisher Scientific; Waltham, MA, USA; Strahl lab, respectively) prior to loading. GeneRuler DNA Ladder Mix (#SM0332, Thermo Fisher Scientific; Waltham, MA, USA) was used as a size reference.
For cloning purposes, DNA fragments were purified from agarose gels using DNA the GeneJET™ Gel Extraction Kit from Fermentas (#K0692).

TBE buffer:

90 mM	Tris base
90 mM	Boric acid
2 mM	EDTA pH 8.0

3.2.7 Polymerase chain reaction (PCR)

PCR was performed using the thermocycler T3000 from Biometra (Göttingen, Germany). DreamTaq DNA Polymerase Green PCR Master Mix (#K1081, Thermo Fisher Scientific) was used for analytical PCR. All reactions were optimized according to oligonucleotide length and oligonucleotide Tm. As standard 20 µL reaction contained 10 ng of plasmid DNA or 1% (v/v) of gDNA prepared as described in 3.2.2. Primers were added to a final concentration of 0.5 µM.

Standard DreamTaq PCR program

Step	**T [°C]**	**Time**	**N° of cycles**
Initial denaturation	95	3 min	-
Denaturation	95	30 s	30
Annealing	Tm	30 s	
Elongation	72	15-30 s/kb	
Final elongation	72	7 min	-

Phusion High-Fidelity DNA Polymerase (#F530, Thermo Fisher Scientific; Waltham, MA, USA) was used for preparative PCR to obtain DNA fragments for cloning or genomic manipulation. All reactions were optimized according to the following criteria: oligonucleotide length, oligonucleotide Tm, $MgCl_2$ concentration and supplied buffer selection (HF or GC). As a standard 50 µL reaction contained 10 ng plasmid DNA or 50-100 ng genomic DNA, 1x concentrated HF/GC reaction buffer, 0.25 µM final concentration of each primer, 200 µM final concentration of each dNTP (#110012, Bioron; Ludwigshafen, Germany), 0.02 U/µL of Phusion High-Fidelity DNA Polymerase and 2mM $MgCl_2$.

Standard Phusion PCR program

Step	T [°C]	Time	N° of cycles
Initial denaturation	98	3 min	-
Denaturation	98	30 s	30
Annealing	Tm	30 s	
Elongation	72	1 min/kb	
Final elongation	72	10 min	-

Two-step Phusion PCR program

Step	T [°C]	Time	N° of cycles
Initial denaturation	98	3 min	-
Denaturation	98	30 s	5
Annealing	Tm	30 s	
Elongation	72	1 min/kb	
Denaturation	98	30 s	30-35
Elongation	72	1 min/kb	
Final elongation	72	10 min	1

3.2.8 DNA purification

Purification of DNA fragments was performed using the GeneJET PCR purification Kit (#K0702, Thermo Fisher Scientific; Waltham, MA, USA), following the manufacturer's instruction.

3.2.9 Real-time Polymerase Chain Reaction (RT-PCR)

Real-time qPCR assays were performed using the Rotor-Gene Q (Qiagen) PCR instrument. All reactions were performed using the qPCRBIO SYGreen Mix L*O*-ROX (#PB20.11, PCR Biosystems Ltd, London, UK). As a standard, 12.5 µL reaction contained 1x qPCRBIO SYGreen

Mix, 0.4 mM oligonucleotide pair and 1:20 dilution of cDNA template. As technical replicates as well as for determination of RT-PCR efficiency, 1:100 and 1:1000 cDNA dilutions were included. Only RT-PCR reactions with efficiencies ranging from 0.9 to 1.1 were considered. To quantify the abundance of HAC1u, oligos annealing on the HAC1 intron were designed (oligos 2264-2272, see 2.3.1). To quantify the abundance of $HAC1^{S}$, oligo 2266 annealing upstream of the intron was used as the forward primer and oligo 2267, annealing on the 5' of exon 1 and 3' of exon 2 was used as the reverse primer.

RT-PCR program

Step	T [°C]	Time	N° of cycles
Initial denaturation	95	2 min	-
Denaturation	95	5 s	40
Annealing	60	25 s	
Melt	63 -> 95 (+ 1 °C/step)	10 min	-

For calculation of either relative gene expression or fold-change in gene expression, both standard curve-based and $2^{-\Delta\Delta Ct}$ methods were used, respectively, depending on the convenience of the output. Statistical analyses were based on three independent biological replicates: Two-tailed Student's t-test on normalized expression values or one-tail Student's t-test on log ($2^{-\Delta\Delta Ct}$) were performed for relative gene expression or fold-change in gene expression, respectively.

3.2.10 Molecular cloning procedures

All DNA manipulations were performed according to Sambrook & Russel, 2001 and the manufacturer's instructions.

Endonuclease digestion was carried out with restriction enzymes purchased from either New England Biolabs (NEB, Frankfurt/Main, Germany) or Thermo Fisher Scientific (Fast digest endonucleases, Waltham, MA, USA) according to manufacturer's instructions. When necessary, DNA fragments were dephosphorylated using FastAP Thermosensitive Alkaline

Phosphatase (#EF0651, Thermo Fisher Scientific; Waltham, MA, USA) following the manufacturer's instructions. When necessary, the blunting of DNA overhangs was performed using T4 DNA Polymerase (#EP0061, Thermo Fisher Scientific; Waltham, MA, USA) according to the manufacturer's instructions. Ligation of DNA fragments was performed using T4 DNA Ligase (#EL0011, Thermo Fisher Scientific; Waltham, MA, USA). A standard 10 µL reaction contained 2 - 3 U of T4 DNA Ligase. For ligation of cohesive or blunt overhangs, vector and insert were mixed in 1.3 or 1:1 molar ratio, respectively. The ligation reaction was routinely performed for either 1h at RT or overnight at 4 °C.

3.2.11 Transformation of *E. coli*

Chemically competent *E. coli* cells were prepared according to Inoue *et al.*, 1990. 100 µl aliquots were frozen in liquid nitrogen and stored at -80 °C.
For the transformation 100 µl aliquots were thawed and incubated for 10 min on ice.
10 - 100 ng of purified DNA was added to the cells and incubated for 30 min on ice. Heat shock was performed at 42 °C for 60 – 90 seconds and samples were quickly transferred to ice. Once chilled, cells were recovered by adding 700 - 900 µL of LB medium and incubating for 30 min. After recovery cells were pelleted by centrifugation and plated on selective solid LB medium. For the transformation of DNA ligation products, 5 µl of ligation reaction mix was used.

3.2.12 Transformation of S. cerevisiae genomic modification of *S. cerevisiae*

All yeast transformations were performed in sterile conditions according to Gietz *et al.*, 1995 with some modifications. To generate yeast competent cells 10 ml overnight liquid culture was diluted to OD_{600} of 0.3 – 0.4 (approximately 50 ml) in the corresponding medium and grown for 3 – 6h at 30 °C with 200 rpm agitation. Cells equivalent to 0.5 - 1 OD_{600} were harvested by centrifugation 5 min at 1,500 – 3,000 g_{av}, washed with TE buffer, resuspended in 1 ml LiAc/TE buffer and incubated 10 – 30 at RT. Next, cells were pelleted and resuspended in a final volume of 50µl LiAc/TE buffer.
In parallel, DNA transformation mix was prepared by mixing transforming DNA (0.5 – 1 µg plasmid DNA or 5 – 10 µg of purified linear DNA) and 50 – 100 ng of salmon sperm DNA carrier (#201190, Agilent Technologies; Santa Clara, CA, USA) previously boiled for 5 min at

95 °C in a total of 10 µl TE buffer. DNA transformation mix was added to the competent yeast suspension together with 300 µl of LiAc/40%PEG-3350/TE and the solution was mixed by pipette action. Samples were incubated 30 min at 30 °C with agitation. Heat shock was performed for 15-20 min at 42 °C. Cells were collected by centrifugation 5 min at 3,000 g_{av} washed with TE buffer and resuspended in 100 µl of either TE buffer or ddH_2O. Cells were plated onto the appropriate selective solid medium in two serial 1:10 dilutions to facilitate the pickup of the future colonies.

As an optional step to increase transformation efficiency, 44 µl of DMSO was added to the cell suspension and mixed by pipette action prior to the heat shock.

For antibiotic-based selection, after the heat shock and before transferring them to selective medium, cells were recovered in YPD medium for 2 - 3h at 30 °C with agitation.

TE-LiAc:	
100 mM	LiAc
10 mM	Tris-HCl pH 8.0
1 mM	EDTA pH 8.0

TE-LiAc-PEG:	
100 mM	LiAc
10 mM	Tris-HCl pH 8.0
1 mM	EDTA pH 8.0
40 % (w/v)	PEG 3350

3.2.13 Genomic modification of *S. cerevisiae*

Yeast genomic modifications were performed based on homologous recombination (Longtine *et al.*, 1998). Integrative cassettes for knockout, knockdown or for HA-genomic tagging were generated by Phusion PCR using pJUG6, genomic DNA or pJH24 as a template as described in 3.2.7. Oligonucleotides contained 50 – 60 bp 5' and 3' homologous sequences to the target genomic locus. PCR fragments were purified after agarose gel electrophoresis. For the generation of UPRE-GFP strains, the PN001 integrative vector was linearized via KpnI/NotI endonuclease digestion and purified as described in 3.2.8.

The transformation of linear DNA fragments was performed as described in 3.2.12 and optimized for every single case.

3.3 Synthetic genetic array (SGA) procedures

3.3.1 ER-GFP screening and data analyses

These experiments were performed by Lihi Gal in the frame of a collaboration with the group of Prof. Maya Schuldiner (Weizmann Institute of Science, Rehovot, Israel).

To create the collection of haploid strains containing the ER-GFP reporter on the background of all yeast mutants, the starting query strain JEY06 expressing ER-GFP was generated on the basis of an SGA compatible strain, YMS721 (Papic *et al.*, 2013).
The yeast deletion library (Giaever *et al.*, 2002) and the DAmP library (Breslow *et al.*, 2008) were crossed with the query strain JEY06 on 1536-colony format plates using a RoToR bench top colony arrayer (Singer Instruments, Somerset, UK) following SGA methodology described in (Cohen & Schuldiner, 2011) and (Tong & Boone, 2006). In brief, genetic libraries and JEY06 were mated on YPD plates and the resulting diploids were selected for both deletion/DaMP libraries and ER-GFP markers; *KanR* and *URA3*, respectively. Sporulation was induced by transferring cells to nitrogen starvation media plates for 7 days. Haploid cells containing the desired mutations were selected by transferring cells to SD-plates with the above selections for both genetic alterations alongside the toxic amino acid derivatives canavanine and thialysine (Sigma-Aldrich) to select against remaining diploids, and lacking histidine to select for spores with an A mating type.
The haploid collection carrying both the deletion/hypomorphic allele and ER-GFP was visualized using an automated microscopy setup described in Breker *et al.*, 2013. In brief, cells were transferred from agar plates into 384-well polystyrene plates for growth in liquid media using the RoToR arrayer robot. Liquid cultures were grown in a LiCONiC incubator (LiCONiC instruments, Liechtenstein) overnight at 30 °C in SD medium. A JANUS liquid handler (PerkinElmer; Waltham, MA, USA) connected to the incubator was used to dilute the strains to an OD_{600} of ~0.2 into plates containing SD. Plates were incubated at 30 °C for 4 h. The cultures in the plates were then transferred by the liquid handler into glass-bottom 384-well microscope plates (Matrical Bioscience; Spokane, WA, USA) coated with Concanavalin A (Sigma-Aldrich). After 20 minutes, wells were washed twice with SD-Riboflavin complete medium to remove non-adherent cells and to obtain a cell monolayer. The plates were then transferred to the ScanR automated inverted fluorescent microscope system (Olympus,

Shinjuku, Japan) using a robotic swap arm (Hamilton, Bonaduz, Switzerland). Images of cells in the 384-well plates were recorded in SD-Riboflavin complete medium at 24 °C at GFP (excitation at 490/20 nm, emission at 535/50 nm) channel using a 60x air lens (NA 0.9) and with an ORCA-ER charge-coupled device camera (Hamamatsu, Shizuoka, Japan).

Analysis of ER-GFP intensity was performed using the Olympus ScanR analysis software. Images were preprocessed by background subtraction and segmentation was done with the brightfield images and a series of shape conditions were applied as filters. The median GFP intensity for each strain was measured from the remaining objects for each strain. Dead cells appear as high fluorescent outlier values and were removed with the ScanR software in an automated manner. Strains with an insufficient number of objects detected (<25) as well as contaminated strains were removed from the analyses.

3.3.2 Tandem fluorescent protein timers screening and data analyses

A subset of query strains from the tFT genetic library that were shown to be *O*-mannosylated (Neubert *et al.*, 2016) were recorded to localize to the secretory pathway (by classification of translocation according to Ast *et al.*, 2013 or inferred from high confidence/manual curated database annotations were selected from the library; App. Data 3) and crossed with MLY201 (*pmt1*Δ), MLY202 (*pmt2*Δ) and MLY204 (*pmt4*Δ) on 1536-colony format plates using the ROTOR HDA pinning robot (Singer Instruments, Somerset, UK) following the SGA methodology described in Baryshnikova *et al.*, 2010. In brief, both tFT queries and MLY201, MLY202, or MLY204 were mated, and the resulting diploids were selected, sporulated, and selected for haploids carrying both the tFT-tagged protein and the *pmt* deletion by sequential pinning followed by selection on appropriate media, as described in (Khmelinskii *et al.*, 2014). Three technical replicates of each cross were arranged next to each other. Fluorescence intensities of the final colonies were measured after 24 h of growth on synthetic complete medium lacking leucine at 30 °C using Infinite M1000 Pro plate readers equipped with stackers for automated plate loading (Tecan, Männedorf, Switzerland) and custom temperature control chambers. Measurements in mCherry (587/10 nm excitation, 610/10 nm emission, fixed detector gain) and sfGFP (488/10 nm excitation, 510/10 nm emission, fixed detector gain) channels were performed at 400 Hz frequency of the flash lamp, with ten flashes averaged for each measurement.

Failed crosses after haploid selection were excluded from the measurement based on colony size. For background correction, the fluorescence intensities of three negative control colonies arranged next to each sample were subtracted from the average of sample colonies. Fluorescence intensity measurements were log-transformed, and the data for each plate were normalized to the median fluorescence of a reference strain set that was present on every plate as described in Meurer *et al.*, 2018. Changes in protein stability between wild-type and mutant were estimated by subtracting the log-ratios of mCherry and sfGFP intensities, yielding a Δ-score. A moderated *t*-test implemented in the R package limma was used to compute *p*-values (R Development Core Team, 2017). Plots were generated using the *ggplot2* (v2.2.1) package (Wickham, 2009). Data labels were introduced using functions of the *ggrepel* (v0.7.0) package (Slowikowski), and heatmaps were generated using the heatmap.2 function of the *gplots* (v3.0.1) package (Warnes).

3.4 Protein Biochemistry

3.4.1 Determination of protein concentrations

Protein concentrations were measured with the DC protein assay (#500112, Bio-Rad; Hercules, CA, USA) in 96-well plate format according to the manufacturer's instructions. BSA (#A5611, Sigma-Aldrich Chemie; Munich, Germany) was used for calibration.

3.4.2 Preparation of total cell extracts and total membranes from *S. cerevisiae*

To prepare total cell extracts, all procedures were performed on ice and/or at 4 °C. Cells were grown to mid-log phase in the corresponding selective medium at 30 °C with 200 rpm shacking. For end-point analyses or time-course experiments, ice-cold NaN_3 was added to the culture to a final concentration of 100 - 200 mM. Cells equivalent to 10 or 20 OD_{600} were harvested by centrifugation 5 min at 3,000 g_{av}, washed with ddH2O or breaking buffer and resuspended in 50 or 100 µl (for 10 and 20 OD_{600}, respectively) of breaking buffer supplemented with protease inhibitors (1 mM PMSF, 1 mM benzamidine, 0.25 mM 1-chloro-3-tosylamido-7-amino-2-heptanone, 50 µg/mL of l-1-tosylamido-2-phenylethyl chloromethyl ketone, 10 µg/mL of antipain, 1 µg/mL of leupeptin, and 1 µg/mL of pepstatin). Cell solution was transferred to a screw-cap tube and glass beads (ø 0.25 – 0.5 mm, #A553.1; Roth,

Karlsruhe, Germany) were added to reach 1 – 2 mm below the solution's meninge. Cells were subjected to mechanic lysis using the Hybaid RiboLyser Homogenizer (Thermo Scientific, Bonn, Germany) in 4 rounds of 25 s at 4.5-speed level. After lysis, screw-cap tubes were punctuated with a needle and the suspension was transferred to a fresh tube by centrifugation 30 s – 1 min at 500 g_{av}. To generate total cell extracts, cell debris was pelleted by centrifugation 5 min at 1,500 g_{av} and supernatant was collected. To prepare total membranes, total cell extracts were centrifuged 1 h at 20,000 × $g_{av.}$ Membrane pellets were resuspended with the aid of a 0.3 mm syringe in an equivalent volume of membrane buffer supplemented with protease inhibitors (as described above).

Breaking buffer:		Membrane buffer:	
50 mM	Tris-HCl pH 7.4	20 mM	Tris-HCl pH 8.0
5 mM	$MgCl_2$	10 mM	EDTA pH 8.0
		15 % (v/v)	Glycerol

3.4.3 Cycloheximide chase

Cycloheximide chase experiments were performed as described in Tran & Brodsky, 2012. In brief, cells expressing the plasmid pJC08 were grown overnight in SD-URA medium at 30 °C to mid-log phase. Cells were initially sampled as time point zero, and cycloheximide was immediately added to a final concentration of 100 or 200 µM. Equal amounts of cells were sampled at the following time points: 15, 30, 60 and 120 min. After sampling, the chase was stopped at each time point by adding NaN_3 to a final concentration of 20 mM, and cells were kept on ice until the last sample was collected. Total cell extracts were prepared from cells sampled at each time point as described in 3.4.2.

3.4.4 Analysis of Hsp150

Hsp150 analysis was performed as described in (Russo *et al.*, 1992). In brief, yeast cells were grown to mid-log phase at 30 °C and 200 rpm shaking. Cells equivalent to 20 OD_{600} were harvested by centrifugation 5 min at 3,000 g_{av} and resuspended in 100 µl of fresh YPD. Heat shock was performed for 1.5 h at 37 °C and cells were pelleted by centrifugation 5 min at

3,000 $g_{av.}$ 10 µl of the supernatant was transferred to a new tube and 5 µl of 3x Laemmli buffer was added prior to load in 8% SDS-PAGE (see 3.4.6).

3.4.5 Immunoprecipitation of FLAG-tagged ER-GFP

Cells expressing ER-GFP-3xFLAG (transformed with the plasmid pPN014) were grown in SD-URA to mid-log phase at 30 °C and 200 rpm shaking. Cells equivalent to 20 OD_{600} were harvested by centrifugation 5 min at 3,000 g_{av}. Total membrane preparation was performed as described in 3.4.2 with the following modifications: Centrifugation of total cell extracts to generate total membrane pellets was performed for 30 min at maximum speed (30,130 g_{max}). Membrane pellets were resuspended in 200 µl of TBS buffer supplemented with 1 mM PMSF. For membrane solubilization, Triton X-100 was added to a final concentration of 1% (v/v) and samples were placed on a rotator mixer (#7-0045; Neolab, Heidelberg, Germany; Mode B4, 75rpm) for 10 min at RT. Next, to generate the immunoprecipitation input, samples were diluted 1:4 in TBS supplemented with 1mM PMSF (reaching a final Triton X-100 concentration of 0.25% v/v) and centrifuged 15 min at 20,000 g_{av} to remove insolubilized material.

For immunoprecipitation, 100 µl of slurry anti-FLAG M2 magnetic beads (#M8823, Sigma-Aldrich Chemie, Munich, Germany) were transferred to 2 ml low-binding tube (Sarstedt; Nümbrecht, Germany) and equilibrated with 3 x 5 min washing steps with 500 µl TBS supplemented with 0.25% Triton X-100 (v/v). Next, 100 µl of TBS 0.25% v/v Triton X-100 supplemented with 1mM PMSF was added to the tube together with 200 µl immunoprecipitation input. The sample was incubated 4 h at 4 °C and the unbound fraction was collected. Beads were then washed three times using TBS 0.25% v/v Triton X-100 and the bound fraction was eluted by addition of FLAG peptide in TBS 0.25% v/v Triton X-100 to a final concentration 0.3 µg/µl and further incubation in the rotator mixer 1 h at 4 °C. ER-GFP presence in unbound and bound protein fractions was analyzed in 12% SDS-PAGE (see 3.4.6) followed by Western blot (see 3.4.7).

TBS:

150 mM	NaCl
50 mM	Tris-HCl pH 7.4

3.4.6 *In vitro* de-mannosylation of ER-GFP

De-mannosylation of ER-GFP was carried out using α(1-2,3,6)-mannosidase (#9025-42-7, Sigma-Aldrich Chemie; Munich, Germany) and the supplied buffer according to the manufacturer's instructions. In brief, 10 or 20 µl of immunoprecipitated ER-GFP (see 3.4.4) was incubated overnight with 0.3 U of α(1-2,3,6)-mannosidase at 37 °C. Mock treatment lacking α(1-2,3,6)-mannosidase was performed in parallel. Both mock and enzyme-treated samples were analyzed in 12% SDS-PAGE followed by Western blot (see 3.4.6 and 3.4.7).

3.4.7 SDS polyacrylamide gel electrophoresis (SDS-PAGE)

Sodium dodecyl sulfate polyacrylamide gel electrophoresis (SDS-PAGE) was performed according to (Laemmli, 1970). In brief, protein fractions were denatured in the presence of Laemmli SDS-PAGE sample buffer for 10 min at 70 °C as standard with shaking at 1,000 rpm and separated on self-prepared 6 – 15 % glycine SDS polyacrylamide (PAA) gels. Electrophoresis was performed at 60 - 80 V for 30 min for the stacking gel and at 140 V for the resolving gel until complete run-off of the dye from Laemmli SDS-PAGE.

Laemmli SDS-PAGE sample buffer:		Running buffer:	
62.5 mM	Tris-HCl pH 6.8	62.5 mM	Tris-HCl pH 6.8
10 % (v/v)	Glycerol	10 % (v/v)	Glycerol
5 % (v/v)	2-Mercaptoethanol	5 % (v/v)	2-Mercaptoethanol
2 % (w/v)	SDS	2 % (w/v)	SDS
0.02 %(w/v)	bromophenol blue	0.02 %(w/v)	bromophenol blue

4 % Stacking gel:	6 – 15 % Resolving gel:	
12.5 mM	37.5 mM	Tris-HCl pH 6.8
0.1 (w/v)	0.1 % (w/v)	SDS
4 % (w/v)	6 – 15 % (w/v)	Acrylamide/Bis-acrylamide (37.5:1)
0.1 % (w/v)	0.1 % (w/v)	APS
0.15 % (v/v)	0.1 % (v/v)	TEMED

3.4.8 Colloidal Coomassie staining

Coomassie staining of polyacrylamide gels was performed according to Kang *et al.*, 2002. In brief, gels resulting from SDS-PAA electrophoresis were rinsed twice with ddH_2O incubated overnight in Coomassie solution (5 % $Al_2SO4_3 \cdot 18\ H_2O$, 10 % EtOH, 0.02 % Coomassie-G250, 2 % *ortho*-H_2PO_4). Gels were then destained in ddH_2O until completion.

3.4.9 Western blot/ immunoblot analysis

Proteins were transferred from PAA gel to a nitrocellulose membrane (#RPN203D, GE Healthcare; Chicago, IL, USA) at 100 V for 60 min in transfer buffer including an ice-cold cooler. Transfer efficiency was monitored by the presence of the protein marker and confirmed by reversible ponceau staining. As standard, membranes were blocked with TBST (TBS with 0.1% Tween 20, see 3.4.5)– 5% milk powder buffer for 15 – 30 min at RT.
The primary antibody was added in the corresponding dilution (see 2.4.1) to TBST – 5% milk powder and incubated either at RT for 1 – 2 h or overnight at 4 °C (depending on the convenience of the output). Membranes were then washed three times 10 – 15 min with TBST at RT and secondary antibodies were added and subsequently incubated 1 h at RT. Prior to detection, membranes were washed 2 – 3 times 10 min with TBST.
Protein-antibody complexes were detected using ECL Prime Western Blotting Detection Reagent (#RPN2232, GE Healthcare; Chicago, IL, USA) and imager ImageQuant LAS 4000 (GE Healthcare; Chicago, IL, USA).

Transfer buffer:		Ponceau S solution:	
150 mM	Glycine	3 % (w/v)	TCA
20 mM	Tris base	3 % (w/v)	Sulfosalicylic acid
20 % (v/v)	Methanol	0.2 % (w/v)	Ponceau S
0.02 % (w/v)	SDS		

3.5 Cell biology

3.5.1 Cell fractionation coupled to RNA preparation.

Cell fractionation by 1-step ultracentrifugation

3.5.1.1 To fractionate cells into soluble and total membrane fraction the method described in 2.5.2 was adapted to the purpose of extracting total mRNA from each fraction as described in Aronov *et al.*, 2013 and Kraut-Cohen *et al.*, 2013. Cells were grown to mid-log phase in the corresponding medium at 30 °C with 200 rpm shaking. Cycloheximide was added to the cultures to a final concentration of 100 µg/ml and cells were further grown for 15 min. Cells equivalent to 20 OD_{600} were harvested by centrifugation 5 min at 3,000 g_{av}, washed with ice-cold SK buffer and incubated 5 min on ice. Cells were pelleted by centrifugation 3 min at 500 g_{av}, resuspended in 250 µl BRS buffer supplemented with protease inhibitors as described in 2.5.2 and transferred to a screw-tap tube. Cell lysis was performed after adding glass beads (see 2.5.2) using the Hybaid RiboLyser Homogenizer in 5 rounds of 35 s at 4.5-speed level. After lysis, screw-cap tubes were punctuated with a needle and the suspension was transferred to a fresh tube by centrifugation 30 s – 1 min at 500 g_{av}. To generate total cell extracts, cell debris was pelleted by centrifugation 10 min at 1,000 g_{av} and supernatant was collected. 200 µl of total cell extracts were fractionated by ultracentrifugation (rotor TLA-100.4, Beckman, Indianapolis, IN, USA) at 48,000 g_{av}, resulting in the soluble fraction (supernatant) and membrane pellet. Next, membrane pellets were resuspended in 400 - 500 µl BMRS buffer with the aid of a 0.3 mm syringe and ultracentrifugation was repeated using the same settings. Final membrane pellets were resuspended in 200 µl BMRS buffer. To confirm the successful separation of soluble and total membrane fractions, 1 µl of each was used for SDS-PAGE and immunodetection of Sec61 and G6PDH as described in 3.4.7 and 3.4.9. Total RNA was prepared from 100 µl of each cell fractions using the Universal RNA Purification Kit (ROBOKLON GMBH, Berlin, Germany) according to manufacturer's indications for purification of RNA from molecular biological reactions or from buffer solutions (Appendix 3 of the user's manual)

SK buffer:

1.2 M	Sorbitol
0.1 M	KPO_4 ph 7.5
100 µg/ml	Cycloheximide (freshly added)

BRS buffer:

50 mM	Tris-HCl ph 7.6
150 mM	NaCl
250 mM	Sorbitol
30 mM	$MgCl_2$
200 U/ml	Rnasin ribonuclease inhibitor (#N2511, Promega; Madison, WI, USA) (freshly added)
100 µg/ml	Cycloheximide (freshly added)

BMRS buffer is prepared as BRS buffer except it contains80 U/ml Rnasin ribonuclease inhibitor.

3.5.1.2 Cell fractionation by sucrose step-gradient centrifugation

This method is adapted from Aronov *et al.*, 2013 and Kraut-Cohen *et al.*, 2013. Cells were grown to mid-log phase in YPD at 30 °C with 200 rpm shaking. Cells equivalent to 300 OD_{600} were harvested by centrifugation 5 min at 2,500 - 3,000 g_{av}, washed with ice-cold SK buffer and incubated 5 min on ice. Cells were pelleted by centrifugation 5 min at 2,500 $g_{av,}$ resuspended in 1.2 ml lysis buffer supplemented with protease inhibitors as described in 3.4.2, transferred to a screw-tap tube and lysed with the Hybaid RiboLyser Homogenizer in 4 rounds of 45 s at 4.5-speed level. Total cell extracts were prepared as in 3.5.1.1.
900 µl of total cell extracts were transferred to a fresh tube and diluted with lysis buffer supplemented with protease inhibitors to 2 ml final volume.
In parallel, a discontinuous sucrose gradient was freshly prepared by adding 3 ml of 1.5 M and 1.2 M sucrose buffer layers on top of a 2 M sucrose cushion as shown in figure 4.29A.

Total cell extract was loaded on top of the gradient and centrifuged 2.5 h at 232,000 g_{max} in a TST14.41 swinging rotor. Gradients were then manually fractionated in 0.5 ml fractions. To analyze protein content on selected fractions they were diluted 1:4 in sucrose-base buffer (10mM Tris-HCl ph 7.5, 150 mM KCl 10mM $MgCl_2$) and 5 µl were used for SDS-PAGE and immunodetection as described in 3.4.7 and 3.4.9. Total RNA was isolated from 300 µl of selected fractions as described in 2.6.1.1.

Lysis buffer

10 mM	Tris-HCl ph 7.5
0.25 M	Sucrose
30 mM	$MgCl_2$
1 mM	DTT
200 U/ml	RNasin ribonuclease inhibitor (#N2511, Promega; Madison, WI, USA) (freshly added)
100 µg/ml	Cycloheximide (freshly added)

Sucrose buffer

10 mM	Tris-HCl ph 7.5
X	Sucrose
150 mM	KCl
10 mM	$MgCl_2$

X: Concentration of sucrose in each fraction is described in the text.

3.5.2 Microscopy

Cells were routinely grown to mid-log phase in the corresponding medium at 30 °C with 200 rpm shaking. Microscopy was performed on standard glass plates adjusting the number of cells to the desired density. For end-point analyses, NaN_3 was added to the culture prior to sampling to a final concentration of 10 mM.

Yeast strains expressing UPRE-GFP or ER-GFP were viewed by using an LSM510-Meta confocal microscope (Carl Zeiss, Jena, Germany) with either ×100 or x40 PlanApochromat objective (numerical aperture 1.4). The fluorescence signal of GFP (excitation 488 nm, Ar laser) was detected by using a bandpass emission filter 505–530 nm. Single plane images

were taken using identical conditions per experiment and are presented without undergoing processing steps.

Cells expressing tFT-fusion proteins were grown to the mid-log phase in synthetic complete medium. Prior to imaging, cells were treated with the vital dye 7-amino-4-chloromethylcoumarin (CMAC, #C2110 Thermo Fischer) to a concentration of 10 µM to stain the lumen of yeast vacuoles. After 15 min incubation at 30 °C, cells were washed once and resuspended in fresh medium. Single plane images were acquired on a Delta Vision Elite system (Applied Precision, Issaquah, WA, USA) consisting of an inverted epifluorescence microscope (IX71; Olympus, Tokio, Japan) equipped with an LED light engine (SpectraX, Lumencor, Beaverton, OR, USA), 390/18-, 475/28- and 575/25-nm excitation and 435/48-, 525/50- and 624/40-nm emission filters (Semrock, Rochester, NY, USA), a dual-band beam splitter 89021 (Chroma Technology, Bellows Falls, VT, USA), using either a 100× NA 1.4 UPlanSApo or a 60× NA 1.42 Plan ApoN oil immersion objective (Olympus), an sCMOS camera (pco.edge 4.2, PCO), and a motorized stage contained in a temperature-controlled chamber. Image processing and quality control were performed using ImageJ. sfGFP, as well as mCherry images obtained for wild-type and corresponding *pmt*Δ mutant, were processed in the same manner.

3.5.3 Flow cytometry

Cells expressing ER-GFP or tFT-fusion proteins were grown to the mid-log phase in the corresponding medium at 30 °C. The fluorescence intensities of 20,000 cells were measured in the appropriate channel using the cell analyzer BD FACSCanto™ (BD Biosciences; Heidelberg, Germany), in collaboration with Flow Cytometry & FACS Core Facility (ZMBH, Heidelberg University; Heidelberg, Germany).

For strains expressing ER-GFP background fluorescence was routinely measured by analyzing cells not expressing the fluorescent protein in parallel and subtracted the obtained values. To estimate the representativeness of the positive events over the whole population, fluorescence intensity was multiplied by the percentage of positive cells, obtaining an R value. R values of mutant strains were normalized to R_{WT} and plotted as fold-change. One tail student's *t*-test was applied to obtain the statistical significance of the changes in R.

To define the age of a certain tFT-fusion protein, a first ratio mCherry/sfGFP was calculated for both wild-type and *pmt*Δ mutant based on the intensity of all measured events, and the

corresponding *p*-value was calculated using Student's *t*-test and considering the null hypothesis as no showing difference between variances of each dataset. To address the impact of the deletion on protein age, a second ratio was calculated as $WT_{mCherry/sfGFP}/pmt\Delta_{mCherry/sfGFP}$.

3.6 Ribosome profiling

These experiments were performed by Ilgin Cotan in the frame of a collaboration with the group of Prof. Bern Bukau and Dr. Gunter Kramer (Zentrum für Molekulare Biologie, Heidelberg, Germany).

3.6.1 Sample preparation

Wild type and *bfr1*Δ cells were grown to mid-log phase at 30 °C and approximately 150 OD_{600} units were harvested using rapid filtration and flash freezing in liquid nitrogen. Frozen cell pellets were mixed with 750 µl of frozen lysis buffer droplets and a metal ball in pre-chilled metal jars and lysed by mixer milling 2 min at 30 Hz (MM400 Retsch, Haan, Germany). Cell lysates were thawed in a water bath at 30 °C, transferred to low-binding tubes and RNA concentration was determined by Nanodrop. Lysates were next subjected to RNase I digestion (10U of RNase I per Abs_{260} unit) 30 min at 4 °C, reaction was stopped by adding 10 µl of Superase-In Rnase inhibitor (#LSAM2694, Invitrogen) and lysates were cleared by 5 min centrifugation at 20,000 x $g_{av.}$

<u>lysis buffer:</u>

20 mM	Tris-HCl pH 8
140 mM	KCl
10 mM	$MgCl_2$
20% (v/v)	NP-40
100 µg/ml	Cycloheximide
1 x	EDTA-free protease inhibitor cocktail (Roche, Basel, Switzerland)
0.02 U/µl	DNase I (Roche, Basel, Switzerland)
40µg/ml	Bestatin

Total ribosomes were collected by sucrose cushion centrifugation. A maximum of 400 µl of cleared lysate was loaded onto 800 µl of sucrose cushion buffer in sucrose cushion tubes and centrifuged 90 min at 75,000 rpm and 4 °C in a TLA120-rotor (Beckman, Indianapolis, IN, USA). Pellets were resuspended in lysis buffer by continuous agitation at 4 °C and transferred to non-stick tubes.

Sucrose cushion buffer:

20 mM	Tris-HCl pH 8
140 mM	KCl
10 mM	$MgCl_2$
100 µg/ml	Cycloheximide
1 x	EDTA-free protease inhibitor cocktail (Roche, Basel, Switzerland)
25% (v/v)	Sucrose

3.6.2 Ribosome-protected footprint mRNA extraction

mRNA footprints were extracted from processed samples by phenol-chloroform extraction. In brief, ribosome pellets were top to a final volume of 700 µl with lysis buffer and mixed with 40 µl 20% (v/v) SDS to precipitate the protein content. 750 µl of pre-warmed (65 °C) acid phenol was added and samples were incubated 5 min at 65 °C and 1,400 rpm shaking, and chilled 5 min on ice. Next, samples centrifuged 2 min at 20,000 x g_{av} and the aqueous phase was transferred to a new tube. 700 µl of hot phenol were again added and samples were incubated 5 min at room temperature with occasional vortexing. 600 µl of chloroform was added and mixed by vortexing. Samples were centrifuged 1 min at 20,000 x g_{av} and the aqueous phase was transferred to a new tube. To precipitate nucleic acids, approximately 650 µl of the sample was mixed with 1:9 equivalence volume of 3 M NaOAc pH 5.5, 1 equivalence volume of isopropanol and 2 µl of Glycoblue, mixed by vortexing and chilled overnight at 80 °C.

Next, RNA samples were centrifuged 2 h at 20,000 x g_{av} and 4 °C and the pellet was washed with 750 µl ice-cold 70% ethanol. Centrifugation was repeated for 2 min and the pellet was dried for 2 min at 65 °C. Pellets were finally resuspended in 20 - 50 µl of 10 mM Tris-HCl ph 7. RNA enrichment was verified by Bioanalyzer RNA Nano chip (Agilent) and total RNA concentration was determined by nanodrop after diluting RNA samples in water and 10 mM Tris-HCl ph 7, respectively.

3.6.3 Deep sequencing library preparation

The method for the analysis of total translatome in yeast is based on what described in Doring *et al.*, 2017 with some modifications. RNA samples were heated at 80 °C for 2 min and 40-50 mg of RNA were loaded onto a 15% TBE-Urea polyacrylamide gels (Invitrogen) in 1xTBE (Ambion) and run for 65 min at 200 V. Gels were stained for 20 min with SYBR gold (Invitrogen) and ribosome footprints were recovered from the gels by excising sections according to 21 to 33 nucleotide size. Gel pieces were placed into 0.5 mL gel breaker tubes and centrifuged for 3 min at 20,000 x g_{av}. The remaining pieces were transferred to a fresh 1.5 ml tube, resuspended with 10 mM Tris-HCl ph 7 and incubated 15 min at 70 °C in a thermomixer with maximum shaking. The gel slurry was then transferred to a Spin-X cellulose acetate column (#60702, Thermo Fisher Scientific; Waltham, MA, USA) and centrifuged 3 min at 20,000 x $g_{av.}$ Flow-through was transferred to a fresh pre-cooled nonstick tube on ice. Nucleic acid samples were precipitated as described previously (See 3.6.2). Next, RNA samples were centrifuged 2 h at 20,000 x g_{av} and 4 °C and the pellet was washed with 750 µl ice-cold 70% ethanol. Centrifugation was repeated for 2 min and the pellet was dried for 2 min at 65 °C. Pellets were finally resuspended in 15 µl of 10 mM Tris-HCl ph 7 and transferred to a fresh nonstick tube.

To dephosphorylate 3' ends of ribosome footprints, a master mix was prepared containing 2 µl 10 x T4 polynucleotide kinase buffer without ATP (NEB) and 1 µl murine RNase-Inhibitor per sample and 3 µl were added to each sample together with 2 µl truncated T4 polynucleotide kinase (Frankfurt/Main, Germany). Samples were incubated 2 h at 37 °C and the enzyme was deactivated after the reaction by 10 min incubation at 75 °C. At this point, nucleic acids were again precipitated as previously indicated.

Samples were centrifuged 1 h at 20,000 x g_{av} and 4 °C and RNA pellet was washed with 70% ethanol and resuspended in 15 µl of 10 mM Tris-HCl ph 7 and transferred to a fresh nonstick tube as previously indicated. At this point, RNA concentration was measured again by Bioanalyzer RNA Nano chip (Agilent) and by nanodrop after diluting RNA samples in water and 10 mM Tris-HCl ph 7, respectively.

For 3' L1 linker ligation, samples were diluted to a final RNA concentration of 10 pmol in 10 µl of 10 mM Tris-HCl ph 7 and denatured 2 min at 80 °C. A master mix was prepared to contain 16 µl 50% sterile filtered PEG MW 8000, 4 µl DMSO, 4 µl 10x T4 RNA Ligase 2 buffer and 2 µl murine RNase-Inhibitor. The master mix was added to each sample together with 1 µl truncated T4 RNA Ligase 2 (NEB, Frankfurt/Main, Germany). Ligation was carried out for 2 h at 23 °C and nucleic acids were precipitated, RNA pellets washed with 70% ethanol as previously indicated and resuspended in 6 µl of 10 mM Tris-HCl ph 7.

3' –linked footprints were denatured at 80 °C for 2 min and purified on 10% TBE-Urea polyacrylamide gels (Invitrogen) in 1xTBE (Ambion) run for 50 min at 200 V. Gels were stained for 20 min with SYBR gold (Invitrogen) and 3' –linked footprints were recovered from the gels by excising sections according to 64 nucleotide size (footprint + L1).

Similar to the previous in-gel purification, gel pieces were placed into 0.5 mL gel breaker tubes and centrifuged for 5 min at 20,000 x g_{av}. The remaining pieces were transferred to a fresh 1.5 ml tube, resuspended with 10 mM Tris-HCl ph 7 and incubated 15 min at 70 °C in a thermomixer with maximum shaking. The gel slurry was then transferred to a Spin-X cellulose acetate column (#60702, Thermo Fisher Scientific; Waltham, MA, USA) and centrifuged 3 min at 20,000 x $g_{av.}$ Flow-through was transferred to a fresh pre-cooled nonstick tube on ice. nucleic acids were precipitated, RNA pellets washed with 70% ethanol as previously indicated and resuspended in 6 µl of 10 mM Tris-HCl ph 7.

To generate ssDNA, 3' linked footprint fragments were reverse transcribed. A master mix containing 1 µl 10 mM dNTP mix, 1 µl 25 µM Linker L1'L20 and 1.5 µl DEPC H_2O was prepared and added to the samples. Samples were incubated 5 min at 65 °C and 4 ml 5x FSB buffer (Invitrogen), 1 ml murine RNase inhibitor, 1 ml 0.1 M DTT and 1 ml Superscript III (#18080085, Invitrogen) was added. Reverse transcription was performed 30 min at 50 °C and the reaction was quenched by adding 2.3 ml 1 N NaOH and further incubating 15 min at 95 °C.

Samples were denatured 2 min at 70°C and run on a 10% TBE-Urea polyacrylamide gel for 70 min at 200 V. Gels were stained as described before, desired bands were excised, and nucleic acids were extracted as mentioned earlier except that remaining gel pieces were mixed with 0.5 ml 10 mM Tris-HCl ph 8. Nucleic acids were precipitated by adding 1:16 equivalence volume of 5 M NaCl and 1:500 equivalence volume of 0.5 M EDTA together with 1 equivalence volume of isopropanol and 2 µl of Glycoblue. Precipitation was performed at -20 °C overnight and pellets were washed with 70% ethanol and resuspended in 15 µl 10 mM Tris-HCl ph 8 as previously described.

To Circularize ssDNA, a master mix containing 2 µl 10x CircLigase buffer, 1 µl 1 mM ATP, 1 µl 50 mM $MnCl_2$ was added to the samples together with 1 µl CircLigase (EPICENTRE). The reaction was carried out for 1h at 60 °C and the enzyme was deactivated by further incubation for 10 min at 80 °C. 1 µl of circularized ssDNA was used as a template for 4 technical replicates of Phusion-based PCR using the following mix and PCR program:

62.6 µl	DEPC H_20
16.7 µl	5x HF buffer
1.7 µl	10 mM dNTPs
0.4 µl	100 mM barcoding primer
0.4 µl	0.4 ml 100 mM PCR primer L1’
0.8 µl	Phusion polymerase

Step	**T [°C]**	**Time**	**N° of cycles**
Initial denaturation	98	30 s	-
Denaturation	98	10 s	
Annealing	60	10 s	10
Elongation	72	5 s	

One tube was removed from the PCR reaction after cycles 7, 8, 9, 10. Samples were run on an 8% TBE polyacrylamide gel (Invitrogen, Waltham, MA, USA) in 1x TBE (Ambion) for 55 min at 180 V. Gels were stained as mentioned before, desired bands from each PCR reaction were excised and DNA was extracted as described before for the ssDNA samples. The size

distribution of DNA fragments was determined by Bioanalyzer, concentration was determined by Qubit (#Q32852, Invitrogen) and samples were sequenced on a HiSeq (Illumina).

Sequenced reads were processed as described previously using standard analysis tools (Bowtie2, Tophat2) and in-house generated python scripts adapted to *S. cerevisiae*.

For **metagene analyses**, genes were normalized to their expression level by dividing the read density of each nucleotide by the average read density per nucleotide of the respective gene. For all normalized regions, reads from each gene were binned into the respective length and each bin was averaged.

3.7 *In silico* analysis of PMT promoter motifs

For PMT promoter analysis, 500 bp upstream of each ORF coding sequence was retrieved from the SGD database. The presence of transcription factor DNA binding motifs was analyzed using the YETFASCO tool (see materials). Based on the DNA motifs present, potential transcription factors were assigned to each ORF and plotted in a Venn diagram using Venny 2.1 (Oliveros, 2007-2015).

4 RESULTS

4.1 The protein *O*-mannosyl transferase family is integrated in the ER folding stress response

PMT proteins were firstly linked to protein folding stress using transcriptomic approaches (Travers *et al.*, 2000). The following studies showed the presence of constitutive UPR activation in both *pmt1*Δ and *pmt2*Δ mutants (Jonikas *et al.*, 2009) and synthetic lethality between PMTs and the UPR transcription factor *HAC1* (Arroyo *et al.*, 2011). In this context, the first aim of this work was to test the transcriptional link between PMTs and ER folding stress as well as to unravel the potential specificity of the different *pmt* mutants with respect to the constitutive activation of the UPR.

4.1.1 *PMT1* and *PMT2* are specifically regulated by the UPR

In order to approach the transcriptional regulation of the major members of the PMT family *PMT1*, *PMT2* and *PMT4* the presence of transcription factor binding motifs in the promoter region of these genes was investigated (Figure 4.1A). The promoter regions of the major PMTs *PMT1*, *PMT2* and *PMT4* were subtracted from the SGD database and searched for transcription factor binding motifs using the YETFASCO platform (detailed in 3.7). Unique and redundant binding motifs were associated with transcription factors based on sequence prediction. Results yielded a high number of transcription factors shared by all three members (69) and some overlap between, at least, two of the three (21, 8 and 19; *PMT1-PMT2*, *PMT2-PMT4,* and *PMT1-PMT4* respectively). Notably, the highest number of unique motifs that would indicate unique regulation of each PMT isoform is present in *PMT4* promoter (24; in comparison to 15 and 12 in *PMT1* and *PMT2*, respectively). A valid interpretation of this observation is that the expression of the Pmt4 homomeric complex is regulated by additional transcription factors on top of a common PMT regulation. Prediction of a higher number of *PMT4* unique transcription factors is consistent with published data (Figure App.1).

In regard to ER stress, all *PMT1, PMT2,* and *PMT4* are predicted to have Hac1 DNA binding motifs but in different numbers: 5, 3 and 1 motif for *PMT1*, *PMT2*, and *PMT4*, respectively.

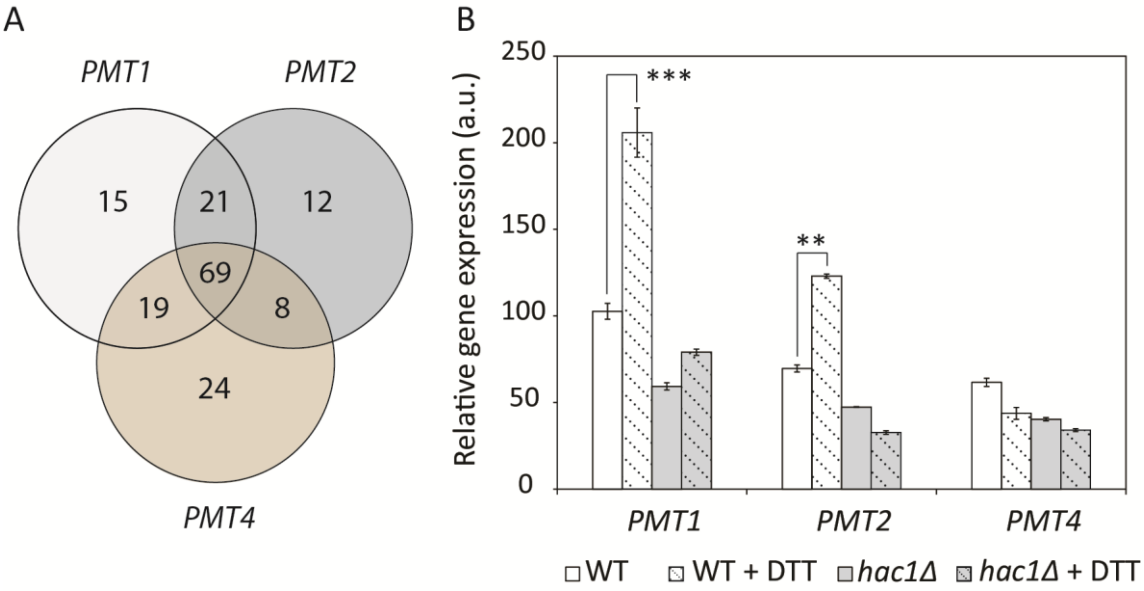

Figure 4.1. (**A**) *In silico* analysis of potential transcription factors regulating PMT expression. Transcription factor binding DNA motifs in 500 bp upstream of *PMT1*, *PMT2,* and *PMT4* were predicted by the YETFASCO database (see 3.7). (**B**) Relative mRNA levels of *PMT1*, *PMT2,* and *PMT4* in response to DTT in wild type and *hac1*Δ (Euroscarf) cells. Wild type (BY4741) and *hac1*Δ (Euroscarf) cultures were treated with 2.2 mM DTT for 60 min. cDNA was prepared from total mRNA according to 3.2.3 and 3.2.4 and RT-PCR was performed according to 3.2.9. Results show averages of mRNA abundance ± SD with respect to *ACT1*. For statistical significance, a two-tailed t-Student's test was applied (n=3).

To analyze the effect of UPR on each major PMT member, the quantification of all three transcripts in response to the folding stress agent DTT was performed in wild type and in *hac1*Δ cells, which are unable to activate the UPR (Figure 4.1B). Results show DTT treatment specifically upregulating the expression of *PMT1* and *PMT2* by approximately a factor of two in a *HAC1* dependent manner. Therefore, in agreement with previous high throughput data (Travers *et al.*, 2000), the Pmt1-Pmt2 heteromeric complex is a target of the UPR, whereas *PMT4* expression is insensitive to ER stress, suggesting that the function of the Pmt4 homomeric complex might be unconnected to the role of PMTs in protein quality control.

4.1.2 Absence of specific members of the PMT family triggers the UPR

To further characterize the relation between the UPR and *O*-mannosylation, a RT-PCR-based method was established (see 3.2.9) to precisely quantify the level of UPR present in the cells by looking at the abundance of both unspliced (inactive, $HAC1^{u}$) and spliced (active, $HAC1^{s}$) forms of HAC1 mRNA (Cox & Walter, 1996). The abundance of KAR2 mRNA was also quantified as *KAR2* is shown to be a major UPR target gene (Nikawa *et al.*, 1996).

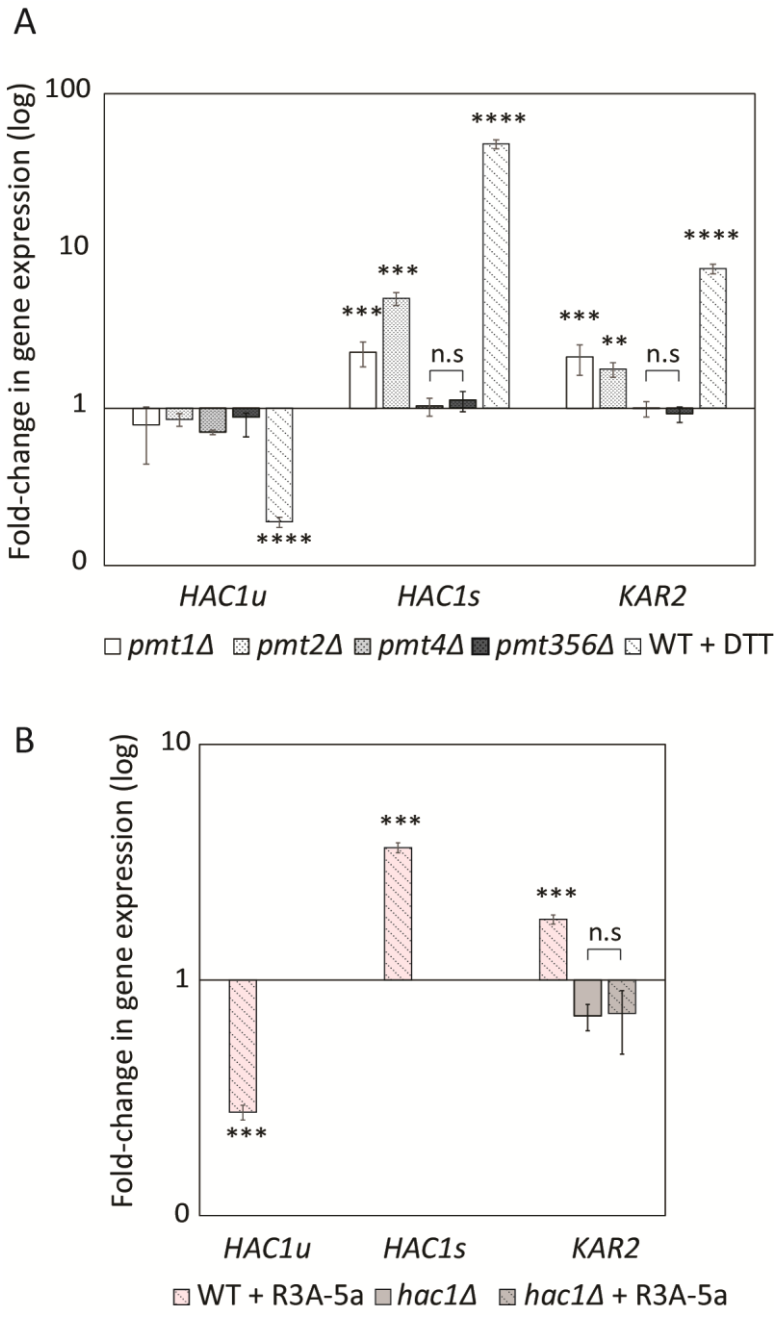

Figure 4.2. Compromising *O*-mannosylation activates the UPR. Fold- change in mRNA levels of $HAC1^{u}$, $HAC1^{s}$ and KAR2 upon either deletion of different members of the PMT family (**A**) or treatment with 10 µM R3A-5a (**B**). Total RNA was extracted either from wild type (BY4741), MLY213 (*pmt1*Δ), MLY214 (*pmt2*Δ), MLY16 (*pmt4*Δ), MLY231 (*pmt356*Δ) and wild type (BY4741) treated with 2.2mM DTT for1h (**A**); or from wild type (BY4741) and *hac1*Δ (Euroscarf) cells mock or treated with 10 µM R3A-5a (**B**); according to 3.2.3 and 3.2.4. (**A**, **B**) Fold-change was calculated by averaged Cts with respect to *ACT1*. Errors bars show the confidence interval. For statistical significance, a one-tailed t-Student's test was applied to log ($2^{-\Delta\Delta Ct}$), n=3.

Results yielded an increase of 2 and 5-fold in the levels of HAC1^{S} in *pmt1*Δ and *pmt2*Δ, respectively (Figure 4.2A). Together with this, the levels of KAR2 were also increased by ~2 fold in both mutants, indicating a mild but constitutive UPR activation when *PMT1* or *PMT2* is absent. Interestingly, no changes in the transcript level of HAC1^{S} or KAR2 were observable when deleting PMT4 or in the strain *pmt356*Δ, where minor PMT members are deleted.
As stated above, the deletion of PMTs together with HAC1 results in synthetic lethality (Arroyo *et al.*, 2011). In order to validate that the increased level of KAR2 upon defective *O*-mannnosylation is *HAC1*-dependent wild type and *hac1*Δ cells were treated with the *O*-mannosylation inhibitor R3A-5a (Figure 4.2B). Consistent with what observed in *pmt1*Δ and *pmt2*Δ, chemical inhibition of *O*-mannosylation also results in an increased level of HAC1^{S} and KAR2 transcripts in wild type cells (3.6 and 2 fold-change, respectively). On the contrary, levels were unaffected in *hac1*Δ cells confirming that the transcript upregulation observed in wild type is representative for UPR activation.
As a second readout GFP under the control of a UPR responsive element (UPRE) was genomically integrated into different PMT deletion mutants (Figure 4.3A, left panel). In line with the transcript analysis, UPR activation in *pmt1*Δ and *pmt2*Δ was observed whereas upon deletion of other PMT members, GFP fluorescence levels were indistinguishable from wild type cells. In this second approach also the multiple deletion mutant *pmt*1356Δ and *pmt*4356Δ, which only keep the minimal set of PMTs for the cells to remain viable (Martin Loibl, unpublished data) were included. UPR activation was only observable in *pmt1356*Δ and not in *pmt4356*Δ indicating that only the Pmt1-Pmt2 heteromeric complex prevents UPR activation under standard conditions. As control for the capacity to activate the UPR of the mutants tested, the response to DTT of all the PMT mutants was also tested using the UPRE-GFP reporter and no significant difference in GFP intensity was observed with respect to wild type cells (Figure 4.3, right panel).

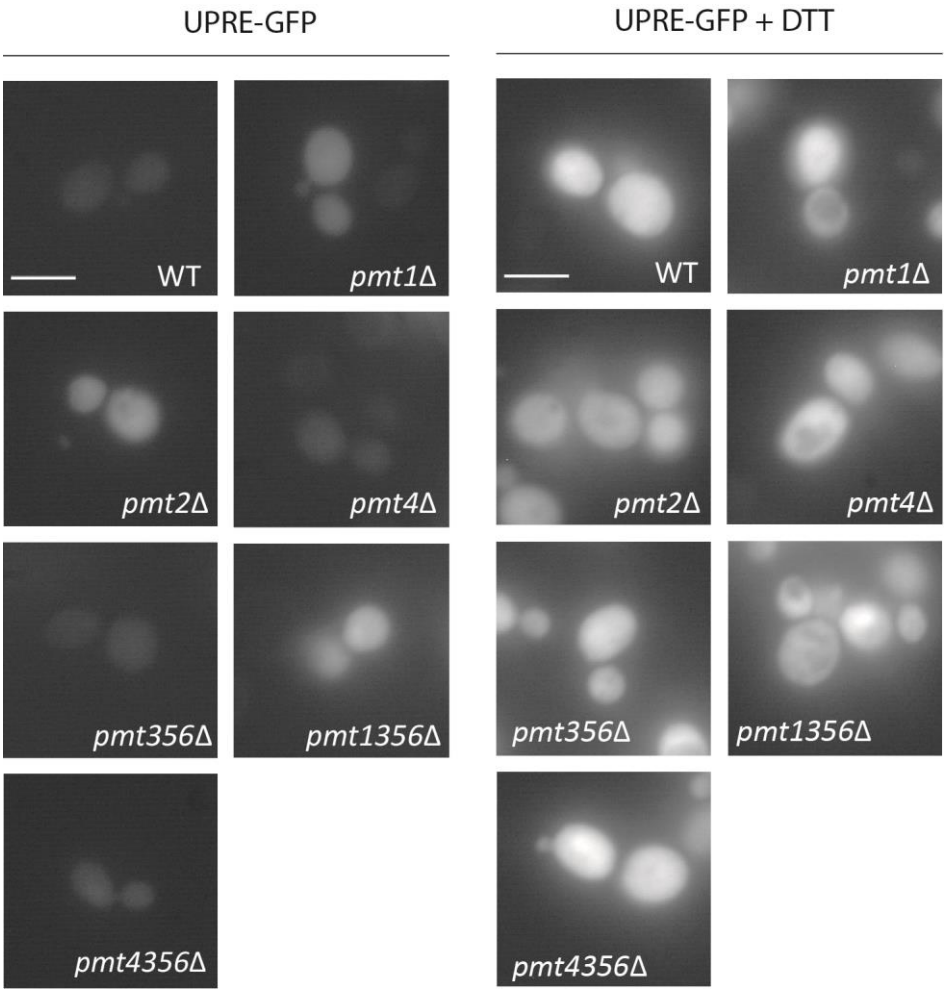

Figure 4.3. Analysis of UPRE-GFP reporter in PMT deleted strains. JCY001 (wild type), JCY002 (*pmt1*Δ), JCY003 (*pmt2*Δ), JCY004 (*pmt4*Δ), JCY005 (*pmt356*Δ), JCY006 (*pmt1356*Δ) and JCY007 (*pmt4356*Δ) were grown in YPD and imaged under standard conditions as detailed in 3.5.2 (left panel). JCY002 (*pmt1*Δ), JCY003 (*pmt2*Δ) and JCY006 (*pmt1356*Δ) show an increase in GFP intensity. The same strains were treated with 2.2Mm DTT for 1h (right panel). Scale bar 5 μM.

In order to clearly rule out that PMTs interfere with the capacity of the ER to activate the UPR wild type and *pmt2*Δ cells were treated with DTT in a time-course experiment (Figure 4.4). Under the conditions tested, maximum UPR activation was achieved after 15-30 min after the induction with DTT. After 60 min UPR decayed to a level close to the initial state. In particular, for *HAC1*^{S}*,* increased levels (4.3 fold-change) of transcript remained even after 4h.

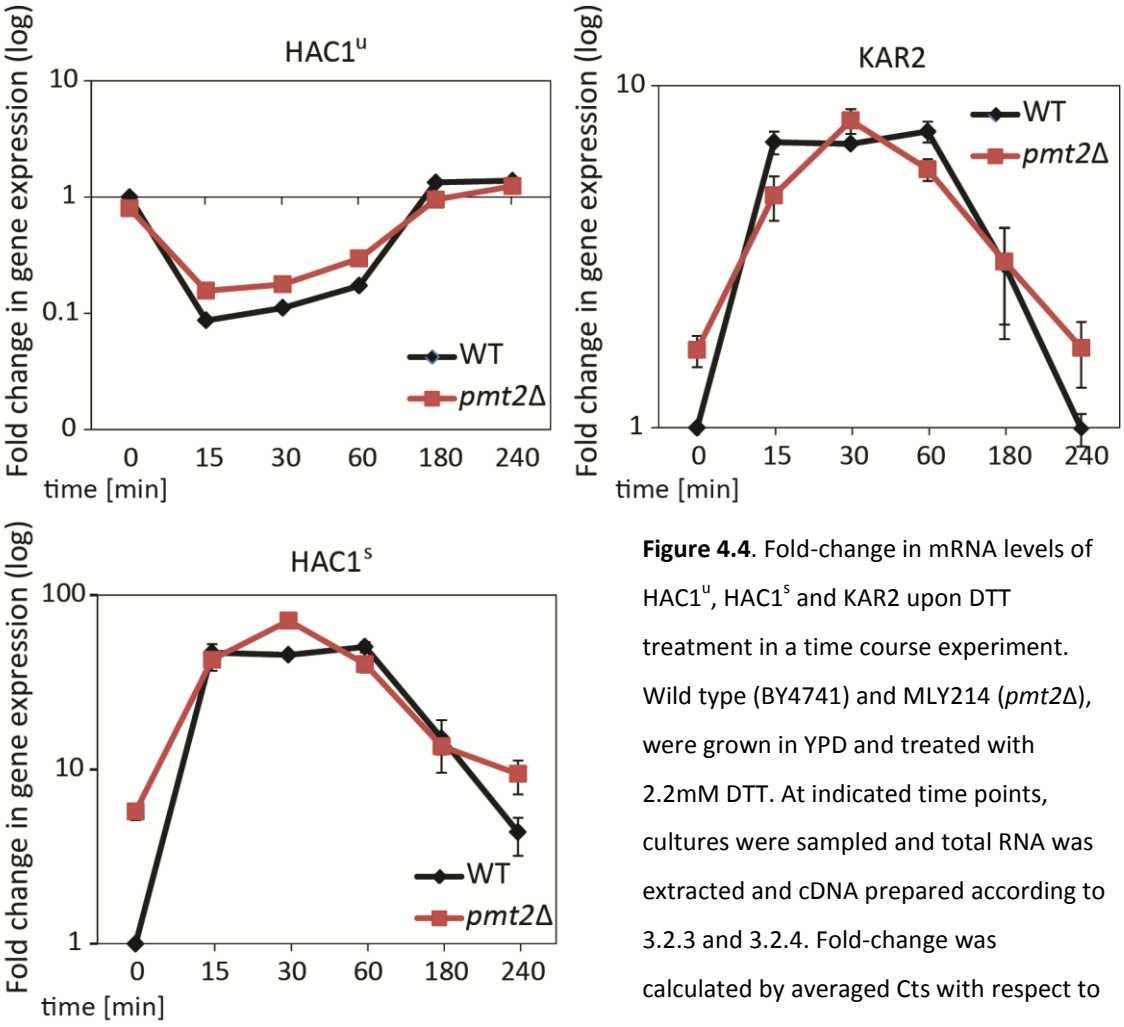

Figure 4.4. Fold-change in mRNA levels of HAC1^{u}, HAC1^{s} and KAR2 upon DTT treatment in a time course experiment. Wild type (BY4741) and MLY214 (*pmt2*Δ), were grown in YPD and treated with 2.2mM DTT. At indicated time points, cultures were sampled and total RNA was extracted and cDNA prepared according to 3.2.3 and 3.2.4. Fold-change was calculated by averaged Cts with respect to *ACT1*. Errors bars show the confidence interval. For statistical significance, a one tailed t-Student's test was applied to log ($2^{-\Delta\Delta Ct}$). n=3.

No striking changes were observed in the response to DTT upon the absence of *PMT2* except for the increased basal and final levels of HAC1^{s} and KAR2 in the assay, supporting the constitutive activation of the UPR in *pmt2*Δ observed in figure 4.2A and 4.3 and indicating no interference of Pmt2 with the UPR machinery.

Taken all together, these results highlight the relevance of the Pmt1-Pmt2 complex during the response to ER folding stress. The basis of the relationship between the Pmt1-Pmt2 complex and the UPR is bidirectional: Pmt1-Pmt2 is needed upon folding stress and causes folding stress when it is absent.

4.2 Searching for genes involved in the unfolded protein *O*-mannosylation (UPOM)

O-mannosylation has emerged in the past years as a potential contributor to ER homeostasis and protein quality control with promising perspectives. As described in the introduction, the fate of many different unfolded protein models is determined by the presence of covalently attached *O*-glycans but yet, only certain PMTs define what has been named unfolded protein *O*-mannosylation (UPOM). Due to the high genetic redundancy of the PMT family and the fact that *O*-mannosylation was initially thought to have a structural function at the cell wall, UPOM components have remained out of the spotlight in the ER quality control field.

When unraveling cell biological pathways and assigning novel protein functions, yeast genetics has proven its proficiency in multiple studies (Cohen & Schuldiner, 2011; Breker *et al.*, 2013; Aviram *et al.*, 2016; Geva *et al.*, 2017). The availability of a vast diversity of yeast libraries as well as the accessibility for researchers to high-throughput methodologies facilitates to obtain a broad picture of a certain biological process.

To unravel the role of *O*-mannosylation in ERQC, the relation between *O*-mannosyltransferases and ER folding stress was initially clarified. In this second part, yeast genetics were used as a tool to investigate what integrates the UPOM machinery. For this purpose, the efficiency of UPOM was characterized in a collection of gene deletion mutants, aiming to find genes that are crucial for this branch of the ER protein quality control.

4.2.1 ER-GFP as a UPOM protein model

ER-GFP has been shown as a target for the Pmt1-Pmt2 complex as a consequence of its inefficient folding ((C. Xu *et al.*, 2013), detailed in 1.4.2). In contrast to other unfolded protein models previously used to study UPOM, the native conformation of GFP is fluorescent and therefore allows us to infer the degree of PMT contribution to the folding state of the protein by monitoring and quantifying fluorescence intensity. This peculiarity of ER-GFP over other UPOM targets described was encouraging to choose it as an *O*-mannosylation reporter in a fluorescence-based high-throughput genetic screen for unknown UPOM components.

ER-GFP is *O*-mannosylated by the Pmt1-Pmt2 complex

4.2.1.1

Taking advantage of ER-GFP as a UPOM model required additional characterization of the physiological effects of its expression as well as additional methods to examine its glycosylation state besides *in vivo* fluorescence intensity. Xu and colleagues (2013) showed that the absence of Pmt1 and/or Pmt2 results in hypoglycosylation of ER-GFP and thereby improves its folding competency. Comparable enhancement in folding efficiency was observed when analyzing ER-GFP$_{fast}$ (referred from now on as ER-GFP$_f$) which skips UPOM due to its improved folding kinetics (C. Xu *et al.*, 2013; C. Xu & Ng, 2015). ER targeting of GFP is driven by the *N*-terminal fusion of GFP to the Kar2 signal peptide. Additionally, in order to avoid bulk-flow of GFP along the secretory pathway, a C-terminal HDEL retention signal is added (This point is further developed in 4.2.1.3)

A starting strain for the screen was generated by genomically integrating ER-GFP in the innoxious HO locus. Further, the major members of the PMT family were deleted to confirm the data published in C. Xu *et al.*, 2013. Indeed, the deletion of *PMT1* or *PMT2* results in an increase in overall fluorescence of ER-GFP (Figure 4.5A). Consistent with this, a fraction of ER-GFP (represented by two smeary bands) was detected migrating slower in SDS-PAGE followed by western blot (Figure 4.5B, indicated with white arrow). This fraction of ER-GFP was absent in *pmt1*Δ and *pmt2*Δ mutants or in ER-GFP$_f$, suggesting that it represents the fraction of ER-GFP that receives *O*-glycans and thereby increases its molecular mass. To confirm this hypothesis a C-terminally flag tagged version of ER-GFP was purified and subjected to α-mannosidase treatment *in vitro*, which cleaves terminal α-mannoses on glycans (Einhoff & Rudiger, 1988). Results show that the higher molecular mass fraction of ER-GFP collapses to the main 35 KDa band after α-mannosidase treatment (Figure 4.5C, indicated with black arrow), indicating that it corresponds to *O*-mannosylated ER-GFP. These results provided a qualitative straight forward method to analyze the glycosylation state of ER-GFP.

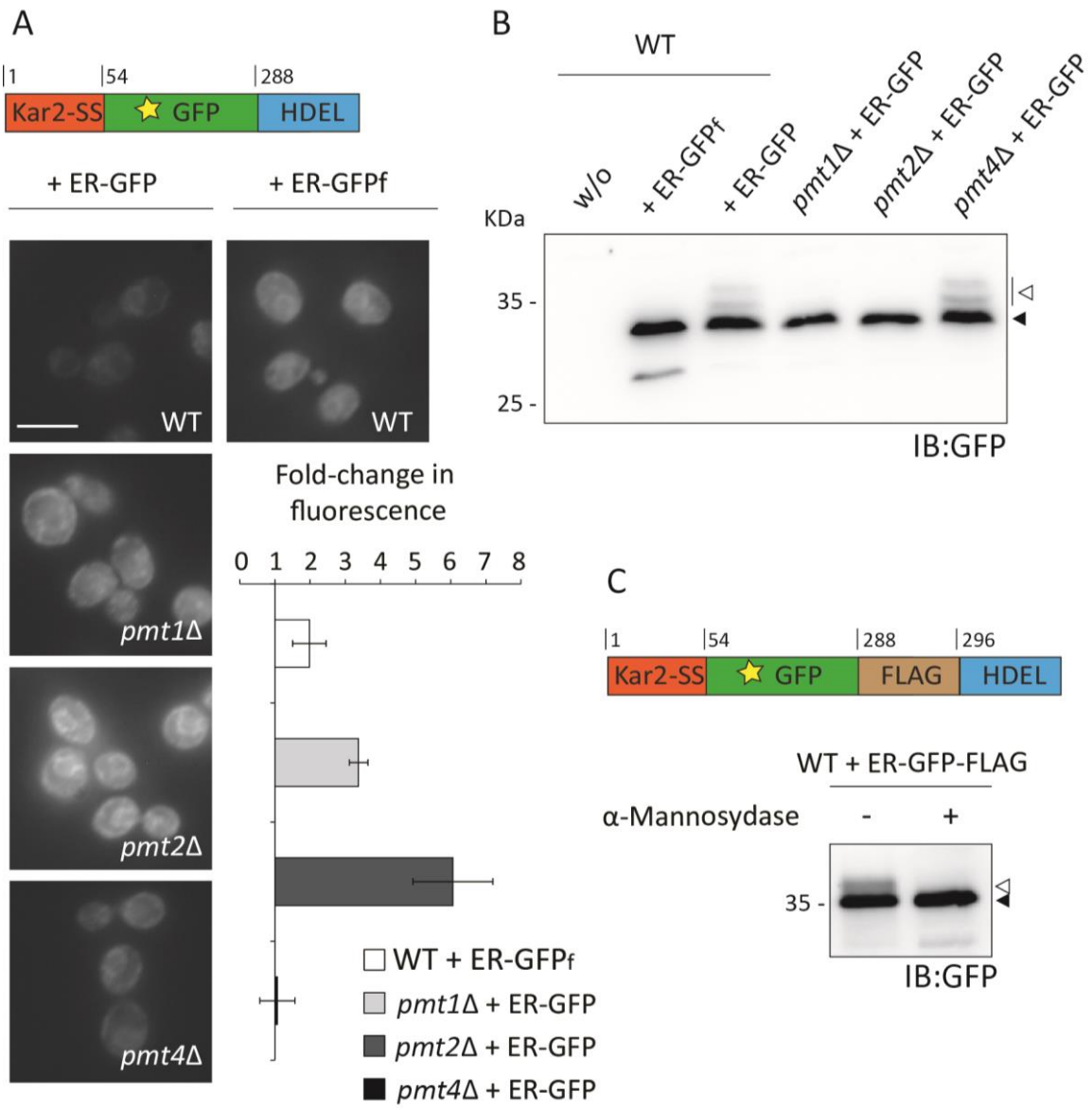

Figure 4.5. ER-GFP is *O*-mannosylated by the Pmt1-Pmt2 complex. (**A**) Microscopy of strains with the ER-GFP cassette genomically integrated (GFP appended with the Kar signal peptide and an HDEL retention sequence). JEY06 (wild type), JCY010 (*pmt1*Δ), JCY011 (*pmt2*Δ), JCY012 (*pmt4*Δ) and JEY05 (wild type expressing ER-GFP$_f$ as control) were grown in YPD and imaged under standard conditions (lower-left panel), scale bar 5 µM. The same strains were grown under identical conditions and analyzed by flow cytometry (lower-right panel). R values indicative of the cell population's fluorescence intensity (see 3.5.3) are normalized to R_{WT} and results are plotted as fold-change (n=3). (**B**) Total cell extracts were prepared from the same strains shown in (A). 20 µg of protein were resolved on a 12% PAA gel and subjected to Western blot analysis using anti-GFP antibody. An *O*-mannosylated fraction (white arrow) coexists with a less or non-modified fraction (black arrow) in wild type and *pmt4*Δ cells whereas is absent in *pmt1*Δ and *pmt2*Δ. (**C**) FLAG-tagged ER-GFP (upper panel) was expressed *via* plasmid pN014 in wild type cells and immunoprecipitated from total cell extracts according to 3.4.5. Purified ER-GFP-FLAG was subjected to α(1-2,3,6)-mannosidase treatment (3.4.6) overnight at 37 °C, resolved on a 12% PAA gel and subjected to Western blot analysis using anti-GFP antibody. The *O*-mannosylated fraction (white arrow) collapses onto the main band (black arrow) after treatment.

ER-GFP expression triggers the activation of the UPR

4.2.1.2

ER-GFP is under the control of the *TDH3* promoter which drives a strong protein overexpression. Previous studies have shown how overexpression of misfolded protein models results in ER stress and UPR activation (Umebayashi *et al.*, 2001; Spear & Ng, 2003). Clarifying the effect of ER-GFP overexpression with respect to stress is particularly relevant since in an ER-stress scenario the levels of Pmt1 and Pmt2, as well as components of the ER folding machinery, are significantly increased (Travers *et al.*, 2000, Figure 4.1B).

The levels of UPR-related transcripts were measured in wild type cells overexpressing both, ER-GFP$_f$ and ER-GFP (Figure 4.6A). Consistent with prolonged time in achieving the native conformation, expression of ER-GFP yielded a very relevant increase for *HAC1*^{s} and *KAR2* (8 and 4 fold-change, respectively). Although still statistically significant, expression of ER-GFP$_f$ only resulted in a mild increase of the same transcripts (1.5 and 1.2, respectively). The different impact of either version of ER-GFP on ER homeostasis is understandable taking into account that the requirement of folding factors for a protein that does not fold efficiently would be higher than for its folding competent counterpart. In line with the UPR activation observed at the transcript level, increased levels of HAC1^s and KAR2 were correlated with increased protein abundance for Kar2, Pmt1, and Pmt2; whereas Pmt4 remained unaffected (Figure 4.6B).

With respect to the use of ER-GFP as a UPOM reporter in a high throughput screen, these results picture a scenario where the ER suffers from folding stress and therefore components of the folding machinery, as well as the Pmt1-Pmt2 complex, are more abundant.

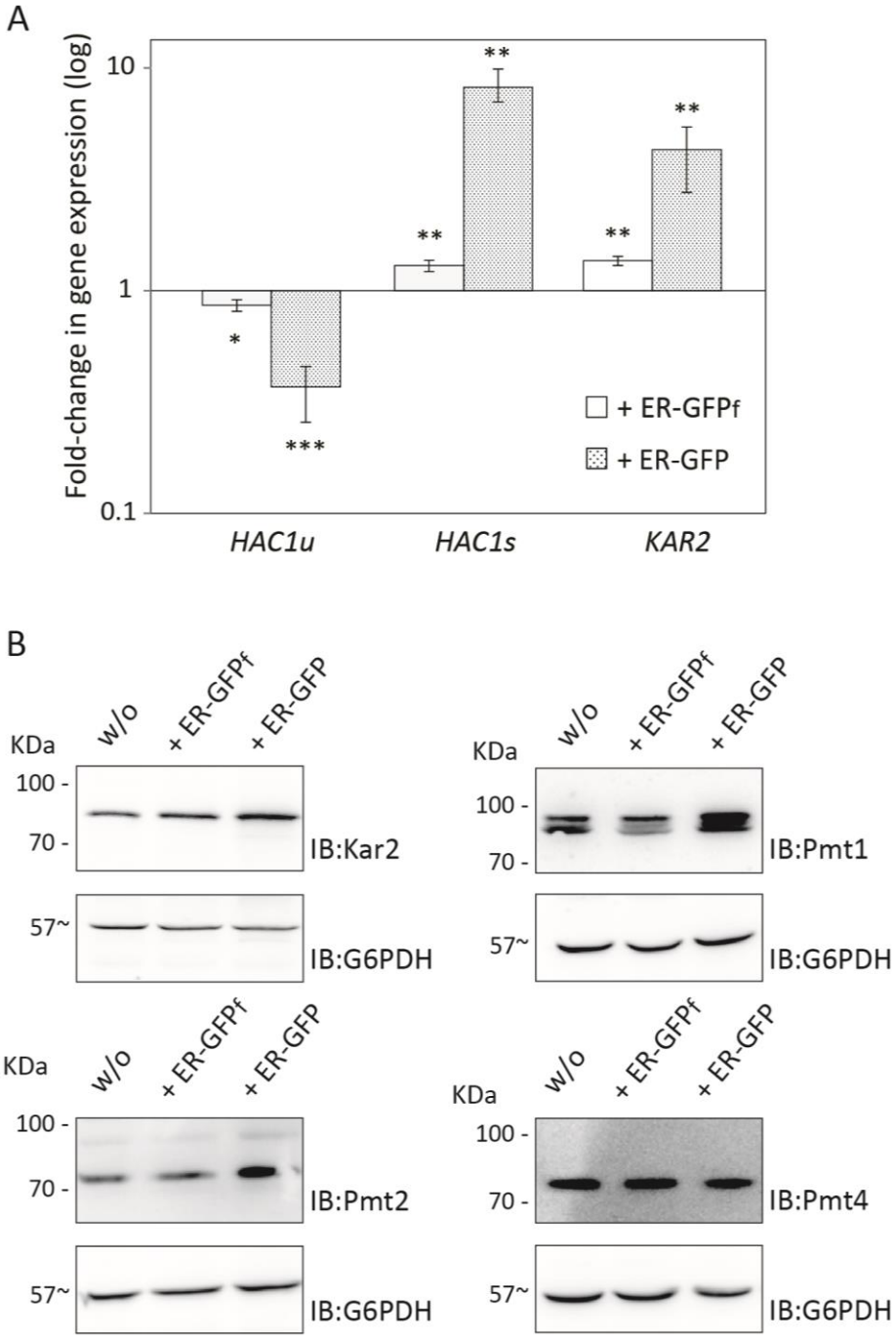

Figure 4.6. Impact of ER-GFP expression on the UPR. (**A**) Fold- change in mRNA levels of HAC1^{u}, HAC1^{s,} and KAR2 upon ER-GFP$_f$ and ER-GFP expression. Total RNA was extracted (3.2.3) from wild type (BY4741), JEY05 (ER-GFP$_f$) and JEY06 (ER-GFP) grown in YPD, cDNA was prepared (3.2.4) and used as a template for RT-PCR. Fold-change is calculated by averaging Cts with respect to *ACT1*. Errors bars show the confidence interval. For statistical significance, a one-tailed t-Student's test was applied to log ($2^{-\Delta\Delta Ct}$), n=3. (**B**) Total cell extracts were prepared from the same strains. 20 µg of protein were resolved on a 12% PAA gel and subjected to Western blot analysis using the antibodies indicated. G6PDH served as loading control (n=2-3).

4.2.1.3 ER-GFP can be targeted for vacuolar degradation

Another important aspect to consider when working with ER-GFP as a model is to account for its stability. Most misfolded protein models studied to date are either recognized by the ERAD system, retro-translocated to the cytosol and degraded at the proteasome or sent to the vacuole for degradation (Nakatsukasa & Brodsky, 2008, Hong *et al.*, 1996; Haynes *et al.*, 2002; Coughlan *et al.*, 2004).

ER-GFP is stable in the ER lumen (C. Xu & Ng, 2015), which in principle should rule out protein stability as a major contributor to its fluorescent intensity. However vacuolar turnover is still a scenario to consider. Soluble proteins functioning at the ER lumen require specific mechanisms to avoid their stochastic escape along the secretory pathway. These ER-resident proteins are central contributors to ER homeostasis since most of them include chaperones, oxidoreductases, and proteins involved in lipid biogenesis. To avoid depletion of these proteins from the ER due to bulk flow, ER-resident proteins bear specific sequences, conserved in higher eukaryotes that function as signals for cargo receptors of the ER retrieval system along the secretory pathway. In yeast, the ER retrieval system is defined by the transmembrane receptor Erd2, which recognizes the canonical motif HDEL of ER-residents and contributes to their retrograde transport into COPI-coated vesicles (reviewed in Perez-Linero & Muniz, 2015).

When studying the *O*-mannosylation of ER-GFP, a canonical C-terminal HDEL sequence was included to prevent bulk flow interfering with the function of PMTs. The presence of the HDEL sequence, however, does not ensure the full efficiency of the retrieval system since it has been observed that some genes, including cargo receptors and others, are required for competent retrieval (Copic *et al.*, 2009). In line with this, as shown in 4.2.1.2 the screen was performed under ER stress conditions which causes upregulation of chaperones such as Kar2, bearing an HDEL signal that might contribute to saturate the Erd2 receptor. These considerations were encouraging to study the effect of the HDEL signal on the stability of ER-GFP. When including a C-terminal HDEL sequence in the ER-GFP construct, fluorescence microscopy indicates a clear ER and secretory pathway localization (Figure 4.5A). Consistent with this and with previous studies (C. Xu *et al.*, 2013), this version of ER-GFP is stable in a cycloheximide chase experiment (Figure App. 2).

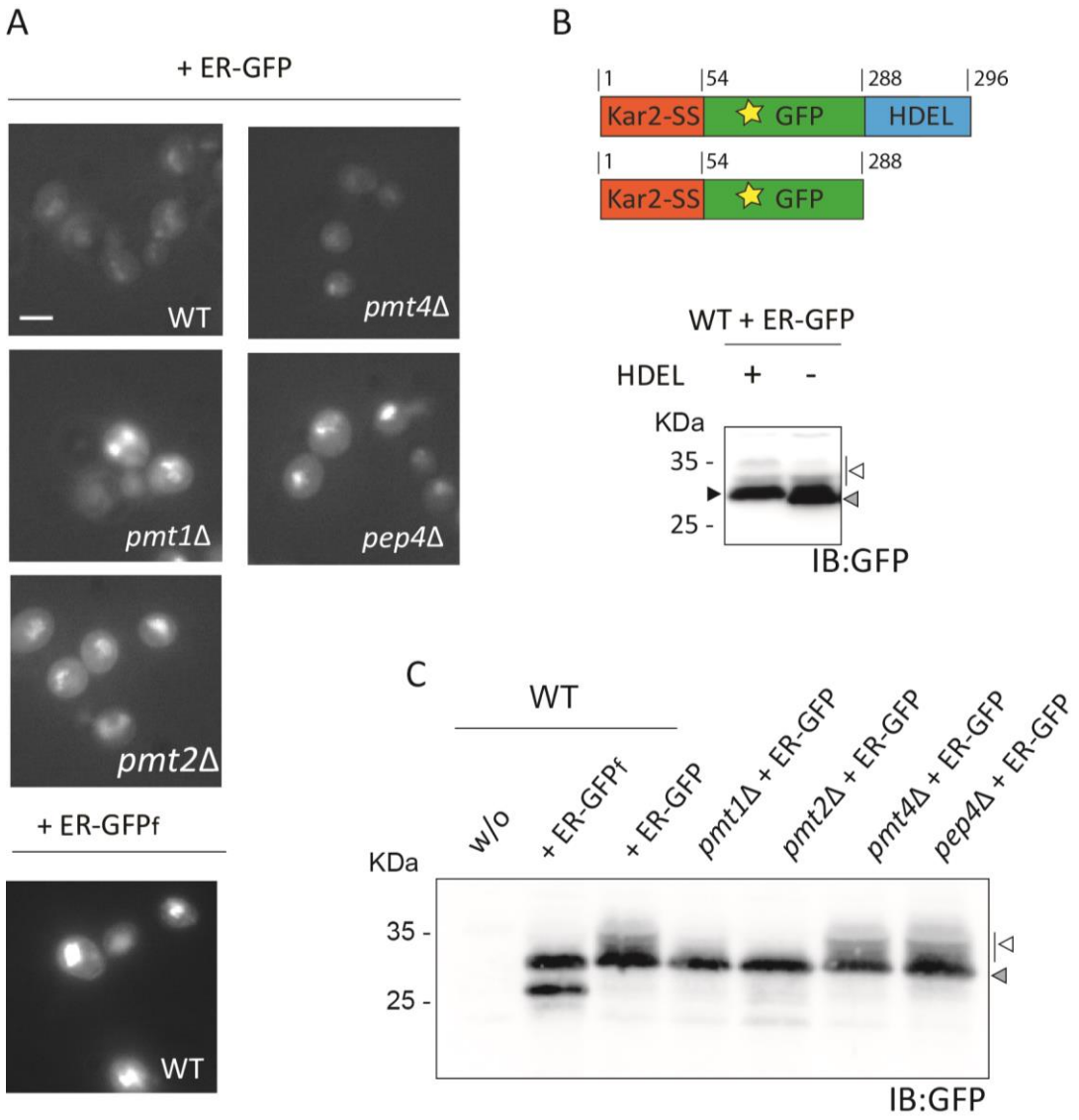

Figure 4.7. Analysis of non-retained ER-GFP. (**A**) Microscopy of strains expressing non-retained ER-GFP. Wild type (BY4741), MLY213 (*pmt1*Δ), MLY214 (*pmt2*Δ), MLY16 (*pmt4*Δ) transformed with pJC08 (ER-GFP) were grown in SD-URA and imaged under standard conditions. As a control, wild type (BY4741) was transformed with pJC07 (ER-GFP$_f$) and analyzed in parallel. Given the strong difference in intensity, two different exposures were used for ER-GFP and ER-GFP$_f$ (200 and 90 ms, respectively). Scale bar 5 µM. (**B, C**) Western blot analysis of non-retained ER-GFP. Comparison between the ER-GFP construct (**B**, upper panel) analyzed in figure 4.5 and non-retained ER-GFP. Total cell extracts were prepared from wild type cells transformed with either pWXB206 (ER-GFP) or pJC08 (non-retained ER-GFP) (**B**, lower panel) or from the same strains as in (A) (**C**). Equivalent to 0.2 OD_{600} of protein were resolved on a 12% PAA gel and subjected to Western blot analysis using anti-GFP antibody. Black and gray arrows indicate the predominant protein fraction of ER-GFP and non-retained ER-GFP respectively. White arrow indicates the *O*-mannosylated ER-GFP fraction (n=2, representative results are shown).

On the contrary, expressing ER-GFP that lacks HDEL (referred to as non-retained ER-GFP) shows a central dotted pattern that suggests vacuolar localization (Figure 4.7A). Regarding the influence of *O*-mannosylation in the folding competency of ER-GFP, the presence of *O*-mannosylated protein fraction is shown by western blot for non-retained ER-GFP and an increase of fluorescence correlates with the absence of this higher molecular size fraction in *pmt1*Δ and *pmt2*Δ (Figure 4.7A and 4.7C). This indicates that despite non-retained ER-GFP does not localize to the ER, this has no major influence on the effect of *O*-mannosylation on its folding state.

To test the vacuolar localization, non-retained ER-GFP was expressed in a *pep4*Δ mutant, where vacuolar degradation is deficient. Similar to *pmt1*Δ or *pmt2*Δ, the deletion of *PEP4* resulted in an increase of fluorescence of ER-GFP (Figure 4.7A).

When analyzing the *O*-mannosylation state, Pep4 did not have any observable influence in the presence of a modified protein fraction. This suggests that the folding competency of ER-GFP is not enhanced in *pep4*Δ but the observed increase in fluorescence might be the result of protein stabilization. To test this hypothesis a cycloheximide chase experiment was performed in wild type and *pep4*Δ expressing non-retained GFP (Figure 4.8). In contrast to the ER-retained counterpart, non-retained GFP is efficiently degraded in wild type and degradation is largely prevented in *pep4*Δ cells.

From these experiments, it was concluded that firstly, prolonged stay in the ER has no major influence in UPOM of ER-GFP since a version of ER-GFP unrestricted to move along the secretory pathway also receives *O*-glycans in a Pmt1-Pmt2-dependent manner. Secondly, although ER-GFP is a stable protein when retained at the ER, the absence of ER-retention results in its vacuolar turnover. This point is relevant for the high throughput screen since as mentioned, ER-retention efficiency can be compromised in the absence of certain genes and the ER-escape of GFP will likely result in protein degradation.

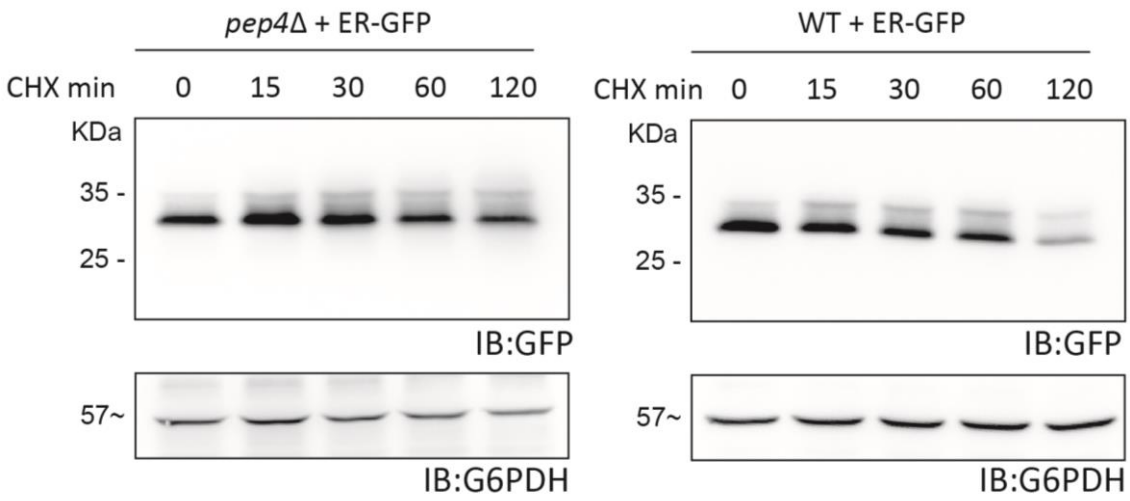

Figure 4.8. **Cycloheximide chase analysis of non-retained ER-GFP**. Wild type (BY4741) and *pep4*Δ were transformed with pJC08 (non-retained ER-GFP) and treated with 200 µg/ml cycloheximide. Equivalent to 10 OD_{600} cells was sampled at the indicated time points. Equivalent to 0.2 OD_{600} of total cell extract was resolved on a 12% PAA gel and subjected to Western blot analysis using an anti-GFP antibody. G6PDH served as a loading control (n=2, representative results are shown).

4.2.2 High throughput screen for UPOM factors

In order to get a comprehensive picture of unfolded protein *O*-mannosylation, a genome-wide screen was performed using ER-GFP as an *O*-mannosylation reporter. The screen was performed by Lihi Gal in collaboration with the group of Prof. Maya Schuldiner (Weizmann Institute of Science, Rehovot, Israel).

Folding competency of ER-GFP is impeded by *O*-mannosylation by the Pmt1-Pmt2 complex and therefore deletion of *PMT1* or *PMT2* results in increased fluorescence intensity (Figure 4.5A). Hypothetically, the deletion of genes involved in UPOM should yield a similar fluorescence increase. To analyze the fluorescence of ER-GFP upon the disruption of every single gene in yeast the workflow depicted in figure 4.9 (and detailed in 3.3.1) was followed. In brief, an automated crossing of a starting wild type strain with ER-GFP genomically integrated (JEY06) with two different libraries was carried out: single deletion mutants and DAmP (decreased abundance by mRNA perturbation) yeast collections. The DAmP collection is a library of hypomorphic alleles for essential genes generated by the fusion of an antibiotic resistance marker to the 3'UTR of the target gene, inducing instability and decay of the transcript (Breslow *et al.*, 2008).

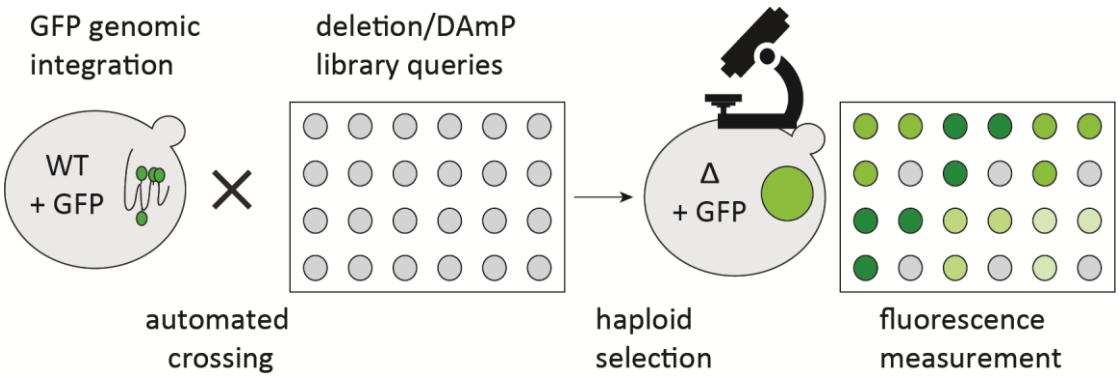

Figure 4.9. Workflow of the ER-GFP screening. In brief, a wild type strain with ER-GFP genomically integrated (JEY06) was crossed with both, single-gene deletion (Giaever *et al.*, 2002) and DAmP (Breslow *et al.*, 2008) genetic libraries using SGA methodology (see 3.3.1). Haploid yeast strains carrying both genetic modifications (ER-GFP integration and single-gene deletion/DAmP allele) were selected. The fluorescence intensity of ER-GFP was calculated based on the software analysis of microscopy images as described in (Breker *et al.*, 2013).

Haploids carrying both ER-GFP and the corresponding mutation (deletion or DAmP) were selected, fluorescence microscopy was performed, and intensity was quantified (see 3.3.1). 109 mutants were yielded as positive hits (Table App 1, Figure 4.10A). As an indication of the validity of the screen, *pmt1*Δ and *pmt2*Δ were found among the positive hits, being *pmt2*Δ the third top hit in the list (Figure 4.10A). Together with PMT mutants GO term enrichment showed a low enrichment score (approximately 2) and included very heterogeneous categories such as *glycosylation*, *protein metabolic process*, *proteolysis* or *chromatic organization*, indicating no ontologically enriched biological pathway or process influencing ER-GFP fluorescence (Figure 4.10B).

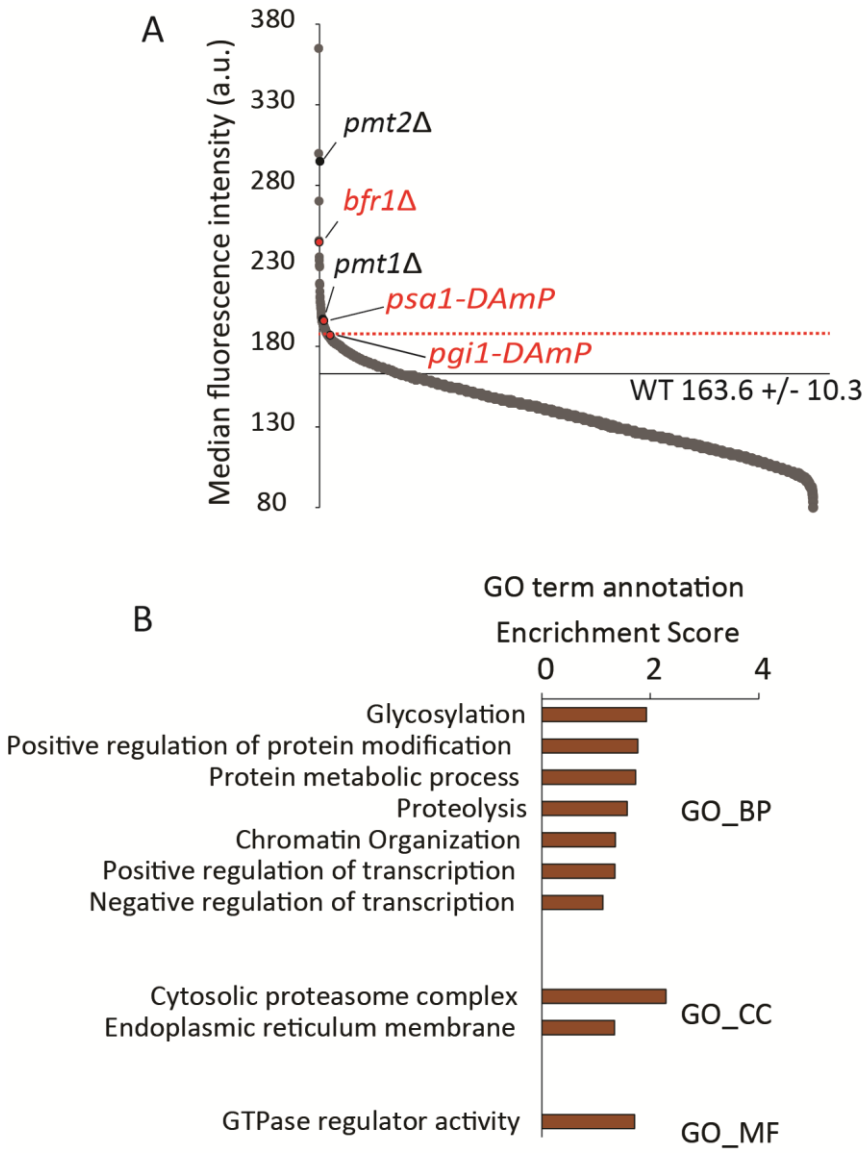

Figure 4.10. Identification of potential UPOM factors. (**A**) Distribution of the median fluorescence intensity (y-axis) displayed by each mutant analyzed in the ER-GFP screening (x-axis) with respect to the median average of wild type cells. The threshold for positive hit selection is depicted as a red dashed line. (**B**) GO term enrichment analysis using DAVID (v6.7). GO term enrichment was performed on 100 mutants considered as a hit (Table App. 1) using GO ALL terms, an EASE score of 0.1, and the *S. cerevisiae* reference list. Enrichment scores were extracted for the respective GO term clusters and clusters were named by representative terms. Biological process (GO_BP), molecular function (GO_MF) and cellular compartment (GO_CC) are shown.

4.2.2.2 Systematic analysis of the positive mutants

Next to *O*-mannosylation, multiple scenarios resulting from gene deletion might impact on the fluorescence of ER-GFP: incorrect ER-targeting, deficient ER-retention (as shown in 4.2.1.3) or inability to maintain the ER-GFP-induced stress response since the UPR is needed to optimize the protein quality control mechanisms. In line with this, it is important to note that genes that affect canonical glycosylation would also be potentially found in the screening. Although it is also of interest targeting core components of the glycosylation pathway, the goal was to find genes that might particularly function in the context of ER-stress and UPOM.

A first analysis of the mutants consisted of manual curation of the ER-localization of ER-GFP in the ER. Of the 109 positive hits, only *spf1*Δ (top hit of the screen, figure 4.10A) showed partial localization of ER-GFP in the cytosol, which was validated in an independent *spf1*Δ deletion mutant (Figure App.3) and excluded from further analyses.

In order to restrict the analysis to those mutants involved in UPOM, two parallel strategies were developed: In a first strategy, to find genes that affect general *O*-mannosylation, it was taken advantage of the extensively *O*-mannosylated protein Hsp150. Hsp150 is a cell wall protein that is induced and secreted to the medium by heat shock (Russo *et al.*, 1992). When analyzing medium containing Hsp150 by SDS-PAGE followed by western blot, deletion of either *PMT1* or *PMT2* results in a shift of the above 150 KDa main fraction to lower molecular mass fractions, resulting in a smeary pattern that likely represents hypoglycosylated subspecies of Hsp150 (Figure 4.11, indicated with white arrow). The medium from 100 heat-shocked positive mutants from the ER-GFP screen was isolated and analyzed. None of the mutants resulted in a major shift of the 150 KDa band (Figure 4.11, indicated with black arrow), however, 12 of them, clustered as *pop2*Δ-like mutants, showed a smear comparable to what shown by the PMT mutants (Table App. 1). Other positive mutants clustered as *ost3*Δ-like, showed an increased presence of two protein fractions of about 70 and 50 KDa, which might correspond to immature forms of Hsp150.

In conclusion from this first filtering, the 12 mutants that showed the *pop2*Δ-like phenotype are promising candidates to suffer from general *O*-mannosylation defects whereas mutants showing the *ost3*Δ-like phenotype are likely unrelated to *O*-mannosylation.

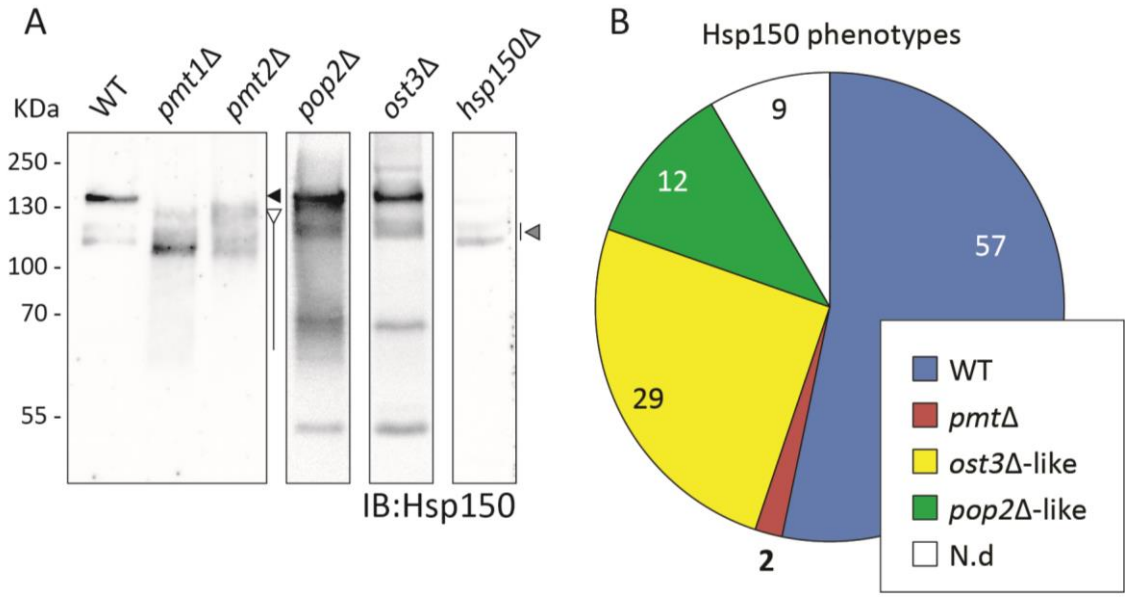

Figure 4.11. Systematic western blot analysis of Hsp150 in the ER-screening positive hits. Viable single deletion mutants considered a hit in the ER-GFP screening (Figure 4.10, Table App.1) were retrieved from the Euroscarf collection and their *O*-mannosylation capacity was analyzed based on the cell wall component Hsp150. (**A**) As detailed in 3.4.4, mutants were subjected to heat shock to induce secretion of Hsp150, proteins of the medium were loaded and resolved on 8% PAA gels and subjected to Western blot analysis using anti-Hsp150 antibody. To ensure reproducibility, wild type and *hsp150*Δ-derived medium were included in each PAA gel as controls. Hsp150 fully glycosylated and hypoglycosylated protein fractions are indicated with black and white arrows, respectively. (**B**) Hsp150 phenotypes were grouped according to the following criteria: protein size shift (*pmt*Δ-like), presence of lower molecular size smear (*pop2*Δ-like) and accumulation of Hsp150 immature species (*ost3*Δ-like). The number of mutants included in each cluster is shown.

In a second strategy, the aim was to select the positive mutants that might affect UPOM in particular. SDS-PAGE followed by western blot was used to evaluate the presence of the *O*-mannosylated fraction of ER-GFP. Although this method denies the quantification of the glycosylation state of ER-GFP, it is proven to be qualitatively suitable when *PMT1* or *PMT2* are deleted (Figure 4.5 B and C). Five mutants among the positive hits were found presenting either absence or strong reduction of the *O*-mannosylated fraction of ER-GFP (Figure 4.12A and B): *pmt1*Δ, *pmt2*Δ, *bfr1*Δ, *psa1-DAmP,* and *pgi1-DAmP*.

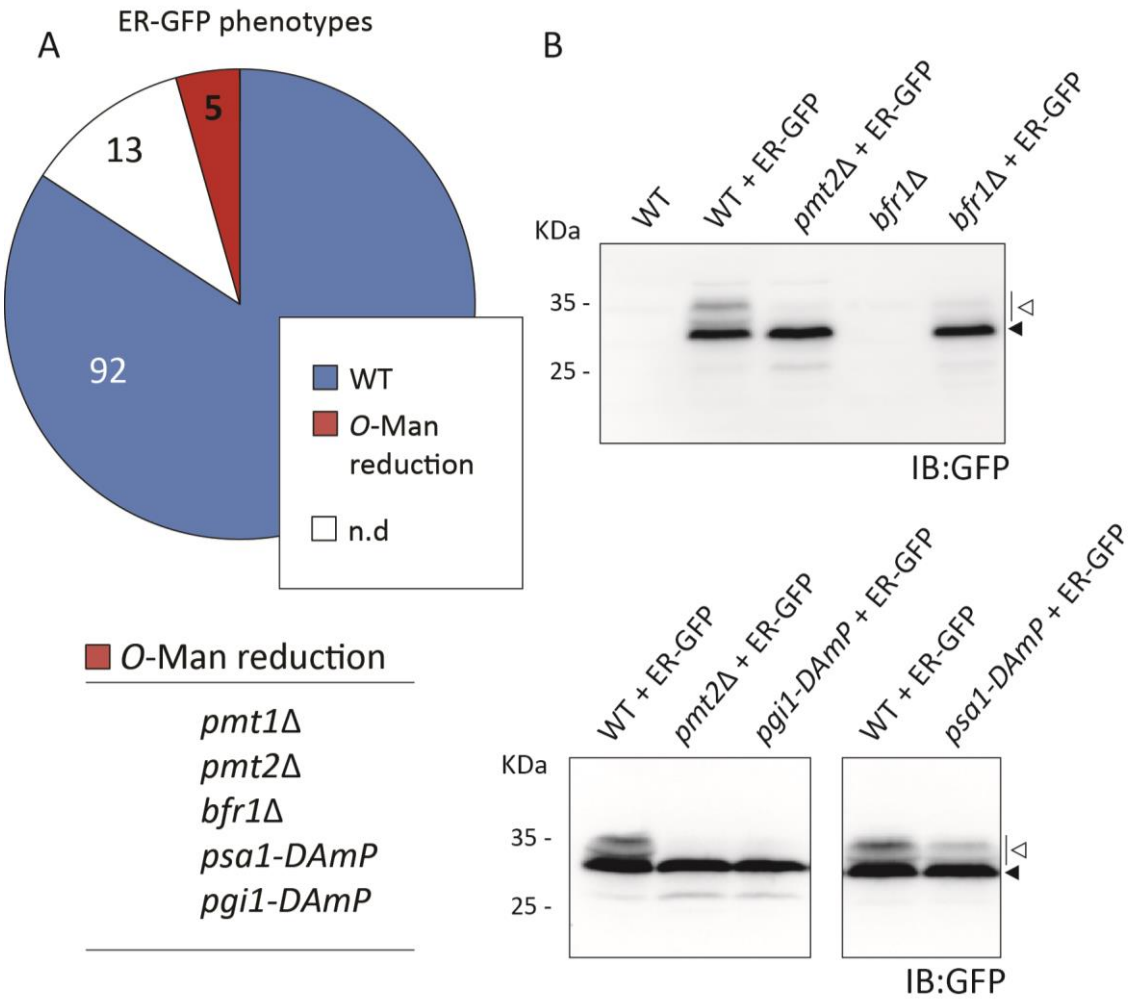

Figure 4.12. Systematic analysis of *O*-mannosylation of ER-GFP in the positive hits of the ER-GFP screening. Selected haploids resulting from SGA crosses and considered a hit in the screening (Figure 4.10A, Table App.1) were analyzed with respect to the glycosylation state of ER-GFP. Total cell extracts were prepared according to 3.4.2 and equivalents to 0.2 OD_{600} were resolved on a 12% PAA gel and subjected to Western blot analysis using anti-GFP antibody. To ensure reproducibility, total cell extracts from wild type expressing ER-GFP (JEY06) were included in each PAA gel as controls. (**A**) ER-GFP phenotypes were clustered with respect to the reduction of the presence of the *O*-mannosylated protein fraction. (**B**) *bfr1*Δ, *pgi1-DAmP,* and *psa1-DAmP* were identified as mutants with deficient UPOM indicated by the reduction of the *O*-mannosylated protein fraction (white arrow). Blots showing *pgi1-DAmP* and *psa1-DAmP* were obtained by Dr. Daniela Bausewein.

The mutants *bfr1*Δ and *pgi1-DAmP* showed strong hypoglycosylation of ER-GFP whereas the effect was milder but still significant for *psa1-DAmP* (Figure 4.12B, indicated with white arrow). In *pgi1-DAmP,* the fluorescence intensity of ER-GFP, although significantly higher than in wild type cells (Table App. 1, Figure 4.10A), was slightly below the threshold. Nevertheless, *pgi1-DAmP* was included in this analysis because of two reasons: First, *pgi1-DAmP* has been shown to cause ER-retention defects (Copic *et al.*, 2009) which in turn would

lead to lower ER-GFP fluorescence level irrespective of UPOM. Second, the involvement of *PGI1* in the glycolic pathway in part necessary for the production of GDP-mannose in the cytosol (Aguilera & Zimmermann, 1986) suggesting a functional link to PMTs.

4.2.3 The role of *PGI1* in UPOM

PGI1 and *PSA1* are essential genes encoding the glycolytic enzymes glucose-6-phosphate isomerase and GDP-mannose pyrophosphorylase, respectively.
Pgi1 catalyzes the isomerization of glucose-6-phosphate into fructose-6-phosphate, a critical reaction of the pathway that metabolizes the glucose taken up by the cell (Aguilera & Zimmermann, 1986; Green *et al.*, 1988). Psa1 catalyzes the synthesis of GDP-mannose using mannose 1-phosphate and GTP as substrates (Hashimoto *et al.*, 1997, Figure 4.13).

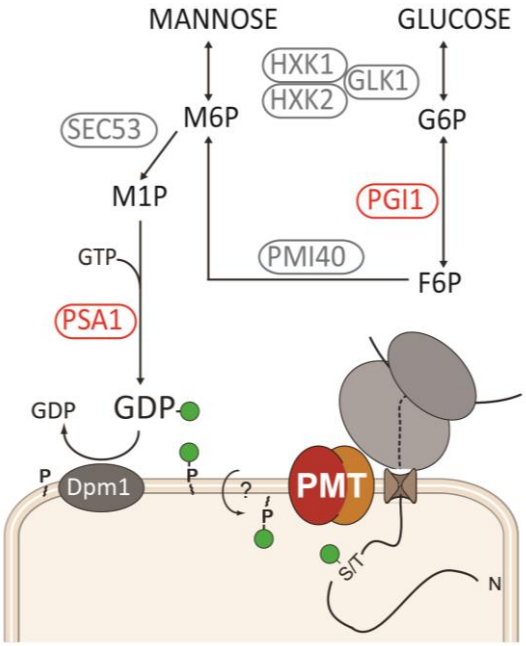

Figure 4.13. Representation of the cytosolic pathways that result in the production of GDP-mannose. After phosphorylation, internalized glucose is isomerized into fructose-6-phosphate by Pgi1. Fructose-6-phosphate is then converted into mannose-6-phosphate which can also be internalized in the cell as mannose and then phosphorylated. Mannose-6-phosphate is used as a substrate to synthesize GDP-mannose by Sec53 and Psa1. GDP-mannose is used as a substrate for the different ER glycosylation machinery, including the PMT machinery via Dol-P mannose (See 1.2.1 and 1.2.2).

Both genes have been found to be necessary to ensure proper UPOM of ER-GFP (Figure 4.12B). In order to validate the results of the screen and to characterize the extent of the downregulation of these two genes by the DAmP methodology, both mutants were generated *de novo* and the mRNA levels were quantified to confirm the knockdown. RT-PCR yielded about 10 and 5 fold-change reduction for *PGI1* and *PSA1*, respectively in comparison to wild type (Figure 4.14)

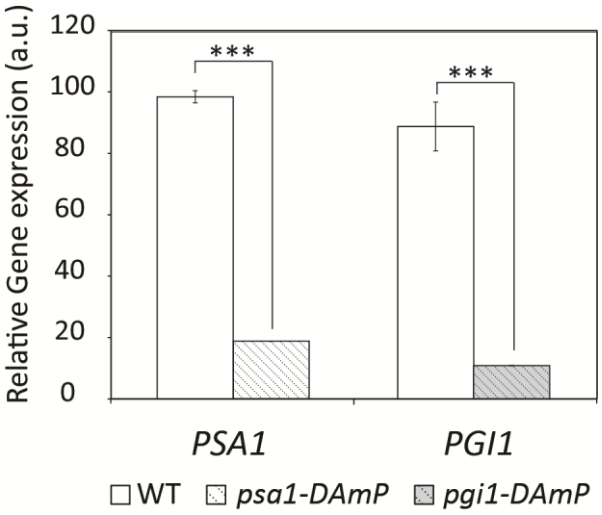

Figure 4.14. Relative mRNA levels of *PSA1* and *PGI1* in wild type, JCY014 (*pgi1-DAmP*) and JCY015 (*psa1-DAmP*). Cell cultures were grown in YPD. cDNA was prepared from total mRNA according to 3.2.3 and 3.2.4 and RT-PCR was performed according to 3.2.9. Results show averages of *PSA1* and *PGI1* mRNA abundance ± SD with respect to *ACT1*. For statistical significance, a two-tailed t-Student's test was applied (n=3).

One logic hypothesis to explain the need of glycolytic enzymes for efficient *O*-mannosylation is given by the fact that both enzymes are involved in the pathway that produces GDP-mannose in the cytosol, thereby providing Dpm1 (see 1.2.1 and 1.2.2) with the substrate to form Dol-P-Man, the sugar donor for *N*-glycosylation, *O*-mannosylation, and GPI-anchor biosynthesis.

In humans, mutations in the homolog of *PSA1* have been associated with different congenital disorders of glycosylation (CDGs) defined as muscular α-dystroglycanopathies (Carss *et al.*, 2013; Koehler *et al.*, 2013; Belaya *et al.*, 2015). In contrast, *PGI1* deficiency has been reported to cause a rare type of hereditary hemolytic anemia sometimes associated with neurological disorders (Kanno *et al.*, 1996; Kugler *et al.*, 1998). In particular, for *PGI1* most of the symptoms of its deficiency have been assumed to be the result of impaired metabolism of glucose and no effect on protein glycosylation and consequently on ER protein quality control has been described so far. The lack of CDGs associated with *PGI1* to date and the modest reduction of *O*-mannosylation of ER-GFP found in *psa1-DAmP* (Figure 4.12B) were encouraging to put the focus on *PGI1* as a link between sugar metabolism and ER homeostasis.

UPOM in *pgi1-DAmP* is mannose-dependent

4.2.3.1

To test that compromised UPOM in *pgi1-DAmP* is related to GDP-mannose production, the glycosylation state of ER-GFP was analyzed in *pgi1-DAmP* cells grown using glucose, mannose or a combination of both as carbon source (Figure 4.15).

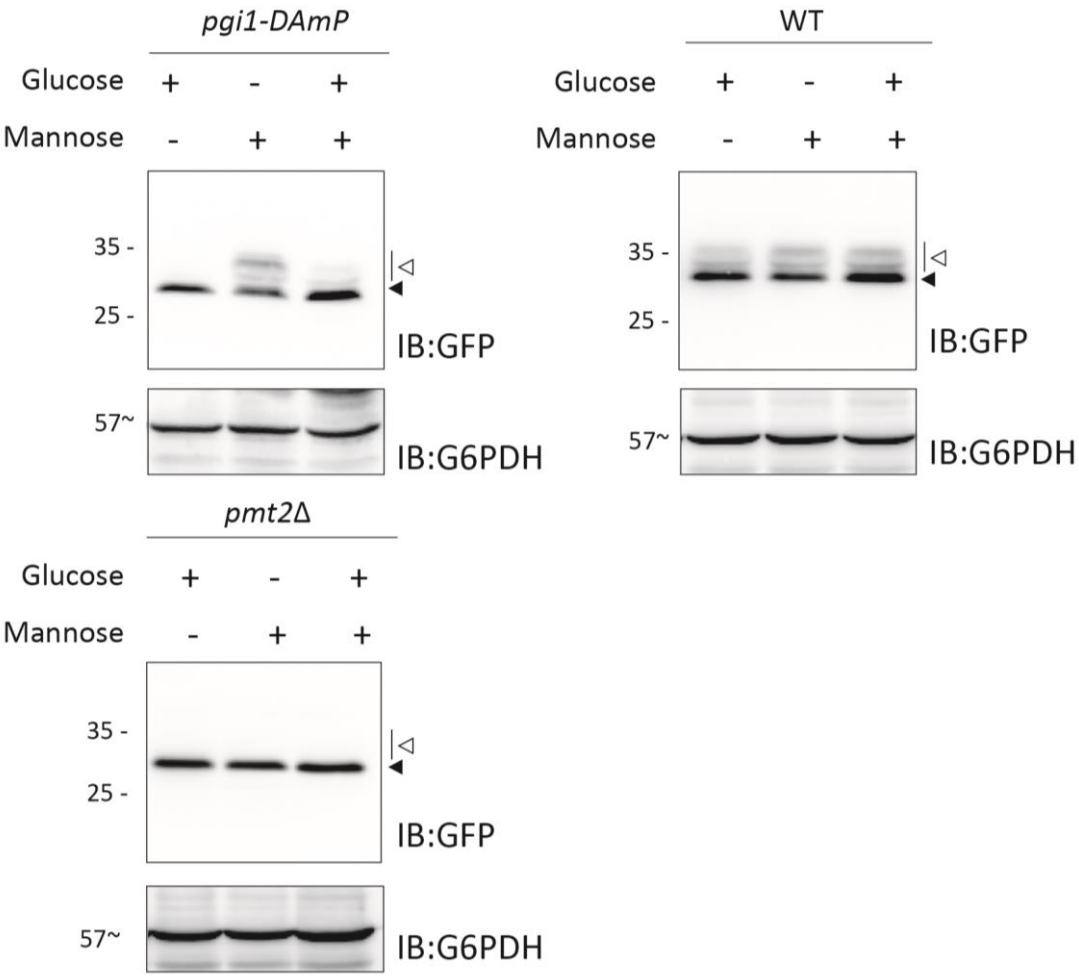

Figure 4.15. Characterization of the requirement of mannose supplementation in *pgi1-DAmP* for UPOM. Yeast strains JEY06 (wild type), JCY011 (*pmt2*Δ) and *pgi1-DAmP* ER-GFP (strain resulting from SGA crosses) were grown in synthetic medium using 2% of the indicated sugar as carbon source. Total cell extracts were prepared according to 3.4.2 and equivalents to 0.2 OD_{600} of protein were resolved on a 12% PAA gel and blotted with anti-GFP antibody. G6PDH served as a loading control. The presence of the *O*-mannosylated fraction of ER-GFP (indicated with a white arrow, see figure 4.5) depends on the presence of mannose as a carbon source. These experiments were performed by Dr. Daniela Bausewein in collaboration with the author.

Mannose supplementation resulted in the rescue of hypoglycosylation of ER-GFP in *pgi1-DAmP* as shown by the presence of the *O*-mannosylated fraction by western blot (indicated with white arrow). A combination of both glucose and mannose resulted in a partial rescue likely due to the preference of the cell to take up glucose. No evident effect of the presence of mannose on the *O*-mannosylation of ER-GFP was observed either wild type or *pmt2*Δ when using mannose, indicating that mannose supplementation does not impact severely in UPOM when *PGI1* remains unaffected.

To further characterize the functional relationship between *PGI1* and the PMT machinery a *pmt2Δpgi1-DAmP* double mutant was generated. In the absence of mannose, *pmt2Δpgi1-DAmP* exhibits a very strong growth defect that can be rescued by mannose supplementation (Figure 4.16). This indicates that the downregulation of *PGI1* and *O*-mannosylation defects have negative additive effects for growth and highlights that the mannose-based rescue of ER-GFP glycosylation can be also extended to a functional rescue.

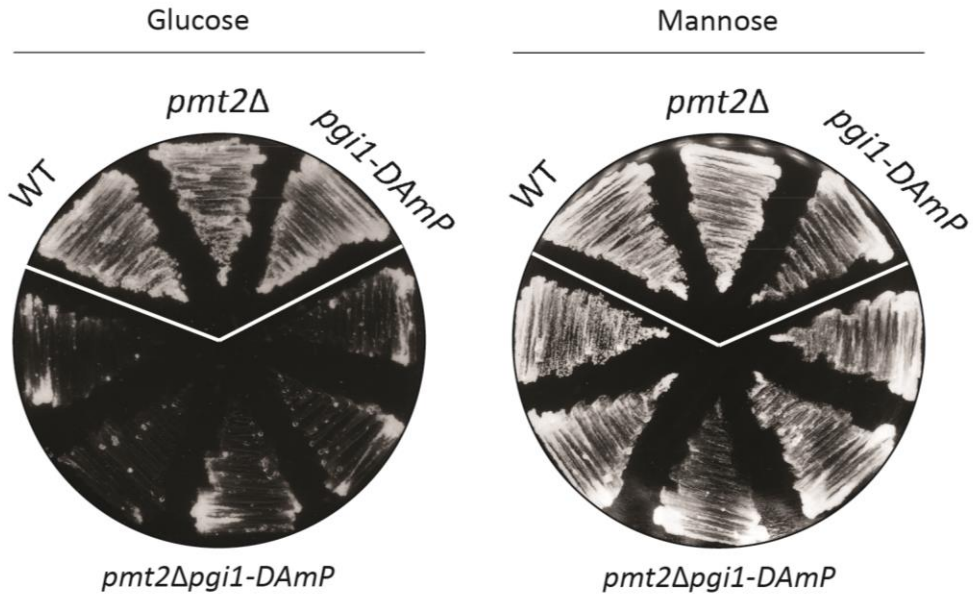

Figure 4.16. Characterization of the mannose-dependent negative genetic interaction between *PGI1* and *PMT2*. Yeast strains JEY06 (wild type), JCY011 (*pmt2*Δ) and JCY014 (*pgi1-DAmP)* were streaked together with five independent transformants of JCY033 (*pmt2*Δ*pgi1-DAmP*) on YP-based plates containing 2% of the indicated sugar as carbon source. Plates were imaged after 24h growth at 30 °C.

4.2.3.2 *PGI1* knockdown affects ER-homeostasis

The finding of *PGI1* as necessary for UPOM adds sugar metabolisms to the requirements for ER homeostasis. The idea of cytosolic sugar content influencing the efficiency of protein folding in the ER encouraged to characterize this relationship.

In 4.2.3.1 it is shown how mannose supplementation can rescue the hypoglycosylation phenotype of *pgi1-DAmP.* In order to check whether mannose is also able to influence protein folding ER-GFP was expressed in *pgi1-DAmP* and fluorescence intensity was measured by flow cytometry under different carbon source conditions.

For this specific assay, the non-retained version of ER-GFP (see 4.2.1.3) was used. *PGI1* has been described as one of the genes that when downregulated, results in the secretion of the ER-resident chaperone Kar2 (Copic *et al.*, 2009). By using the non-retained version of ER-GFP the ER retention defect in *pgi1-DAmP* was anticipated and prevented, which in turn would have biased the analysis.

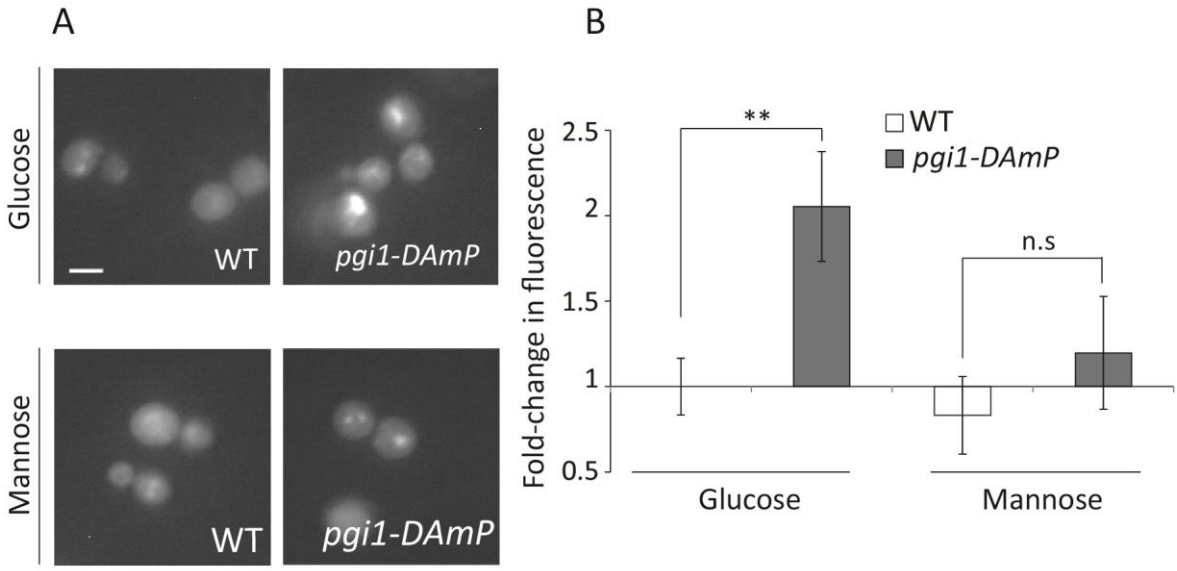

Figure 4.17. Characterization of the effect of mannose supplementation on ER-GFP folding in *pgi1-DAmP*. (**A**) Wild type (BY4741) and JCY014 (*pgi1-DAmP*) cells were transformed with pJC08 (non-retained ER-GFP), grown in SD-URA-based medium containing 2% of the indicated sugar as carbon source and imaged under standard conditions, scale bar 5µm. (**B**)The same strains were grown under identical conditions and analyzed by flow cytometry. R values indicative of the cell population's fluorescence intensity (see 3.5.3) are normalized to R_{WT} and results are plotted as fold-change. For statistical significance, a one-tail Student's test was applied (n=3).

Under mannose limiting conditions, the fluorescence intensity of ER-GFP in *pgi1-DAmP* was about 2-fold higher than in wild type cells (Figure 4.17). Consistent with the restoration of the *O*-mannosylation state of ER-GFP, mannose supplementation reduced fluorescence of *pgi1-DAmP* to almost wild type levels. No effect in fluorescence could be observed upon mannose supplementation in wild type cells (Figure 4.16). In conclusion from these results, upon *PGI1* knockdown, UPOM is impaired and hence inefficient folding of ER-GFP is not prevented.

In 4.1.2 it is shown that the absence of either *PMT1* or *PMT2* causes UPR activation. As discussed in 5.1, a valid explanation is that the Pmt1-Pmt2 complex actively contributes to the quality control of aberrant proteins in the ER, as it is shown for ER-GFP (Figure 4.5, C. Xu *et al.*, 2013). In *pgi1-DAmP*, quality control of ER-GFP is also prevented (Figure 4.17) suggesting that, by extension, UPR might be also activated to cope with a hypothetical increase in the load of unfolded proteins.

UPR in *pgi1-DAmP* activation was evaluated by quantitative RT-PCR analysis of UPR-related transcripts. This experiment yielded a clear increase in $HAC1^{S}$ and KAR2 levels in *pgi1-DamP* (6 and 3 fold-change, respectively) indicative of constitutive activation of the UPR (Figure 4.18B). Consistent with this, *pgi1-DAmP* cells were more sensitive to the ER stress agent tunicamycin (Figure 4.18A).

Given that mannose supplementation is able to restore quality control of ER-GFP (Figure 4.17), the effect of this rescue was also analyzed with regard to the UPR. Both UPR levels and growth sensitivity to tunicamycin in *pgi1-DAmP* were restored upon mannose supplementation making this mutant indistinguishable from wild type (Figure 4.18A and B). These results confirm *PGI1* as an important contributor to the ER protein quality control, expanding the requirements for proper ER homeostasis to the substrate sugar content in the cytosol.

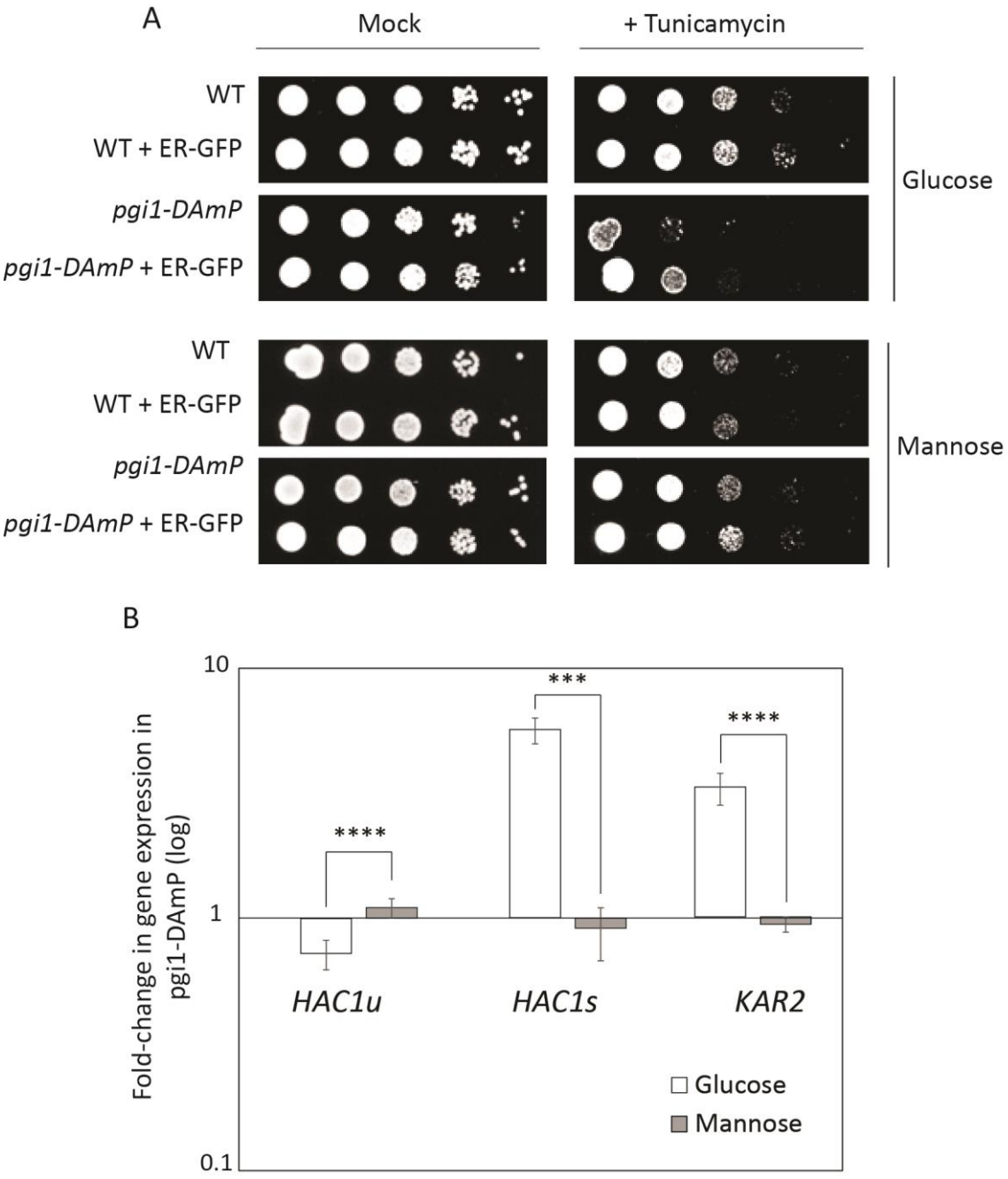

Figure 4.18. Characterization of the *pgi1-DAmP* mutant in the context of ER-stress. (**A**) Spotting assay of wild type (BY4741), wild type expressing ER-GFP (JEY06), JCY014 (*pgi1-DAmP*) and *pgi1-DAmP* ER-GFP (strain resulting from SGA crosses). Serial 10-fold dilutions cells were spotted on solid SD-based medium containing 2% of the indicated sugar as a carbon source together with no (control) or 0.5 µg/ml tunicamycin. This experiment was performed by Sven Klassa under the author's supervision and included in the bachelor thesis: "*Phosphoglucose isomerase 1 function in the frame of protein O-mannosylation and ER homeostasis"*, submitted to the Ruprecht-Karls-University (Heidelberg faculty of Biosciences) in 2017. (**B**) Fold- change in mRNA levels of $HAC1^{u}$, $HAC1^{s,}$ and KAR2 in JCY014 (*pgi1-DAmP*). Total RNA was extracted (3.2.3) from cells grown in YP-based medium containing 2% of the indicated sugar as a carbon source, cDNA was prepared (3.2.4) and used as a template for RT-PCR. Fold-change is calculated by averaging Cts with respect to *ACT1*. Errors bars show the confidence interval. For statistical significance one-tailed, t-Student's test was applied to log ($2^{-\Delta\Delta Ct}$), n=3.

4.2.4 The role of *BFR1* in UPOM

The deletion of *BFR1* was found to be an enhancer of fluorescence intensity and hence folding of the *O*-mannosylation reporter ER-GFP (Figure 4.19A and B). Western blot analysis confirmed the inefficient UPOM of ER-GFP as the cause of improved folding competence (4.2.2.1). In order to validate the results of the screen, a *BFR1* knockout was *de novo* generated in the parental wild type starting strain of the screen and measured the fluorescence of ER-GFP by flow cytometry (Figure App. 4). At this point, it is important to note that although the majority of the transformants confirmed by PCR showed the expected increase in fluorescence intensity there was significant variability among transformants.

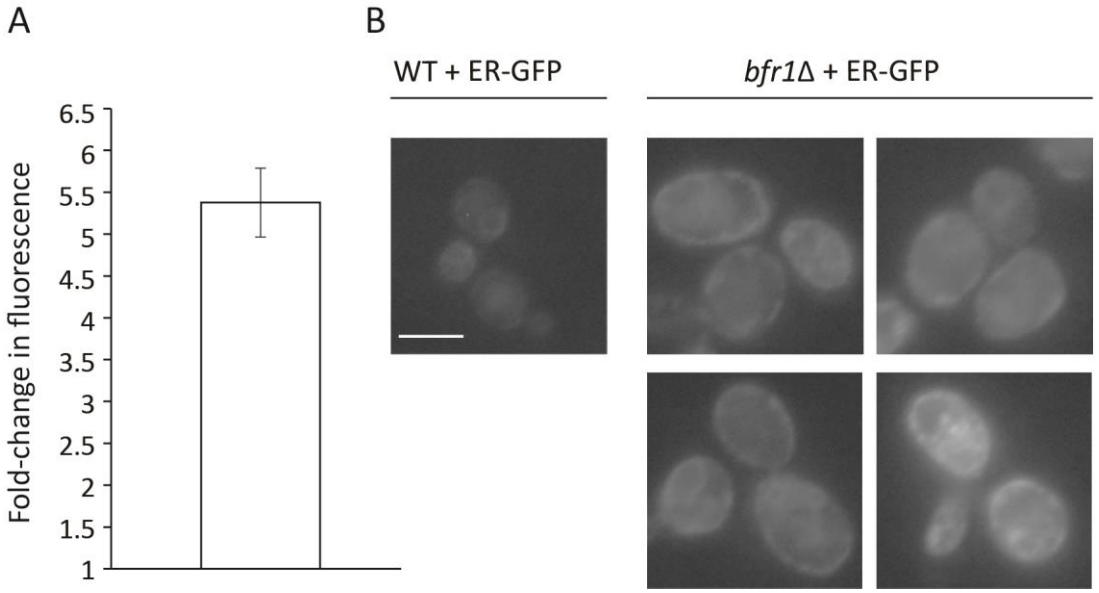

Figure 4.19. The deletion of *BFR1* enhances ER-GFP folding. (**A**) Flow cytometry of strains JEY06 (wild type expressing ER-GFP) and *bfr1*Δ ER-GFP (strain resulting from SGA crosses) grown in YPD under standard conditions. R values indicative of the cell population's fluorescence intensity (see 3.5.3) are normalized to R_{WT} and results are plotted as fold-change (n=3). (**B**) Microscopy of the same strains grown under identical conditions, scale bar 5 µM.

BFR1 encodes a 55 KDa cytosolic protein first identified as a multicopy suppressor of brefeldin A-induced lethality (Jackson & Kepes, 1994), suggesting a link of *BFR1* to protein secretion. Furthermore, this study also pointed out note worth phenotypes associated with *BFR1* deletion: abnormal cell ploidy described as pseudo haploidy, with polynucleated cells and non-nucleated cells found in the same population; and abnormally increased cell size.

Later studies showed Bfr1 as part of a ribonucleoprotein complex mainly represented by the protein Scp160 and associated with the polyribosome mRNP machinery (Lang *et al.*, 2001). Moreover, RNA immunoprecipitation (RIP)-CHIP experiments showed that Bfr1 is capable to associate with multiple RNAs (Hogan *et al.*, 2008). Since then, multiple functions related to mRNA post-transcriptional regulation have been assigned to Bfr1. On one hand, Bfr1 mediates the re-localization of certain mRNAs to P-bodies (Simpson *et al.*, 2014), which are conserved, complex and dynamic ribonucleoprotein complexes where mRNA de-adenylation and decay occurs (reviewed in Luo *et al.*, 2018). In terms of optimizing and adjusting the proper mRNA levels next to gene transcription, P-bodies become especially relevant under conditions that require attenuating protein translation such as cell starvation or stress. In this context, Bfr1 and Scp160 have been shown to prevent the appearance of P-bodies under normal conditions (Weidner *et al.*, 2014), suggesting a role as a gate for mRNA from polyribosomes to the decay system.

How can a cytosolic protein work in the context of mRNA transport and metabolism be linked to protein *O*-mannosylation? Insights to answer this question came with the publication of the mRNA targets of Bfr1 in a novel *in vivo* RNA tagging approach (Lapointe *et al.*, 2015). Interestingly, Bfr1 binds more than a 1000 mRNAs significantly enriched with transcripts that undergo ER-localized translation (Jan *et al.*, 2014), including PMT mRNAs as main Bfr1 targets. Therefore, although functionally unclear, the link of Bfr1 to mRNA regulation, and in particular along with PMTs being mRNA targets of Bfr1 raised the hypothesis of Bfr1 regulating the expression of PMTs and thereby impacting on *O*-mannosylation of ER-GFP.

4.2.4.1 *BFR1* deletion impacts negatively on the abundance of Pmt1 and Pmt2

To explore whether inefficient UPOM in *bfr1Δ* is a consequence of abnormal PMT expression the steady-state levels of Pmt1 and Pmt2 were quantified by Western blot. Considering the ER stress scenario triggered by the expression of ER-GFP, WT, and *bfr1Δ* without ER-GFP expression were included as controls.

In a no ER-stress scenario, the results of three independent experiments show a significant reduction of 2-fold in the protein level for both Pmt1 and Pmt2 when *BFR1* is deleted (Figure 4.20). Interestingly, Pmt1 and Pmt2 showed a reduction of 2-fold and 3.7-fold upon ER-GFP

expression, indicating that the upregulation of both PMTs, expected due to ER stress (see Figure 4.6), is also absent in *bfr1*Δ.

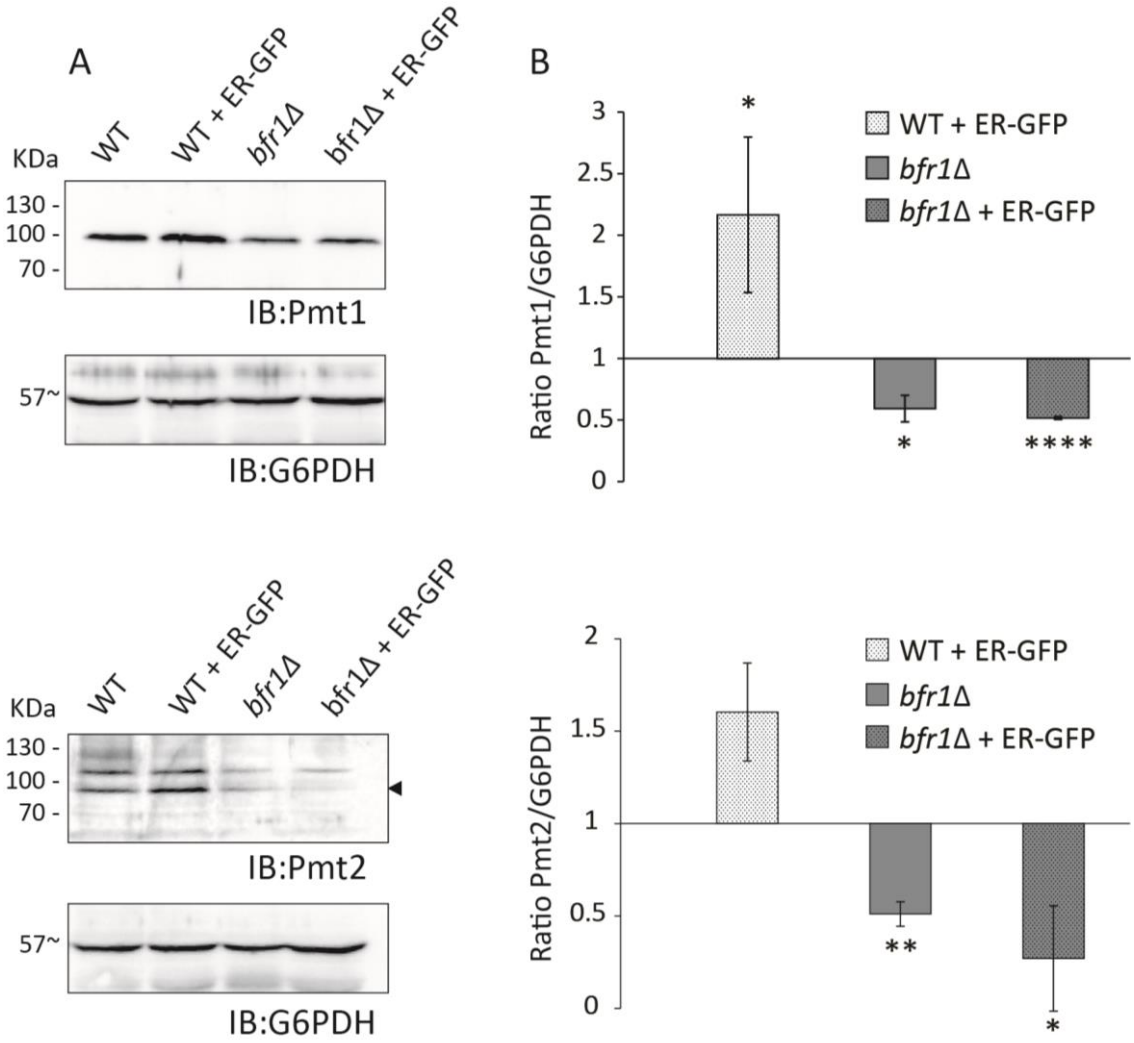

Figure 4.20. The deletion of *BFR1* affects negatively Pmt1 and Pmt2 protein levels. (**A**) Total cell extract was prepared from yeast strains wild type (BY4741), JEY06 (wild type ER-GFP), *bfr1*Δ (Euroscarf) and *bfr1*Δ ER-GFP (strain resulting from SGA crosses) grown in YPD under standard conditions. 20 µg of protein were resolved on a 12% PAA gel and subjected to Western blot analysis using either anti-Pmt1 or anti-Pmt2 antibody (Pmt2 signal indicated with black arrow). G6PDH served as a loading control. (**B**) Western blot signals were quantified using Image Studio Lite V.5.2 as a Pmt/G6PDH ratio, normalized to Pmt/G6PDH$_{WT}$, averaged and plotted as fold-change. For statistical significance, a one-tail Student's test was applied to averaged fold-change values (n=3).

As described in the literature, *bfr1*Δ cells display a very complex and pleiotropic phenotype that might impact in ER-GFP intensity at multiple levels. Therefore, in order to confirm that decreased protein abundance of PMTs is the reason for inefficient UPOM a functional rescue of *bfr1*Δ was performed by overexpressing *PMT2* from a centromeric plasmid. The

overexpression of *PMT2* results in a significant rescue of the ER-GFP intensity in *bfr1*Δ (Figure 4.21A), whereas no effect was detectable in wild type cells. This observation on wild type cells indicates that the rescue in *bfr1*Δ is due to the restoration of the physiological levels of Pmt2 to some extent and rules out that increasing the *PMT2* load over physiological levels impacts in ER-GFP folding. In line with this, overexpression of *PMT2* also restores the presence of the hypoglycosylated fraction of ER-GFP in *bfr1*Δ (Figure 4.21B), confirming that decreased PMT protein levels is the cause for increased ER-GFP folding in absence of Bfr1. Besides analyzing the rescue of UPOM, *PMT2* overexpression conditions were used to question whether Pmt2 abundance is also diminished in *bfr1*Δ when additional *PMT2* is expressed. These conditions would mimic the scenario of ER-GFP expression, where *PMT2* is transcriptionally upregulated via the UPR. When comparing Pmt2 steady-state levels under *PMT2* overexpression conditions *bfr1*Δ (with or without ER-GFP) fails to fully overexpress Pmt2 to the same extent as in wild type cells (Figure 4.21C, compare lanes two and four without ER-GFP expression and lanes six and eight with ER-GFP expression). Still, some increase in Pmt2 levels can be observed in *bfr1*Δ, explaining the partiality of the functional rescue observed in Figure 4.21A and indicating that Pmt2 expression is just reduced in *bfr1*Δ and not fully impeded.

One indicator of *O*-mannosylation capacity is the sensitivity to the general *O*-mannosylation inhibitor R3A-5a (Arroyo *et al.*, 2011). Consistent with the reduction in the levels of Pmt1 and Pmt2 in absence of Bfr1, a previous study showed *bfr1*Δ to be significantly more sensitive to R3A-5a (Zatorska *et al.*, 2017). In order to confirm the data and to test whether *PMT2* overexpression is also able to rescue sensitivity to R3A-5a in *bfr1*Δ a spotting assay was performed (Figure 4.22). A mild decrease in cell growth upon R3A-5a could be observed for *bfr1*Δ independently of ER-GFP expression (indicated with black arrows), supporting decreased *O*-mannosylation capacity. However, in this assay, overexpression of *PMT2* was unable to rescue the R3A-5a sensitivity phenotype in either case, suggesting that although *PMT2* overexpression is enough to restore UPOM of ER-GFP, the rescue of the general *O*-mannosylation capacity likely requires complementation with also *PMT1* or even with additional PMTs. These results indicate that the reduction in the Pmt1 and Pmt2 levels in *bfr1*Δ compromise the efficiency of *O*-mannosylation and highlight that the role of Bfr1 is not restricted to UPOM, but it also involves *O*-mannosylation in general. In agreement, *bfr1*Δ was clustered among the *pop2*Δ-like mutants when analyzing Hsp150 (Figure 4.11) and has

been shown to have negative genetic interaction with *PMT1* and *PMT2* (Schuldiner *et al.*, 2005) suggesting that they work in parallel pathways.

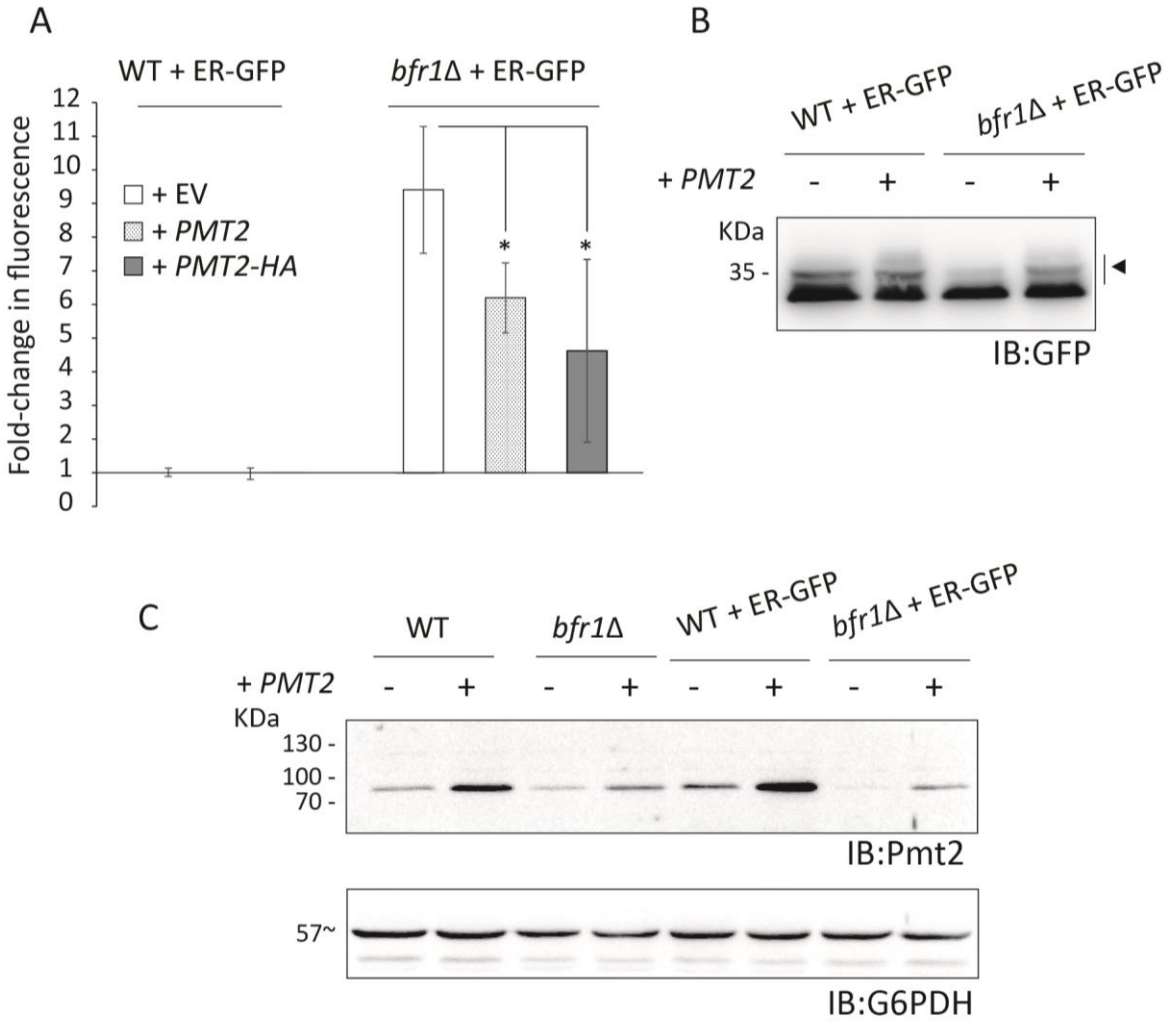

Figure 4.21. (**A**) *PMT2* overexpression partially rescues ER-GFP fluorescence in *bfr1*Δ. Flow cytometry analyses of JEY06 (wild type ER-GFP) and *bfr1*Δ ER-GFP expressing either pRS41N (empty vector, EV), pJC09 (*PMT2*) or pJC10 (*PMT2-3xHA*) grown under standard conditions in YPD supplemented with nourseothricin for selection. R values indicative of the cell population's fluorescence intensity (see 3.5.3) are normalized to R_{WT} and results are plotted as fold-change. For statistical significance, a one-tail Student's test was applied (n=3). (**B**) Total cell extract was prepared from the same strains as in A transformed with either pRS41N or pJC09 and grown under identical conditions. 20 µg of protein were resolved on a 12% PAA gel and subjected to Western blot analysis using anti-GFP antibody. *O*-mannosylated fraction (indicated with black arrow) is restored by *PMT2* overexpression in *bfr1*Δ. (**C**) *bfr1*Δ cells fail to fully overexpress *PMT2*. Total cell extracts were prepared from wild type (BY4741), *bfr1*Δ, JEY06 (wild type ER-GFP) and *bfr1*Δ ER-GFP transformed with either pRS41N or pJC09 and grown as in A. 20 µg of protein were resolved on a 12% PAA gel and blotted with anti-Pmt2 antibody. G6PDH served as a loading control.

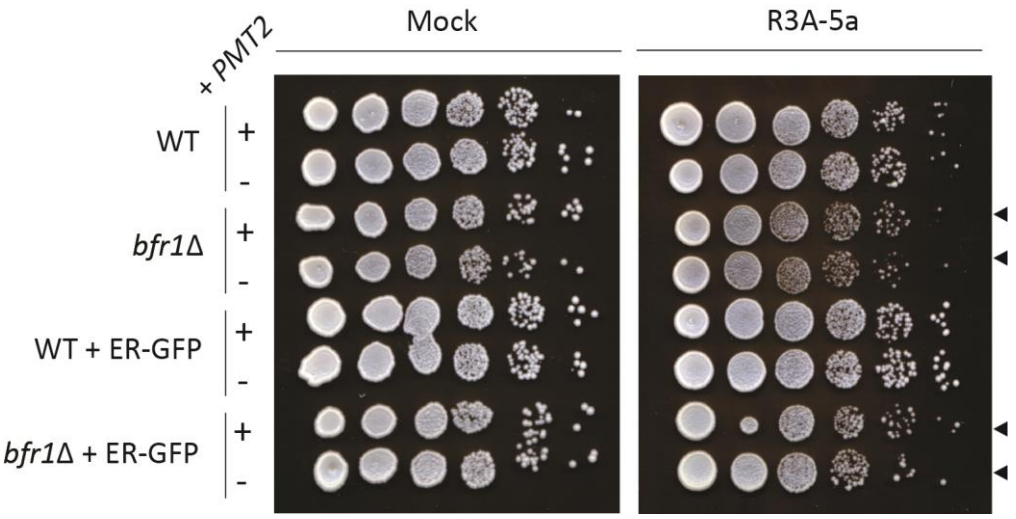

Figure 4.22. Spotting assay of wild type (BY4741), *bfr1*Δ, JEY06 (wild type expressing ER-GFP) and *bfr1*Δ ER-GFP expressing either pRS41N (empty vector, EV) or pJC09 (*PMT2*). Serial 10-fold dilutions cells were spotted on solid YPD medium containing nourseothricin for selection together with no (control) or 5 µM of the PMT inhibitor R3A-5a (Arroyo *et al.*, 2011) and grown at 30 °C for 24h. *bfr1*Δ are slightly more sensitive to R3A-5a (indicated with black arrows).

Before addressing how Bfr1 regulates PMT protein expression, the reduction in protein levels of other Bfr1 targets was investigated. As shown in Lapointe *et al.*, 2015, Bfr1 preferentially targets transcripts coding for secretory proteins, some of them functionally linked to PMTs. Bfr1 targets representative for different protein classes linked to *O*-mannosylation were selected and analyzed their protein abundance in *bfr1*Δ. Among the Bfr1 targets selected there is Gas1 as representative for GPI-anchored proteins (Nuoffer *et al.*, 1991), Kar2 as soluble ER Hsp70 chaperone (Rose *et al.*, 1989), Ost3 and Wbp1 as subunits of the OST complex (te Heesen *et al.*, 1992; Karaoglu *et al.*, 1995) and Sec61 as main subunit of the translocon complex (Deshaies & Schekman, 1987). Despite the previously observed increased values of Kar2 upon ER-GFP expression (Figure 4.6), no significant differences were found in the protein abundance of other Bfr1 targets upon *BFR1* deletion (Figure 4.23, Figure App.5), restricting the effect on protein expression to PMTs, so far. The specificity observed for PMTs over other Bfr1 transcript targets implies that the capacity to interact with Bfr1 does not necessarily result in a change in protein expression. In addition to binding, Bfr1 must drive additional events for PMT transcripts that result in correct protein expression.

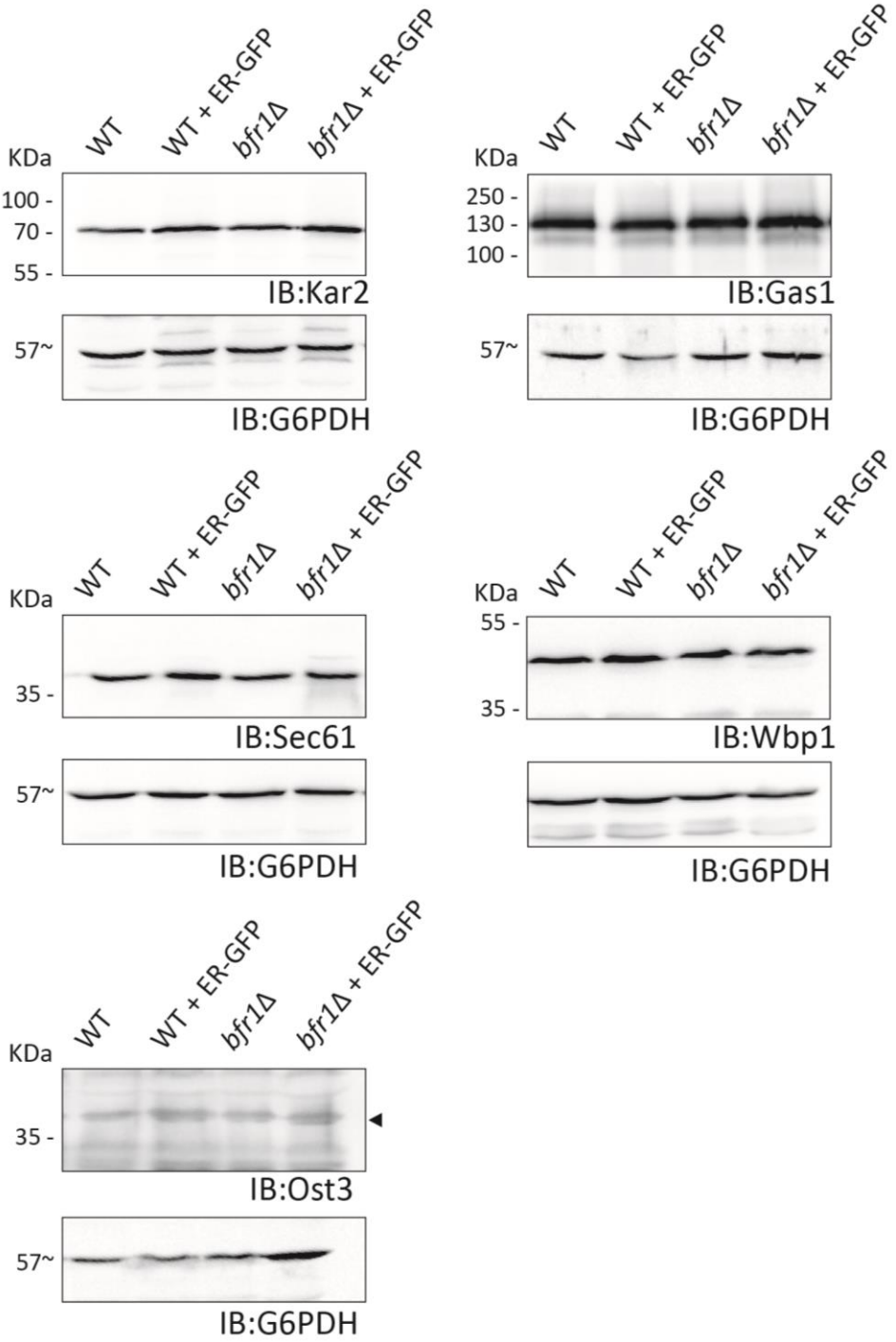

Figure 4.23. *BFR1* deletion does not affect the steady-state levels of other representative secretory proteins. Total cell extract was prepared from yeast strains wild type (BY4741), JEY06 (wild type ER-GFP), *bfr1*Δ (Euroscarf) and *bfr1*Δ ER-GFP (strain resulting from SGA crosses) grown in YPD under standard conditions. 20 µg of protein were resolved on a 12% PAA gel and subjected to Western blot analysis using the indicated antibodies. G6PDH served as a loading control. Proteins analyzed are described as Bfr1 targets at the mRNA level according to (Lapointe *et al.*, 2015). Quantification of the Western blot signals based on three biological replicates is shown in Figure App.5.

PMT protein abundance does not correlate with transcript levels

4.2.4.2

Given that *BFR1* is suggested in the literature to play a role in mRNA transport and very closely linked functionally to mRNA catabolism (Simpson *et al.*, 2014; Weidner *et al.*, 2014), whether the decrease in Pmt1 and Pmt2 protein abundance is a consequence of decreased transcript level was analyzed by RT-PCR.

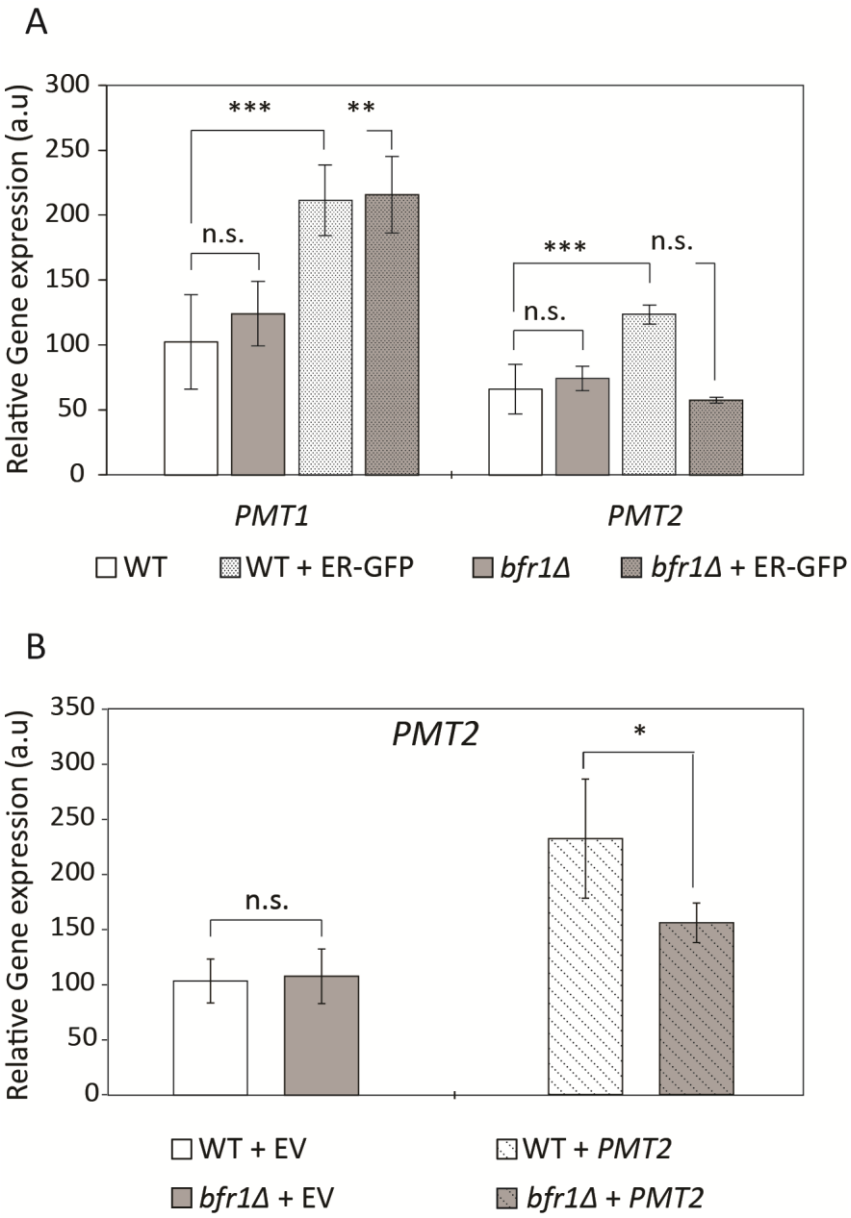

Figure 4.24. Relative mRNA levels of *PMT1* and *PMT2* in wild type (BY4741), JEY06 (wild type ER-GFP), *bfr1*Δ (Euroscarf) and *bfr1*Δ ER-GFP (strain resulting from SGA crosses) (**A**); and *PMT2* in wild type (BY4741) and *bfr1*Δ (Euroscarf), expressing either pRS41N (empty vector, EV) or pJC09 (*PMT2*) (**B**) grown in YPD or YPD supplemented with nourseothricin. cDNA was prepared from total mRNA according to 3.2.3 and 3.2.4 and RT-PCR was performed according to 3.2.9. Results show averages of PMT1 and PMT2 mRNA abundance ± SD with respect to *TAF10* (**A**) or *ACT1* (**B**)**.** For statistical significance, a two-tailed t-Student's test was applied (n=3).

When comparing wild type and *bfr1*Δ, no difference in the transcript level was observed for either *PMT1* or *PMT2*. In contrast, upon ER-GFP expression, which results in a 2-fold transcriptional upregulation of both PMTs in wild type cells, such an increase in transcript level was absent specifically for *PMT2* in *bfr1*Δ (Figure 4.24A). In agreement, a similar reduction of the *PMT2* transcript level is observed in *bfr1*Δ in comparison to wild type under *PMT2* overexpression conditions (Figure 4.24B).

These data pictures a complex scenario where two conclusions were drawn: First, comparable *PMT1* and *PMT2* transcript levels between wild type and *bfr1*Δ result in lower protein abundance in *bfr1*Δ. Second, when *PMT2* is overexpressed at the mRNA level, either mediated the UPR caused by ER-GFP expression or by extra copies of *PMT2*, *bfr1*Δ affects specifically *PMT2* transcript levels.

Likely the reduction in *PMT2* transcript observed in *bfr1*Δ upon ER-GFP expression contributes to the hypoglycosylation of ER-GFP. However, *PMT2* transcript decrease occurs only upon the excess of *PMT2* expression. This suggests that the general role of Bfr1 in PMT protein expression is independent of the changes observed at the mRNA level for *PMT2*.

Given that Bfr1 is described to function in the context of mRNA processing, further analyses were performed to explain the effect observed for *PMT2* transcript in *bfr1*Δ upon stress. The inability of *bfr1*Δ ER-GFP to produce or maintain correct levels of *PMT2* transcript upon ER stress can be due to transcriptional downregulation as well as enhanced mRNA turnover. Since the Bfr1 function is somehow linked to P-body formation, both questions were addressed by replacing the *PMT2* native promoter by the *GAL1* inducible promoter (P_{GAL1}). P_{GAL1} is known to be tightly repressed in cells grown in glucose and to drive a strong overexpression in cells grown in galactose. The strain selected included PMT2-HA-tagged driven by P_{GAL1} and an *N*-terminal UbiR protein degron (Hwang *et al.*, 2010), which works as a signal for proteasomal degradation. The reason for using a degradable Pmt2-HA version is that a growth defect was detected when overexpressing *PMT2-HA* in particular in *bfr1*Δ (Figure App. 7, indicated with black arrow) and therefore the potential lethality that could result by the strong overexpression driven by P_{GAL1}in *bfr1*Δ was anticipated. Yet, the reason behind why specifically HA-tagged *PMT2* is harmful to *bfr1*Δ cells in contrast to untagged *PMT2* remains unknown.

Analysis of Pmt2-HA expression under the control of P_{GAL1} showed that the deletion of *BFR1* results in lower protein abundance in comparison to wild type (Figure 4.25A). Upon

replacement of *PMT2* promoter, no difference in P_{GAL1}-PMT2-HA transcript level was observed between wild type and *bfr1*Δ (Figure 4.25B, left panel), and identical results were obtained when expressing ER-GFP (Figure 4.25B, right panel) indicating that the reduction in native PMT2 transcript level observed in Figure 4.24 is promoter-dependent.

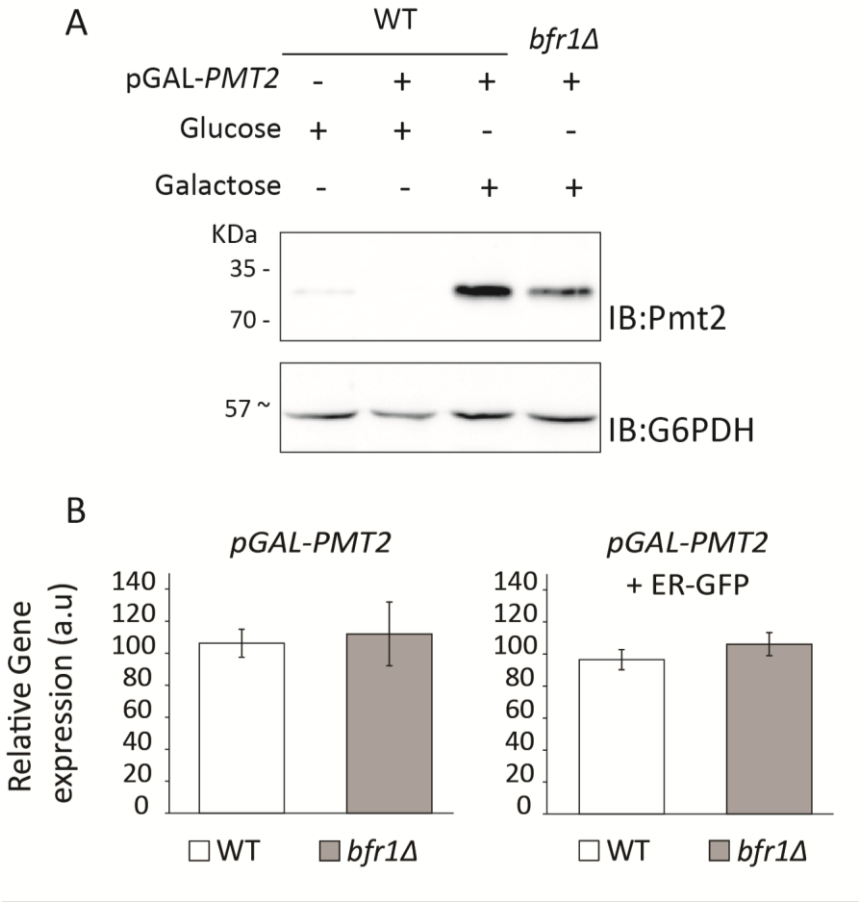

Figure 4.25. The effect of *BFR1* deletion on *PMT2* transcript level is promoter-dependent. (**A**) Total cell extract was prepared from yeast strains MLY014 (wild type, *PMT2-3xHA*), MLY098 (wild type, P_{GAL1}-*UBI4*-R-*PMT2)* and JCY034 (*bfr1*Δ, P_{GAL1}-*UBI4*-R-*PMT2-HA*) grown in YP medium containing 2% of the indicated sugar. Equivalent of 0.2 OD_{600} (lanes 1 and 2) or 20 µg protein (lanes 3 and 4) were resolved on a 12% PAA gel and subjected to Western blot analysis using anti-Pmt2 antibody. G6PDH served as loading control. (**B**) Relative *PMT2* mRNA levels in MLY098 (wild type, P_{GAL1}-*UBI4*-R-*PMT2-HA)* and JCY034 (*bfr1*Δ, P_{GAL1}-*UBI4*-R-*PMT2-HA*) (left panel) or in the same strains transformed with pJC16 (ER-GFP) (right panel) grown in YP or synthetic medium (left and right panel, respectively) containing 2% Galactose as carbon source. Results show averages ± SD with respect to or *ACT1,* (n=3).

In addition, the capacity of P_{GAL1} to be repressed by glucose was used to perform a transcriptional shutdown and the turnover of P_{GAL1}-PMT2-HA transcript was analyzed over time. As anticipated by the comparable steady-state mRNA levels (Figure 4.25B), no

significant changes were detected in the P_{GAL1}-PMT2-HA mRNA decay with or without ER-GFP expression (Figure 4.26).

As a conclusion from these results, the reduction observed in the *PMT2* transcript in *bfr1*Δ is uncoupled from the defects in PMT protein expression. Despite the effect at the transcript level likely contributes to the hypoglycosylation phenotype in *bfr1*Δ, it is promoter-dependent and possibly caused by downstream effects of *BFR1* deletion.

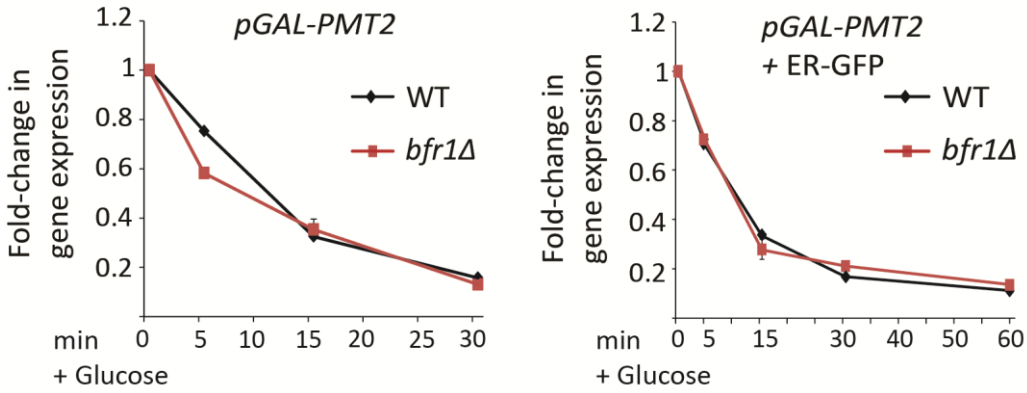

Figure 4.26. PMT2 mRNA decay is not affected in *bfr1*Δ. MLY098 (wild type, P_{GAL1}-*UBI4*-R-*PMT2-HA)* and JCY034 (*bfr1*Δ, P_{GAL1}-*UBI4*-R-*PMT2-HA*) (left panel) or in the same strains transformed with pJC16 (ER-GFP) (right panel) were grown in YP or synthetic medium (left and right panel, respectively) containing 2% Galactose as carbon source. Glucose was added to the medium at t_0 and fold-change in *PMT2* transcript abundance is calculated by averaged Cts with respect to *ACT1* at the indicated time points and normalized to t_0. Errors bars show the confidence interval.

4.2.4.3 Bfr1 is involved in the translation of PMTs and PMT-related transcripts

Decreased PMT protein abundance (Fig 4.20) while unchanged transcript levels in *bfr1*Δ under standard conditions (Fig 4.24) suggested a defect in protein production. Bfr1 has been shown to interact with translating ribosomes (Lang *et al.*, 2001) but no functional relationship to translation is known to date.

In order to explore potential defects in PMT mRNA translation in the *bfr1*Δ mutant, a ribosome profiling experiment was carried out for both wild type and *bfr1*Δ cells in collaboration with the group of Prof. Bern Bukau and Dr. Güenter Kramer (Zentrum für Molekulare Biologie, Heidelberg, Germany). The experiments were performed by Ilgin Kotan and are detailed in methods (see 3.6.1).

Ribosome profiling compares the abundance of ribosome-protected mRNA footprints of all translating ribosomes allowing to obtain a snapshot of the translatome under desired conditions (Figure 4.27A, Becker *et al.*, 2013; Doring *et al.*, 2017). A ratio of transcript abundance determined by RNA deep sequencing was obtained between *bfr1*Δ and wild type for every ORF in yeast based on normalized values of sequencing reads (RPKM, Reads Per Kilobase per Million) of the respective footprints. The experiment was performed in duplicate for both yeast strains wild type and *bfr1*Δ. In both cases, data sets showed a high correlation (coefficient of determination r^2 of 0.99 and 0.97 for wild type and *bfr1*Δ, respectively, Figure App.9). When comparing wild type and *bfr1*Δ translatome high correlation was also observed (r^2 of 0.97, Figure 4.27B), indicating no major defects on general translation. This is consistent with the analysis of polyribosomes of *bfr1*Δ shown in Lang *et al.*, 2001.

First focusing on *PMT1* and *PMT2,* RNA deep sequencing data showed about 1.7 fold reduction in the presence of both *PMT1* and *PMT2* among the ribosome-protected footprints in *bfr1*Δ ($RPKM_{bfr1\Delta}/RPKM_{WT}$ ratios of 0.58 and 0.59, respectively), revealing a decrease in the engagement of PMT1 and PMT2 transcripts to ribosomes in absence of *BFR1* (Figure 4.27B, App. Data 1). In addition to PMT1 and PMT2, all other different PMT family members (PMT3, 4, 5 and 6) are also found to be downregulated in *bfr1*Δ with $RPKM_{bfr1\Delta}/RPKM_{WT}$ ratios below 0.6 in all cases (App. Data 1). Since the underrepresentation of *PMT1* and *PMT2* footprints in *bfr1*Δ was consistent with the reduction observed at the protein level (Figure 4.20) these values were used as a basis to set a threshold to define significant changes in footprint distribution of 1.5 fold-change for both –under and overrepresented footprints in *bfr1*Δ. The additional ER proteins analyzed in *bfr1*Δ showing no obvious change in abundance (Figure 4.23) serve as negative controls for the translatome data. Based on the 1.5 fold-change threshold, Sec61, Gas1, Ost3, and Wbp1 appear to be unchanged whereas similar to PMTs, Kar2 shows approximately 1.7 fold reduction in *bfr1*Δ translatome. The reason behind the inconsistency between ribosome profiling and western blot data for Kar2 is unknown.

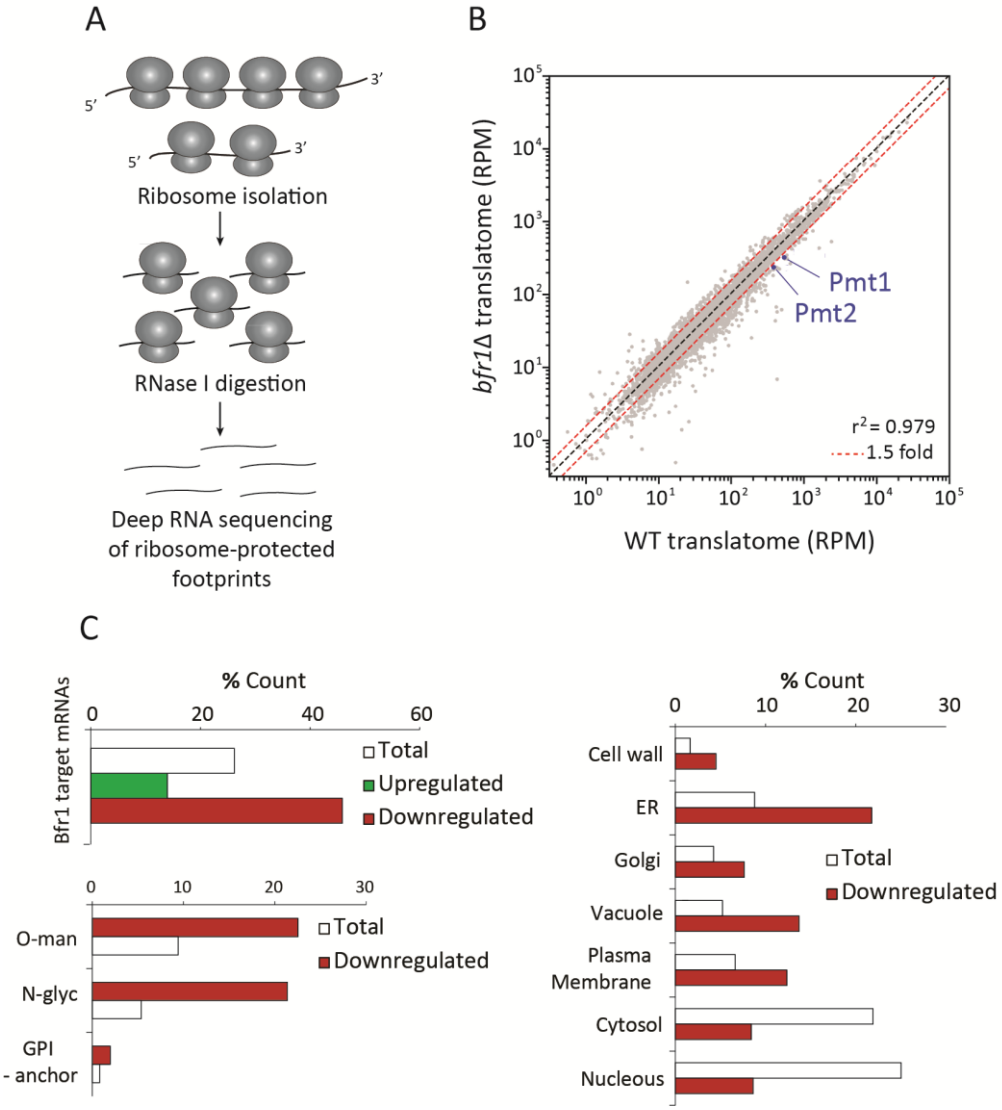

Figure 4.27. Ribosome profiling of *bfr1*Δ. (**A**) Workflow of a ribosome profiling approach to obtain a snapshot of the translatome (see 3.6). The total ribosome fraction was isolated from wild type (BY4741) and *bfr1*Δ (Euroscarf) in duplicate and digested with RNase I. Ribosome footprints remain protected from digestion and represent the mRNA fraction being actively translated in the cell. mRNA footprints were further isolated and subjected to deep RNA sequencing, assigned to the corresponding ORF and quantified on reads per million (RPM). For translatome comparison RPMs were normalized to the corresponding transcript length (reads per kilobase per million, RPKM). (**B**) Scatter plot illustrating the correlation between wild type and *bfr1*Δ translatome. *PMT1* and *PMT2* appear as underrepresented footprints in *bfr1*Δ. Red dashed lines account for the 1.5 fold change threshold applied to define translatome changes upon *BFR1* deletion, (n=2). (**C**) Analyses of functional categories enriched among ORFS below and/or above the threshold with respect to the total translatome. Gene annotation is based on (Lapointe *et al.*, 2015) for Bfr1 targets, (Neubert *et al.*, 2016) for *O*-mannosylated proteins, (Zielinska *et al.*, 2012) for *N*-glycosylated proteins, (Pittet & Conzelmann, 2007) for GPI-anchored proteins and SGD (Saccharomyces genome database) and UniportKB/Compartments databases for cell compartment localization.

By applying the 1.5 fold-change threshold, about 10% (510) of the measured ORFs were considered as underrepresented in *bfr1*Δ, whereas 5% (258) were overrepresented.
When mining the available data on Bfr1 transcript targets (Lapointe *et al.*, 2015) a significant enrichment of Bfr1 known targets was found among underrepresented ORFs in comparison with the entire translatome (45 % versus 26%, respectively) (Figure 4.27C, upper panel; App. Data 1). On the contrary, such overlap does not hold true when looking at the overrepresented ORF fraction, where only 14% are known targets of Bfr1. This observation, together with the higher number of ORFs that are downregulated suggests that *BFR1* positively affects translation of its transcript targets, whereas upregulated ORFs are mainly unrelated to Bfr1 function and might respond to a compensatory mechanism for *BFR1* loss.

In order to gain insight on the biological relevance of Bfr1 at the translation level, downregulated ORFs were clustered based on their annotated cell localization and their distribution in the translatome was analyzed (Figure 4.27C, right panel). Interestingly, secretory proteins localizing to the ER, Golgi, vacuole, plasma membrane or cell wall were enriched among downregulated transcripts when comparing to the total translatome, whereas cytosolic and nuclear proteins were dis-enriched. Moreover, similar enrichment within downregulated transcripts was observed when looking at the distribution of *O*-mannosylated, *N*-glycosylated or GPI-anchored proteins. This indicates that together with PMTs, mainly other secretory proteins rely on Bfr1 for effective translation. Whether the effect on the translatome impacts on the steady-state protein abundance for those downregulated ORFs as it is the case for PMTs is still pending of investigation.
In addition, gene ontology analysis was performed for the genes that rely on Bfr1 for translation (ORFs below the 1.5 fold-change, Figure 4.28). The most enriched clusters showed terms closely linked to protein *O*-mannosylation: *glycosylation*, *GPI anchor metabolic process* or *response to endoplasmic reticulum stress*. Most ORFs are clustered as *intrinsic component of membranes* and *hexosyl transferase*, *across-membrane transport* or *oxidoreductase activity* terms were also highlighted, rendering a functionally and spatially interconnected catalog of Bfr1 clients.
What determines the dependence on Bfr1 for effective translation besides the described interaction at the mRNA level for many of them (Lapointe *et al.*, 2015, Figure 4.27C, left-upper panel) still remains unknown.

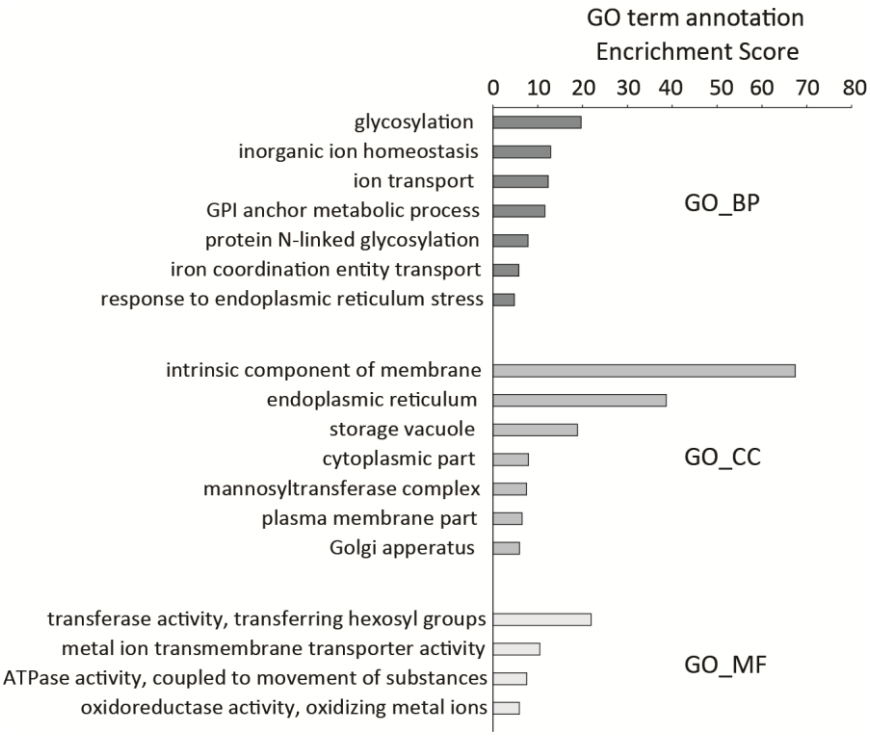

Figure 4.28. Gene ontology analysis of ORFs underrepresented in the translatome of *bfr1Δ*. GO term enrichment analysis using DAVID (v6.8). GO term enrichment was performed on 504 ORFs considered as downregulated in the ribosome profiling experiment (Figure 4.27B, App. Data 1) using GO ALL terms, a very stringent EASE score of 0.0001, and the *S. cerevisiae* reference list. Enrichment scores were extracted for the respective GO term clusters and clusters were named by representative terms. Biological process (GO_BP), molecular function (GO_MF) and cellular compartment (GO_CC) are shown.

In order to approach the potential molecular mechanism behind Bfr1 function, metagene analyses of footprint distribution along the mRNA sequences was performed for the downregulated ORFs (see Doring *et al.*, 2017 as an example), revealed a slight trend of increased ribosome occupancy in the first 100 codons in *bfr1*Δ relative to wild type (Figure App. 9C), suggestive of defects in translation elongation. However, the weakness of the observed effect and the data available are not enough to robustly conclude whether the translational speed is certainly affected.

In conclusion, these data indicate that Bfr1 is required for effective translation of *PMT1* and *PMT2*. Furthermore, 510 ORFs whose expression is also hampered by the absence of Bfr1 were identified. Most ORFs identified as Bfr1-dependent for translation are proteins localizing to the different organelles of the secretory pathway and that mainly fulfill functions at least partially related to protein *O*-mannosylation. The molecular mechanism of the Bfr1 function is yet to be elucidated since at the time of this current work more specialized analysis of the ribosome profiling data is part of the future perspectives. Both the

implications of these findings in the context of *O*-mannosylation and insights on the potential molecular mechanisms are outlined in the discussion (see 5.3).

PMT mRNA localization to the ER-membrane is Bfr1-independent

4.2.4.4 Bfr1 is required for the translation of *PMT1* and *PMT2* gene products. One immediate question that arises after the ribosome profiling data is whether the function of Bfr1 is restricted to translation when the ribosomal subunits have assembled or rather implies some sort of RBP-dependent mRNA localization mechanism. Transcript localization in eukaryotes is long known to be a source for directed protein synthesis not only providing polarity during cell differentiation but also contributing to optimize protein translation and translocation into different cell organelles (Beach *et al.*, 1999; Singer-Kruger & Jansen, 2014). Previous evidence of ER localization has been already shown for *PMT2* transcript in an *in vivo* mRNA localization study (Kraut-Cohen *et al.*, 2013). The well-known model of translation-dependent protein targeting to the ER via signal recognition particle (SRP) would predict the hydrophilic amino acid sequence of transmembrane domains of PMTs to act as a signal for ER delivery (reviewed in Aviram & Schuldiner, 2017). There is however emerging evidence of protein targeting mechanisms to the ER that rely not on the protein sequence but in signals present in the mRNA itself (Kraut-Cohen & Gerst, 2010).

In this context, one role shown for Bfr1 is mRNA transport to P-bodies upon glucose starvation (Simpson *et al.*, 2014). Also, Scp160, which forms a complex with Bfr1 (Lang *et al.*, 2001) has been described in the context of specific mRNA localization during mating (Guo *et al.*, 2003). The fact that most ORFs affected in *bfr1*Δ are enriched for secretory proteins (Figure 4.27C) raised the hypothesis of Bfr1 mediating mRNA transport of specific PMT transcripts to the ER, where they are translated (Jan *et al.*, 2014), perhaps as a backup mechanism to optimize ER targeting when SRP is inefficient.

ER localization of PMT transcripts was analyzed by two parallel strategies of subcellular fractionation. In a first approach, sucrose step-gradient centrifugation of total cell extracts was performed and the fractions containing the interphase between each step were selected (Figure 4.29A). In order to track the cellular localization of Bfr1 in the gradient, a C-terminal HA-tagged *BFR1* shown to keep the functionality of the protein (Fig App. 6) was used as a wild type strain.

Analysis of the mRNA content of the fractions showed enrichment of ribosomes in two pools represented by fractions F2 and F3 (Figure 4.29A and B). As a control the experiment was performed under EDTA conditions and both, a shift of the Abs_{260} peaks to soluble fractions and disassembly of the ribosomal subunits were observed (Figure App.7A). Ribosome-rich fraction F2 contained residual cytosolic G6PDH whereas Sec61 was exclusively found in F3, confirming successful isolation of ER-associated and ER-free ribosomal cell pools in F2 and F3 fractions, respectively. Bfr1-HA was present in all fractions together with the ribosomal 60S subunit protein Rpl5, consistent with the described engagement of Bfr1 protein with the translation machinery (Figure 4.29C, Lang *et al.*, 2001). Analysis of the mRNA of F2 and F3 by semi-quantitative RT-PCR (Figure 4.25D) yielded strong engagement of *PMT1*, *PMT2* and *SEC61* transcripts to ER-associated ribosomes (F3) whereas for *ACT1* transcript was also significantly present at the ER-free ribosome pool (F2). It not surprising to observe *ACT1* transcript, coding for a cytosolic protein, associated with the ER since it is postulated that this organelle works as a hub for general translation, including proteins that function at the cytosol (Diehn *et al.*, 2000). When analyzing *bfr1*Δ, no changes were observed in the distribution of these transcripts in all cases.

In a second approach, total cell membranes were isolated by ultracentrifugation and the presence of specifically *PMT2* transcript associated with either the membrane (TM) or the soluble fraction (SF) was analyzed. Western blot on soluble and membrane fractions confirmed successful isolation of Sec61-containing membranes whereas G6PDH was found exclusively in the soluble fraction (Figure 4.30A). Both fractions contained ribosomes (Figure App.8). When analyzing the presence of *PMT2* mRNA, one of the advantages of this strategy is that the simplicity of separating the cell in only two fractions allows relative quantification by standard RT-PCR.

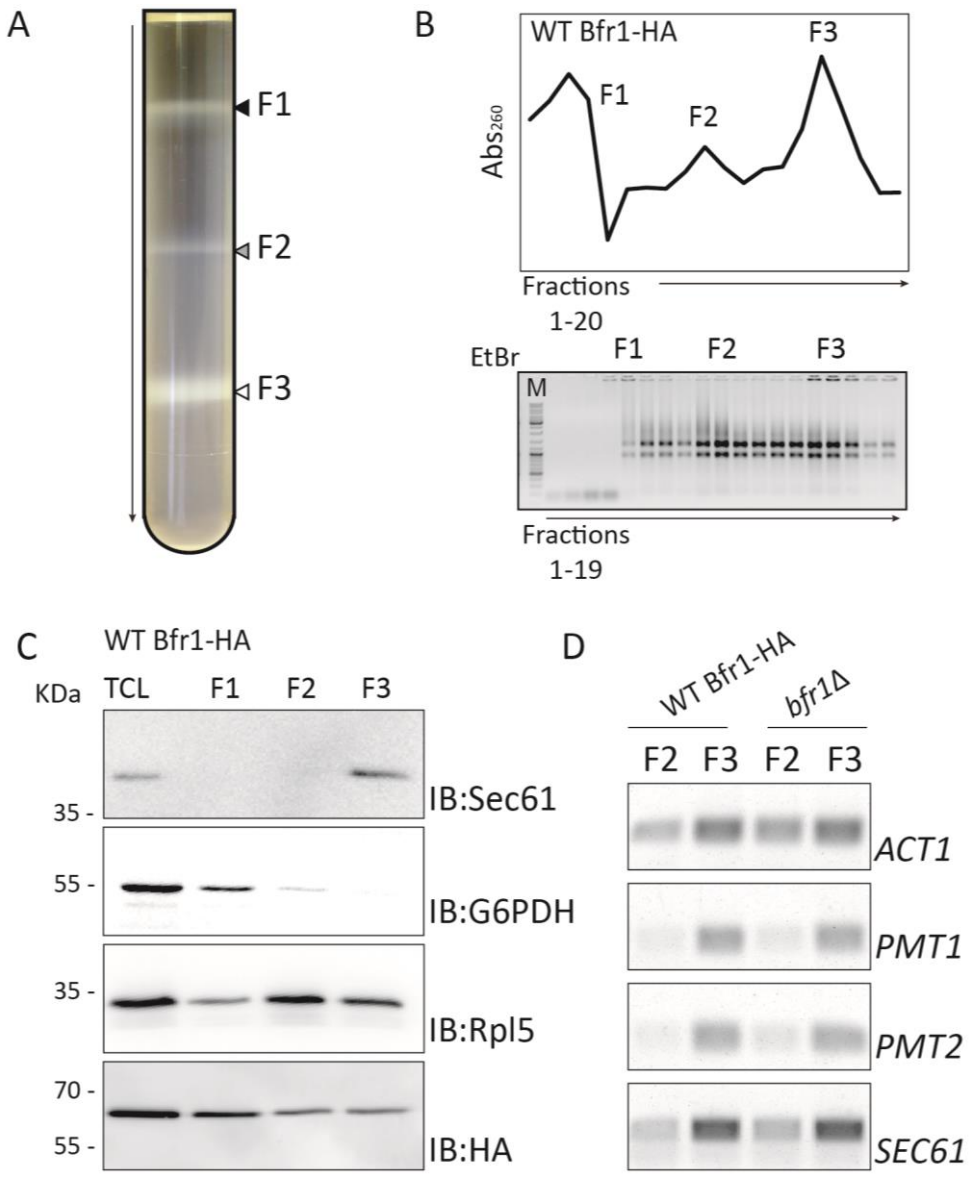

Figure 4.29. Analysis of *PMT1* and *PMT2* transcript localization by sucrose gradient cell fractionation. JCY017 (wild type, *BFR1-3xHA*) and *bfr1*Δ (Euroscarf) strains were grown in YPD under standard conditions, harvested, lysed and subjected to sucrose step gradient centrifugation as described in 3.5.1.2. (**A**) Image of a representative sucrose step gradient (wild type, strain JCY017). Black, grey and white arrows indicate the fractions selected. (**B,** upper panel) Abs_{260} at each fraction sampled from the sucrose gradient (JCY017). (**B**, lower panel) The equivalents of each fraction were loaded in an agarose gel and stained with ethidium bromide (JCY017). (**C**) 0.25 OD_{600} units of total cell extract (TCE) and equivalents of each sucrose fraction (wild type, strain JCY017) were resolved on a 12% PAA gel and subjected to Western blot analysis using the indicated antibodies. (**D**) Semi-quantitative PCR performed on cDNA prepared from total RNA extracted from selected sucrose fractions. 1:20 cDNA dilution was used as a template in a standard dreamtaq PCR program (see 3.2.7) using 23 or 25 cycles for amplification of *ACT1* or *PMT1*, *PMT2,* and *SEC61*, respectively. Representative results of two independent fractionations are shown.

Thus, the relative abundance of *PMT2* transcript with respect to *ACT1* was quantified in each fraction and a ratio between fractions was calculated. In agreement with the results shown in Figure 4.29D, *PMT2* mRNA was found associated with the membrane fraction to a higher extent and no significant difference in *PMT2* distribution was observed in *bfr1*Δ with respect to wild type cells (Figure 4.30B, upper panel).

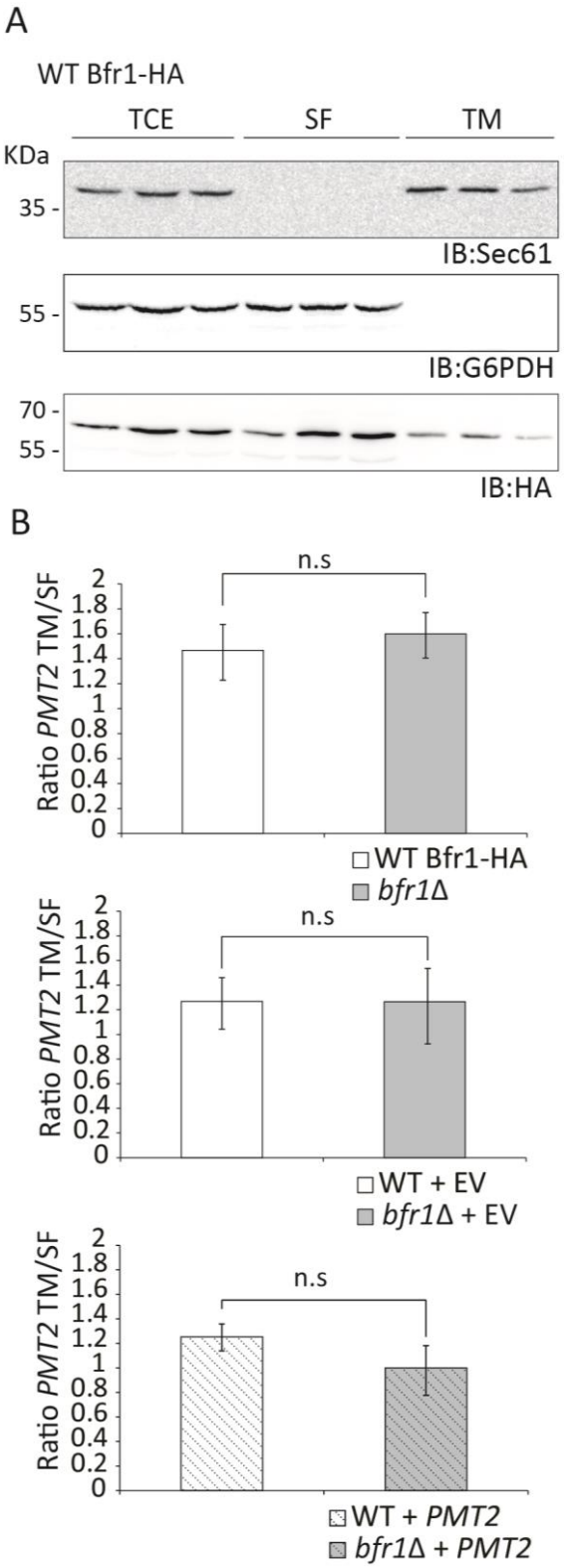

Figure 4.30. Analysis of *PMT2* transcript localization by one step gradient cell fractionation. Either JCY017 (wild type, *BFR1-3xHA*) and *bfr1*Δ (Euroscarf) (**A; B,** upper panel) or wild type (BY4741) and *bfr1*Δ transformed with pRS41N (empty vector, EV) or pJC09 (*PMT2*) (**B**, lower panel) were grown in YPD or YPD supplemented with nourseothricin under standard conditions, harvested, lysed and subjected to one-step ultracentrifugation as described in 3.5.1.2. (**A**) Western blot analysis of the protein content of total cell extract (TCE) soluble fraction (SF) and total membrane fraction (TM) prepared from JCY017. Equivalents to 0.25 OD_{600} of each fraction were resolved on a 12% PAA gel and subjected to Western blot analysis using the indicated antibodies (**B**) cDNA was synthesized from total RNA prepared from TCE, SF, and TM fractions and used as a template for quantitative RT-PCR (3.2.9). Results show the ratio between the relative *PMT2* abundance normalized to *ACT1* in TM with respect to SF. Error bars show the confidence interval. For statistical significance, a one-tailed t-Student's test was applied to log ($2^{-\Delta\Delta Ct}$), n=3.

Further, whether increasing the total levels of *PMT2* would also increase the need for functional Bfr1 was questioned. Perhaps performing these experiments under PMT2 overexpression conditions could reveal changes in transcript distribution that are undetectable under standard conditions. Analysis of mRNA distribution in wild type and *bfr1*Δ overexpressing *PMT2* yielded a transcript distribution comparable to standard conditions and no significant change was observed in *bfr1*Δ (Figure 4.30B, lower panel). Taken together, the two strategies used to track PMT transcript distribution show that PMT transcripts are preferentially associated with the ER membrane and that the reduction in PMT protein expression observed in *bfr1*Δ is not caused by changes in PMT transcript mislocalization. The reduction of PMT protein expression in *bfr1*Δ is therefore restricted to translation, suggesting that Bfr1 might be required when the ribosome has already been recruited to the ER membrane.

4.2.4.5 Bfr1 functions in the UPR

As detailed in the introduction, the Pmt1-Pmt2 complex is specifically integrated in the UPR and therefore is upregulated upon ER-GFP expression. The role of Bfr1 in Pmt1-Pmt2 protein expression is particularly relevant upon ER-GFP expression, where the expected increase in PMT protein abundance upon ER stress is also prevented in the absence of *BFR1* (Figure 4.20). One possible explanation already suggested by transcriptomic data (Travers *et al.*, 2000) is that *BFR1* also functions, together with PMTs, during the UPR.

This hypothesis was tested by measuring the expression of *BFR1* upon DTT treatment in both wild type and the UPR-deficient mutant *hac1*Δ. As shown in Figure 4.31A, DTT causes a 2-fold upregulation in the *BFR1* transcript level and such an effect is absent when *HAC1* is deleted, confirming that *BFR1* is a target of the UPR. These data point out that Bfr1 function is particularly important when the ER faces folding stress, which makes sense since among the ORFs that require Bfr1 for translation there are key members of the ER quality control system such as the Hsp70 chaperone Lhs1, or the central E3-ligase Hrd1 (App. Data 1).

The deletion of *BFR1* was also analyzed for constitutive UPR activation (Figure 4.31B). Like what shown for PMT mutants (see 4.1.1), quantification of UPR-related transcripts in *bfr1*Δ yielded a very poor increase in the level of $HAC1^{S}$ (1.5 fold-change) and no change in the levels of KAR2, indicating no UPR activation under standard conditions. This suggests that the reduction in expression of the mainly secretory proteins showed by the ribosome

profiling experiment (Figure 4.27C) is insufficient to cause detectable stress. However, since *IRE1* is one of the ORFs affected at the translational level in *bfr1*Δ (App. Data 1), the capacity of this mutant to fully activate the UPR should be analyzed in more detail.

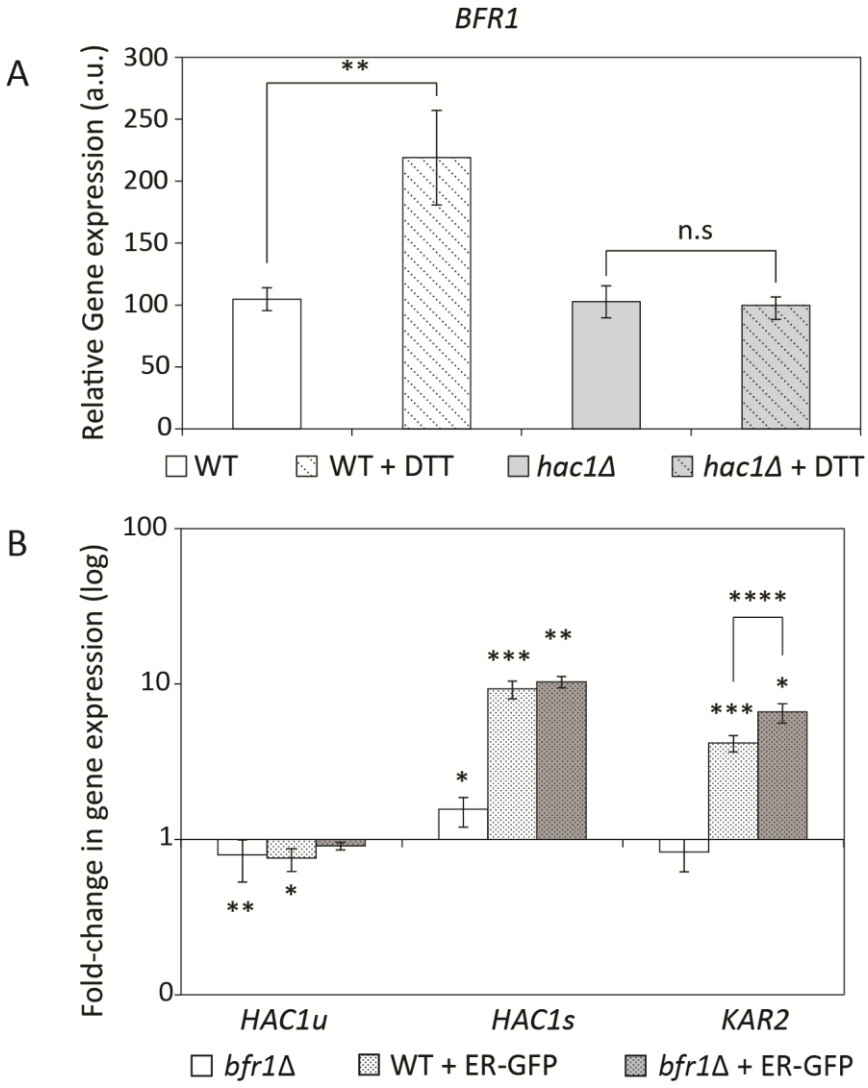

Figure 4.31. Characterization of *BFR1* in the context of the UPR. (**A**) Relative mRNA levels of *BFR1* in response to DTT in wild type and *hac1*Δ cells. Wild type (BY4741) and *hac1*Δ (Euroscarf) cultures were treated with 2.2 mM DTT for 60 min. (**B**) Fold- change in mRNA levels of $HAC1^{u}$, $HAC1^{s,}$ and KAR2 upon either deletion of *BFR1*. Total RNA was extracted either from yeast strains wild type (BY4741), JEY06 (wild type ER-GFP), *bfr1*Δ (Euroscarf) and *bfr1*Δ ER-GFP (strain resulting from SGA crosses) grown in YPD under standard conditions. (**A**, **B**) cDNA was prepared from total mRNA according to 3.2.3 and 3.2.4 and RT-PCR was performed according to 3.2.9. (**A**) Results show averages of mRNA abundance ± SD with respect to *ACT1*. For statistical significance, a two-tailed t-Student's test was applied (n=3). (**B**) Fold-change is calculated by averaging Cts with respect to *TAF10*. Errors bars show the confidence interval. For statistical significance, a one-tailed t-Student's test was applied to log ($2^{-\Delta\Delta Ct}$), n=3.

4.3 Monitoring the role of protein *O*-mannosylation in protein dynamics

In the context of investigating the role of *O*-mannosylation in maintaining protein homeostasis, the aim was to systematically approach the opposite effects described for *O*-mannosylation in protein stability (see 1.4.2 and 1.4.3).

In order to get a comprehensive picture of the impact of *O*-mannosylation on protein stability, the first interest was to unravel the complexity of the redundant PMT family by looking at the contribution of each major PMT member. Secondly, the spotlight was put on those *O*-mannosylated proteins whose stability is increased upon PMT deletion, seeking for endogenous targets for a PMT-dependent quality control mechanism.

One possibility to account for protein stability *in vivo* in a high throughput manner is the use of tandem protein timers (tFT). This method is based on the C-terminal fusion of the protein of interest to two different fluorescent proteins: mCherry and sfGFP; whose fluorophores have distinct maturation time (Figure 4.32A, Khmelinskii *et al.*, 2012). While sfGFP is very efficiently folded after translation and thereby becomes rapidly fluorescent, mCherry takes longer time to fold and fluorescence can only be detected when the fused protein of interest was stable long enough to permit mCherry complete maturation.

By using this system different aspects of protein dynamics can be investigated *in vivo*. One aspect of particular interest for this study is to account for protein stability. On one hand, the sfGFP signal allows the quantification of steady-state protein abundance since due to its folding kinetics it will become fluorescent independently of the age of the fused protein of interest. On the other hand, combining sfGFP and mCherry signals allows measuring differences in protein stability since only stable proteins will display mCherry fluorescence (Khmelinskii *et al.*, 2012). Hence, conditions that decrease the mCherry/sfGFP ratio are indicative of decreased stability whereas increased ratios indicate protein stabilization.

Besides stability, this system also allows to track protein localization and provides valuable information about the physical environment of the tFT. The fluorescence of each fusion protein with tTF facing the lumen will be differently affected by conditions that vary throughout the secretory pathway such as pH.

4.3.1 High throughput screen of dynamics of *O*-mannosylated proteins by tandem fluorescent timers

The recently described yeast *O*-mannose glycoproteome, which includes 293 *O*-mannosylated PMT-target proteins (Neubert *et al.*, 2016) was used to select queries for the tFT screening. Fluorescence of a total of 137 tFT fusion proteins was analyzed in *pmt1*Δ, *pmt2*Δ, and *pmt4*Δ mutants *in vivo* (App. Data 2).

*pmt1*Δ, *pmt2*Δ, and *pmt4*Δ deletions mutants were generated in the selected subset of *O*-mannosylated proteins tFT-fused by automated crossing following synthetic genetic array (SGA) methodology (see 3.3.2). Three replicates for each resulting cross as well as untagged negative controls were plated onto the corresponding selective medium and fluorescence for both sfGFP and mCherry of the resulting colonies was measured after growth at 30 °C for 24h using a fluorescent plate reader (Figure 4.32B). A Δ-score was calculated based on the intensities of both fluorescent proteins for each mutant versus wild type. Δ-score for sfGFP accounts for changes in protein abundance upon PMT deletion whereas Δ-score for mCherry/sfGFP accounts for protein stability. In line with this, negative mCherry/sfGFP Δ-score values indicate stabilization, while positive values mean destabilization of the tFT-fusion protein in the mutant compared to the wild-type. While the deletion of PMTs had no major influence on the majority of proteins analyzed (App. Data 3, Figure App. 10), significant changes were observed for 39 individual proteins in total in the three *pmtΔ* mutants (Figure 4.33A and B). Among those, the tFT-fusion proteins Pmt3, Tsc3, Kre6, Opy2, Vth2, Ted1, Fab1, Lam6, YNL058c, Coy1, Osm1, YCR061w, Sec12, Nis1, and Mnl2 showed the most relevant changes in Δ-score (App. Data 3; net Δ-score > 0.5; *p*-value < 0.1).

Fluorescence of luminal tFT can be affected by the change in localization induced by PMT deletion. This scenario was addressed first in order to narrow down the effects in Δ-score to changes in protein abundance and/or stability.

Based on prediction (TOPCONS, Bernsel *et al.*, 2009) C-terminal tFT of 59% of the identified proteins is localized at the cytosol (Figure 4.33C). As a proof of principle, localization of the fluorescent signal was analyzed for different representative C-terminally oriented proteins of the selected 39 positive fusions (e.g., Axl2, Coy1, Kre6, Mnn11, Osm1, Sec12, Ted1, Tsc3, Vrg4 and Wsc2, data not shown). No difference was observed in localization upon PMT

deletion (eg. Figure 4.36B), suggesting that the effects on Δ-score are restricted to changes in protein abundance and/or stability.

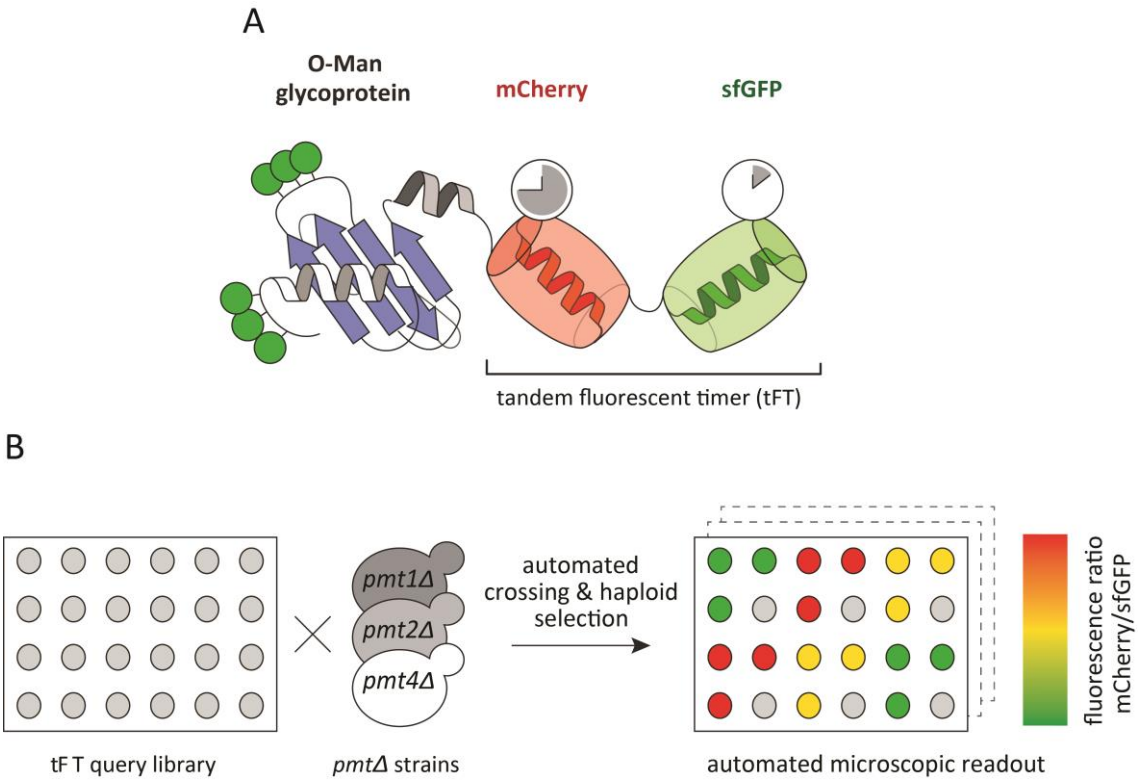

Figure 4.32. Tandem fluorescent protein timer (tFT) screening. (**A**) Representation of a C-terminal tFT-fusion protein analyzed. The slow maturing mCherry and the fast maturing sfGFP are fused in tandem to the C-terminus of *O*-mannosylated proteins of interest. Figure section designed by Patrick Neubert. (**B**) Workflow of the screening of the selected fusion proteins. In brief, 137 individual tFT fusions of the tFT library established by Khmelinskii and coworkers (Khmelinskii *et al.*, 2014) were selected based on the presence of *O*-mannosyl glycans on these proteins (Neubert *et al.*, 2016). The 137 tFT query strains were crossed with *pmt1*Δ (MLY201), *pmt2*Δ (MLY202), or *pmt4*Δ (MLY204) mutants using synthetic genetic array methodology (Baryshnikova *et al.*, 2010). Haploid yeast strains carrying both genetic modifications (tFT-fusion and *pmt* deletion) were selected. mCherry/sfGFP ratio was calculated for each protein and used for comparison between wild-type and mutants. Figure published in Castells-Ballester *et al.*, 2018.

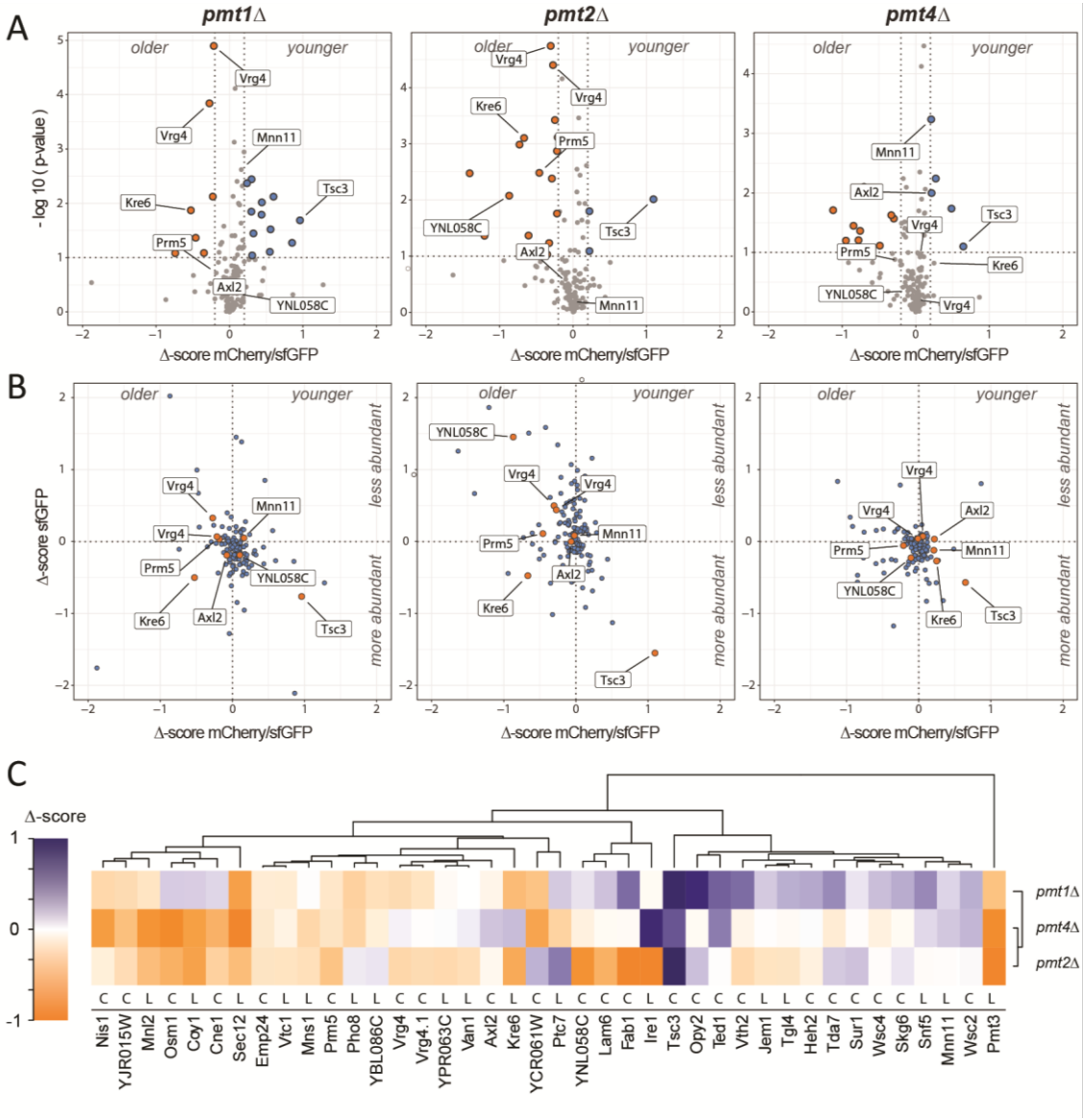

Figure 4.33. **Identification of proteins affected in *pmt1*Δ, *pmt2*Δ, and *pmt4*Δ deletion mutants.** (**A**) Volcano plots illustrating changes in tFT-fusion protein stability in the indicated mutant strains in regard to the statistical significance of data as inferred from variance analysis. Plots show Δ-scores mCherry/sfGFP for changes in protein stability on the x-axis and the negative logarithm of *p*-values on the y-axis. Data were subset for relevance based on thresholds as indicated by red dashed lines (*p*-value < 0.1 and net Δ-score > 0.2). (**B**) Correlation of Δ-scores mCherry/sfGFP, as a measure of tFT-fusion protein stability and turnover (x-axis), and Δ-scores sfGFP, as a measure of the change in protein abundance (y-axis). (**A**, **B**) Data referring to proteins further analyzed or discussed in this study are labeled in red. The example of Vrg4-tFT shows that even minor effects could be reproducibly detected. (**C**) Heatmap with hierarchical clustering of Δ-scores mCherry/sfGFP from a subset of data that passes the thresholds of significance in at least one of the indicated mutant strains (*p*-value < 0.1 and net Δ-score > 0.2). Cytosolic and luminal orientation of the tFT reporter is indicated with C and L, respectively. Analyses and figure designs made by Patrick Neubert and published in Castells-Ballester *et al.*, 2018.

To further analyze the effect of each PMT deletion Δ-scores of each *pmt* mutant were hierarchically clustered (4.33C). Clustering shows a group of proteins with comparable responses to all *pmt* deletions. For example, Pmt3 and Sec12 are stabilized in all three deletions whereas Tsc3 and Wsc2 are destabilized. Consistent with these results, the effect of PMT deletion on Pmt3, as well as defects in Wsc2 maturation, has been shown in previous studies (Verna *et al.*, 1997; Lodder *et al.*, 1999; Girrbach & Strahl, 2003; Lommel *et al.*, 2004). On the contrary, other tFT fusions show unique effects upon the combined deletion of specific PMTs. This is the case of the destabilization effect is observed for Opy2 in *pmt1*Δ and *pmt2*Δ but not *pmt4*Δ or the opposing case for Axl2, which is destabilized only in *pmt4*Δ. The diversity observed among the different PMT deletions likely represents the substrate specificity of the Pmt1-Pmt2 and Pmt4-Pmt4 complexes.

In summary, by a biased (*O*-mannoprotein directed) high throughput screen 39 tFT-fusion proteins were identified as potential candidates for altered protein abundance or stability upon deletion of PMTs. Noteworthy, both effects protein stabilization and destabilization can be inferred from the changes obtained on the reporters Δ-score.

4.3.2 *O*-mannosylation impacts differently on the stability of secretory proteins

As indicated by the Δ-score from the tFT screen, some tFT fusions are likely affected by PMT deletion in terms of abundance and/or protein stability. To evaluate the solidity of these results the analyses were first focused on the previously shown example of Axl2. Axl2 is a type I plasma membrane glycoprotein required for yeast axial budding and shown to require Pmt4 for proper maturation (Roemer *et al.*, 1996; Sanders *et al.*, 1999). In the tFT screen, Axl2 shows a Δ-score consistent with destabilization upon *PMT4* deletion specifically (Figure 4.33A and C).

Next, it was of particular interest to address those tFT fusions that showed a Δ-score compatible with protein stabilization upon PMT deletion as potential targets of an *O*-mannosylation-directed quality control system. Among the potentially stabilized tFT fusions, Kre6, Vrg4, and Ynl058C were selected based on the most relevant Δ-scores identified with a *p*-value < 0.015 in *pmt1*Δ or *pmt2*Δ (App. Data 3). To confirm Axl2, Kre6, Vrg4, and Ynl058C PMT deletions were generated *de novo* on the respective parental tFT fusion strains and the Δ-scores shown in the screen were confirmed under logarithmic growth conditions by flow cytometry (Table 1).

Table 1. Fluorescence flow cytometry of selected candidate strains. Fluorescence intensities of sfGFP and mCherry were measured by flow cytometry in mutants EZY107 (*pmt4*Δ, Axl2-tFT), EZY91 (*pmt1*Δ, Kre6-tFT), EZY96 (*pmt1*Δ, Vrg4-tFT), EZY106 (*pmt2*Δ, YNL058C-tFT) and the corresponding wild-type strains. Intensity ratios were calculated as detailed in 3.3.2. Ratios > 1 and < 1 are indicative for protein destabilization and stabilization, respectively. Mean ± SD values of three measurements are shown. Indicated *p*-values were calculated using a two-tailed *t*-test. The experiment was performed in collaboration with Dr. Ewa Zatorska. Table published in Castells-Ballester *et al.*, 2018

***pmt*Δ Mutant**	**tFT-Fusion Protein**	**$WT_{mCherry/sfGFP}/pmt\Delta_{mCherry/sfGFP}$ ± SD**	***p*-Value**
*pmt4*Δ	Axl2	1.118 ± 0.033	0.088
*pmt1*Δ	Kre6	0.842 ± 0.027	0.037
*pmt1*Δ	Vrg4	0.873 ± 0.040	0.047
*pmt2*Δ	YNL058C	0.787± 0.042	0.010

Consistent with what previously shown for Axl2, Axl2-tFT was found at the bud site of mother cells forming ring-like structures when tracking the sfGFP signal (Figure 4.34A, Roemer & Bussey, 1991; Sanders *et al.*, 1999). The mCherry signal, however, was predominantly found at the vacuole, suggesting that this is the older fraction of the protein that undergoes vacuolar turnover. In contrast to wild type cells, *PMT4* deletion results in vacuolar localization of the sfGFP signal, indicating that even younger protein undergoes turnover in *pmt4*Δ. When comparing the steady-state abundance of previously shown functional Axl2-HA with Axl2-tFT, a similar increase in the presence of degradation products was detected (Sanders *et al.*, 1999, Figure 4.34B), indicating decreased stability in *pmt4*Δ. This data on Axl2-tFT is largely in agreement with what previously described and allows to further infer changes in protein stability from the Δ-score yielded in the tFT screen.
Once confident with the solidity of the tFT screening, the effect of PMT deletion on protein stabilization was next investigated. In principle, increased protein stability should be also reflected in an increase in steady-state abundance. Among the confirmed tFT fusions Kre6, Vrg4 and YNL058C, Kre6-tFT was selected for further analyses because the Δ-score of both sfGFP and sfGFP/mCherry ratio met both criteria (Figure 4.33B).

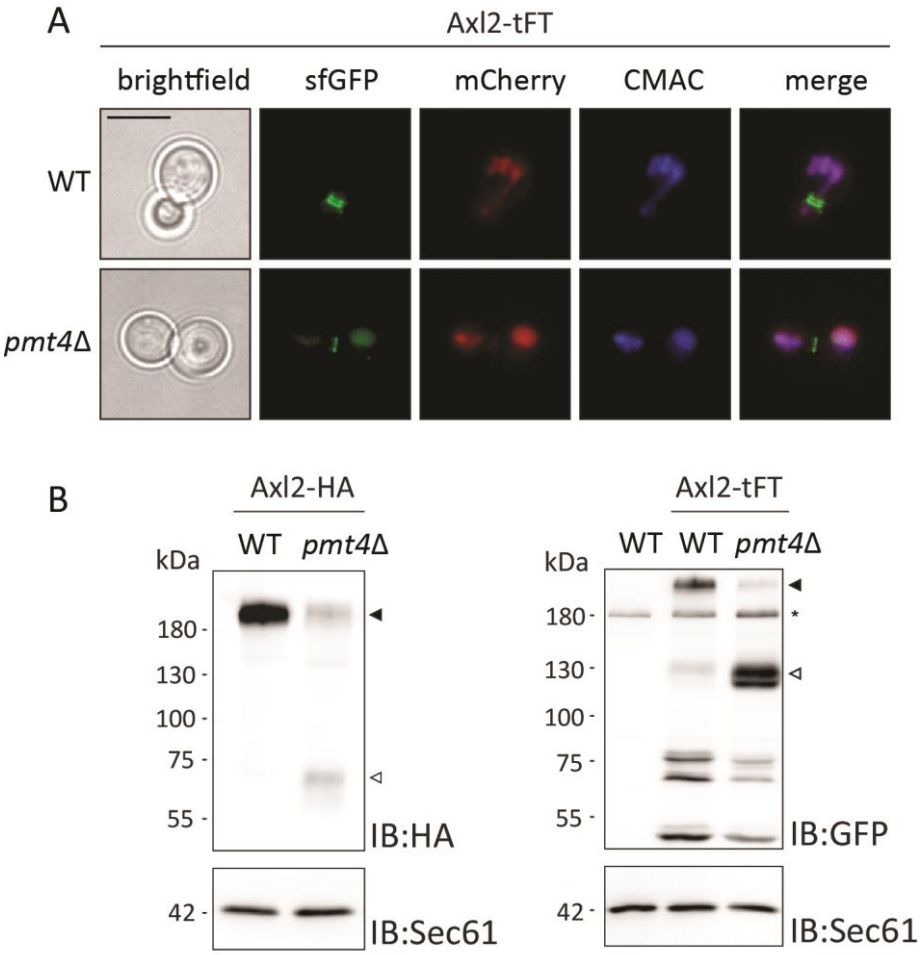

Figure 4.34. **Analyses of Axl2-tFT protein.** (**A**) Wild type and *pmt4*Δ (EZY107) cells expressing the Axl2-tFT (WT Axl2-tFT resulting from SGA crosses, (Khmelinskii *et al.*, 2012); and EZY107 strains) were grown in SD medium and imaged under standard conditions. Prior to imaging, cells were stained with the vacuolar vital dye 7-amino-4-chloromethylcoumarin (CMAC). Scale bar, 5 µm. Figure section designed by Dr. Ewa Zatorska. (**B**) Membranes (equivalent to 1 OD_{600} units of yeast cells) from wild-type (MGY69) and *pmt4*Δ (MGY72) cells expressing Axl2-HA or wild-type (WT Axl2-tFT, strain resulting from SGA crosses, Khmelinskii *et al.*, 2012) and *pmt4*Δ (EZY107) cells expressing Axl2-tFT, were resolved on 8% polyacrylamide gels and subjected to Western blot analysis using anti-HA and anti-GFP antibodies, respectively. The full-length form of tagged Axl2 (black arrows) is less abundant in *pmt4*Δ than in corresponding wild-type cells. In the cells lacking Pmt4, C-terminal proteolytic fragments of the protein (white arrows) are detected. Differences in the apparent molecular masses of the full-length forms and proteolytic fragments observed for Axl2-HA and Axl2-tFT, respectively, correspond to the calculated mass difference (−60 kDa) of the tags. Asterisks indicate an unrelated cross-reactive band, present also in the membranes isolated from wild-type cells without tFT-fusion protein (YMaM330). Sec61 served as a loading control. Experiments have been replicated three times; representative results are shown. Figure published in Castells-Ballester *et al.*, 2018.

Kre6 is a type II transmembrane protein that functions in the synthesis of β-1,6-glucan that is deposited in the yeast cell wall (Roemer & Bussey, 1991). According to previous studies, Kre6 localizes to the ER and to a lesser extent to the plasma membrane at sites of cell wall remodeling (Kurita *et al.*, 2012). Kre6-tFT showed partial ER localization from the sfGFP signal, however, the majority of the protein was found at the vacuole in both sfGFP and mCherry signals (Figure 4.35A). This result indicates that the addition of a large C-terminal tag might affect the stability or the localization of Kre6 itself, which likely undergoes vacuolar turnover. When analyzing Kre6-tFT in *pmt1*Δ (Figure 4.35A), an overall increase for both sfGFP and mCherry signals was observed. A stronger presence of ER localization could be observed from the sfGFP signal, which would be in agreement with the longer persistence of Kre6-tFT at the secretory pathway. Nevertheless, the overall increase in total fluorescence signal complicates drawing definitive conclusions. Still, although largely consistent with protein stabilization in *pmt1*Δ, Kre6-tFT shows unexpected vacuolar localization regardless of the genetic background.

Kre6 has been described to require interaction with a set of chaperones for proper function (Takahashi *et al.*, 2001; Kurita *et al.*, 2012) and therefore it is possible that the tFT tag, which faces the lumen, might be hampering this interaction and thereby causing folding defects that trigger vacuolar turnover. To rule out that tFT induces general mislocalization of the type II proteins, correct localization of the Golgi mannosyltransferase Mnn11-tFTwas confirmed (Figure 4.36A and B). In order to test the increased stability of Kre6-tFT upon *PMT1* deletion, Western blot was performed to address increased protein abundance, and cycloheximide chase followed by Western blot to address changes in protein stability. In agreement with the Δ-score yielded at the screen, *pmt1*Δ results in an increased abundance of Kre6-tFT (Figure 4.34B, left panel). Increased Kre6-tFT turnover was observed in wild type cells in comparison with *pmt1*Δ, where Kre6-tFT remains even after 3h after the addition of cycloheximide (Figure 4.35B, right panel).

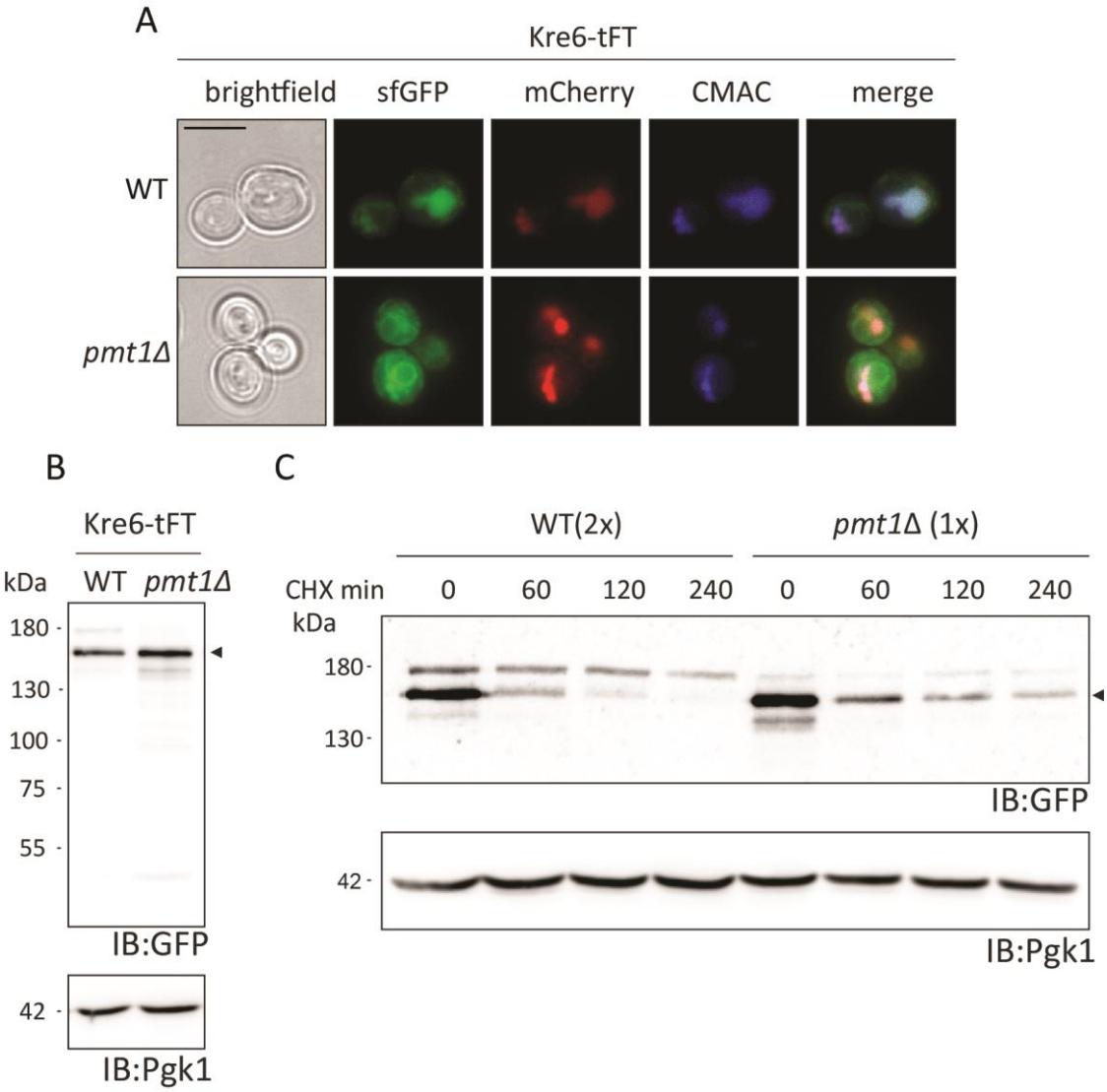

Figure 4.35. **Analyses of Kre6-tFT protein**. (**A**) Localization of Kre6-tFT protein. Wild-type and *pmt1*Δ cells expressing the Kre6-tFT (strains WT Kre6-tFT and EZY91, respectively) were grown in SD and imaged under standard conditions. Prior to imaging, cells were stained with the vacuolar vital dye CMAC. In wild-type and *pmt1*Δ cells Kre6-tFT is present in the ER, but mainly in the vacuole. Scale bar, 5 µm. Figure section designed by Dr. Ewa Zatorska (**B, C)** Cell lysates from wild-type (WT Kre6-tFT) and *pmt1*Δ (EZY91) cells expressing Kre6-tFT were resolved on 8% polyacrylamide gels and subjected to Western blot analysis using anti-GFP antibodies. Pgk1 served as a loading control. (**B**) Steady-state levels of Kre6-tFT. Cell lysates equivalent to 0.2 OD_{600} units of yeast cells were analyzed. (**C**) Cycloheximide chase analysis. Cell lysates equivalent to 0.2 OD_{600} units (1x; *pmt1*Δ) and 0.4 OD_{600} units (2x; WT) of yeast cells were analyzed, to allow for better comparability. (**B**, **C**) Three forms of Kre6-tFT were detected as previously demonstrated for the native protein (Takeuchi *et al.*, 2008). The major band is more abundant at steady state (**B**) and slower degraded (C) in mutant *pmt1*Δ. Experiments have been replicated at least two times; representative results are shown. Figure published in Castells-Ballester *et al.*, 2018.

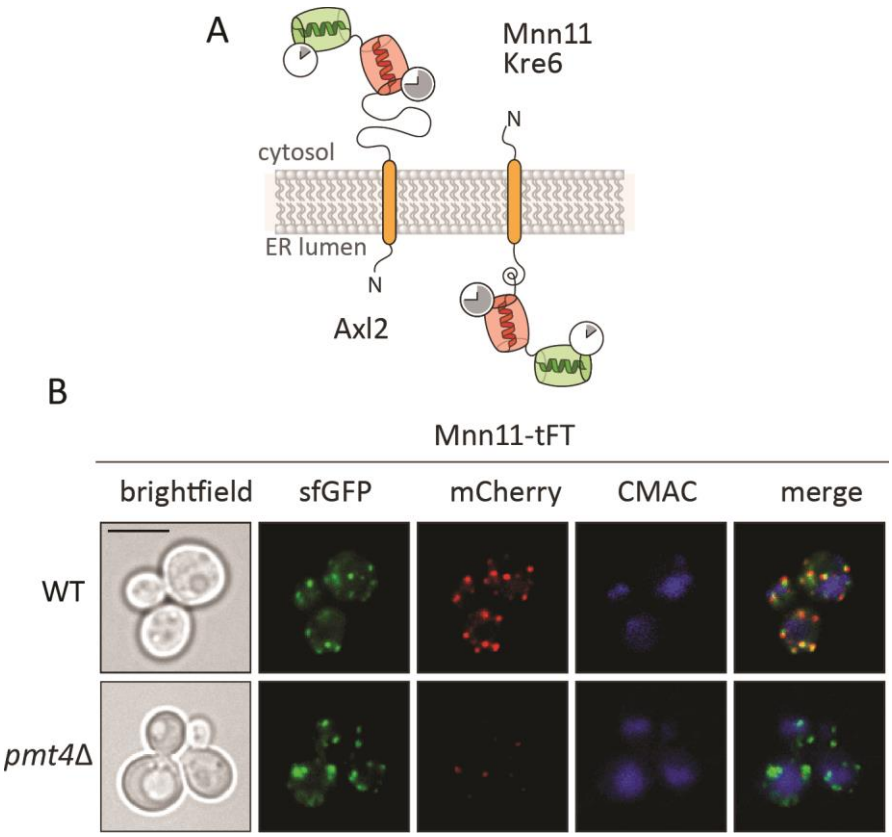

Figure 4.36. (**A**)Topology model of Axl2, Kre6 and Mnn11 depicting the orientation of the tFT timer for type I and type II transmembrane proteins. Figure section designed by Patrick Neubert. (**B**) Localization of another type II transmembrane protein, Mnn11-tFT, to the Golgi is not affected by the C-terminal tFT reporter. Lower abundance of old Mnn11-tFT (mCherry) in *pmt4*Δ cells when compared to wild-type strain confirms the destabilization of this protein observed upon decreased *O*-mannosylation. Prior to imaging, cells were stained with the vacuolar vital dye CMAC. Scale bar, 5 µm. Figure section (B) designed by Dr. Ewa Zatorska. Figure published in Castells-Ballester *et al.*, 2018.

In summary, these results show the suitability of using in vivo fluorescent timers to monitor the influence of *O*-mannosylation on protein stability. 137 secretory *O*-mannoproteins were analyzed upon the deletion of the major members of the PMT family and confirmed previous data on the requirements of this post-translational modification for protein maturation. More interestingly, *O*-mannosylation is likely required for the turnover of a set of endogenous secretory proteins. Putting the spotlight on Kre6, vacuolar mislocalization was observed for Kre6-tFT, where *PMT1* becomes necessary for efficient turnover. Therefore, it was concluded that *O*-mannosylation is an important contributor for protein stability and that whether the influence of *O*-glycans is positive or negative largely depends on the nature of the substrate.

5 DISCUSSION

5.1 The function of PMTs during protein folding stress

As a start point of this current work, the relationship between protein *O*-mannosylation and ER stress *via* the UPR was investigated. Under conditions where the ER lumen faces an unbalance between an increased load of unfolded polypeptides and the folding machinery, the activation of the UPR becomes vital to restore ER homeostasis (reviewed in Thibault *et al.*, 2011).

Previous studies pointed out the requirement of the UPR when *O*-mannosylation is compromised. *PMT1*, *PMT2* and *PMT4* show synthetic lethality with *HAC1* (Arroyo et al., 2011), also identified by high throughput methods as negative genetic interaction (Ernst, 2013; Costanzo *et al.*, 2016). The sensitivity of the *hac1*Δ mutant to the general PMT inhibitor R3A-5a has been shown (Zatorska *et al.*, 2017). One hypothesis to explain these observations would be that abrogating *O*-mannosylation would result in the accumulation of immature unfolded or misfolded forms of secretory proteins that would be eventually recognized by Ire1. Supporting this hypothesis there is the assumption that *O*-glycans confer solubility to secretory proteins and therefore prevent protein aggregation in the ER lumen (Harty *et al.*, 2001; Vashist *et al.*, 2001; Nakatsukasa *et al.*, 2004; Hirayama *et al.*, 2008; Murakami-Sekimata, Sato, Takashima*, et al.*, 2009).

In this study, a specific and bidirectional relationship within the redundant PMT family is shown between the Pmt1-Pmt2 complex and the activation of the UPR. First, only the Pmt1-Pmt2 complex prevents the activation of the UPR under standard conditions (Figure 4.2). Specifically, for *pmt1*Δ mutant comparable upregulation of KAR2 transcript and protein levels were reported in the course of this current work (Cui *et al.*, 2015). Second, *PMT1* and *PMT2,* in contrast to *PMT4,* are specific targets of the UPR (Figure 4.1). Moreover, during the characterization of ER-GFP as a UPOM substrate, a high correlation was observed between the spliced version of HAC1 mRNA and increased protein abundance of Pmt1 and Pmt2 but not Pmt4 (Figure 4.4).

These data argue against that *O*-mannosylation, in general, prevents UPR, since even the combination of multiple PMT deletions (Figure 4.2, see *pmt4356*), is insufficient to produce detectable stress as it is the case when deleting *PMT1* or *PMT2.* Is then UPR activation a

consequence of a specific function of the Pmt1-Pmt2 complex during protein quality control?

One common feature of the ER quality control system is that malfunction caused by the absence of key components results in UPR activation as it is, for instance, reported for proteins working on ERAD or affecting vacuolar function (Jonikas *et al.*, 2009; Promlek *et al.*, 2011). Likewise, as reviewed in the introduction and showed for the specific example of ER-GFP, UPOM has been so far restricted to the function of the Pmt1-Pmt2 (1.4.2, 4.2.1.1). Furthermore, Pmt1 is shown as necessary for the correct degradation of mislocalized Kre6 (See 4.3.3), which suggests that UPOM might be a relevant pathway to facilitate degradation for certain endogenous secretory proteins (discussed in 5.3). Although not analyzed further, also *pmt2*Δ mutant displayed a phenotype compatible with the stabilization of Kre6-tFT (Figure 4.35) supporting the idea of the Pmt1-Pmt2 complex working in concert with ER protein quality control mechanisms.

However, the pieces of evidence supporting a specific quality control-related function of the Pmt1-Pmt2 complex do not completely rule out that insufficient *O*-mannosylation of *bona fide* substrates may be also a cause of ER stress. It is still possible, that the Pmt1-Pmt2 complex has a broader range of protein targets in comparison with other PMTs. The absence of PMTs that are minor contributors to the overall *O*-mannose glycoproteome may be insufficient to activate the UPR. Although the Pmt1-Pmt2 complex has been considered as the major PMT machinery (Gentzsch & Tanner, 1996), this statement is only supported by the severity of the phenotype manifested by the multiple mutants: In contrast to *PMT4,* deletion of *PMT2* is lethal in combination with the minor *PMT3*, *PMT5,* and *PMT6* (Martin Loibl, unpublished). Moreover, the determinants that define substrate specificity among PMTs remain unknown. Only the Pmt4-Pmt4 complex has been linked to *O*-mannosylation of Serine/threonine rich regions in the vicinity of membrane-anchoring sequences (Hutzler *et al.*, 2007). It is therefore not possible to answer the question of which PMT complex has a stronger contribution to the overall *O*-mannose glycoproteome with the data available so far.

Furthermore, the specificity of the Pmt1-Pmt2 complex being integrated in the UPR could be the consequence of the malfunction of specific downstream effects of the *PMT1* or *PMT2* deletion. Multiple key members of the folding and quality control machinery have been revealed to be *O*-mannosylated (Neubert *et al.*, 2016). In a hypothetical scenario of Pmt1-

Pmt2 complex being specific for one or more of these key quality control factors, hypoglycosylation of those could be the reason behind UPR activation in *pmt1*Δ or *pmt2*Δ. Taken together, by dissecting the PMT family and analyzing the relationship between each major PMT member with the UPR, the relevance of the Pmt1-Pmt2 complex in maintaining ER homeostasis is highlighted. One likely reason is the role described for this particular protein complex as a contributor to the quality control of aberrant proteins. Considering the example of ER-GFP, UPR activation in *pmt1*Δ and *pmt2*Δ could be the cost of abnormally prolonged folding attempts for proteins that would otherwise be discarded by UPOM. Still, it would not be valid to consider a role in protein quality control as the only explanation behind the concert between UPR and the Pmt1-Pmt2 complex, since dissecting the *O*-mannose glycoproteome into each single PMT member's contribution is still a future challenge.

5.2 ER-GFP drives the hunt for UPOM components

Being aware of the obstacles of targeting the complex mechanism of UPOM, it was taken advantage of ER-GFP as a reporter to perform a high throughput screen searching for UPOM components. The initial characterization of ER-GFP confirmed previous data showing that it is indeed a specific target of the Pmt1-Pmt2 and not the Pmt4-Pmt4 complex (Figure 4.5). Contrary to ER-$GFP_{f,}$ expression of ER-GFP causes ER folding stress, triggers the activation of the UPR and thereby the transcriptional upregulation of *PMT1* and *PMT2* (Figure 4.6). Increased levels of the Pmt1-Pmt2 complex likely favor the efficiency of UPOM and therefore factors monitoring ER-stress (E.g. Ire1) and/or driving the upregulation of the Pmt1-Pmt2 complex (E.g. Hac1) could be potentially found in the screening. In the case of *ire1*Δ and *hac1*Δ, haploids resulting from crosses with wild type expressing ER-GFP were inviable (data not shown). Probably the overexpression of ER-GFP when the UPR is impaired results in cell lethality as previously shown for other misfolded protein models (Spear & Ng, 2003).

Moreover, the relevance of the HDEL signal included in the ER-GFP construct was analyzed. As hypothesized in (Harty *et al.*, 2001), UPOM could be favored by the prolonged stay of UPOM targets in the ER lumen. In the case of non-retained ER-GFP, UPOM works independently of ER-retention and contributes to the folding state of non-retained ER-GFP

(Figure 4.7A and C). When qualitatively comparing the extent of UPOM received by ER-GFP with and without HDEL signal, no major difference was observed in the presence of the *O*-mannosylated fraction by Western blot (Figure 4.7B). This implies that ER retention is not crucial for UPOM since this type of *O*-mannosylation seems to precede the recruitment of cargos for ER-Golgi transport, at least in the case of ER-GFP. Supporting this idea, expression of both retained and non-retained ER-GFP cause comparable UPR activation (Figure App 8). If it is assumed that the degree of UPR activation largely depends on the extent of unfolded regions being recognized by chaperones and by Ire1 itself; and that UPOM disengages chaperones from unfolded segments (Nakatsukasa *et al.*, 2004; Pincus *et al.*, 2010; C. Xu *et al.*, 2013), it is deduced that both versions of ER-GFP interact with chaperones during a comparable time window until UPOM takes place. In general, it is accepted that immature proteins, meaning those still interacting with chaperones, are prevented to be packaged into COPII vesicles (reviewed in Geva & Schuldiner, 2014).

In addition, during the characterization of non-retained ER-GFP, it was noticed that ER-GFP is eventually targeted to the vacuole, where it undergoes degradation in a Pep4-dependent manner (Figure 4.7 and 4.8). It is important to note that ER-GFP fluorescence is significantly lower in the vacuole, likely because of both the ongoing protein degradation as well as the acidic environment of the vacuolar lumen. This fact gains importance in the context of a high throughput screen, where efficiency of UPOM was about to be inferred from the fluorescence intensity of ER-GFP in deletion mutant libraries. As described by Copic and colleagues (2009), there are several deletions that interfere with the function of Erd2, the main cargo receptor for proteins bearing HDEL retention signals. These deletions would result in the release of ER-GFP from the ER, vacuolar degradation and thereby decrease of fluorescence intensity, biasing the interpretation of the results of the ER-GFP screening. Precisely, one mutant described at (Copic *et al.*, 2009) is *pgi1-DAmP,* which was found affecting UPOM (Figure 4.12). With these considerations, the non-retained version of ER-GFP was used to anticipate misinterpretations when analyzing the fluorescence intensity of ER-GFP in *pgi1-DAmP* (Figure 4.17)

The screening yielded 107 mutants for genes potentially involved in UPOM. The fraction of mutants considered positive corresponds to about 5% of the total number of mutants tested

and indicates that fluorescence of ER-GFP is not affected upon the deletion of the majority of non-essential genes. The suitability of ER-GFP to report defects in UPOM was proven by the presence of *pmt1*Δ and *pmt2*Δ among the positive hits of the screen. The diversity of GO term categories and the low enrichment score pointed out the absence of a clear biological pathway affecting UPOM. This is consistent with the fact that UPOM is not a preceding step for any quality control pathway but rather works independently, sometimes facilitating degradation depending on the nature of each the UPOM target (see 5.3). In parallel to this work, a conceptually similar study was conducted by the group of Davis Ng and focused on finding factors that diminish the folding capacity of ER-GFP_f (Zhang *et al.*, 2017). Although the purpose of their study largely differed from this current work, the functional heterogeneity in the mutants found in both screenings is comparable. This indicates that despite not so many mutations interfere in ER-GFP intensity, the deletions that do so cause malfunction in many diverse cell machinery, many of which are unconnected to the quality control of secretory proteins.

Given the high noise within the 107 positive mutants, different filters were applied to discriminate those mutants that are directly linked to *O*-mannosylation and UPOM.

First of all, ER localization of the GFP signal was manually curated for the 107 positive mutants and was confirmed for all of them except for *spf1*Δ (Figure App 3). Spf1 is a P-type ATPase that works at the ER membrane as an ion transporter maintaining the homeostasis of Ca^{2+} (Cronin *et al.*, 2002). In the context of this work, deletion of *SPF1* results in partial cytosolic folding of ER-GFP where, due to the folding environment and the absence of *O*-mannosylation (Jain *et al.*, 2001; D. G. Huang & Shusta, 2006), it displays the highest fluorescence intensity of all mutants tested (Figure 4.10). Literature highlighting the importance of Spf1 for ER homeostasis is abundant (Cronin *et al.*, 2002, Y. Chen *et al.*, 2005, Cohen *et al.*, 2013) and although an ER import defect has not been described so far, it is possible that this is a consequence of the strong overexpression conditions of ER-GFP used in the screen in a scenario of already compromised homeostasis.

Qualitative evaluation of the *O*-mannosylation state of the cell wall protein Hsp150 by western blot was used to track general changes in glycosylation and yielded 12 mutants that display Hsp150 phenotype compatible with hypoglycosylation. Among those, one of the most prominent is *pop2*Δ, in which a major subunit of the Ccr4-Not complex is deleted. This complex mediates 3' to 5' mRNA de-adenylation prior to mRNA decay. Although the *pop2*Δ

mutant did not show a clear reduction of *O*-mannosylation of ER-GFP (Figure 4.12), it would be interesting to question whether the post-transcriptional regulation of PMT expression could also include mRNA decay mechanisms. Particularly after the link shown between PMT expression and protein translation efficiency (See 4.2.4)

Unexpected connections of UPOM to *N*-glycosylation were found among the 109 positive mutants such as *cwh41*Δ and *ost3*Δ. *CWH41* encodes the α-glucosidase I in charge of trimming *N*-glycans during glycoprotein folding cycles (See 1.4.1). As it works in mammals with the calnexin-calreticulin cycle (Trombetta & Helenius, 2000), glucose removal sets up a time window for glycoprotein folding before Mns1 and Htm1 mannosidases are recruited and generate a signal recognized by Yos9 for ERAD (Benitez *et al.*, 2011). Interestingly, as it is shown for *O*-mannosylation (see 1.4.2), *CWH41* has been involved in the degradation of misfolded proteins (Hitt & Wolf, 2004). Ost3 is a subunit of the OST complex described to determine the substrate specificity of OST (Schwarz *et al.*, 2005). Ost3 was recently reported to be necessary for Pmt2 *N*-glycosylation although no direct evidence of decreased *O*-mannosylation was observed in *ost3Δ* (Zatorska *et al.*, 2017). However, the formation of ER-GFP oligomers as a consequence of ER-GFP misfolding (C. Xu *et al.*, 2013) was significantly reduced in *ost3*Δ (Ewa Zatorska, 2017, unpublished) indicating that ER-GFP indeed folds more efficiently in the absence of *OST3.* Both *CWH41* and *OST3* do not seem to intrinsically modulate UPOM, but their influence in the quality control of secretory proteins is an attractive scenario to investigate.

Next, the efficiency of UPOM was analyzed in the positive mutants by the presence of the *O*-mannosylated fraction of ER-GFP. Analysis of 97 mutants revealed that UPOM was affected in four of them: *bfr1*Δ, *pgi1-DAmP,* and *Psa1-DAmP,* which showed clear UPOM reduction. At this point, it is relevant to mention that although judging the efficiency of UPOM by the presence of *O*-mannosylated ER-GFP by Western blot was done in a qualitative manner, very stringent criteria were used in terms of only selecting those mutants that showed clear hypoglycosylation of ER-GFP. Therefore, it is still possible that milder but still significant reduction of UPOM in other mutants might have been unnoticed.

5.2.1 A link between sugar metabolism and ER protein folding stress

Among the mutants found in the screening, the deficient UPOM of ER-GFP was confirmed by western blot for both *psa1-DAmP* and *pgi1-DAmP* mutants (Figure 4.12). Both genes *PSA1*

and *PGI1* are involved in the cytosolic reaction cascade that converts glucose-6-phosphate into GDP-mannose, which will be subsequently used as a substrate to generate the sugar donor for both *N*- and *O*- glycosylation machinery as well as for the formation of the GPI anchor.

Two reasons encouraged to put the focus on characterizing *PGI1*: First, *the pgi1-DAmP* mutant displayed a more severe hypoglycosylation of ER-GFP (Figure 4.12B). Second, unlike for *PSA1*, no CDGs have been associated with *PGI1* defects in humans, which indicates that the impact of *PGI1* on protein glycosylation has not been characterized in detail.

The *O*-mannosylation state of ER-GFP in *pgi1-DAmP* strongly relies on the availability of free mannose (Figure 4.15), suggesting that limiting the cytosolic substrate of the PMT machinery has a strong impact on the efficiency of UPOM. Recombinant overexpression of *MPG1*, the homolog of *Trichoderma reesei*, was shown to cause an increase in the intracellular levels of GDP-Man, an increase in the expression of Dpm1 and an overall increase in mannosyltransferase activity (Zakrzewska *et al.*, 2003) Accordingly, the opposite effect could be expected when limiting the accessibility of fructose-6-phosphate (see figure 4.13).

In fact, there is a functional relationship between *PMT2* and *PGI1* since the deletion of *PMT2* on top of the *pgi1-DAmP* knockdown results in a severe growth defect. Although either *pmt2*Δ or *pgi1-DAmP* alone does not impair growth, both *O*-mannosylation and the isomerization of glucose-6-phosphate into fructose-6-phosphate are vital processes and therefore it is not surprising that both mutations have additive negative effects when combined (Figure 4.15, upper panel). Together with PMTs, the potential depletion of GDP-mannose would also impact the efficiency of the *N*-glycosylation as well as the synthesis of the GPI anchor. Since these two processes are also functionally linked to *O*-mannosylation (Ecker *et al.*, 2003; G. Huang *et al.*, 2003), it is likely that their malfunction also contributes to the phenotype of *pmt2*Δ*pgi1-DAmP* double mutant.

UPOM of ER-GFP in *pgi1-DAmP* can be rescued by including mannose as the carbon source in the medium, so presumably, fructose-6-phosphate is no longer a necessary intermediate to synthesize mannose-6-phosphate. Under these conditions, both UPOM in *pgi1-DAmP* and growth in *pmt2*Δ*pgi1-DAmP* are restored (Figure 4.15 and 4.16).

Furthermore, the impact of mannose supplementation in *pgi1-DAmP* in regard to ER-GFP folding was investigated. Upon mannose supplementation, folding of ER-GFP in *the pgi1-DAmP* mutant is prevented similar to wild type (Figure 4.17), confirming that the availability

of mannose contributes to the folding competency of secretory proteins. In agreement, *pgi1-DAmP* cells display constitutive activation of the UPR and increased sensitivity to the ER stress agent tunicamycin (Figure 4.18 A and B). Both phenotypes can be rescued when supplementing *pgi1-DAmP* cells with mannose, indicating that the activation of the UPR occurring at the ER can be tuned by the availability of sugars at the cytosol. This is particularly relevant since there is increasing literature that links the UPR with spatially unconnected processes occurring at the cytosol (Ishiwata-Kimata *et al.*, 2013; Schmidt *et al.*, 2019) or mitochondria (Knupp *et al.*, 2019).

Isomerization of glucose-6-phosphate into fructose-6-phosphate by *PGI1* is a key reaction of glycolysis. Mutations in *GPI1*, the human homolog of *PGI1* have been associated with a rare hereditary hemolytic anemia sometimes accompanied by neurological impairment (W. M. Xu & Beutler, 1994; Kanno *et al.*, 1996). Most of the symptoms of *GPI1* deficiency have been assumed to be caused by impaired metabolism of glucose or explained by the potential neurotrophic properties of *GPI1* (Kugler *et al.*, 1998). No effect on protein glycosylation neither in yeast and humans has been described for *PGI1* mutants so far. Given the high degree of conservation of glycolytic enzymes in eukaryotes it is expected that besides defects in glycolytic metabolism, *GPI1* malfunction also results in hypoglycosylation of secretory proteins that could have well been unnoticed.

In yeast, most of the hypoglycosylation-associated phenotypes of *pgi1-DAmP* can be relieved by bypassing the need for endogenous synthesis of mannose-6-phosphate. It would be relevant to explore whether these observations translatable to human patients of hemolytic anemia. Interestingly, mannose supplementation has been proven to be suitable for patients suffering from CDG associated genes that act downstream of *PGI1* in the pathway such as the mannosephosphate isomerase *MPI* and the phosphomannomutase *PMM2* (homolog to the yeast *PMI40* and *SEC53,* and associated with CDG-Ib and CGD-Ia*,* respectively) (Grunewald *et al.*, 2002; Thiel *et al.*, 2012; Witters *et al.*, 2017). In the case of *GPI1,* It is feasible that its role in glycolysis complicates the use of mannose-based nutritional therapies to cope with the expected CDG due to the existing unbalance in sugar metabolism. Nevertheless, mannose-based therapies can cause osmotic diarrhea among other undesired side effects on CDG-Ib patients (Alton *et al.*, 1997; Freeze & Aebi, 1999). Yet, whether mannose supplementation could be applied to hemolytic anemia patients to alleviate some of the symptoms is an attractive hypothesis that could be explored in the future. Baker's

yeast is a suitable platform to investigate defects in protein glycosylation that are possibly linked to hemolytic anemia as well as to analyze to which extent mannose-based nutritional therapies are a realistic option.

Overall, the data shown in this current work indicate that *PGI1* is a key contributor for ER homeostasis and UPOM and provides a direct link between the UPR and sugar metabolism.

5.2.2 Local protein translation control as a contributor to ER homeostasis

In the frame of the ER-GFP screening, *BFR1* was found as necessary for efficient UPOM (Figure 4.12 and 4.13). Clues on how Bfr1 could influence *O*-mannosylation appeared when looking at the mRNAs previously shown to interact with Bfr1. Among the mainly secretome-related transcripts, there was *PMT1* and *PMT2* (Lapointe *et al.*, 2015), leading to the hypothesis of Bfr1 modulating PMT expression.

The steady-state protein abundance of Pmt1 and Pmt2 is certainly dependent on Bfr1 (Figure 4.20). Further, it was confirmed that the effect of *BFR1* deletion on PMTs is the reason behind ER-GFP hypoglycosylation since *PMT2* overexpression is partially able to restore ER-GFP folding and glycosylation (Figure 4.21A and B). Although previously published data strongly supported a role for Bfr1 in regulating PMT expression, a cycloheximide chase experiment was performed to address potential changes in protein stability. The preliminary results showed that the PMT proteins are very stable, and no changes were detected in *bfr1*Δ (data not shown).

In order to find out at which level Bfr1 regulates PMT expression, whether the decrease in PMT protein levels was the result of transcriptional downregulation was first questioned. RT-PCR analyses showed that the effect at the protein level is not coupled to decreased transcript abundance under normal conditions (Figure 4.24A). Significant reduction of transcript levels was nevertheless observed for *PMT2* both upon ER stress (Figure 4.24A), where *PMT1* and *PMT2* undergo upregulation *via* the UPR, or when mirroring such upregulation by *PMT2* overexpression (Figure 4.24B). By promoter replacement it was clarified that the observed specific effect of *BFR1* deletion on *PMT2* transcript level is promoter-dependent (Figure 4.25B) and uncoupled to the effect at the protein level (Figure 4.25A), which is constant under all conditions tested (Figures 4.20, 4.21C and 4.25A).

The involvement of Bfr1 in post-transcriptional mRNA processing events (Simpson *et al.*, 2014) led to the hypothesis that Bfr1 could perhaps play a protective role for its client

transcripts in addition to its role at the protein level. This idea was also supported by the increase of mRNA decay nodes when Bfr1 and/or its cognate partner Scp160 are deleted (Weidner *et al.*, 2014). By performing the transcriptional shutdown of *PMT2* no link of Bfr1 to altered mRNA decay was observed to explain the above-mentioned particular effect on *PMT2* transcript (Figure 4.26). At this stage of the project, what underlies *PMT2* transcript reduction under certain conditions remains unanswered. One option supported by the dependence of this effect on the gene promoter is that *PMT2* simply undergoes transcriptional downregulation as the sum of downstream effects of *BFR1* deletion and ER-stress. Alternatively, modifications on galactose-induced *PMT2*, which additionally contains a degron and a C-terminal HA tag, might interfere with the transcript decay, burying potential changes that would be only effective for *PMT2* native transcript. This second explanation considers that the mRNA determinants that recruit Bfr1 are unknown. Whether specific transcript recognition by Bfr1 is based on a consensus sequence or perhaps on secondary structures has not been addressed so far. Notably, the interaction between P-body components and mRNAs based on conformational cues has been shown for the RNA helicase Dhh1 (Jungfleisch *et al.*, 2017).

Given that under standard conditions mRNA level of both *PMT1* and *PMT2* remained unchanged in *bfr1*Δ (Figure 4.24A), efforts were focused on characterizing a potential role of Bfr1 on PMT translation. Analysis of ribosome-protected mRNA footprints revealed a decrease in ribosome occupancy of a set of transcripts in the absence of *BFR1* (App. Data 2). Among those, PMT1 and PMT2 transcripts were approximately 1.7 fold-change underrepresented in *bfr1*Δ translatome (Figure 4.27), confirming that Bfr1 regulates UPOM by affecting the translational state of PMT transcripts. Noteworthy, known Bfr1 targets were enriched among those ORFs that are underrepresented in *bfr1*Δ translatome, which indicates that Bfr1 likely functions as a translational enhancer rather than as a repressor (Figure 4.27C).

Although described as part of ribosome-associated mRNP complexes, no previous study pointed out Bfr1 to act at the translational level**.** The first intriguing question is how Bfr1 could modulate the translational state of its client transcripts. The fact that in absence of *BFR1* fewer ribosomes sit on transcripts together with the decreased steady-state protein amounts observed at least for Pmt1 and Pmt2 suggests that Bfr1 might work as a translation

control factor facilitating the recruitment of its client transcripts with the ribosome at the initial stages of translation.

However, metagene analysis of footprint distribution revealed a slight accumulation of footprints in the first 100 codons in *bfr1*Δ (Figure App. 9B), suggestive of defects in translation elongation similar to what previously observed by comparable methods when inducing ribosome stalling or translational slow-down (Gerashchenko & Gladyshev, 2014, Subramaniam *et al.*, 2014, Schuller *et al.*, 2017). Notably, defects in translation elongation coupled to decreased protein production have been linked to the absence of Scp160 (Hirschmann *et al.*, 2014), an RNA-binding protein (RBP) that forms a stable complex with Bfr1 (Lang *et al.*, 2001). The link between Scp160 and translation is based on the analysis of the codon composition of Scp160 mRNA targets and the ribosomal occupancy of tRNAs upon Scp160 loss (Hogan *et al.*, 2008). It is proposed that the absence of Scp160 results in loss of synonym-rich tRNAs by causing either tRNA diffusion or facilitating tRNA recycling, thereby affecting translation efficiency. A similar function could be conceived for Bfr1, however slowing down translational elongation would conceptually result in prolonged engagement with ribosomes and thereby increased ribosome occupancy which is in evident contradiction with the ribosome profiling data. A potential explanation for this discrepancy could rely on the interaction between Bfr1 and Scp160. Despite the fact that deletion of either *BFR1* or *SCP160* causes a very similar phenotype in terms of cells morphology and both proteins have been shown to have partially overlapping functions in different contexts (Lang *et al.*, 2001; Baum *et al.*, 2004; Sezen *et al.*, 2009), the functional relationship between these two RBPs is far from being clear. One interesting observation is the dependence of Scp160 on Bfr1 for interaction with polyribosomes (Lang *et al.*, 2001) which might imply that Scp160 is prevented to function in optimizing translation efficiency in the absence of *BFR1*. Therefore, the slight accumulation of footprint in the first 100 codons of Bfr1 target ORFs might represent the loss of Scp160 function, independent of the more probable role of Bfr1 in facilitating translation initiation for its cognate transcripts.

In order to gain insight into the molecular mechanism of Bfr1, the localization of PMT transcripts to the ER membrane was investigated. No difference was found in transcript localization to the ER membrane in *bfr1*Δ (Figures 4.29 and 4.30), indicating that co-

translational targeting of ribosomes to the ER membrane occurs independently of Bfr1. Both the SRP-dependent or the more recently described SRP-independent (SND) targeting pathways rely on the emergence of hydrophobic polypeptide chains (transmembrane domain or signal peptide)(Aviram *et al.*, 2016; reviewed in Aviram & Schuldiner, 2017), an event that occurs sequentially after the assembly of the translation initiation complex where Bfr1 function might be integrated. Supporting the independence of Bfr1 to ribosome-to-ER targeting pathways, there is no preferential enrichment of SRP –dependent or independent proteins among the ORFs affected in *bfr1*Δ, indicating that the secretory proteins are generally affected (Figure App. 9B).

Co-localization of Bfr1 with the ER membrane seems to correlate fairly well with the presence of ribosomes (Figures 4.29C and App.9D), suggesting that Bfr1 is directly recruited to ribosomes that would eventually carry it to the ER membrane. Supporting this model, the interaction of Bfr1 with the ER membrane is shown to be abolished after RNase treatment (Lang *et al.*, 2001). One interesting factor that could function recruiting Bfr1 to ribosomes is the conserved core component of the 40S ribosomal subunit RACK1/Asc1 (Inada *et al.*, 2002). Asc1 is thought to function as a scaffold protein for multiple kinases and membrane receptors (McCahill *et al.*, 2002; Ben-Shem *et al.*, 2010), integrating inputs from different signaling pathways (Melamed *et al.*, 2010; Schmitt *et al.*, 2017). Furthermore, Asc1 has been directly linked to translation initiation (M. K. Thompson *et al.*, 2016; Gerbasi *et al.*, 2018), as it seems to interact with eIF4G and eIF3b initiation factors (Gavin *et al.*, 2002) and other RBPs such as Sro9p and Gis2p, thought to feed the ribosome with nuclear transcripts (Opitz *et al.*, 2017). Asc1 is also associated with other processes in the context of the ribosome such as ribosome quality control (Brandman *et al.*, 2012; Wolf & Grayhack, 2015; Ikeuchi & Inada, 2016) or translation control of specific mRNAs (Shor *et al.*, 2003). Interestingly Asc1 is associated with Bfr1 and Scp160 in an RNA-dependent manner (Sezen *et al.*, 2009; Opitz *et al.*, 2017) and seems to play a role in local translation control events at the nuclear envelope (Sezen *et al.*, 2009). Interaction of Scp160 with polysomes is also Asc1-dependent (Baum *et al.*, 2004), suggesting that Asc1 could work as a platform to recruit Scp160 and also Bfr1 to the ribosome. Taking all these observations together, a hypothetical model could be that Bfr1 is recruited to the 40S subunit of the ribosome by Asc1 and captures its target transcripts by the time translation initiation occurs. Perhaps Bfr1 is loosely interacting with ribosomes by default and this interaction is stabilized by the presence of a Bfr1 target

transcript. This however does not answer the question of how Bfr1 recognizes and discriminates between its client transcripts. Ribosome profiling of *bfr1*Δ revealed 510 ORFs being at least 1.5 fold-change underrespresented in the translatome (Figure 4.27, App. Data 2). Bfr1-dependent proteins highly correlate with Bfr1 mRNA targets (Lapointe *et al.*, 2015) and are significantly enriched for secretory proteins (Figures 4.27 and App.9), suggesting that Bfr1 represents a novel mechanism of local translation control at the ER membrane, where most of these proteins are actively translated (Jan *et al.*, 2014). Although it is far too early from being able to propose a mechanism behind the specificity shown by Bfr1 towards secretory proteins, one possibility is that the interaction with its target transcripts is achieved by specific determinants on the mRNA sequence that could be recognized and stabilized by Bfr1 on the ribosome. As mentioned above, determinants of client transcripts may consist of both specific sequons and/or secondary structures that would recruit Bfr1. The question of how Bfr1 interacts with mRNA was already raised in previous studies (Hogan *et al.*, 2008; Lapointe *et al.*, 2015). Based on domain prediction Bfr1 protein structure lacks any classical RNA-interacting domains while having three independent coiled-coil domains, regions previously showed to crosslink with mRNA (Kramer *et al.*, 2014) indicating that they most likely represent the effector domains for RNA binding. In line with this, multiple RBPs have been shown in the last years to carry non-canonical RNA-binding domains (Baltz *et al.*, 2012; Beckmann *et al.*, 2015; Hentze *et al.*, 2018). In-depth scrutiny of the ribosome profiling metadata and/or directed mutagenesis of Bfr1 targets are potential approaches to solve the riddle.

5.2.3 At both, sugar donor and enzyme abundance levels: How to fine-tune UPOM

Putting together the findings from the ER-GFP screening, *PGI1* and *BFR1* were confirmed and further characterized to be necessary for efficient *O*-mannosylation of ER-GFP.
First, it is shown that *PGI1* regulates UPOM most likely by defining the availability of GDP-mannose to generate Dol-P Man, the sugar donor of the protein glycosylation machinery at the ER. The data also revealed the RBP Bfr1 to modulate the translational state of PMTs, bringing the first evidence of its potential role as a local translation factor for secretory proteins. Taken together, in the hunt for UPOM components genes involved in the regulation of this process at both substrate and enzyme levels were found. This raises the

question of why PMTs would require such a meticulous tuning of their abundance and enzymatic activity?

The answer might rely on the promiscuity shown by the *O*-mannosylation machinery, which seems to have a very broad and flexible catalog of potential substrates. As recently shown, *O*-mannosylation in baker's yeast is more abundant than initially expected. The *O*-mannose glycoproteome revealed 293 secretory proteins including more than 1900 unique sites that undergo *O*-mannosylation (Neubert *et al.*, 2016). Although features such as the presence of unstructured regions and β-strands seem to favor *O*-mannosylation, no sequon has been identified yet. Along with this, PMTs have shown their capacity to *O*-mannosylate different acceptor peptides in a cell-free microsomal system as long as they emerge long enough into the lumen (Loibl *et al.*, 2014; Zatorska *et al.*, 2017, Ewa Zatorska, unpublished). Moreover, as shown in this and previous studies, the PMT complex is also able to target unfolded protein segments of multiple misfolded protein models (C. Xu & Ng, 2015) and even be the predominant type of glycosylation for proteins recombinantly expressed in yeast (Murakami-Sekimata, Sato, Sato*, et al.*, 2009).

All in all, *O*-mannosylation is pictured as a post-translational modification that, in contrast to *N*-glycosylation, is versatile and seems to target any protein substrate that contains accessible serine/threonine residues. Given that the PMT activity is not limited by a defined consensus sequence, it is possible that the cell regulates the extent of *O*-mannosylation by adapting the abundance of PMTs and the abundance of the PMT sugar donor Dol-P-Man to the existing demand. Thus, optimization of the correct PMT function is accomplished by multiple coordinated regulatory layers: First by transcription, as it is the case of the PMT upregulation upon cell wall damage *via* activation of the CWI pathway (Arroyo *et al.*, 2011); or as it is shown for the *PMT1* and *PMT2*, during UPOM when the ER faces protein folding stress. Second, PMTs are regulated at the level of protein translation by the RBP Bfr1, which ensures the correct expression of the PMT transcripts. Finally, the efficiency of *O*-mannosylation relies on the availability of cytosolic GDP-mannose *via PSA1* and *PGI1*, whose function likely determines the availability of Dol-P-mannose.

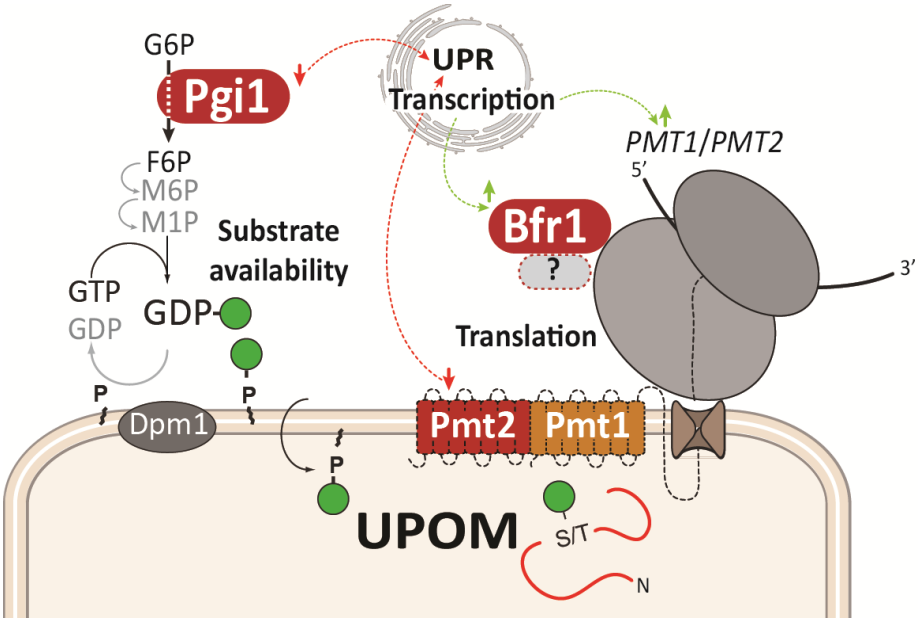

Figure 5. Model of the function of Pgi1 and Bfr1 in the context of UPOM. Model summarizing the highlights of the high throughput screening for UPOM. (left) *PGI1* ensures the efficiency of UPOM by deriving primary metabolites (Fructose-6-phosphate) for the synthesis of GDP-mannose and the sugar donor Dol-P-Man. The downregulation of the *PGI1* function results in hypoglycosylation and UPR activation. (right) *BFR1* works in the frame of translation ensuring the expression of a subset of transcripts mainly functioning across the secretory pathway; including *PMT1* and *PMT2*. The expression of both the Pmt1-Pmt2 complex and Bfr1 is coordinated by the UPR. The mechanism underlying the Bfr1 function remains unknown and it is likely involving additional factors.

As it is for *PMT1* and *PMT2*, both genes *PGI1* and *BFR1* are connected to ER folding stress (Figures 4.18 and 4.31, respectively). What happens during ER stress is a very figurative example of how UPOM, in particular, could be fine-tuned (Figure 5): Expression of the slow folding protein ER-GFP compromises ER homeostasis and the cell responds activating the UPR and therefore increasing the transcript level of *PMT1* and *PMT2*. At this point two conditions determine the efficiency of UPOM: First Dol-P-Man content must be sufficient to ensure effective *O*-mannosylation, resulting in additional ER stress when depleted. Second, *BFR1*, which is also upregulated by the UPR, will ensure efficient translation of PMT transcripts.

An existing question derived from the hypothesis of the PMT promiscuity is whether meticulous regulation of the enzymatic function is also present for other *O*-glycosylation types that lack a consensus sequence. In yeast, *O*-mannosylation is the only type of *O*-glycosylation and it is fairly abundant along the secretory pathway (Neubert *et al.*, 2016). In mammals, however, *O*-mannosylation is so far only present in a few cell surface proteins such as α-dystroglycan, KIAA1549, members of the cadherin and plexin superfamilies and

lecticans (Moore & Hewitt, 2009; Pacharra *et al.*, 2013; Vester-Christensen *et al.*, 2013). Furthermore, *O*-mannosylation in mammals coexists with other types of *O*-glycosylation, being the mucin-type *O*-GalNAc glycosylation the most common modification (Steentoft *et al.*, 2013). Interestingly, *O*-GalNAc also lacks a general consensus sequence and shares a set of substrates with *O*-mannosylation orthologs in yeast, based on glycoproteomic data (Neubert *et al.*, 2016). Perhaps in analogy to PMTs, the expression of GalNAc-transferases also undergoes post-transcriptional regulation to cope with the absence of specificity at the sequence level of target proteins.

The genes *BFR1* and *PGI1* found in the screen to be necessary for UPOM represent the high heterogeneity among the requirements of *O*-mannosylation during ER stress. Especially regarding the function of Bfr1, it is proposed that the existence of manifold regulatory levels of PMT protein abundance serves as a mechanism to adapt the *O*-mannosylation activity at the enzymatic level to the cellular needs, thus compensating for the high versatility of PMTs in finding potential protein substrates.

5.3 *O*-Mannosylation, quality control, and protein fate: substrate's nature matters

In the third part of the study the question of how *O*-mannosylation impacts protein dynamics was approached. The goal of this part was to shed light on the heterogeneity shown by PMT target proteins when it comes to the influence of *O*-glycans on protein turnover. As developed in 1.4.2, the fate of several misfolded protein models that become UPOM targets is to undergo degradation either by ERAD or by vacuolar turnover as the final step of their quality control. Strikingly, *O*-mannosylation is not always a determinant for protein degradation since in the absence of UPOM several misfolded model proteins are nevertheless degraded (C. Xu & Ng, 2015). Else ways, the effect of *O*-mannosylation on protein stability is not restricted to UPOM function. It is long known that *O*-mannosylation is necessary for the complete maturation of a set of secretory proteins. The absence of major members of the PMT family reduces the stability of the plasma membrane proteins Wsc1, Wsc2, Mid2, and Mtl1 (Lommel *et al.*, 2004; Petkova *et al.*, 2012).

It was a goal to confirm the coexisting opposing effects of *O*-mannosylation on protein stability and to overcome the obstacle of redundancy within the PMT family by dissecting the contribution of each major PMT member. In the hope that high throughput

methodologies are suitable to address such complex scenarios, it was taken advantage of tandem fluorescent protein timers to estimate the lifetime of a set of proteins described to be *O*-mannosylated (Neubert *et al.*, 2016) upon deletion of each of the major components of the PMT machinery: *PMT1*, *PMT2* and *PMT4*.

O-mannosylation-dependent changes in protein stability were inferred from Δ-scores obtained by subtracting the ratio mCherry/sfGFP of 137 tFT C-terminal fusion proteins in wild type versus *pmt*Δ mutant. Under the applied conditions, the great majority of tFT fusions did not exhibit severe changes in Δ-score suggesting that *O*-mannosylation might not influence the protein's lifetime (App. Data 2, Figure App.10). However, a total of 39 individual proteins were found clearly affected (Figure 4.32A and C). Δ-scores suggested the presence of both effects, protein stabilization and destabilization upon deletion of individual PMTs. Among the 39 tFT fusions potentially destabilized Wsc2 and Axl2 were found, which were previously described to have maturation defects upon PMT deletion (Sanders *et al.*, 1999; Lommel *et al.*, 2004).

As a proof of principle, the known example of Axl2 was used to validate the findings from the tFT screening. Fluorescence microscopy confirmed the localization of Axl2-tFT to the bud neck in the sfGFP channel whereas additional vacuolar localization was found for the older pool of the protein at the mCherry channel, indicating most likely protein turnover in this organelle. In a *de novo* generated *pmt4*Δ mutant changes in the mCherry/sfGFP intensity ratio were confirmed and in agreement with the destabilization of the protein, vacuolar localization of Axl2-tFT was observed already in the sfGFP channel (Figure 4.33A). Moreover, the running behavior of Axl2-tFT in an SDS-PAGE (Figure 4.33B) was compared with a previously described Axl2 C-terminally HA-tagged (Sanders *et al.*, 1999). A similar degradation pattern was observed upon *PMT4* deletion, confirming what previously shown for Axl2.

Mining the data on tFT fusions destabilized upon PMT deletion yields Tsc3, which appears to be affected in a similar manner in all three *pmt*Δ (Figure 4.33C). Tsc3 is a subunit of the serine palmitoyltransferase involved in the biosynthesis of sphingolipids (Gable *et al.*, 2000). Sphingolipids are particularly relevant for the formation of membrane rafts involved in the ER trafficking of GPI-anchored proteins (Helms & Zurzolo, 2004). GPI-anchored proteins are major targets of PMTs (Neubert *et al.*, 2016) and *O*-mannosylation appears to be necessary for correct ER export of the GPI-anchored protein Gas1 (Goder & Melero, 2011).

Additionally, Ted1, a protein involved in remodeling of GPI glycan moieties, was found destabilized in *pmt1*Δ and *pmt4*Δ. Ted1 is described to act in concert with the members of the p24 family Emp24 and Erv25 promoting cargo exit from the endoplasmic reticulum (Haass *et al.*, 2007). Besides being a target of *O*-mannosylation, Ted1 is, together with Emp24 and Erv25 a physical interactor of the Pmt1-Pmt2 complex (Goder & Melero, 2011). Furthermore, it was recently shown that the deletion of *PMT1* on top of *ted1*Δ suppresses the shortened replicative lifespan of the single deletion (Cui *et al.*, 2018). The fact that the stability of Tsc3 and Ted1 relies on PMT function suggests that *O*-mannosylation might work in concert with sphingolipid biosynthesis and GPI-anchor remodeling enzymes to ensure the correct export of GPI anchored proteins out of the ER. Based on these findings, the functional connection between *O*-mannosylation and the GPI anchor remodeling machinery is indeed an intriguing scenario to be explored in the future.

Next, the focus was put on tFT fusions showing a Δ-score indicative for protein stabilization. This perhaps was the most interesting subset of affected tFT fusions because the role of PMTs in assisting protein turnover has been so far only described for artificial misfolded model proteins in the frame of UPOM. Therefore, finding endogenous proteins that undergo degradation in a PMT-dependent manner is fundamental to understand whether UPOM is a physiologically relevant mechanism. Among the tFT fusions validated by flow cytometry using *de novo* generated *pmt*Δ mutants Kre6-tFT was characterized. Kre6 is a type II integral membrane protein; required for beta-1,6 glucan biosynthesis. Kre6 was described to cycle between the ER and the Golgi to be released to the plasma membrane at sites of polarized growth (Takeuchi *et al.*, 2008; Kurita *et al.*, 2011). The data on Kre6-tFT localization show that a C-terminal tFT-tag interferes with the localization of Kre6, indicated by the presence of the fusion protein largely at the vacuole in both wild type and *pmt1*Δ. Although the potential misfolding or Kre6-tFT and neither the influence of the tFT-tag on the protein function were investigated in this work, the interaction between the C-terminal domain of Kre6 with a set of chaperones and chaperone-like proteins such as Kar2, Rot1, and Keg1 has been described. Under the absence of Keg1 or Rot1, Kre6 is destabilized and degraded in a Pep4 and Ubc7-dependent manner indicating that both ERAD and the vacuole are involved in the turnover of misfolded Kre6 (Takeuchi *et al.*, 2008; Kurita *et al.*, 2012). Based on these observations, it is proposed that an intact C-terminal domain is required for the correct localization of Kre6. Likely the addition of the tFT-tag hampers the interaction of Kre6 with

the above-mentioned proteins causing misfolding defects that direct the protein for vacuolar turnover.

Under conditions that mislocalize Kre6, *O*-mannosylation by Pmt1 becomes a requirement for correct turnover (Figure 4.34A and B). Also, Pmt2 was shown in the tFT screening to contribute to Kre6-tFT stability in a similar manner as Pmt1 (Figure 4.32C), indicating that the effect on the turnover of Kre6-tFT is caused by the Pmt1-Pmt2 complex. The fact that Kre6-tFT was observed at the vacuole suggests that turnover is mainly taking place in this organelle. This, however, does not exclude ERAD as a contributor to Kre6-tFT degradation as previously indicated (Kurita *et al.*, 2012). At this point, there are different scenarios that could explain how the presence of *O*-glycans would enhance Kre6-tFT turnover. One attractive possibility is that *O*-glycans on misfolded proteins might modify the protein structure and enhance the accessibility of vacuolar proteases to cleaving sites that could remain hidden in the non-glycosylated counterparts. This hypothesis is supported by the enhanced sensitivity of ER-GFP to proteases *in vitro* when comparing to ER-GFP$_f$ (C. Xu *et al.*, 2013) and could be an additional contributor to the increased fluorescence intensity of non-retained ER-GFP at the vacuole observed in *pmt1*Δ and *pmt2*Δ (Figure 4.7). It is also possible, that protease activity is modulated by *O*-mannosylation itself since several vacuolar proteases are found to be *O*-mannosylated, including proteinase A (Pep4), proteinase B (Prb1), aminopeptidase Y (Ape3) and carboxypeptidase S (Cps1) (Neubert *et al.*, 2016). In general, protein glycosylation is considered a contributor to protease activity, and both enhancing and inhibiting effects have been described (Goettig, 2016). With these considerations, it is proposed that given the many requirements for proper Kre6 maturation, the dependence of Kre6-tFT stability on the Pmt1-Pmt2 complex might indicate that *O*-mannosylation is a relevant mechanism to facilitate protein disposal under the many conditions that induce Kre6 misfolding.

Other ER stabilized tFT fusions that were not further analyzed include the Pmt2 paralog Pmt3 which shows a very significant Δ-score in all three *pmt1*Δ, *pmt2*Δ and *pmt4*Δ mutants (Figure 4.33C). Pmt3 together with Pmt5 are members of the PMT family considered minor contributors to the overall PMT activity and are described to form redundant complexes with both Pmt1 and Pmt2 (Girrbach & Strahl, 2003). Previous unpublished data from the Strahl lab already pointed out the increase in Pmt3 protein abundance in the absence of the

Pmt1-Pmt2 complex. Another interesting protein is Sec12-tFT involved in COPII vesicle formation and found to be also strongly affected in all three *pmt*Δ mutants. Although some tFT fusions are affected similarly in *pmt1*Δ and *pmt2*Δ, this not always the case. A good example to illustrate this observation is Ire1-tFT, which seems to be stabilized in *pmt2*Δ whereas no effect was notified in *pmt1*Δ (Figure 4.33C). The different effects of each of the three PMT deletions on protein stability might be indicative of the substrate specificity of the different PMT complexes. Therefore, the data provided by the tFT screen could be taken to start dissecting the *O*-mannose glycoproteome into each PMT's contribution while waiting for more robust proteomic data.

Overall, the tFT screen is the first high throughput attempt to clarify the role of *O*-glycans in protein stability. Valuable data with strong potential to infer *O*-mannosylation-dependent changes in protein stability is provided for 137 tFT fusions. Results are in agreement with previous indications of the double-edged sword effect of *O*-mannosylation which on one hand assists protein maturation and on the other actively contributes to protein turnover. The prevalence of either effect seems to be greatly dependent on the nature of the substrate. One ideal explanation for this would arise from classifying proteins with shortened lifetime upon *O*-mannosylation defects as *bona fide* targets that require this modification for their maturation, whereas proteins with increased stability could be considered as targets of an *O*-mannosylation-dependent quality control pathway. Thus, the requirement of the Pmt1-Pmt2 complex for efficient vacuolar turnover of mislocalized and probably misfolded Kre6 were characterized. Whether what these observations are translatable to native Kre6 is pending for investigation. Still, Kre6-tFT could be considered a suitable protein model to characterize in detail the role of *O*-glycans in the efficiency of vacuolar degradation of misfolded proteins.

5.4 Final remarks: Defining UPOM, is it really happening?

Although the term UPOM has not been used until very recently (C. Xu *et al.*, 2013; C. Xu & Ng, 2015), the addition of *O*-glycans on misfolded proteins was described already almost two decades ago (Harty *et al.*, 2001). Throughout this current work it was aimed to i) clarify the relationship between ER stress and *O*-mannosylation; ii), to unravel mechanistically the UPOM machinery in a high throughput screen and iii), to explore the effects of

O-mannosylation on protein stability, mainly aiming to explore the physiological relevance of UPOM.

With a birds-eye-view of all three different parts, it can certainly be stated that *O*-mannosylation and in particular the Pmt1-Pmt2 complex is a key contributor to ER homeostasis in *Saccharomyces cerevisiae* (see 5.1). However, the high throughput screening was unable to find mechanistic differences, in terms of specific factors that define and differentiate UPOM from canonical *O*-mannosylation. On the contrary, evidence was found for *O*-mannosylation being a process that is tightly regulated at multiple layers, perhaps balancing the lack of specificity shown by the PMT machinery (see 5.3). Evidence of *O*-mannosylation being a determinant for protein stability was provided, together with a large number of proteins that likely follow an *O*-mannosylation dependent degradation pathway. However, it is too early to state that UPOM is a process mechanistically different from *O*-mannosylation as it has been recently defined (C. Xu & Ng, 2015). The basis of PMT substrate recognition rather suggests that *O*-mannosylation targets proteins based on confirmation cues, implying a competition mechanism between protein folding and glycosylation during, and likely also after translocation. Who wins the game perhaps depends on each polypeptide's folding intermediates and the accessibility of Ser and Thr residues during its journey to the final native state.

6 APPENDIX

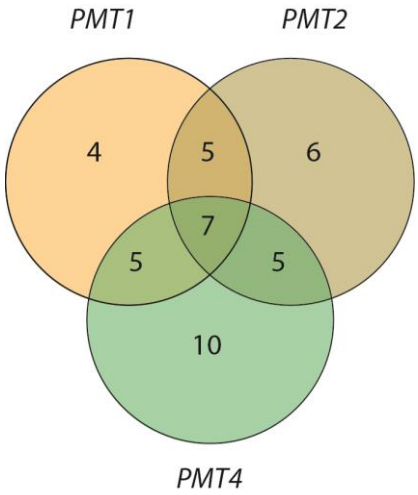

Figure App 1. Analysis of transcription factors associated with *PMT1*, *PMT2* and *PMT4* in the Yeastract database (Teixeira *et al.*, 2018). Results show the number of transcription factors associated with each gene based on bibliographic references.

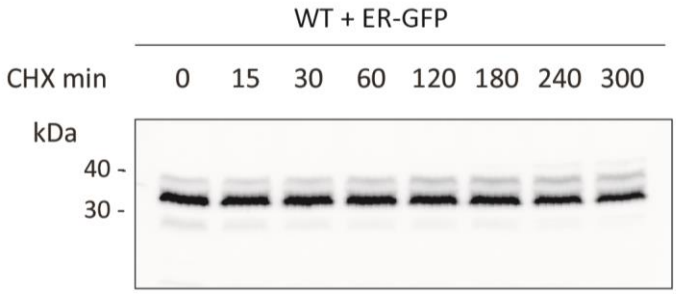

Figure App 2. Cycloheximide chase analysis of ER-GFP. Wild type (BY4741) cells were transformed with plasmid pWXB206 (ER-GFP) and treated with 200 µg/ml cycloheximide. Equivalent to 10 OD_{600} cells was sampled at the indicated time points. The equivalents to 0.2 OD_{600} of total cell extract were resolved on a 12% PAA gel subjected to Western blot analysis using anti-GFP antibody. Consistent with (C. Xu *et al.*, 2013), ER-GFP is stable when retained in the ER. This experiment was performed by Dr. Ewa Zatorska in collaboration with the author.

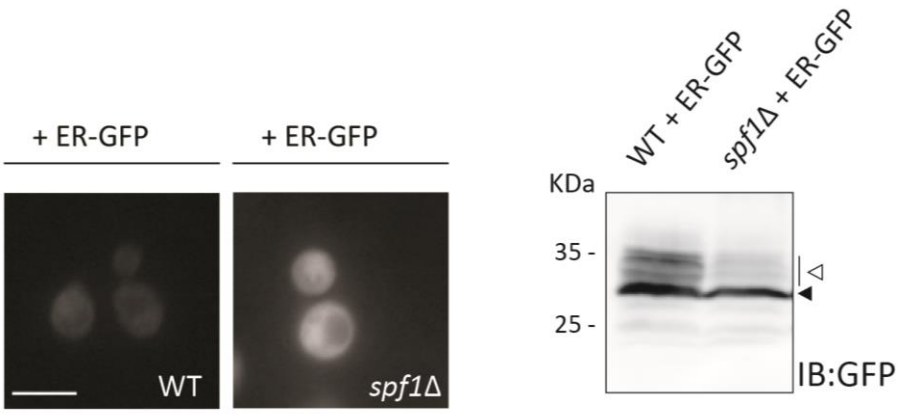

Figure App 3. **Analyses of ER-GFP in *spf1*Δ.** (**A**) Wild type (BY4741) and *spf1*Δ (Euroscarf) cells were transformed with pWXB206 (ER-GFP), grown in SD-Uracil and imaged under standard conditions. The deletion of *SPF1* causes partial cytosolic localization of ER-GFP. This experiment was performed by Karen Schriever under the author's supervision and included in the bachelor thesis: "Assessing a possible role of unfolded protein *O*-mannosylation as a complementary Endoplasmic Reticulum quality control mechanism in *Saccharomyces cerevisiae",* submitted to the Ruprecht-Karls-University (Heidelberg faculty of Biosciences) in 2015. (**B**) Total cell extracts were prepared from the strains shown in (A) and analyzed by western blot. Equivalents of 0.2 OD_{600} of protein were resolved on a 12% PAA gel and blotted with anti-GFP antibody. *SPF1* deletion causes a reduction in the presence of the *O*-mannosylated fraction of ER-GFP (indicated with white arrow).

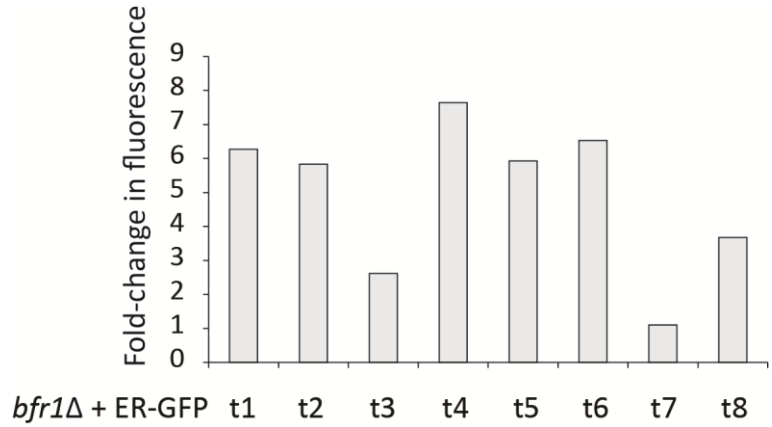

Figure App 4. **Flow cytometry analysis of *bfr1*Δ knockout transformants**. *BFR1* was knocked out in JEY06 (wild type ER-GFP) by homologous recombination. A knockout cassette containing up and downstream *BFR1* homologous regions and *KanMX6* was generated via PCR (oligos 2810-2811) from pUG6 and transformed according to 3.2.12. After selection, KanMX6 insertion was verified by PCR and eight independent transformants (t1-t8) were grown in YPD and analyzed by flow cytometry. R values indicative of the cell population's fluorescence intensity (see 3.5.3) are normalized to R_{WT} and results are plotted as fold-change. Results show heterogeneity in the expected increase of ER-GFP fluorescence.

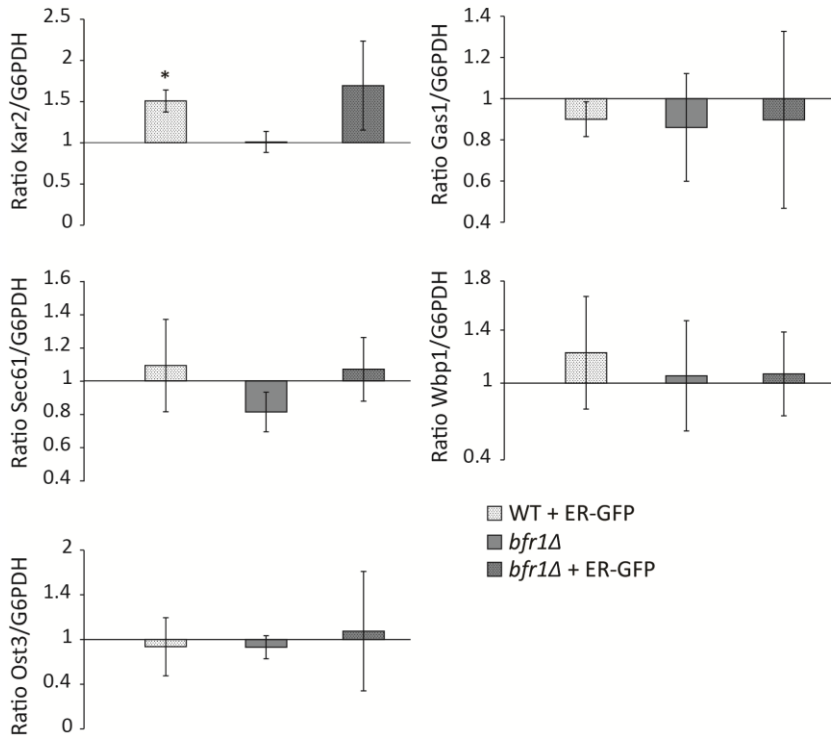

Figure App 5. Quantification of the western blot of representative targets of Bfr1 at the mRNA level (figure 4.23). Western blot signals were quantified using Image Studio Lite V.5.2 as a Pmt/G6PDH ratio, normalized to $Pmt_{WT}/G6PDH_{WT}$ averaged and plotted as fold-change. For statistical significance, a one-tail Student's test was applied to averaged fold-change values (n=3).

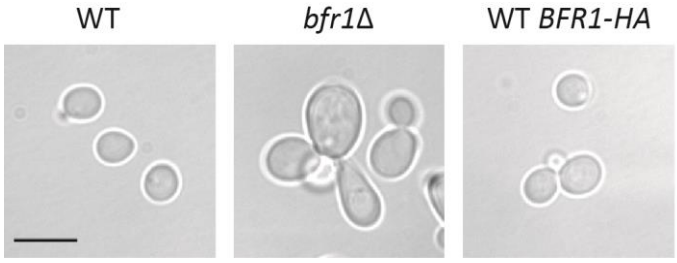

Figure App 6. Evaluation of functionality of Bfr1-3xHA. A yeast strain including a genomic 3xHA c-terminal tag of *BFR1*(JCY017) was generated by homologous recombination. A tagging cassette containing sequences homologous of *BFR1* 3', 3xHA and *KanMX6* was generated via PCR (oligos 2885-2886) from pJH24 and transformed into wild type cells (BY4741) according to 3.2.12. After selection, KanMX6 insertion was verified by PCR. A validated transformant was grown together with wild type (BY4741) and *bfr1*Δ in YPD and imaged under standard conditions, scale bar 5 µm. Results show no phenotypic effect of the 3xHA C-terminal tag.

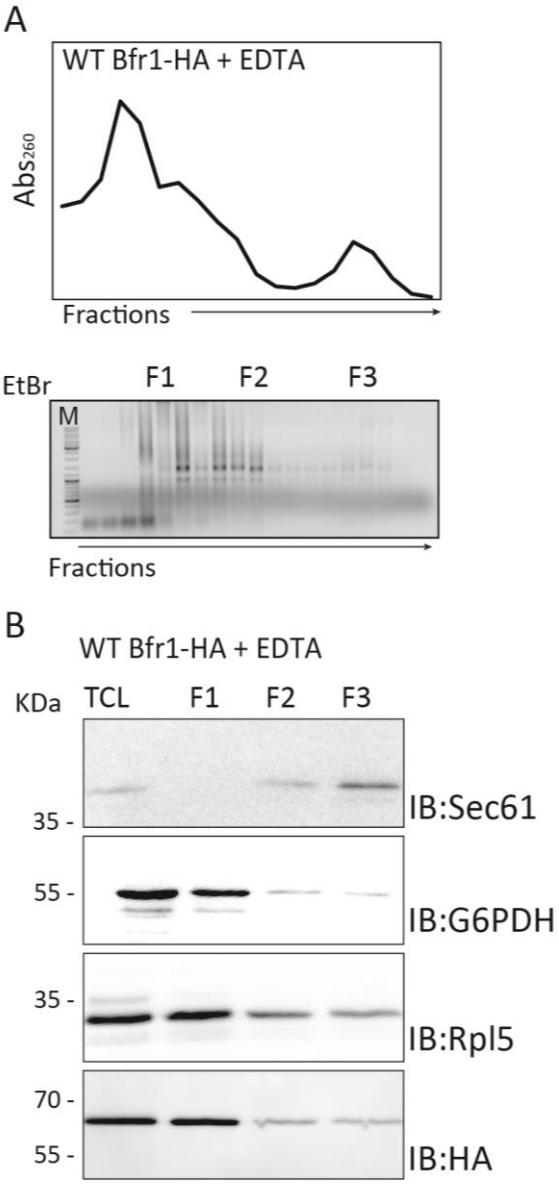

Figure App 7. Analyses of protein and RNA content of EDTA-treated cell lysates after fractionation by sucrose gradient. As a control for what shown in Figure 4.27B, total cell extracts prepared from wild type (*BFR1-HA*, strain JCY017) were supplemented with 30 mM EDTA prior load in a sucrose gradient. (**A**, Upper panel) Abs_{260} of each fraction sampled from the sucrose gradient. (Lower panel) The equivalents of each fraction were resolved ion an agarose gel and stained with ethidium bromide. Addition of EDTA causes both, disengagement of ribosomes from the membrane containing sucrose fraction (F3) and disassembly of the ribosomal subunits at the sucrose fractions where they accumulate (F2 and F3).(**B**) 0.25 OD_{600} units of total cell extract and equivalents of each sucrose fraction were resolved on a 12% PAA gel and analyzed by Western blot using the indicated antibodies. In comparison to Figure 4.29C, EDTA treatment results in decreased prevalence of Rpl5 and Bfr1-HA at F2 and F3 fractions.

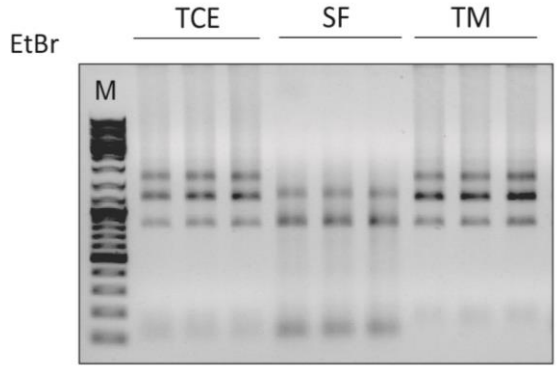

Figure App 8.Analysis of RNA content after cell fractionation by 1-step ultracentrifugation. 400 ng of total mRNA extracted from total cell extract (TCE) soluble fraction (SF) and total membrane fraction (TM) prepared from wild type (*BFR1-HA*, strain JCY017) were resolved in triplicate in an agarose gel and stained with ethidium bromide. Results show the distribution of ribosomal subunits in each fraction.

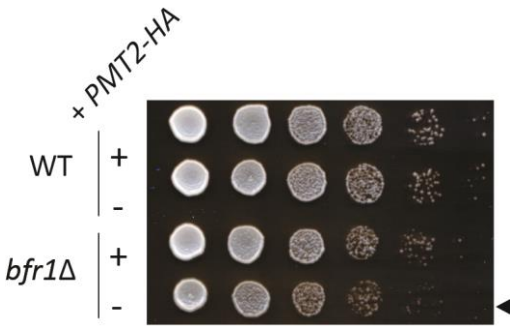

Figure App 7. Spotting assay of wild type (BY4741), *bfr1*Δ (Euroscarf), JEY06 (wild type expressing ER-GFP) and *bfr1*Δ ER-GFP (strain resulting from SGA crosses) expressing either pRS41N (empty vector, EV) or pJC10 (*PMT2-3xHA*). Serial 10-fold dilutions cells were spotted on solid YPD medium containing nourseothricin for selection and grown at 30 °C for 24h. In contrast to the native protein, overexpression of C-terminally tagged Pmt2 in *bfr1*Δ cells results in a modest growth defect (indicated with black arrow).

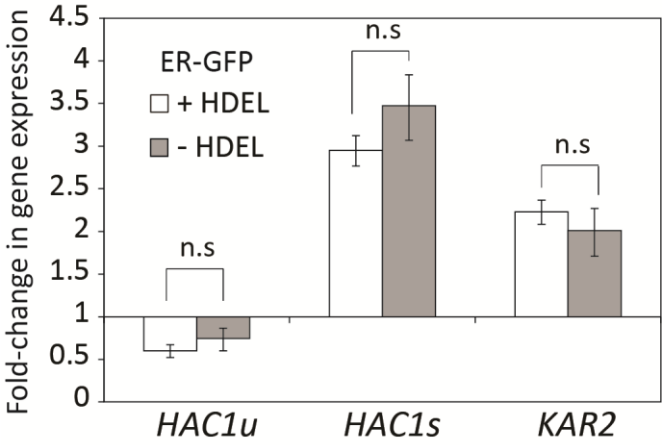

Figure App 8. Fold-change in mRNA levels of HAC1^{u}, HAC1^{s,} and KAR2 upon expression of retained or non-retained ER-GFP. Wild type cells (BY4741) were transformed with either pWXB206 (ER-GFP) or pJC07 (non-retained ER-GFP). Total RNA was extracted either from cells grown in SD (wild type) or SD-Uracil (transformed wild type). cDNA was prepared from total mRNA according to 3.2.3 and 3.2.4 and RT-PCR was performed according to 3.2.9. Fold-change is calculated by averaging Cts with respect to *ACT1*. Errors bars show the confidence interval. For statistical significance, a two-tailed t-Student's test was applied to log ($2^{-\Delta\Delta Ct}$), n=3.

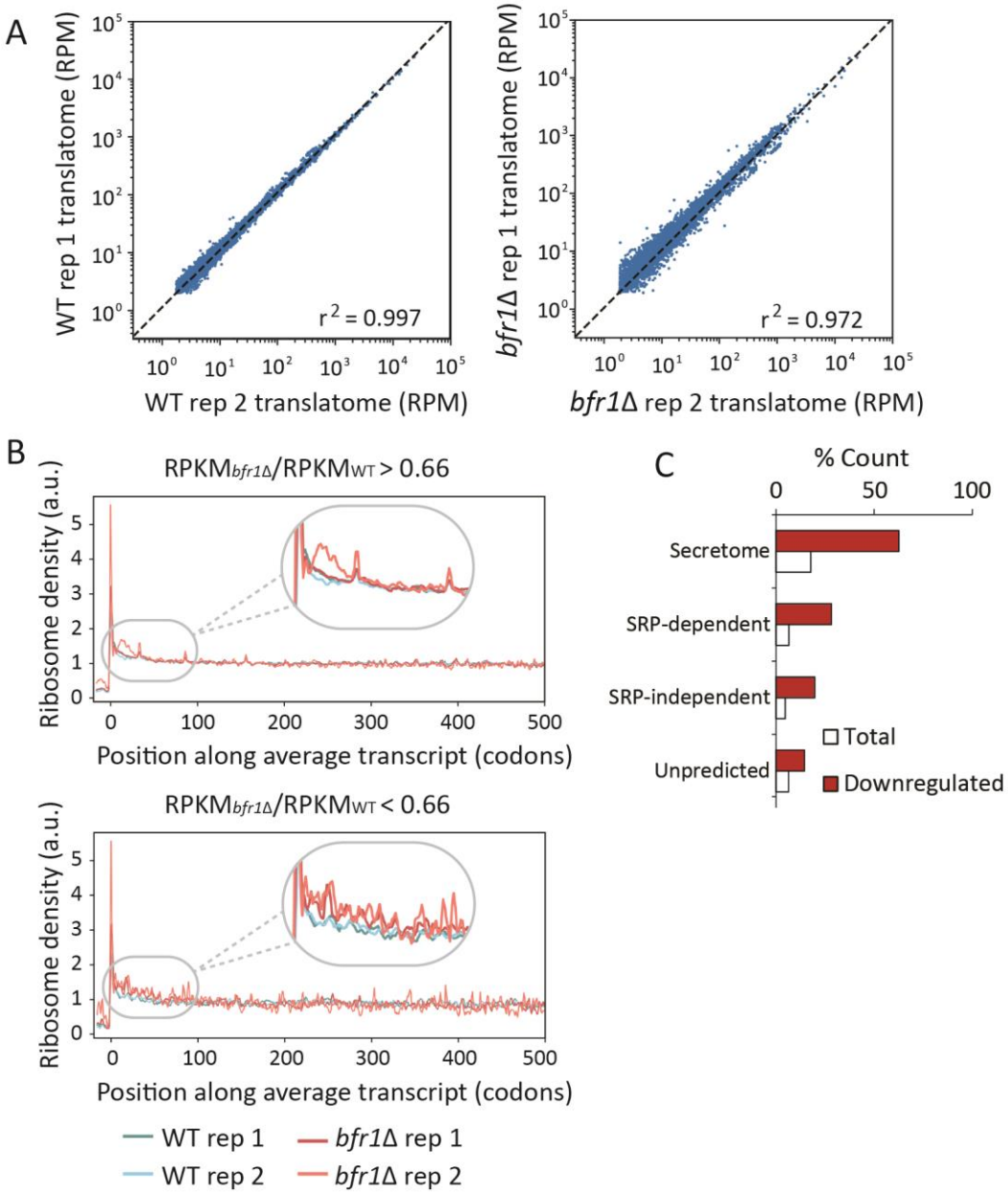

Figure App 9. (**A**) Scatter plot illustrating the correlation between the two replicates for the translatome of wild type and *bfr1*Δ in the ribosome profiling experiment (Figure 4.27). Figure section adapted from Ilgin Kotan (**B**) Metagene analysis of ORF underrepresented in *bfr1*Δ translatome vs the remaining ORFs according to 1.5 fold-change threshold (below or above 0.66 $RPKM_{bfr1\Delta}/RPKM_{WT}$, lower and panel, respectively) in the two replicates for WT and *bfr1*Δ used for ribosome profiling (Figure 4.27). Ribosome protected footprints of underrepresented ORFs show a modest tendency to accumulate in the first 100 codons of averaged ORF sizes. Analyses performed by Ilgin Kotan. (**C**) Analyses of functional categories enriched among ORFS below the threshold with respect to the total translatome. Gene annotation for secretome, SRP-dependent, SRP-independent and unpredicted is based on Ast *et al.*, 2013.

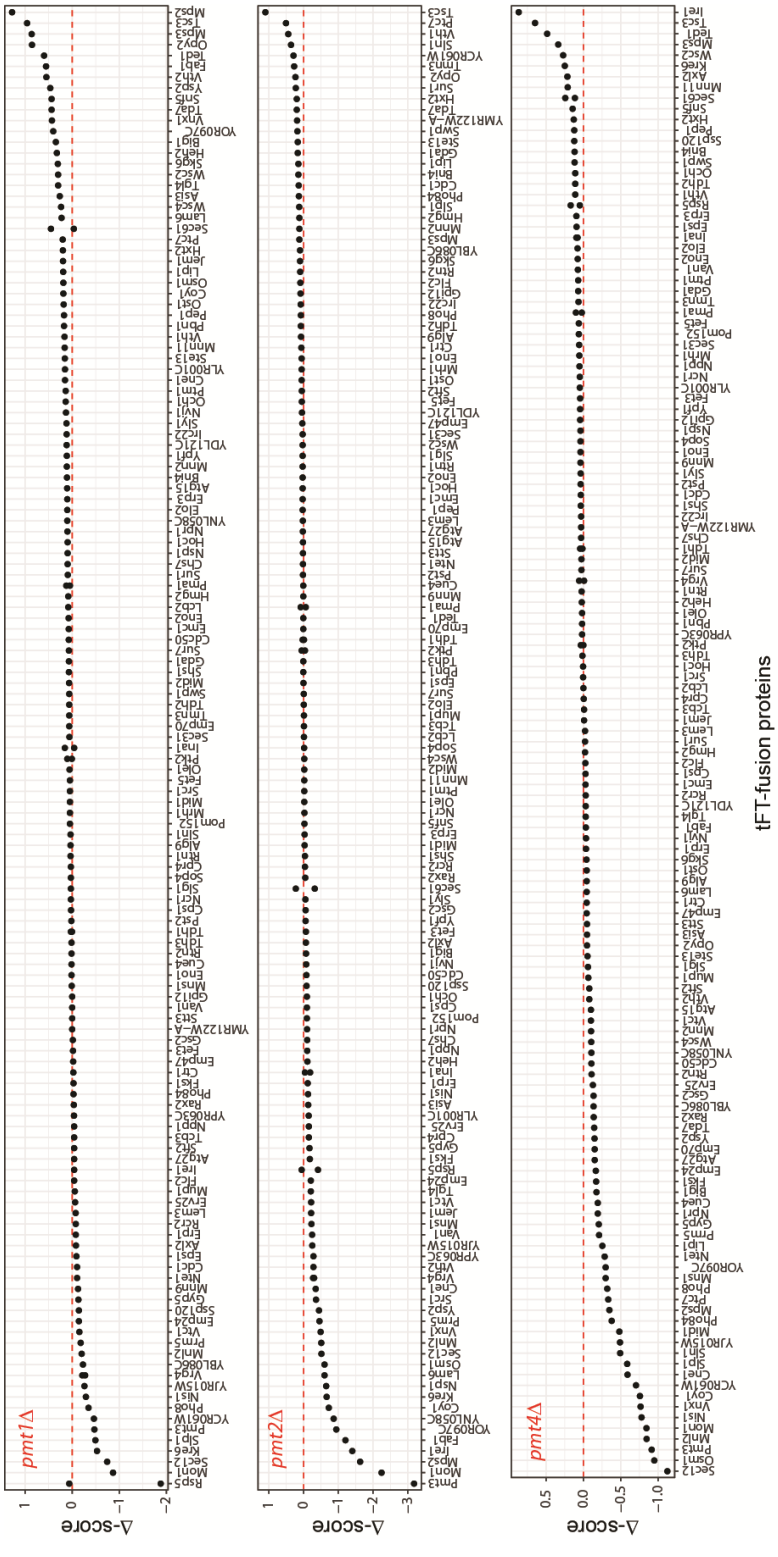

Figure App 10. Dynamics of tFT-fusion proteins in different *pmtΔ* strains. Differences in fluorescence intensities of mCherry and sfGFP are compared between mutant and wildtype strain (Δ-score) and summarized in an ordered dot plot. A negative Δ-score indicates a prolonged lifetime of the tFT-fusion protein in the mutant compared to the wildtype, while a positive Δ-score indicates destabilizing effects and a higher turnover of protein. Measurements were performed by high throughput fluorescence microscopy of triplicates. Proteins with multiple results were spotted on multiple plates for internal control. Results are shown as a measure of variance between experiments. Figure designed by Patrick Neubert and published in Castells-Ballester *et al.*, 2018.

Table App 1. ER-GFP results are shown. Median intensity of ER-GFP intensity of each mutant and median error (MAD) associated. Hsp150 phenotypes according to Figure 4.11. ER-GFP O-mannosylation reduction according to figure 4.12. Mutants below the threshold but with ER-GFP intensities above the wild-type controls are highlighted in grey. N.d – not determined. Experiment performed performed by Lihi Gal in collaboration with the group of Prof. Maya Schuldiner (Weizmann Institute of Science, Rehovot, Israel).

ORF	Gene	Median Intensity Gfp	Error	Hsp150 phenotype	Decreased ER-GFP *O*-mannosylation
YEL031W	SPF1	363	34	*pop*2Δ-like	YES
YDR123C	INO2	299	28	*ost3*Δ-like	NO
YAL023C	PMT2	295	21	WT	YES
YPR049C	ATG11	270	32	WT	NO
YDR195W	REF2	246	31	WT	n.d
YOR198C	BFR1	245	34	*pop*2Δ-like	YES
YNL064C	YDJ1	236	27	WT	NO
YJL006C	CTK2	234	0	*pop*2Δ-like	n.d
YNR052C	POP2	231	29	*pop*2Δ-like	NO
YIL147C	SLN1	230	28	n.d	NO
YEL043W	YEL043W	220	34	*ost3*Δ-like	NO
YGR135W	PRE9	219	33	*ost3*Δ-like	NO
YJL088W	ARG3	219	40	*ost3*Δ-like	NO
YLR087C	CSF1	215	37	WT	NO
YNL208W	YNL208W	212	41	*ost3*Δ-like	NO
YDR025W	RPS11A	211	33	WT	NO
YNL099C	OCA1	209	35	*ost3*Δ-like	NO
YOR085W	OST3	208	40	*ost3*Δ-like	NO
YDL077C	VAM6	208	31	*ost3*Δ-like	NO
YLR079W	SIC1	207	32	*ost3*Δ-like	NO
YDR207C	UME6	207	30	WT	NO
YOL008W	COQ10	207	44	*ost3*Δ-like	n.d
YNL079C	TPM1	205	35	WT	NO
YIL103W	DPH1	205	34	WT	NO
YMR247C	RKR1	204	39	WT	NO
YGL003C	CDH1	202	37	*ost3*Δ-like	NO
YPL238C	YPL238C	202	37	n.d	NO
YDR369C	XRS2	200	33	*pop*2Δ-like	NO

YER151C	UBP3	200	38	*ost3*Δ-like	NO
YML112W	CTK3	199	25	WT	n.d
YDL097C	RPN6	199	32	n.d	NO
YMR306W	FKS3	198	38	WT	NO
YNL198C	YNL198C	197	50	WT	NO
YGL016W	KAP122	197	34	WT	NO
YNL097C	PHO23	197	34	WT	NO
YBR003W	COQ1	197	35	WT	NO
YIL110W	HPM1	197	0	WT	NO
YDL095W	PMT1	197	24	WT	YES
YLR039C	RIC1	196	29	WT	NO
YPR017C	DSS4	196	41	WT	NO
YKR100C	SKG1	196	28	WT	NO
YJL064W	YJL064W	196	43	WT	NO
YNL056W	OCA2	196	29	*ost3*Δ-like	NO
YBR150C	TBS1	196	39	WT	NO
YDL055C	PSA1	196	35	n.d	NO
YKR104W	YKR104W	195	49	WT	NO
YPL094C	SEC62	195	34	n.d	NO
YPL143W	RPL33A	195	33	n.d	NO
YNL199C	GCR2	194	50	WT	NO
YKR048C	NAP1	194	35	WT	NO
YJL065C	DLS1	194	37	WT	NO
YBR131W	CCZ1	194	42	*ost3*Δ-like	NO
YBR001C	NTH2	194	27	WT	NO
YNL120C	YNL120C	194	30	WT	NO
YER161C	SPT2	194	24	WT	NO
YLR140W	YLR140W	194	37	n.d	NO
YHR178W	STB5	194	37	WT	NO
YDR363W-A	SEM1	193	36	WT	NO
YDR250C	YDR250C	193	40	WT	NO
YMR142C	RPL13B	193	28	WT	n.d
YJL063C	MRPL8	193	35	WT	n.d

YBR009C	HHF1	193	37	*pop*2Δ-like	NO
YBR272C	HSM3	193	34	WT	NO
YJL068C	YJL068C	192	37	WT	NO
YNL054W	VAC7	192	30	WT	NO
YBR008C	FLR1	192	30	WT	NO
YBR012C	YBR012C	192	32	WT	NO
YNL115C	YNL115C	192	29	WT	NO
YPR043W	RPL43A	192	36	WT	NO
YER122C	GLO3	192	43	*pop*2Δ-like	NO
YLL039C	UBI4	192	27	WT	NO
YJL115W	ASF1	191	45	*pop*2Δ-like	NO
YPR014C	YPR014C	191	34	WT	NO
YBR005W	RCR1	191	33	WT	NO
YNL104C	LEU4	191	39	WT	NO
YLL038C	ENT4	191	35	WT	NO
YGL028C	SCW11	190	37	WT	NO
YGL027C	CWH41	190	59	*pop*2Δ-like	NO
YMR089C	YTA12	190	42	WT	n.d
YKR103W	NFT1	190	44	*ost3*Δ-like	NO
YNL069C	RPL16B	190	28	*ost3*Δ-like	n.d
YNL100W	MIC27	190	46	*ost3*Δ-like	NO
YDR525W	API2	190	31	*ost3*Δ-like	NO
YDR349C	YPS7	190	42	WT	NO
YCL005W	LDB16	190	38	*ost3*Δ-like	n.d
YDR225W	HTA1	190	36	*ost3*Δ-like	NO
YNL196C	SLZ1	189	44	WT	NO
YIL044C	AGE2	189	46	*ost3*Δ-like	NO
YIL053W	GPP1	189	42	*ost3*Δ-like	NO
YMR125W	STO1	189	40	WT	NO
YKR093W	PTR2	189	41	*ost3*Δ-like	NO
YNL078W	NIS1	189	39	*ost3*Δ-like	NO
YBR276C	PPS1	189	33	*pop*2Δ-like	NO
YDL006W	PTC1	189	32	*ost3*Δ-like	NO

YGL011C	SCL1	189	32	n.d	NO
YGL048C	RPT6	189	31	n.d	NO
YPR135W	CTF4	188	36	*pop*2Δ-like	NO
YGR237C	YGR237C	188	37	WT	NO
YJL073W	JEM1	188	68	WT	NO
YMR311C	GLC8	188	43	WT	NO
YPR020W	ATP20	188	39	WT	NO
YKR098C	UBP11	188	43	WT	NO
YBL099W	ATP1	188	30	WT	n.d
YBR083W	TEC1	188	39	WT	NO
YNL083W	SAL1	188	33	WT	NO
YBR287W	YBR287W	188	31	*ost3*Δ-like	NO
YGL105W	ARC1	188	44	*pop*2Δ-like	NO
YLL024C	SSA2	188	34	WT	NO
YKL048C	ELM1	188	34	*ost3*Δ-like	NO
YNL219C	ALG9	187	28	n.d	NO
YPL158C	AIM44	187	44	n.d	NO
YIL045W	PIG2	187	39	n.d	NO
YMR312W	ELP6	187	50	n.d	NO
YJL057C	IKS1	187	42	n.d	NO
YDL104C	QRI7	187	28	n.d	NO
YJR087W	YJR087W	187	37	n.d	NO
YKR046C	PET10	187	33	n.d	NO
YIL100W	YIL100W	187	27	n.d	NO
YBR270C	BIT2	187	34	n.d	NO
YFL001W	DEG1	187	35	n.d	NO
YBR196C	PGI1	187	30	n.d	YES
YFR050C	PRE4	187	26	n.d	NO
YMR025W	CSI1	187	32	n.d	NO
YGL007W	BRP1	186	40	n.d	NO
YJL099W	CHS6	186	37	n.d	NO
YMR271C	URA10	186	42	n.d	NO

YBL107C	MIX23	186	30	n.d	NO
YNL106C	INP52	186	26	n.d	NO
YNL105W	RRT16	186	36	n.d	NO
YKL172W	EBP2	186	33	n.d	NO
YDL098C	SNU23	186	48	n.d	NO
YOR103C	OST2	186	16	n.d	NO
YML013W	UBX2	186	36	n.d	NO
YOR069W	VPS5	186	37	n.d	NO
YNL211C	YNL211C	185	34	n.d	NO
YNL190W	YNL190W	185	47	n.d	NO
YNL191W	DUG3	185	42	n.d	NO
YJR110W	YMR1	185	30	n.d	NO
YMR279C	YMR279C	185	38	n.d	NO
YPR027C	YPR027C	185	50	n.d	NO
YKR105C	VBA5	185	30	n.d	NO
YJL029C	VPS53	185	36	n.d	NO
YBR006W	UGA2	185	34	n.d	NO
YBR288C	APM3	185	44	n.d	NO
YER169W	RPH1	185	32	n.d	NO
YBR075W	YBR075W	185	30	n.d	NO
YFR052W	RPN12	185	32	n.d	NO
YPL228W	CET1	185	35	n.d	NO
YPL144W	POC4	185	35	n.d	NO
YOL011W	PLB3	185	0	n.d	NO
YNL227C	JJJ1	184	47	n.d	NO
YNL226W	YNL226W	184	41	n.d	NO
YNL192W	CHS1	184	23	n.d	NO
YNL193W	YNL193W	184	38	n.d	NO
YPR069C	SPE3	184	26	n.d	NO
YMR126C	DLT1	184	40	n.d	NO
YLL018C-A	COX19	184	49	n.d	NO
YJL058C	BIT61	184	28	n.d	NO

YJL060W	BNA3	184	49	n.d	NO
YDL096C	OPI6	184	20	n.d	NO
YGR063C	SPT4	184	24	n.d	NO
YNL085W	MKT1	184	34	n.d	NO
YIL099W	SGA1	184	35	n.d	NO
YNL119W	NCS2	184	38	n.d	NO
YDL076C	RXT3	184	36	n.d	NO
YER162C	RAD4	184	27	n.d	NO
YER163C	GCG1	184	35	n.d	NO
YFL033C	RIM15	184	0	n.d	NO
YPL175W	SPT14	184	38	n.d	NO
YJR112W	NNF1	184	32	n.d	NO
YDL060W	TSR1	184	28	n.d	NO
YJR065C	ARP3	184	31	n.d	NO
YBR200W	BEM1	184	24	n.d	NO
YEL054C	RPL12A	184	36	n.d	NO

7 REFERENCES

Adair, W. L., Jr., & Cafmeyer, N. (1987). Characterization of the Saccharomyces cerevisiae cis-prenyltransferase required for dolichyl phosphate biosynthesis. *Arch Biochem Biophys, 259*(2), 589-596.

Aebi, M. (2013). *N*-linked protein glycosylation in the ER. *Biochim Biophys Acta, 1833*(11), 2430-2437. doi: 10.1016/j.bbamcr.2013.04.001

Aebi, M., Gassenhuber, J., Domdey, H., & te Heesen, S. (1996). Cloning and characterization of the ALG3 gene of Saccharomyces cerevisiae. *Glycobiology, 6*(4), 439-444.

Aguilera, A., & Zimmermann, F. K. (1986). Isolation and molecular analysis of the phosphoglucose isomerase structural gene of Saccharomyces cerevisiae. *Mol Gen Genet, 202*(1), 83-89.

Alton, G., Kjaergaard, S., Etchison, J. R., Skovby, F., & Freeze, H. H. (1997). Oral ingestion of mannose elevates blood mannose levels: A first step toward a potential therapy for carbohydrate-deficient glycoprotein syndrome type I. *Biochemical and Molecular Medicine, 60*(2), 127-133. doi: DOI 10.1006/bmme.1997.2574

Apweiler, R., Hermjakob, H., & Sharon, N. (1999). On the frequency of protein glycosylation, as deduced from analysis of the SWISS-PROT database. *Biochim Biophys Acta, 1473*(1), 4-8.

Aronov, S., Dover, S., Geva, P., Halperin, E., Shmoish, M., Duek, L., & Choder, M. (2013). Pheromone-induced transport of the yeast MFA2 mRNA to the mating projection is mediated by specific RNP granules. *Yeast, 30*, 43-43.

Aronson, D. E., Costantini, L. M., & Snapp, E. L. (2011). Superfolder GFP Is Fluorescent in Oxidizing Environments When Targeted via the Sec Translocon. *Traffic, 12*(5), 543-548. doi: 10.1111/j.1600-0854.2011.01168.x

Arroyo, J., Hutzler, J., Bermejo, C., Ragni, E., Garcia-Cantalejo, J., Botias, P., . . . Strahl, S. (2011). Functional and genomic analyses of blocked protein *O*-mannosylation in baker's yeast. *Mol Microbiol, 79*(6), 1529-1546. doi: 10.1111/j.1365-2958.2011.07537.x

Ast, T., Cohen, G., & Schuldiner, M. (2013). A network of cytosolic factors targets SRP-independent proteins to the endoplasmic reticulum. *Cell, 152*(5), 1134-1145. doi: 10.1016/j.cell.2013.02.003

Aviram, N., Ast, T., Costa, E. A., Arakel, E. C., Chuartzman, S. G., Jan, C. H., . . . Schuldiner, M. (2016). The SND proteins constitute an alternative targeting route to the endoplasmic reticulum. *Nature, 540*(7631), 134-138. doi: 10.1038/nature20169

Aviram, N., & Schuldiner, M. (2017). Targeting and translocation of proteins to the endoplasmic reticulum at a glance. *Journal of Cell Science, 130*(24), 4079-4085. doi: 10.1242/jcs.204396

Babczinski, P., & Tanner, W. (1973). Involvement of dolicholmonophosphate in the formation of specific mannosyl-linkages in yeast glycoproteins. *Biochem Biophys Res Commun, 54*(3), 1119-1124. doi: 0006-291X(73)90808-5 [pii]

Bai, L., Kovach, A., You, Q., Kenny, A., & Li, H. (2019). Structure of the eukaryotic protein *O*-mannosyltransferase Pmt1-Pmt2 complex. *Nat Struct Mol Biol, 26*(8), 704-711. doi: 10.1038/s41594-019-0262-6

Bai, L., Wang, T., Zhao, G., Kovach, A., & Li, H. (2018). The atomic structure of a eukaryotic oligosaccharyltransferase complex. *Nature, 555*(7696), 328-333. doi: 10.1038/nature25755

Bai, L., Wang, T., Zhao, G. P., Kovach, A., & Li, H. L. (2018). The atomic structure of a eukaryotic oligosaccharyltransferase complex. *Nature, 555*(7696), 328-+. doi: 10.1038/nature25755

Ballou, C. E. (1990). Isolation, characterization, and properties of Saccharomyces cerevisiae mnn mutants with nonconditional protein glycosylation defects. *Methods Enzymol, 185*, 440-470.

Baltz, A. G., Munschauer, M., Schwanhausser, B., Vasile, A., Murakawa, Y., Schueler, M., . . . Landthaler, M. (2012). The mRNA-bound proteome and its global occupancy profile on protein-coding transcripts. *Mol Cell, 46*(5), 674-690. doi: 10.1016/j.molcel.2012.05.021

Baryshnikova, A., Costanzo, M., Dixon, S., Vizeacoumar, F. J., Myers, C. L., Andrews, B., & Boone, C. (2010). Synthetic genetic array (SGA) analysis in Saccharomyces cerevisiae and Schizosaccharomyces pombe. *Methods Enzymol, 470*, 145-179. doi: 10.1016/S0076-6879(10)70007-0

Baum, S., Bittins, M., Frey, S., & Seedorf, M. (2004). Asc1p, a WD40-domain containing adaptor protein, is required for the interaction of the RNA-binding protein Scp160p with polysomes. *Biochemical Journal, 380*, 823-830. doi: 10.1042/Bj20031962

Bause, E., & Lehle, L. (1979). Enzymatic *N*-glycosylation and *O*-glycosylation of synthetic peptide acceptors by dolichol-linked sugar derivatives in yeast. *Eur J Biochem, 101*(2), 531-540.

Beach, D. L., Salmon, E. D., & Bloom, K. (1999). Localization and anchoring of mRNA in budding yeast. *Curr Biol, 9*(11), 569-578.

Becker, A. H., Oh, E., Weissman, J. S., Kramer, G., & Bukau, B. (2013). Selective ribosome profiling as a tool for studying the interaction of chaperones and targeting factors with nascent polypeptide chains and ribosomes. *Nature Protocols, 8*(11), 2212-2239. doi: 10.1038/nprot.2013.133

Beckmann, B. M., Horos, R., Fischer, B., Castello, A., Eichelbaum, K., Alleaume, A. M., . . . Hentze, M. W. (2015). The RNA-binding proteomes from yeast to man harbour conserved enigmRBPs. *Nat Commun, 6*, 10127. doi: 10.1038/ncomms10127

Belaya, K., Rodriguez Cruz, P. M., Liu, W. W., Maxwell, S., McGowan, S., Farrugia, M. E., . . . Beeson, D. (2015). Mutations in GMPPB cause congenital myasthenic syndrome and bridge myasthenic disorders with dystroglycanopathies. *Brain, 138*(Pt 9), 2493-2504. doi: 10.1093/brain/awv185

Beltran-Valero de Bernabe, D., Currier, S., Steinbrecher, A., Celli, J., van Beusekom, E., van der Zwaag, B., . . . Brunner, H. G. (2002). Mutations in the *O*-mannosyltransferase gene POMT1 give rise to the severe neuronal migration disorder Walker-Warburg syndrome. *Am J Hum Genet, 71*(5), 1033-1043.

Ben-Shem, A., Jenner, L., Yusupova, G., & Yusupov, M. (2010). Crystal Structure of the Eukaryotic Ribosome. *Science, 330*(6008), 1203-1209. doi: 10.1126/science.1194294

Benitez, E. M., Stolz, A., & Wolf, D. H. (2011). Yos9, a control protein for misfolded glycosylated and non-glycosylated proteins in ERAD. *FEBS Lett, 585*(19), 3015-3019. doi: 10.1016/j.febslet.2011.08.021

Bernsel, A., Viklund, H., Hennerdal, A., & Elofsson, A. (2009). TOPCONS: consensus prediction of membrane protein topology. *Nucleic Acids Res, 37*(Web Server issue), W465-468. doi: 10.1093/nar/gkp363

Bickel, T., Lehle, L., Schwarz, M., Aebi, M., & Jakob, C. A. (2005). Biosynthesis of lipid-linked oligosaccharides in Saccharomyces cerevisiae: Alg13p and Alg14p form a complex required for the formation of GlcNAc(2)-PP-dolichol. *J Biol Chem, 280*(41), 34500-34506. doi: 10.1074/jbc.M506358200

Brachmann, C. B., Davies, A., Cost, G. J., Caputo, E., Li, J., Hieter, P., & Boeke, J. D. (1998). Designer deletion strains derived from Saccharomyces cerevisiae S288C: a useful set of strains and plasmids for PCR-mediated gene disruption and other applications. *Yeast, 14*(2), 115-132.

Brandman, O., Stewart-Ornstein, J., Wong, D., Larson, A., Williams, C. C., Li, G. W., . . . Weissman, J. S. (2012). A Ribosome-Bound Quality Control Complex Triggers Degradation of Nascent Peptides and Signals Translation Stress. *Cell, 151*(5), 1042-1054. doi: 10.1016/j.cell.2012.10.044

Breker, M., Gymrek, M., & Schuldiner, M. (2013). A novel single-cell screening platform reveals proteome plasticity during yeast stress responses. *J Cell Biol, 200*(6), 839-850. doi: 10.1083/jcb.201301120

Breslow, D. K., Cameron, D. M., Collins, S. R., Schuldiner, M., Stewart-Ornstein, J., Newman, H. W., . . . Weissman, J. S. (2008). A comprehensive strategy enabling high-resolution functional analysis of the yeast genome. *Nat Methods, 5*(8), 711-718. doi: 10.1038/nmeth.1234

Bullock, W. O., Fernandez, J. M., & Short, J. M. (1987). Xl1-Blue - a High-Efficiency Plasmid Transforming Reca Escherichia-Coli Strain with Beta-Galactosidase Selection. *Biotechniques, 5*(4), 376-&.

Burda, P., & Aebi, M. (1998). The ALG10 locus of Saccharomyces cerevisiae encodes the alpha-1,2 glucosyltransferase of the endoplasmic reticulum: the terminal glucose of the lipid-linked oligosaccharide is required for efficient *N*-linked glycosylation. *Glycobiology, 8*(5), 455-462.

Burda, P., Jakob, C. A., Beinhauer, J., Hegemann, J. H., & Aebi, M. (1999). Ordered assembly of the asymmetrically branched lipid-linked oligosaccharide in the endoplasmic reticulum is ensured by the substrate specificity of the individual glycosyltransferases. *Glycobiology, 9*(6), 617-625.

Cannon, WB. (1926). Physiological regulation of normal states: some tentative postulates concerning biological homeostatics. *In: Pettit A, editor. A Charles Richet: ses amis, ses collègues, ses élèves (in French) Paris: Les Éditions Médicales*, p. 91.

Cappellaro, C., Hauser, K., Mrsa, V., Watzele, M., Watzele, G., Gruber, C., & Tanner, W. (1991). Saccharomyces cerevisiae a- and alpha-agglutinin: characterization of their molecular interaction. *EMBO J, 10*(13), 4081-4088.

Carss, K. J., Stevens, E., Foley, A. R., Cirak, S., Riemersma, M., Torelli, S., . . . Muntoni, F. (2013). Mutations in GDP-mannose pyrophosphorylase B cause congenital and limb-girdle muscular dystrophies associated with hypoglycosylation of alpha-dystroglycan. *Am J Hum Genet, 93*(1), 29-41. doi: 10.1016/j.ajhg.2013.05.009

Carvalho, P., Goder, V., & Rapoport, T. A. (2006). Distinct ubiquitin-ligase complexes define convergent pathways for the degradation of ER proteins. *Cell, 126*(2), 361-373. doi: 10.1016/j.cell.2006.05.043

Carvalho, P., Stanley, A. M., & Rapoport, T. A. (2010). Retrotranslocation of a Misfolded Luminal ER Protein by the Ubiquitin-Ligase Hrd1p. *Cell, 143*(4), 579-591. doi: 10.1016/j.cell.2010.10.028

Castells-Ballester, J., Zatorska, E., Meurer, M., Neubert, P., Metschies, A., Knop, M., & Strahl, S. (2018). Monitoring Protein Dynamics in Protein *O*-Mannosyltransferase Mutants In

Vivo by Tandem Fluorescent Protein Timers. *Molecules, 23*(10). doi: 10.3390/molecules23102622

Chawla, A., Chakrabarti, S., Ghosh, G., & Niwa, M. (2011). Attenuation of yeast UPR is essential for survival and is mediated by IRE1 kinase. *Journal of Cell Biology, 193*(1), 41-50. doi: 10.1083/jcb.201008071

Chen, M. H., Shen, Z. M., Bobin, S., Kahn, P. C., & Lipke, P. N. (1995). Structure of Saccharomyces cerevisiae alpha-agglutinin. Evidence for a yeast cell wall protein with multiple immunoglobulin-like domains with atypical disulfides. *J Biol Chem, 270*(44), 26168-26177.

Chen, X., Karnovsky, A., Sans, M. D., Andrews, P. C., & Williams, J. A. (2010). Molecular characterization of the endoplasmic reticulum: insights from proteomic studies. *Proteomics, 10*(22), 4040-4052. doi: 10.1002/pmic.201000234

Chen, Y., Feldman, D. E., Deng, C., Brown, J. A., De Giacomo, A. F., Gaw, A. F., . . . Koong, A. C. (2005). Identification of mitogen-activated protein kinase signaling pathways that confer resistance to endoplasmic reticulum stress in Saccharomyces cerevisiae. *Mol Cancer Res, 3*(12), 669-677. doi: 3/12/669 [pii] 10.1158/1541-7786.MCR-05-0181

Christianson, T. W., Sikorski, R. S., Dante, M., Shero, J. H., & Hieter, P. (1992). Multifunctional yeast high-copy-number shuttle vectors. *Gene, 110*(1), 119-122. doi: 0378-1119(92)90454-W [pii]

Cipollo, J. F., Trimble, R. B., Chi, J. H., Yan, Q., & Dean, N. (2001). The yeast ALG11 gene specifies addition of the terminal alpha 1,2-Man to the Man5GlcNAc2-PP-dolichol *N*-glycosylation intermediate formed on the cytosolic side of the endoplasmic reticulum. *J Biol Chem, 276*(24), 21828-21840. doi: 10.1074/jbc.M010896200

Clerc, S., Hirsch, C., Oggier, D. M., Deprez, P., Jakob, C., Sommer, T., & Aebi, M. (2009). Htm1 protein generates the *N*-glycan signal for glycoprotein degradation in the endoplasmic reticulum. *Journal of Cell Biology, 184*(1), 159-172. doi: 10.1083/jcb.200809198

Cohen, Y., Megyeri, M., Chen, O. C. W., Condomitti, G., Riezman, I., Loizides-Mangold, U., . . . Schuldiner, M. (2013). The Yeast P5 Type ATPase, Spf1, Regulates Manganese Transport into the Endoplasmic Reticulum. *Plos One, 8*(12). doi: UNSP e85519 10.1371/journal.pone.0085519

Cohen, Y., & Schuldiner, M. (2011). Advanced methods for high-throughput microscopy screening of genetically modified yeast libraries. *Methods Mol Biol, 781*, 127-159. doi: 10.1007/978-1-61779-276-2_8

Copic, A., Dorrington, M., Pagant, S., Barry, J., Lee, M. C., Singh, I., . . . Miller, E. A. (2009). Genomewide analysis reveals novel pathways affecting endoplasmic reticulum homeostasis, protein modification and quality control. *Genetics, 182*(3), 757-769. doi: 10.1534/genetics.109.101105

Cormier, J. H., Pearse, B. R., & Hebert, D. N. (2005). Yos9p: A sweet-toothed bouncer of the secretory pathway. *Molecular Cell, 19*(6), 717-719. doi: 10.1016/j.molcel.2005.08.029

Costanzo, M., VanderSluis, B., Koch, E. N., Baryshnikova, A., Pons, C., Tan, G., . . . Boone, C. (2016). A global genetic interaction network maps a wiring diagram of cellular function. *Science, 353*(6306). doi: 10.1126/science.aaf1420

Coughlan, C. M., Walker, J. L., Cochran, J. C., Wittrup, K. D., & Brodsky, J. L. (2004). Degradation of mutated bovine pancreatic trypsin inhibitor in the yeast vacuole suggests post-endoplasmic reticulum protein quality control. *J Biol Chem, 279*(15), 15289-15297. doi: 10.1074/jbc.M309673200

M309673200 [pii]
Couto, J. R., Huffaker, T. C., & Robbins, P. W. (1984). Cloning and expression in Escherichia coli of a yeast mannosyltransferase from the asparagine-linked glycosylation pathway. *J Biol Chem, 259*(1), 378-382.
Cox, J. S., Shamu, C. E., & Walter, P. (1993). Transcriptional induction of genes encoding endoplasmic reticulum resident proteins requires a transmembrane protein kinase. *Cell, 73*(6), 1197-1206. doi: 0092-8674(93)90648-A [pii]
Cox, J. S., & Walter, P. (1996). A novel mechanism for regulating activity of a transcription factor that controls the unfolded protein response. *Cell, 87*(3), 391-404. doi: S0092-8674(00)81360-4 [pii]
Credle, J. J., Finer-Moore, J. S., Papa, F. R., Stroud, R. M., & Walter, P. (2005). On the mechanism of sensing unfolded protein in the endoplasmic reticulum. *Proc Natl Acad Sci U S A, 102*(52), 18773-18784. doi: 10.1073/pnas.0509487102
Cronin, S. R., Rao, R. J., & Hampton, R. Y. (2002). Cod1p/Spf1p is a P-type ATPase involved in ER function and Ca2+ homeostasis. *Journal of Cell Biology, 157*(6), 1017-1028. doi: 10.1083/jcb.200203052
Cui, H. J., Cui, X. G., Zhao, W., He, X., Zhou, T., Yuan, Y., . . . Liu, X. G. (2018). PMT1 deficiency extends the shortened replicative lifespan of TED1-deficient yeast in a Hac1p-dependent manner. *FEMS Microbiol Lett, 365*(21). doi: 10.1093/femsle/fny234
Cui, H. J., Liu, X. G., McCormick, M., Wasko, B. M., Zhao, W., He, X., . . . Feng, W. L. (2015). PMT1 deficiency enhances basal UPR activity and extends replicative lifespan of Saccharomyces cerevisiae. *Age, 37*(3). doi: ARTN 46 10.1007/s11357-015-9788-7
Dancourt, J., & Barlowe, C. (2009). Erv26p-Dependent Export of Alkaline Phosphatase from the ER Requires Lumenal Domain Recognition. *Traffic, 10*(8), 1006-1018. doi: 10.1111/j.1600-0854.2009.00936.x
Dancourt, J., & Barlowe, C. (2010). Protein Sorting Receptors in the Early Secretory Pathway. *Annual Review of Biochemistry, Vol 79, 79*, 777-802. doi: 10.1146/annurev-biochem-061608-091319
de Boer, C. G., & Hughes, T. R. (2012). YeTFaSCo: a database of evaluated yeast transcription factor sequence specificities. *Nucleic Acids Res, 40*(Database issue), D169-179. doi: 10.1093/nar/gkr993
Dean, N. (1999). Asparagine-linked glycosylation in the yeast Golgi. *Biochim Biophys Acta, 1426*(2), 309-322. doi: S0304-4165(98)00132-9 [pii]
Dell, A., Galadari, A., Sastre, F., & Hitchen, P. (2010). Similarities and differences in the glycosylation mechanisms in prokaryotes and eukaryotes. *Int J Microbiol, 2010*, 148178. doi: 10.1155/2010/148178
Denic, V., Quan, E. M., & Weissman, J. S. (2006). A luminal surveillance complex that selects misfolded glycoproteins for ER-associated degradation. *Cell, 126*(2), 349-359. doi: 10.1016/j.cell.2006.05.045
Deshaies, R. J., & Schekman, R. (1987). A Yeast Mutant Defective at an Early Stage in Import of Secretory Protein Precursors into the Endoplasmic-Reticulum. *Journal of Cell Biology, 105*(2), 633-645. doi: DOI 10.1083/jcb.105.2.633
Diehn, M., Eisen, M. B., Botstein, D., & Brown, P. O. (2000). Large-scale identification of secreted and membrane-associated gene products using DNA microarrays. *Nature Genetics, 25*(1), 58-62. doi: Doi 10.1038/75603

Doring, K., Ahmed, N., Riemer, T., Suresh, H. G., Vainshtein, Y., Habich, M., . . . Bukau, B. (2017). Profiling Ssb-Nascent Chain Interactions Reveals Principles of Hsp70-Assisted Folding. *Cell, 170*(2), 298-311 e220. doi: 10.1016/j.cell.2017.06.038

Dorner, A. J., Wasley, L. C., & Kaufman, R. J. (1992). Overexpression of Grp78 Mitigates Stress Induction of Glucose Regulated Proteins and Blocks Secretion of Selective Proteins in Chinese-Hamster Ovary Cells. *Embo Journal, 11*(4), 1563-1571. doi: DOI 10.1002/j.1460-2075.1992.tb05201.x

Ecker, M., Mrsa, V., Hagen, I., Deutzmann, R., Strahl, S., & Tanner, W. (2003). *O*-mannosylation precedes and potentially controls the *N*-glycosylation of a yeast cell wall glycoprotein. *EMBO Rep, 4*(6), 628-632. doi: 10.1038/sj.embor.embor864

Einhoff, W., & Rudiger, H. (1988). The alpha-mannosidase from Canavalia ensiformis seeds: chemical and kinetic properties and action on animal lymphocytes. *Biol Chem Hoppe Seyler, 369*(3), 165-169.

Ernst, R. (2013). A lipid E-MAP identifies Ubx2 as a critical regulator of lipid saturation and lipid bilayer stress. *Yeast, 30*, 65-65.

Fedorov, A. N., & Baldwin, T. O. (1997). Cotranslational protein folding. *Journal of Biological Chemistry, 272*(52), 32715-32718. doi: DOI 10.1074/jbc.272.52.32715

Frank, C. G., & Aebi, M. (2005). ALG9 mannosyltransferase is involved in two different steps of lipid-linked oligosaccharide biosynthesis. *Glycobiology, 15*(11), 1156-1163. doi: 10.1093/glycob/cwj002

Freeze, H. H., & Aebi, M. (1999). Molecular basis of carbohydrate-deficient glycoprotein syndromes type I with normal phosphomannomutase activity. *Biochimica Et Biophysica Acta-Molecular Basis of Disease, 1455*(2-3), 167-178. doi: Doi 10.1016/S0925-4439(99)00072-1

Gable, K., Slife, H., Bacikova, D., Monaghan, E., & Dunn, T. M. (2000). Tsc3p is an 80-amino acid protein associated with serine palmitoyltransferase and required for optimal enzyme activity. *J Biol Chem, 275*(11), 7597-7603.

Gardner, B. M., & Walter, P. (2011). Unfolded proteins are Ire1-activating ligands that directly induce the unfolded protein response. *Science, 333*(6051), 1891-1894. doi: science.1209126 [pii] 10.1126/science.1209126

Gauss, R., Kanehara, K., Carvalho, P., Ng, D. T., & Aebi, M. (2011). A complex of Pdi1p and the mannosidase Htm1p initiates clearance of unfolded glycoproteins from the endoplasmic reticulum. *Mol Cell, 42*(6), 782-793. doi: 10.1016/j.molcel.2011.04.027

Gauss, R., Sommer, T., & Jarosch, E. (2006). The Hrd1p ligase complex forms a linchpin between ER-lumenal substrate selection and Cdc48p recruitment. *Embo Journal, 25*(9), 1827-1835. doi: 10.1038/sj.emboj.7601088

Gavin, A. C., Bosche, M., Krause, R., Grandi, P., Marzioch, M., Bauer, A., . . . Superti-Furga, G. (2002). Functional organization of the yeast proteome by systematic analysis of protein complexes. *Faseb Journal, 16*(4), A523-A523.

Gentzsch, M., Immervoll, T., & Tanner, W. (1995). Protein *O*-glycosylation in Saccharomyces cerevisiae: the protein *O*-mannosyltransferases Pmt1p and Pmt2p function as heterodimer. *FEBS Lett, 377*(2), 128-130.

Gentzsch, M., & Tanner, W. (1996). The PMT gene family: protein *O*-glycosylation in Saccharomyces cerevisiae is vital. *EMBO J, 15*(21), 5752-5759.

Gentzsch, M., & Tanner, W. (1997). Protein-*O*-glycosylation in yeast: protein-specific mannosyltransferases. *Glycobiology, 7*(4), 481-486.

Gerashchenko, M. V., & Gladyshev, V. N. (2014). Translation inhibitors cause abnormalities in ribosome profiling experiments. *Nucleic Acids Res, 42*(17), e134. doi: 10.1093/nar/gku671

Gerbasi, V. R., Browne, C. M., Samir, P., Shen, B. X., Sun, M., Hazelbaker, D. Z., . . . Link, A. J. (2018). Critical Role for Saccharomyces cerevisiae Asc1p in Translational Initiation at Elevated Temperatures. *Proteomics, 18*(23). doi: Artn 1800208 10.1002/Pmic.201800208

Geva, Y., Crissman, J., Arakel, E. C., Gomez-Navarro, N., Chuartzman, S. G., Stahmer, K. R., . . . Schuldiner, M. (2017). Two novel effectors of trafficking and maturation of the yeast plasma membrane H(+) -ATPase. *Traffic, 18*(10), 672-682. doi: 10.1111/tra.12503

Geva, Y., & Schuldiner, M. (2014). The back and forth of cargo exit from the endoplasmic reticulum. *Curr Biol, 24*(3), R130-136. doi: 10.1016/j.cub.2013.12.008

Giaever, G., Chu, A. M., Ni, L., Connelly, C., Riles, L., Veronneau, S., . . . Johnston, M. (2002). Functional profiling of the Saccharomyces cerevisiae genome. *Nature, 418*(6896), 387-391. doi: 10.1038/nature00935

Gietz, R. D., Schiestl, R. H., Willems, A. R., & Woods, R. A. (1995). Studies on the transformation of intact yeast cells by the LiAc/SS-DNA/PEG procedure. *Yeast, 11*(4), 355-360. doi: 10.1002/yea.320110408

Girrbach, V., & Strahl, S. (2003). Members of the evolutionarily conserved PMT family of protein *O*-mannosyltransferases form distinct protein complexes among themselves. *J Biol Chem, 278*(14), 12554-12562.

Girrbach, V., Zeller, T., Priesmeier, M., & Strahl-Bolsinger, S. (2000). Structure-function analysis of the dolichyl phosphate-mannose: protein *O*-mannosyltransferase ScPmt1p. *J Biol Chem, 275*(25), 19288-19296.

Goder, V., & Melero, A. (2011). Protein *O*-mannosyltransferases participate in ER protein quality control. *J Cell Sci, 124*(Pt 1), 144-153. doi: 10.1242/jcs.072181

Goettig, P. (2016). Effects of Glycosylation on the Enzymatic Activity and Mechanisms of Proteases. *Int J Mol Sci, 17*(12). doi: 10.3390/ijms17121969

Gonzalez, M., Brito, N., & Celedonio, G. (2012). High abundance of Serine/Threonine-rich regions predicted to be hyper-*O*-glycosylated in the secretory proteins coded by eight fungal genomes. *BMC Microbiol, 12*(1), 213. doi: 1471-2180-12-213 [pii] 10.1186/1471-2180-12-213

Goto, M. (2007). Protein *O*-glycosylation in fungi: diverse structures and multiple functions. *Biosci Biotechnol Biochem, 71*(6), 1415-1427. doi: JST.JSTAGE/bbb/70080 [pii]

Green, J. B., Wright, A. P., Cheung, W. Y., Lancashire, W. E., & Hartley, B. S. (1988). The structure and regulation of phosphoglucose isomerase in Saccharomyces cerevisiae. *Mol Gen Genet, 215*(1), 100-106.

Grunewald, S., Matthijs, G., & Jaeken, J. (2002). Congenital disorders of glycosylation: A review. *Pediatric Research, 52*(5), 618-624. doi: 10.1203/01.Pdr.0000031921.02259.35

Güldener, U., Heck, S., Fielder, T., Beinhauer, J., & Hegemann, J. H. (1996). A new efficient gene disruption cassette for repeated use in budding yeast. *Nucleic Acids Res, 24*(13), 2519-2524. doi: 6w0051 [pii]

Guo, M., Aston, C., Burchett, S. A., Dyke, C., Fields, S., Rajarao, S. J., . . . Dohlman, H. G. (2003). The yeast G protein alpha subunit Gpa1 transmits a signal through an RNA binding effector protein Scp160. *Mol Cell, 12*(2), 517-524.

Haass, F. A., Jonikas, M., Walter, P., Weissman, J. S., Jan, Y. N., Jan, L. Y., & Schuldiner, M. (2007). Identification of yeast proteins necessary for cell-surface function of a

potassium channel. *Proc Natl Acad Sci U S A, 104*(46), 18079-18084. doi: 10.1073/pnas.0708765104

Hammond, C., Braakman, I., & Helenius, A. (1994). Role of *N*-linked oligosaccharide recognition, glucose trimming, and calnexin in glycoprotein folding and quality control. *Proc Natl Acad Sci U S A, 91*(3), 913-917.

Harding, H. P., Zhang, Y., & Ron, D. (1999). Protein translation and folding are coupled by an endoplasmic-reticulum-resident kinase. *Nature, 397*(6716), 271-274. doi: 10.1038/16729

Hartl, F. U., & Martin, J. (1995). Molecular chaperones in cellular protein folding. *Curr Opin Struct Biol, 5*(1), 92-102.

Harty, C., Strahl, S., & Romisch, K. (2001). *O*-mannosylation protects mutant alpha-factor precursor from endoplasmic reticulum-associated degradation. *Mol Biol Cell, 12*(4), 1093-1101.

Haselbeck, A. (1989). Purification of GDP mannose:dolichyl-phosphate *O*-beta-D-mannosyltransferase from Saccharomyces cerevisiae. *Eur J Biochem, 181*(3), 663-668.

Hashimoto, H., Sakakibara, A., Yamasaki, M., & Yoda, K. (1997). Saccharomyces cerevisiae VIG9 encodes GDP-mannose pyrophosphorylase, which is essential for protein glycosylation. *Journal of Biological Chemistry, 272*(26), 16308-16314. doi: DOI 10.1074/jbc.272.26.16308

Haynes, C. M., Caldwell, S., & Cooper, A. A. (2002). An HRD/DER-independent ER quality control mechanism involves Rsp5p-dependent ubiquitination and ER-Golgi transport. *Journal of Cell Biology, 158*(1), 91-101. doi: 10.1083/jcb.200201053

Heesen, S., Lehle, L., Weissmann, A., & Aebi, M. (1994). Isolation of the ALG5 locus encoding the UDP-glucose:dolichyl-phosphate glucosyltransferase from Saccharomyces cerevisiae. *Eur J Biochem, 224*(1), 71-79. doi: 10.1111/j.1432-1033.1994.tb19996.x

Helms, J. B., & Zurzolo, C. (2004). Lipids as targeting signals: lipid rafts and intracellular trafficking. *Traffic, 5*(4), 247-254.

Hentze, M. W., Castello, A., Schwarzl, T., & Preiss, T. (2018). A brave new world of RNA-binding proteins. *Nat Rev Mol Cell Biol, 19*(5), 327-341. doi: 10.1038/nrm.2017.130

Hese, K., Otto, C., Routier, F. H., & Lehle, L. (2009). The yeast oligosaccharyltransferase complex can be replaced by STT3 from Leishmania major. *Glycobiology, 19*(2), 160-171. doi: 10.1093/glycob/cwn118

Hirayama, H., Fujita, M., Yoko-o, T., & Jigami, Y. (2008). *O*-mannosylation is required for degradation of the endoplasmic reticulum-associated degradation substrate Gas1*p via the ubiquitin/proteasome pathway in Saccharomyces cerevisiae. *J Biochem, 143*(4), 555-567. doi: mvm249 [pii] 10.1093/jb/mvm249

Hirschmann, W. D., Westendorf, H., Mayer, A., Cannarozzi, G., Cramer, P., & Jansen, R. P. (2014). Scp160p is required for translational efficiency of codon-optimized mRNAs in yeast. *Nucleic Acids Research, 42*(6), 4043-4055. doi: 10.1093/nar/gkt1392

Hitt, R., & Wolf, D. H. (2004). DER7, encoding alpha-glucosidase I is essential for degradation of malfolded glycoproteins of the endoplasmic reticulum. *Fems Yeast Research, 4*(8), 815-820. doi: 10.1016/j.femsyr.2004.04.002

Hogan, D. J., Riordan, D. P., Gerber, A. P., Herschlag, D., & Brown, P. O. (2008). Diverse RNA-binding proteins interact with functionally related sets of RNAs, suggesting an extensive regulatory system. *PLoS Biol, 6*(10), e255. doi: 10.1371/journal.pbio.0060255

Hollien, J., & Weissman, J. S. (2006). Decay of endoplasmic reticulum-localized mRNAs during the unfolded protein response. *Science, 313*(5783), 104-107. doi: 10.1126/science.1129631

Hong, E., Davidson, A. R., & Kaiser, C. A. (1996). A pathway for targeting soluble misfolded proteins to the yeast vacuole. *Journal of Cell Biology, 135*(3), 623-633. doi: DOI 10.1083/jcb.135.3.623

Huang, D. G., & Shusta, E. V. (2006). A yeast platform for the production of single-chain antibody-green fluorescent protein fusions. *Applied and Environmental Microbiology, 72*(12), 7748-7759. doi: 10.1128/Aem.01403-06

Huang, G., Zhang, M., & Erdman, S. E. (2003). Posttranslational modifications required for cell surface localization and function of the fungal adhesin Aga1p. *Eukaryot Cell, 2*(5), 1099-1114.

Hutzler, J., Schmid, M., Bernard, T., Henrissat, B., & Strahl, S. (2007). Membrane association is a determinant for substrate recognition by PMT4 protein *O*-mannosyltransferases. *Proc Natl Acad Sci U S A, 104*(19), 7827-7832. doi: 10.1073/pnas.0700374104

Hwang, C. S., Shemorry, A., Auerbach, D., & Varshavsky, A. (2010). The *N*-end rule pathway is mediated by a complex of the RING-type Ubr1 and HECT-type Ufd4 ubiquitin ligases. *Nature Cell Biology, 12*(12), 1177-U1120. doi: 10.1038/ncb2121

Ikeuchi, K., & Inada, T. (2016). Ribosome-associated Asc1/RACK1 is required for endonucleolytic cleavage induced by stalled ribosome at the 3 ' end of nonstop mRNA. *Scientific Reports, 6*. doi: Artn 28234 10.1038/Srep28234

Immervoll, T., Gentzsch, M., & Tanner, W. (1995). PMT3 and PMT4, two new members of the protein-*O*-mannosyltransferase gene family of Saccharomyces cerevisiae. *Yeast, 11*(14), 1345-1351.

Inada, T., Winstall, E., Tarun, S. Z., Yates, J. R., Schieltz, D., & Sachs, A. B. (2002). One-step affinity purification of the yeast ribosome and its associated proteins and mRNAs. *Rna-a Publication of the Rna Society, 8*(7), 948-958. doi: 10.1017/S1355838202026018

Inoue, H., Nojima, H., & Okayama, H. (1990). High efficiency transformation of Escherichia coli with plasmids. *Gene, 96*(1), 23-28. doi: 0378-1119(90)90336-P [pii]

Ishida, Y., & Nagata, K. (2009). Autophagy eliminates a specific species of misfolded procollagen and plays a protective role in cell survival against ER stress. *Autophagy, 5*(8), 1217-1219. doi: DOI 10.4161/auto.5.8.10168

Ishiwata-Kimata, Y., Yamamoto, Y. H., Takizawa, K., Kohno, K., & Kimata, Y. (2013). F-actin and a Type-II Myosin Are Required for Efficient Clustering of the ER Stress Sensor Ire1. *Cell Structure and Function, 38*(2), 135-143. doi: Doi 10.1247/Csf.12033

Ismail, N., & Ng, D. T. W. (2006). Have you HRD? Understanding ERAD is DOAble! *Cell, 126*(2), 237-239. doi: 10.1016/j.cell.2006.07.001

Izquierdo, L., Schulz, B. L., Rodrigues, J. A., Guther, M. L., Procter, J. B., Barton, G. J., . . . Ferguson, M. A. (2009). Distinct donor and acceptor specificities of Trypanosoma brucei oligosaccharyltransferases. *EMBO J, 28*(17), 2650-2661. doi: 10.1038/emboj.2009.203

Jackson, C. L., & Kepes, F. (1994). BFR1, a multicopy suppressor of brefeldin A-induced lethality, is implicated in secretion and nuclear segregation in Saccharomyces cerevisiae. *Genetics, 137*(2), 423-437.

Jain, R. K., Joyce, P. B. M., Molinete, M., Halban, P. A., & Gorr, S. U. (2001). Oligomerization of green fluorescent protein in the secretory pathway of endocrine cells. *Biochemical Journal, 360*, 645-649. doi: Doi 10.1042/0264-6021:3600645

Jakob, C. A., Burda, P., Roth, J., & Aebi, M. (1998). Degradation of misfolded endoplasmic reticulum glycoproteins in Saccharomyces cerevisiae is determined by a specific oligosaccharide structure. *Journal of Cell Biology, 142*(5), 1223-1233. doi: DOI 10.1083/jcb.142.5.1223

Jan, C. H., Williams, C. C., & Weissman, J. S. (2014). Principles of ER cotranslational translocation revealed by proximity-specific ribosome profiling. *Science, 346*(6210), 716-+. doi: Artn 1257521 10.1126/Science.1257521

Johansen, P. G., Neuberger, A., & Marshall, R. D. (1961). Carbohydrates in Protein .3. Preparation and Some of Properties of a Glycopeptide from Hens-Egg Albumin. *Biochemical Journal, 78*(3), 518-&. doi: Doi 10.1042/Bj0780518

Jonikas, M. C., Collins, S. R., Denic, V., Oh, E., Quan, E. M., Schmid, V., . . . Schuldiner, M. (2009). Comprehensive characterization of genes required for protein folding in the endoplasmic reticulum. *Science, 323*(5922), 1693-1697. doi: 323/5922/1693 [pii] 10.1126/science.1167983

Jungfleisch, J., Nedialkova, D. D., Dotu, I., Sloan, K. E., Martinez-Bosch, N., Bruning, L., . . . Diez, J. (2017). A novel translational control mechanism involving RNA structures within coding sequences. *Genome Research, 27*(1), 95-106. doi: 10.1101/gr.209015.116

Jurado, L. A., Coloma, A., & Cruces, J. (1999). Identification of a human homolog of the Drosophila rotated abdomen gene (POMT1) encoding a putative protein *O*-mannosyl-transferase, and assignment to human chromosome 9q34.1. *Genomics, 58*(2), 171-180.

Kampf, M., Absmanner, B., Schwarz, M., & Lehle, L. (2009). Biochemical characterization and membrane topology of Alg2 from Saccharomyces cerevisiae as a bifunctional alpha1,3- and 1,6-mannosyltransferase involved in lipid-linked oligosaccharide biosynthesis. *J Biol Chem, 284*(18), 11900-11912. doi: 10.1074/jbc.M806416200

Kang, D., Gho, Y., Suh, M., & Kang, C. (2002). Highly Sensitive and Fast Protein Detection with Coomassie Brilliant Blue in Sodium Dodecyl Sulfate-Polyacrylamide Gel Electrophoresis. *Bull Korean Chem Soc, 23*(11), 1511-1512.

Kanno, H., Fujii, H., Hirono, A., Ishida, Y., Ohga, S., Fukumoto, Y., . . . Miwa, S. (1996). Molecular analysis of glucose phosphate isomerase deficiency associated with hereditary hemolytic anemia. *Blood, 88*(6), 2321-2325.

Karaoglu, D., Kelleher, D. J., & Gilmore, R. (1995). Functional-Characterization of Ost3p - Loss of the 34-Kd Subunit of the Saccharomyces-Cerevisiae Oligosaccharyltransferase Results in Biased Underglycosylation of Acceptor Substrates. *Journal of Cell Biology, 130*(3), 567-577. doi: DOI 10.1083/jcb.130.3.567

Kelleher, D. J., & Gilmore, R. (2006). An evolving view of the eukaryotic oligosaccharyltransferase. *Glycobiology, 16*(4), 47R-62R. doi: cwj066 [pii] 10.1093/glycob/cwj066

Khmelinskii, A., Blaszczak, E., Pantazopoulou, M., Fischer, B., Omnus, D. J., Le Dez, G., . . . Knop, M. (2014). Protein quality control at the inner nuclear membrane. *Nature, 516*(7531), 410-413. doi: 10.1038/nature14096

Khmelinskii, A., Keller, P. J., Bartosik, A., Meurer, M., Barry, J. D., Mardin, B. R., . . . Knop, M. (2012). Tandem fluorescent protein timers for in vivo analysis of protein dynamics. *Nat Biotechnol, 30*(7), 708-714. doi: 10.1038/nbt.2281

Kimata, Y., Ishiwata-Kimata, Y., Ito, T., Hirata, A., Suzuki, T., Oikawa, D., . . . Kohno, K. (2007). Two regulatory steps of ER-stress sensor Ire1 involving its cluster formation and interaction with unfolded proteins. *Journal of Cell Biology, 179*(1), 75-86. doi: 10.1083/jcb.200704166

Kimata, Y., Shimizu, Y., Oikawa, D., Kimata, Y., & Kohno, K. (2004). A role of BiP as an adjustor for the endoplasmic reticulum stress-sensing protein Ire1. *Cell Structure and Function, 29*, 94-94.

Kincaid, M. M., & Cooper, A. A. (2007). Misfolded proteins traffic from the endoplasmic reticulum (ER) due to ER export signals. *Molecular Biology of the Cell, 18*(2), 455-463. doi: 10.1091/mbc.E06-08-0696

Klis, F. M., Boorsma, A., & De Groot, P. W. (2006). Cell wall construction in Saccharomyces cerevisiae. *Yeast, 23*(3), 185-202. doi: 10.1002/yea.1349

Knupp, J., Arvan, P., & Chang, A. (2019). Increased mitochondrial respiration promotes survival from endoplasmic reticulum stress. *Cell Death Differ, 26*(3), 487-501. doi: 10.1038/s41418-018-0133-4

Koehler, K., Malik, M., Mahmood, S., Giesselmann, S., Beetz, C., Hennings, J. C., . . . Hubner, C. A. (2013). Mutations in GMPPA cause a glycosylation disorder characterized by intellectual disability and autonomic dysfunction. *Am J Hum Genet, 93*(4), 727-734. doi: 10.1016/j.ajhg.2013.08.002

Kohno, K., Normington, K., Sambrook, J., Gething, M. J., & Mori, K. (1993). The Promoter Region of the Yeast Kar2 (Bip) Gene Contains a Regulatory Domain That Responds to the Presence of Unfolded Proteins in the Endoplasmic-Reticulum. *Molecular and Cellular Biology, 13*(2), 877-890. doi: Doi 10.1128/Mcb.13.2.877

Korennykh, A. V., Egea, P. F., Korostelev, A. A., Finer-Moore, J., Zhang, C., Shokat, K. M., . . . Walter, P. (2009). The unfolded protein response signals through high-order assembly of Ire1. *Nature, 457*(7230), 687-U682. doi: 10.1038/nature07661

Kowarik, M., Kung, S., Martoglio, B., & Helenius, A. (2002). Protein folding during cotranslational translocation in the endoplasmic reticulum. *Molecular Cell, 10*(4), 769-778. doi: Doi 10.1016/S1097-2765(02)00685-8

Kramer, K., Sachsenberg, T., Beckmann, B. M., Qamar, S., Boon, K. L., Hentze, M. W., . . . Urlaub, H. (2014). Photo-cross-linking and high-resolution mass spectrometry for assignment of RNA-binding sites in RNA-binding proteins. *Nat Methods, 11*(10), 1064-1070. doi: 10.1038/nmeth.3092

Kraut-Cohen, J., Afanasieva, E., Haim-Vilmovsky, L., Slobodin, B., Yosef, I., Bibi, E., & Gerst, J. E. (2013). Translation- and SRP-independent mRNA targeting to the endoplasmic reticulum in the yeast Saccharomyces cerevisiae. *Mol Biol Cell, 24*(19), 3069-3084. doi: 10.1091/mbc.E13-01-0038

Kraut-Cohen, J., & Gerst, J. E. (2010). Addressing mRNAs to the ER: cis sequences act up! *Trends Biochem Sci, 35*(8), 459-469. doi: 10.1016/j.tibs.2010.02.006

Kriangkripipat, T., & Momany, M. (2009). Aspergillus nidulans protein *O*-mannosyltransferases play roles in cell wall integrity and developmental patterning. *Eukaryot Cell, 8*(10), 1475-1485. doi: EC.00040-09 [pii] 10.1128/EC.00040-09

Kugler, W., Breme, K., Laspe, P., Muirhead, H., Davies, C., Winkler, H., . . . Lakomek, M. (1998). Molecular basis of neurological dysfunction coupled with haemolytic anaemia

in human glucose-6-phosphate isomerase (GPI) deficiency. *Hum Genet, 103*(4), 450-454.

Kurita, T., Noda, Y., Takagi, T., Osumi, M., & Yoda, K. (2011). Kre6 Protein Essential for Yeast Cell Wall beta-1,6-Glucan Synthesis Accumulates at Sites of Polarized Growth. *Journal of Biological Chemistry, 286*(9), 7429-7438. doi: 10.1074/jbc.M110.174060

Kurita, T., Noda, Y., & Yoda, K. (2012). Action of Multiple Endoplasmic Reticulum Chaperon-like Proteins Is Required for Proper Folding and Polarized Localization of Kre6 Protein Essential in Yeast Cell Wall beta-1,6-Glucan Synthesis. *Journal of Biological Chemistry, 287*(21), 17415-17424. doi: 10.1074/jbc.M111.321018

Laboratories, Bethesda Research. (1986). BRL pUC host: E. coli DH5α competent cells. *Focus 8(2): 9*.

Laemmli, U. K. (1970). Cleavage of structural proteins during the assembly of the head of bacteriophage T4. *Nature, 227*(5259), 680-685.

Lang, B. D., Li, Am, Black-Brewster, H. D., & Fridovich-Keil, J. L. (2001). The brefeldin A resistance protein Bfr1p is a component of polyribosome-associated mRNP complexes in yeast. *Nucleic Acids Res, 29*(12), 2567-2574.

Lapointe, C. P., Wilinski, D., Saunders, H. A., & Wickens, M. (2015). Protein-RNA networks revealed through covalent RNA marks. *Nat Methods, 12*(12), 1163-1170. doi: 10.1038/nmeth.3651

Larriba, G., Elorza, M. V., Villanueva, J. R., & Sentandreu, R. (1976). Participation of dolichol phospho-mannose in the glycosylation of yeast wall manno-proteins at the polysomal level. *FEBS Lett, 71*(2), 316-320.

Lee, K. P. K., Dey, M., Neculai, D., Cao, C., Dever, T. E., & Sicheri, F. (2008). Structure of the dual enzyme ire1 reveals the basis for catalysis and regulation in nonconventional RNA splicing. *Cell, 132*(1), 89-100. doi: 10.1016/j.cell.2007.10.057

Lee, M. C. S., Miller, E. A., Goldberg, J., Orci, L., & Schekman, R. (2004). Bi-directional protein transport between the ER and Golgi. *Annual Review of Cell and Developmental Biology, 20*, 87-123. doi: 10.1146/annurev.cellbio.20.010403.105307

Lehle, L., Strahl, S., & Tanner, W. (2006). Protein glycosylation, conserved from yeast to man: a model organism helps elucidate congenital human diseases. *Angew Chem Int Ed Engl, 45*(41), 6802-6818. doi: 10.1002/anie.200601645

Lesage, G., & Bussey, H. (2006). Cell wall assembly in Saccharomyces cerevisiae. *Microbiol Mol Biol Rev, 70*(2), 317-343. doi: 70/2/317 [pii] 10.1128/MMBR.00038-05

Li, H., Korennykh, A. V., Behrman, S. L., & Walter, P. (2010). Mammalian endoplasmic reticulum stress sensor IRE1 signals by dynamic clustering. *Proceedings of the National Academy of Sciences of the United States of America, 107*(37), 16113-16118. doi: 10.1073/pnas.1010580107

Li, S., Spooner, R. A., Hampton, R. Y., Lord, J. M., & Roberts, L. M. (2012). Cytosolic entry of Shiga-like toxin a chain from the yeast endoplasmic reticulum requires catalytically active Hrd1p. *PLoS One, 7*(7), e41119. doi: 10.1371/journal.pone.0041119

Li, S. Y., Spooner, R. A., Hampton, R. Y., Lord, J. M., & Roberts, L. M. (2012). Cytosolic Entry of Shiga-Like Toxin A Chain from the Yeast Endoplasmic Reticulum Requires Catalytically Active Hrd1p. *Plos One, 7*(7). doi: ARTN e41119 10.1371/journal.pone.0041119

Lis, H., & Sharon, N. (1993). Protein glycosylation. Structural and functional aspects. *Eur J Biochem, 218*(1), 1-27.

Lizak, C., Gerber, S., Numao, S., Aebi, M., & Locher, K. P. (2011). X-ray structure of a bacterial oligosaccharyltransferase. *Nature, 474*(7351), 350-355. doi: 10.1038/nature10151

Lodder, A. L., Lee, T. K., & Ballester, R. (1999). Characterization of the Wsc1 protein, a putative receptor in the stress response of Saccharomyces cerevisiae. *Genetics, 152*(4), 1487-1499.

Loibl, M., Wunderle, L., Hutzler, J., Schulz, B. L., Aebi, M., & Strahl, S. (2014). Protein *O*-mannosyltransferases associate with the translocon to modify translocating polypeptide chains. *J Biol Chem, 289*(12), 8599-8611. doi: 10.1074/jbc.M113.543116

Lommel, M., Bagnat, M., & Strahl, S. (2004). Aberrant processing of the WSC family and Mid2p cell surface sensors results in cell death of Saccharomyces cerevisiae *O*-mannosylation mutants. *Mol Cell Biol, 24*(1), 46-57.

Lommel, M., Schott, A., Jank, T., Hofmann, V., & Strahl, S. (2011). A conserved acidic motif is crucial for enzymatic activity of protein o-mannosyltransferases. *J Biol Chem, 286*(46), 39768-39775. doi: M111.281196 [pii] 10.1074/jbc.M111.281196

Lommel, M., & Strahl, S. (2009). Protein *O*-mannosylation: conserved from bacteria to humans. *Glycobiology, 19*(8), 816-828. doi: cwp066 [pii] 10.1093/glycob/cwp066

Longtine, M. S., McKenzie, A., 3rd, Demarini, D. J., Shah, N. G., Wach, A., Brachat, A., . . . Pringle, J. R. (1998). Additional modules for versatile and economical PCR-based gene deletion and modification in Saccharomyces cerevisiae. *Yeast, 14*(10), 953-961. doi: 10.1002/(SICI)1097-0061(199807)14:10<953::AID-YEA293>3.0.CO;2-U

Looke, M., Kristjuhan, K., & Kristjuhan, A. (2011). Extraction of genomic DNA from yeasts for PCR-based applications. *Biotechniques, 50*(5), 325-328. doi: 10.2144/000113672

Luo, Y., Na, Z., & Slavoff, S. A. (2018). P-Bodies: Composition, Properties, and Functions. *Biochemistry, 57*(17), 2424-2431. doi: 10.1021/acs.biochem.7b01162

Lussier, M., Gentzsch, M., Sdicu, A. M., Bussey, H., & Tanner, W. (1995). Protein *O*-glycosylation in yeast. The PMT2 gene specifies a second protein *O*-mannosyltransferase that functions in addition to the PMT1-encoded activity. *J Biol Chem, 270*(6), 2770-2775.

Mayinger, P., & Meyer, D. I. (1993). An Atp Transporter Is Required for Protein Translocation into the Yeast Endoplasmic-Reticulum. *Embo Journal, 12*(2), 659-666. doi: DOI 10.1002/j.1460-2075.1993.tb05699.x

McCahill, A., Warwicker, J., Bolger, G. B., Houslay, M. D., & Yarwood, S. J. (2002). The RACK1 scaffold protein: A dynamic cog in cell response mechanisms. *Molecular Pharmacology, 62*(6), 1261-1273. doi: DOI 10.1124/mol.62.6.1261

McCracken, A. A., & Brodsky, J. L. (1996). Assembly of ER-associated protein degradation in vitro: dependence on cytosol, calnexin, and ATP. *J Cell Biol, 132*(3), 291-298.

Melamed, D., Bar-Ziv, L., Truzman, Y., & Arava, Y. (2010). Asc1 Supports Cell-Wall Integrity Near Bud Sites by a Pkc1 Independent Mechanism. *Plos One, 5*(6). doi: ARTN e11389 10.1371/journal.pone.0011389

Meunier, L., Usherwood, Y. K., Chung, K. T., & Hendershot, L. M. (2002). A subset of chaperones and folding enzymes form multiprotein complexes in endoplasmic reticulum to bind nascent proteins. *Mol Biol Cell, 13*(12), 4456-4469. doi: 10.1091/mbc.E02-05-0311

Meurer, M., Duan, Y., Sass, E., Kats, I., Herbst, K., Buchmuller, B. C., . . . Knop, M. (2018). Genome-wide C-SWAT library for high-throughput yeast genome tagging. *Nat Methods, 15*(8), 598-600. doi: 10.1038/s41592-018-0045-8

Moore, C. J., & Hewitt, J. E. (2009). Dystroglycan glycosylation and muscular dystrophy. *Glycoconj J, 26*(3), 349-357. doi: 10.1007/s10719-008-9182-0

Mori, K., Ma, W., Gething, M. J., & Sambrook, J. (1993). A transmembrane protein with a cdc2+/CDC28-related kinase activity is required for signaling from the ER to the nucleus. *Cell, 74*(4), 743-756. doi: 0092-8674(93)90521-Q [pii]

Mrsa, V., Ecker, M., Strahl-Bolsinger, S., Nimtz, M., Lehle, L., & Tanner, W. (1999). Deletion of new covalently linked cell wall glycoproteins alters the electrophoretic mobility of phosphorylated wall components of Saccharomyces cerevisiae. *J Bacteriol, 181*(10), 3076-3086.

Murakami-Sekimata, A., Sato, K., Sato, K., Takashima, A., & Nakano, A. (2009). *O*-Mannosylation is required for the solubilization of heterologously expressed human beta-amyloid precursor protein in Saccharomyces cerevisiae. *Genes to Cells, 14*(2), 205-215. doi: 10.1111/j.1365-2443.2008.01263.x

Murakami-Sekimata, A., Sato, K., Takashima, A., & Nakano, A. (2009). *O*-Mannosylation is required for the solubilization of heterologously expressed human beta-amyloid precursor protein in Saccharomyces cerevisiae. *Genes Cells, 14*(2), 205-215. doi: GTC1263 [pii]
10.1111/j.1365-2443.2008.01263.x

Nagai, K., Ihara, Y., Wada, Y., & Taniguchi, N. (1997). *N*-glycosylation is requisite for the enzyme activity and Golgi retention of *N*-acetylglucosaminyltransferase III. *Glycobiology, 7*(6), 769-776. doi: DOI 10.1093/glycob/7.6.769

Nakatsukasa, K., & Brodsky, J. L. (2008). The recognition and retrotranslocation of misfolded proteins from the endoplasmic reticulum. *Traffic, 9*(6), 861-870. doi: 10.1111/j.1600-0854.2008.00729.x

Nakatsukasa, K., Okada, S., Umebayashi, K., Fukuda, R., Nishikawa, S., & Endo, T. (2004). Roles of *O*-mannosylation of aberrant proteins in reduction of the load for endoplasmic reticulum chaperones in yeast. *J Biol Chem, 279*(48), 49762-49772. doi: 10.1074/jbc.M403234200

Nasab, F. P., Schulz, B. L., Gamarro, F., Parodi, A. J., & Aebi, M. (2008). All in one: Leishmania major STT3 proteins substitute for the whole oligosaccharyltransferase complex in Saccharomyces cerevisiae. *Molecular Biology of the Cell, 19*(9), 3758-3768. doi: 10.1091/mbc.E08-05-0467

Neubert, P., Halim, A., Zauser, M., Essig, A., Joshi, H. J., Zatorska, E., . . . Strahl, S. (2016). Mapping the *O*-Mannose Glycoproteome in Saccharomyces cerevisiae. *Mol Cell Proteomics, 15*(4), 1323-1337. doi: 10.1074/mcp.M115.057505

Neubert, P., Halim, A., Zauser, M., Essig, A., Joshi, H. J., Zatorska, E., . . . Strahl, S. (2016). Mapping the *O*-mannose glycoproteome in Saccharomyces cerevisiae. *Mol Cell Proteomics*. doi: 10.1074/mcp.M115.057505

Nikawa, J., Akiyoshi, M., Hirata, S., & Fukuda, T. (1996). Saccharomyces cerevisiae IRE2/HAC1 is involved in IRE1-mediated KAR2 expression. *Nucleic Acids Research, 24*(21), 4222-4226. doi: DOI 10.1093/nar/24.21.4222

Nishikawa, S., Fewell, S. W., Kato, Y., Brodsky, J. L., & Endo, T. (2001). Molecular chaperones in the yeast endoplasmic reticulum maintain the solubility of proteins for retrotranslocation and degradation. *Journal of Cell Biology, 153*(5), 1061-1069. doi: DOI 10.1083/jcb.153.5.1061

Nishikawa, S. I., Fewell, S. W., Kato, Y., Brodsky, J. L., & Endo, T. (2001). Molecular chaperones in the yeast endoplasmic reticulum maintain the solubility of proteins for retrotranslocation and degradation. *J Cell Biol, 153*(5), 1061-1070.

Nuoffer, C., Jeno, P., Conzelmann, A., & Riezman, H. (1991). Determinants for glycophospholipid anchoring of the Saccharomyces cerevisiae GAS1 protein to the plasma membrane. *Mol Cell Biol, 11*(1), 27-37. doi: 10.1128/mcb.11.1.27

O'Reilly, M. K., Zhang, G., & Imperiali, B. (2006). In vitro evidence for the dual function of Alg2 and Alg11: essential mannosyltransferases in *N*-linked glycoprotein biosynthesis. *Biochemistry, 45*(31), 9593-9603. doi: 10.1021/bi060878o

Oikawa, D., Kimata, Y., & Kohno, K. (2007). Self-association and BiP dissociation are not sufficient for activation of the ER stress sensor Ire1. *Journal of Cell Science, 120*(9), 1681-1688. doi: 10.1242/jcs.002808

Oliveros, J.C. (2007-2015). Venny. An interactive tool for comparing lists with Venn's diagrams. *Available online: https://bioinfogp.cnb.csic.es/tools/venny/index.html*

Olson, G. M., Fox, D. S., Wang, P., Alspaugh, J. A., & Buchanan, K. L. (2007). Role of protein *O*-mannosyltransferase Pmt4 in the morphogenesis and virulence of Cryptococcus neoformans. *Eukaryot Cell, 6*(2), 222-234. doi: EC.00182-06 [pii] 10.1128/EC.00182-06

Opitz, N., Schmitt, K., Hofer-Pretz, V., Neumann, B., Krebber, H., Braus, G. H., & Valerius, O. (2017). Capturing the Asc1p/Receptor for Activated C Kinase 1 (RACK1) Microenvironment at the Head Region of the 40S Ribosome with Quantitative BioID in Yeast. *Molecular & Cellular Proteomics, 16*(12), 2199-2218. doi: 10.1074/mcp.M116.066654

Orlean, P., Albright, C., & Robbins, P. W. (1988). Cloning and sequencing of the yeast gene for dolichol phosphate mannose synthase, an essential protein. *J Biol Chem, 263*(33), 17499-17507.

Pacharra, S., Hanisch, F. G., Muhlenhoff, M., Faissner, A., Rauch, U., & Breloy, I. (2013). The lecticans of mammalian brain perineural net are *O*-mannosylated. *J Proteome Res, 12*(4), 1764-1771. doi: 10.1021/pr3011028

Papic, D., Elbaz-Alon, Y., Koerdt, S. N., Leopold, K., Worm, D., Jung, M., . . . Rapaport, D. (2013). The role of Djp1 in import of the mitochondrial protein Mim1 demonstrates specificity between a cochaperone and its substrate protein. *Mol Cell Biol, 33*(20), 4083-4094. doi: 10.1128/MCB.00227-13

Perez-Linero, A. M., & Muniz, M. (2015). Membrane trafficking: returning to the fold(ER). *Curr Biol, 25*(7), R288-290. doi: 10.1016/j.cub.2015.02.007

Petkova, M. I., Pujol-Carrion, N., & de la Torre-Ruiz, M. A. (2012). Mtl1 *O*-mannosylation mediated by both Pmt1 and Pmt2 is important for cell survival under oxidative conditions and TOR blockade. *Fungal Genet Biol, 49*(11), 903-914. doi: 10.1016/j.fgb.2012.08.005 S1087-1845(12)00155-7 [pii]

Pincus, D., Chevalier, M. W., Aragon, T., van Anken, E., Vidal, S. E., El-Samad, H., & Walter, P. (2010). BiP binding to the ER-stress sensor Ire1 tunes the homeostatic behavior of the unfolded protein response. *PLoS Biol, 8*(7), e1000415. doi: 10.1371/journal.pbio.1000415

Pittet, M., & Conzelmann, A. (2007). Biosynthesis and function of GPI proteins in the yeast Saccharomyces cerevisiae. *Biochim Biophys Acta, 1771*(3), 405-420. doi: 10.1016/j.bbalip.2006.05.015

Popolo, L., Grandori, R., Vai, M., Lacana, E., & Alberghina, L. (1988). Immunochemical characterization of gp115, a yeast glycoprotein modulated by the cell cycle. *Eur J Cell Biol, 47*(2), 173-180.

Promlek, T., Ishiwata-Kimata, Y., Shido, M., Sakuramoto, M., Kohno, K., & Kimata, Y. (2011). Membrane aberrancy and unfolded proteins activate the endoplasmic reticulum stress sensor Ire1 in different ways. *Mol Biol Cell, 22*(18), 3520-3532. doi: 10.1091/mbc.E11-04-0295

Proszynski, T. J., Simons, K., & Bagnat, M. (2004). *O*-glycosylation as a sorting determinant for cell surface delivery in yeast. *Mol Biol Cell, 15*(4), 1533-1543.

Quan, E. M., Kamiya, Y., Kamiya, D., Denic, V., Weibezahn, J., Kato, K., & Weissman, J. S. (2008). Defining the glycan destruction signal for endoplasmic reticulum-associated degradation. *Mol Cell, 32*(6), 870-877. doi: 10.1016/j.molcel.2008.11.017

Reiss, G., te Heesen, S., Zimmerman, J., Robbins, P. W., & Aebi, M. (1996). Isolation of the ALG6 locus of Saccharomyces cerevisiae required for glucosylation in the *N*-linked glycosylation pathway. *Glycobiology, 6*(5), 493-498.

Rine, J., Hansen, W., Hardeman, E., & Davis, R. W. (1983). Targeted selection of recombinant clones through gene dosage effects. *Proc Natl Acad Sci U S A, 80*(22), 6750-6754.

Robinson, J. S., Klionsky, D. J., Banta, L. M., & Emr, S. D. (1988). Protein sorting in Saccharomyces cerevisiae: isolation of mutants defective in the delivery and processing of multiple vacuolar hydrolases. *Mol Cell Biol, 8*(11), 4936-4948.

Roemer, T., & Bussey, H. (1991). Yeast beta-glucan synthesis: KRE6 encodes a predicted type II membrane protein required for glucan synthesis in vivo and for glucan synthase activity in vitro. *Proc Natl Acad Sci U S A, 88*(24), 11295-11299.

Roemer, T., Madden, K., Chang, J., & Snyder, M. (1996). Selection of axial growth sites in yeast requires Axl2p, a novel plasma membrane glycoprotein. *Genes Dev, 10*(7), 777-793.

Rose, M. D., Misra, L. M., & Vogel, J. P. (1989). Kar2, a Karyogamy Gene, Is the Yeast Homolog of the Mammalian Bip/Grp78 Gene. *Cell, 57*(7), 1211-1221. doi: Doi 10.1016/0092-8674(89)90058-5

Rubenstein, E. M., Kreft, S. G., Greenblatt, W., Swanson, R., & Hochstrasser, M. (2012). Aberrant substrate engagement of the ER translocon triggers degradation by the Hrd1 ubiquitin ligase. *Journal of Cell Biology, 197*(6), 761-773. doi: 10.1083/jcb.201203061

Rubio, C., Pincus, D., Korennykh, A., Schuck, S., El-Samad, H., & Walter, P. (2011). Homeostatic adaptation to endoplasmic reticulum stress depends on Ire1 kinase activity. *Journal of Cell Biology, 193*(1), 171-184. doi: 10.1083/jcb.201007077

Rush, J. S., & Waechter, C. J. (1995). Transmembrane movement of a water-soluble analogue of mannosylphosphoryldolichol is mediated by an endoplasmic reticulum protein. *J Cell Biol, 130*(3), 529-536.

Russo, P., Kalkkinen, N., Sareneva, H., Paakkola, J., & Makarow, M. (1992). A heat shock gene from Saccharomyces cerevisiae encoding a secretory glycoprotein. *Proc Natl Acad Sci U S A, 89*(9), 3671-3675.

Sambrook, J., & Russel, D.W. (2001). *Molecular cloning : a laboratory manual* (3rd ed.): Cold Spring Harbor Laboratory Press, Cold Spring Harbor, NY.

Sanders, S. L., Gentzsch, M., Tanner, W., & Herskowitz, I. (1999). *O*-Glycosylation of Axl2/Bud10p by Pmt4p is required for its stability, localization, and function in daughter cells. *J Cell Biol, 145*(6), 1177-1188.

Schenk, B., Fernandez, F., & Waechter, C. J. (2001). The ins(ide) and out(side) of dolichyl phosphate biosynthesis and recycling in the endoplasmic reticulum. *Glycobiology, 11*(5), 61R-70R.

Schmidt, R. M., Schessner, J. P., Borner, G. H. H., & Schuck, S. (2019). The proteasome biogenesis regulator Rpn4 cooperates with the unfolded protein response to promote ER stress resistance. *Elife, 8*. doi: ARTN e43244 10.7554/eLife.43244

Schmitt, K., Smolinski, N., Neumann, P., Schmaul, S., Hofer-Pretz, V., Braus, G. H., & Valerius, O. (2017). Asc1p/RACK1 Connects Ribosomes to Eukaryotic Phosphosignaling. *Molecular and Cellular Biology, 37*(3). doi: UNSP e00279-16 10.1128/MCB.00279-16

Schneider, C. A., Rasband, W. S., & Eliceiri, K. W. (2012). NIH Image to ImageJ: 25 years of image analysis. *Nat Methods, 9*(7), 671-675.

Schuldiner, M., Collins, S. R., Thompson, N. J., Denic, V., Bhamidipati, A., Punna, T., . . . Krogan, N. J. (2005). Exploration of the function and organization of the yeast early secretory pathway through an epistatic miniarray profile. *Cell, 123*(3), 507-519. doi: S0092-8674(05)00868-8 [pii] 10.1016/j.cell.2005.08.031

Schuller, A. P., Wu, C. C., Dever, T. E., Buskirk, A. R., & Green, R. (2017). eIF5A Functions Globally in Translation Elongation and Termination. *Mol Cell, 66*(2), 194-205 e195. doi: 10.1016/j.molcel.2017.03.003

Schulz, B. L., & Aebi, M. (2009). Analysis of glycosylation site occupancy reveals a role for Ost3p and Ost6p in site-specific *N*-glycosylation efficiency. *Mol Cell Proteomics, 8*(2), 357-364. doi: 10.1074/mcp.M800219-MCP200

Schwarz, M., Knauer, R., & Lehle, L. (2005). Yeast oligosaccharyltransferase consists of two functionally distinct sub-complexes, specified by either the Ost3p or Ost6p subunit. *FEBS Lett, 579*(29), 6564-6568. doi: S0014-5793(05)01315-3 [pii] 10.1016/j.febslet.2005.10.063

Selkoe, D. J. (2003). Folding proteins in fatal ways. *Nature, 426*(6968), 900-904. doi: 10.1038/nature02264

Sentandreu, R., & Northcote, D. H. (1968). The structure of a glycopeptide isolated from the yeast cell wall. *Biochem J, 109*(3), 419-432.

Sezen, B., Seedorf, M., & Schiebel, E. (2009). The SESA network links duplication of the yeast centrosome with the protein translation machinery. *Genes & Development, 23*(13), 1559-1570. doi: 10.1101/gad.524209

Shamu, C. E., Cox, J. S., & Walter, P. (1994). The unfolded-protein-response pathway in yeast. *Trends Cell Biol, 4*(2), 56-60.

Shibatani, T., David, L. L., McCormack, A. L., Frueh, K., & Skach, W. R. (2005). Proteomic analysis of mammalian oligosaccharyltransferase reveals multiple subcomplexes that contain Sec61, TRAP, and two potential new subunits. *Biochemistry, 44*(16), 5982-5992. doi: 10.1021/bi047328f

Shimoi, H., Kitagaki, H., Ohmori, H., Iimura, Y., & Ito, K. (1998). Sed1p is a major cell wall protein of Saccharomyces cerevisiae in the stationary phase and is involved in lytic enzyme resistance. *J Bacteriol, 180*(13), 3381-3387.

Shor, B., Calaycay, J., Rushbrook, J., & McLeod, M. (2003). Cpc2/RACK1 is a ribosome-associated protein that promotes efficient translation in Schizosaccharomyces pombe. *Journal of Biological Chemistry, 278*(49), 49119-49128. doi: 10.1074/jbc.M303968200

Sidrauski, C., Cox, J. S., & Walter, P. (1996). tRNA ligase is required for regulated mRNA splicing in the unfolded protein response. *Cell, 87*(3), 405-413. doi: Doi 10.1016/S0092-8674(00)81361-6

Simpson, C. E., Lui, J., Kershaw, C. J., Sims, P. F., & Ashe, M. P. (2014). mRNA localization to P-bodies in yeast is bi-phasic with many mRNAs captured in a late Bfr1p-dependent wave. *J Cell Sci, 127*(Pt 6), 1254-1262. doi: 10.1242/jcs.139055

Singer-Kruger, B., & Jansen, R. P. (2014). Here, there, everywhere. mRNA localization in budding yeast. *RNA Biol, 11*(8), 1031-1039. doi: 10.4161/rna.29945

Slowikowski, K. Repulsive Text and Label Geoms for 'ggplot2'. *Available online: https://CRAN.R-project.org/package=ggrepel (accessed on 12 September 2018)*.

Solda, T., Galli, C., Kaufman, R. J., & Molinari, M. (2007). Substrate-specific requirements for UGT1-dependent release from calnexin. *Molecular Cell, 27*(2), 238-249. doi: 10.1016/j.molcel.2007.05.032

Spear, E. D., & Ng, D. T. (2003). Stress tolerance of misfolded carboxypeptidase Y requires maintenance of protein trafficking and degradative pathways. *Mol Biol Cell, 14*(7), 2756-2767. doi: 10.1091/mbc.E02-11-0717
E02-11-0717 [pii]

Spirig, U., Bodmer, D., Wacker, M., Burda, P., & Aebi, M. (2005). The 3.4-kDa Ost4 protein is required for the assembly of two distinct oligosaccharyltransferase complexes in yeast. *Glycobiology, 15*(12), 1396-1406. doi: cwj025 [pii]
10.1093/glycob/cwj025

Spiro, R. G. (2002). Protein glycosylation: nature, distribution, enzymatic formation, and disease implications of glycopeptide bonds. *Glycobiology, 12*(4), 43R-56R. doi: 10.1093/glycob/12.4.43r

Stagljar, I., te Heesen, S., & Aebi, M. (1994). New phenotype of mutations deficient in glucosylation of the lipid-linked oligosaccharide: cloning of the ALG8 locus. *Proc Natl Acad Sci U S A, 91*(13), 5977-5981.

Steentoft, C., Vakhrushev, S. Y., Joshi, H. J., Kong, Y., Vester-Christensen, M. B., Schjoldager, K. T., . . . Clausen, H. (2013). Precision mapping of the human *O*-GalNAc glycoproteome through SimpleCell technology. *EMBO J, 32*(10), 1478-1488. doi: 10.1038/emboj.2013.79

Stirling, C. J., Rothblatt, J., Hosobuchi, M., Deshaies, R., & Schekman, R. (1992). Protein translocation mutants defective in the insertion of integral membrane proteins into the endoplasmic reticulum. *Mol Biol Cell, 3*(2), 129-142.

Strahl-Bolsinger, S., Immervoll, T., Deutzmann, R., & Tanner, W. (1993). PMT1, the gene for a key enzyme of protein *O*-glycosylation in Saccharomyces cerevisiae. *Proc Natl Acad Sci U S A, 90*(17), 8164-8168.

Strahl-Bolsinger, S., & Scheinost, A. (1999). Transmembrane topology of pmt1p, a member of an evolutionarily conserved family of protein *O*-mannosyltransferases. *J Biol Chem, 274*(13), 9068-9075.

Strahl-Bolsinger, S., & Tanner, W. (1991). Protein *O*-glycosylation in Saccharomyces cerevisiae. Purification and characterization of the dolichyl-phosphate-D-mannose-protein *O*-D-mannosyltransferase. *Eur J Biochem, 196*(1), 185-190.

Subramaniam, A. R., Zid, B. M., & O'Shea, E. K. (2014). An integrated approach reveals regulatory controls on bacterial translation elongation. *Cell, 159*(5), 1200-1211. doi: 10.1016/j.cell.2014.10.043

Takahashi, S., Sasaki, T., Manya, H., Chiba, Y., Yoshida, A., Mizuno, M., . . . Endo, T. (2001). A new beta-1,2-*N*-acetylglucosaminyltransferase that may play a role in the biosynthesis of mammalian *O*-mannosyl glycans. *Glycobiology, 11*(1), 37-45.

Takeuchi, M., Kimata, Y., & Kohno, K. (2008). Saccharomyces cerevisiae Rot1 is an essential molecular chaperone in the endoplasmic reticulum. *Molecular Biology of the Cell, 19*(8), 3514-3525. doi: 10.1091/mbc.E07-12-1289

Tanner, W., Gentzsch, M., Immervoll, T., Scheinost, A., & Strahl-Bolsinger, S. (1995). Fungal glycoproteins and their biosynthetic pathway as potential targets for antifungal agents. *Acta Biochim Pol, 42*(4), 505-508.

Taxis, C., & Knop, M. (2006). System of centromeric, episomal, and integrative vectors based on drug resistance markers for Saccharomyces cerevisiae. *Biotechniques, 40*(1), 73-78. doi: 10.2144/000112040

te Heesen, S., Janetzky, B., Lehle, L., & Aebi, M. (1992). The yeast WBP1 is essential for oligosaccharyl transferase activity in vivo and in vitro. *Embo J, 11*(6), 2071-2075.

te Heesen, S., Knauer, R., Lehle, L., & Aebi, M. (1993). Yeast Wbp1p and Swp1p form a protein complex essential for oligosaccharyl transferase activity. *EMBO J, 12*(1), 279-284.

Team, R Development Core. (2017). *R: A Language and Environment for Statistical Computing* (Vol. Available online: https://www.R-project.org/ (accessed on12 September 2018)). Vienna, Austria, 2017: R Foundation for statistical Computing.

Teixeira, M. C., Monteiro, P. T., Palma, M., Costa, C., Godinho, C. P., Pais, P., . . . Sa-Correia, I. (2018). YEASTRACT: an upgraded database for the analysis of transcription regulatory networks in Saccharomyces cerevisiae. *Nucleic Acids Res, 46*(D1), D348-D353. doi: 10.1093/nar/gkx842

Thibault, G., Ismail, N., & Ng, D. T. W. (2011). The unfolded protein response supports cellular robustness as a broad-spectrum compensatory pathway. *Proceedings of the National Academy of Sciences of the United States of America, 108*(51), 20597-20602. doi: 10.1073/pnas.1117184109

Thibault, G., & Ng, D. T. (2012). The endoplasmic reticulum-associated degradation pathways of budding yeast. *Cold Spring Harb Perspect Biol, 4*(12). doi: 10.1101/cshperspect.a013193

Thiel, C., Schneider, A., Rindermann, J., DeRossi, C., Popovici, D., Hoffmann, G. F., . . . Korner, C. (2012). Successful prenatal mannose treatment for congenital disorder of glycosylation-Ia in mice. *European Journal of Pediatrics, 171*(9), 1423-1423.

Thompson, J. D., Higgins, D. G., & Gibson, T. J. (1994). CLUSTAL W: improving the sensitivity of progressive multiple sequence alignment through sequence weighting, position-specific gap penalties and weight matrix choice. *Nucleic Acids Res, 22*(22), 4673-4680.

Thompson, M. K., Rojas-Duran, M. F., Gangaramani, P., & Gilbert, W. V. (2016). The ribosomal protein Asc1/RACK1 is required for efficient translation of short mRNAs. *Elife, 5*. doi: ARTN e11154 10.7554/eLife.11154

Tong, A. H., & Boone, C. (2006). Synthetic genetic array analysis in Saccharomyces cerevisiae. *Methods Mol Biol, 313*, 171-192.

Tran, J. R., & Brodsky, J. L. (2012). Assays to measure ER-associated degradation in yeast. *Methods Mol Biol, 832*, 505-518. doi: 10.1007/978-1-61779-474-2_36

Travers, K. J., Patil, C. K., Wodicka, L., Lockhart, D. J., Weissman, J. S., & Walter, P. (2000). Functional and genomic analyses reveal an essential coordination between the unfolded protein response and ER-associated degradation. *Cell, 101*(3), 249-258. doi: S0092-8674(00)80835-1 [pii]

Trombetta, E. S., & Helenius, A. (2000). Conformational requirements for glycoprotein reglucosylation in the endoplasmic reticulum. *Journal of Cell Biology, 148*(6), 1123-1129. doi: DOI 10.1083/jcb.148.6.1123

Umebayashi, K., Fukuda, R., Hirata, A., Horiuchi, H., Nakano, A., Ohta, A., & Takagi, M. (2001). Activation of the Ras-cAMP signal transduction pathway inhibits the proteasome-independent degradation of misfolded protein aggregates in the endoplasmic reticulum lumen. *Journal of Biological Chemistry, 276*(44), 41444-41454. doi: DOI 10.1074/jbc.M105829200

Varki, A. (1993). Biological roles of oligosaccharides: all of the theories are correct. *Glycobiology, 3*(2), 97-130.

Vashist, S., Kim, W., Belden, W. J., Spear, E. D., Barlowe, C., & Ng, D. T. (2001). Distinct retrieval and retention mechanisms are required for the quality control of endoplasmic reticulum protein folding. *J Cell Biol, 155*(3), 355-368. doi: 10.1083/jcb.200106123
jcb.200106123 [pii]

Verna, J., Lodder, A., Lee, K., Vagts, A., & Ballester, R. (1997). A family of genes required for maintenance of cell wall integrity and for the stress response in Saccharomyces cerevisiae. *Proc Natl Acad Sci U S A, 94*(25), 13804-13809.

Vester-Christensen, M. B., Halim, A., Joshi, H. J., Steentoft, C., Bennett, E. P., Levery, S. B., . . . Clausen, H. (2013). Mining the *O*-mannose glycoproteome reveals cadherins as major *O*-mannosylated glycoproteins. *Proc Natl Acad Sci U S A, 110*(52), 21018-21023. doi: 10.1073/pnas.1313446110

Wang, S. Y., & Ng, D. T. W. (2010). Evasion of Endoplasmic Reticulum Surveillance Makes Wsc1p an Obligate Substrate of Golgi Quality Control. *Molecular Biology of the Cell, 21*(7), 1153-1165. doi: 10.1091/mbc.E09-10-0910

Warnes, G.R.; Bolker, B.; Bonebakker, L.; Gentleman, R.; Huber, W.; Liaw, A.; Lumley, T.; Maechler, M.; Magnusson, A.; Moeller, S. Various R Programming Tools for Plotting Data. *Available online:https://CRAN.R-project.org/package=gplots (accessed on 12 September 2018)*.

Weidner, J., Wang, C., Prescianotto-Baschong, C., Estrada, A. F., & Spang, A. (2014). The polysome-associated proteins Scp160 and Bfr1 prevent P body formation under normal growth conditions. *J Cell Sci, 127*(Pt 9), 1992-2004. doi: 10.1242/jcs.142083

Weston, A., Nassau, P. M., Henly, C., & Marriott, M. S. (1993). Protein *O*-mannosylation in Candida albicans. Determination of the amino acid sequences of peptide acceptors for protein *O*-mannosyltransferase. *Eur J Biochem, 215*(3), 845-849.

Whitley, P., Nilsson, I. M., & von Heijne, G. (1996). A nascent secretory protein may traverse the ribosome/endoplasmic reticulum translocase complex as an extended chain. *J Biol Chem, 271*(11), 6241-6244.

Wickham, H. (2009). *Elegant Graphics for Data Analysis; Springer*. New York,.

Willer, T., Amselgruber, W., Deutzmann, R., & Strahl, S. (2002). Characterization of POMT2, a novel member of the PMT protein *O*-mannosyltransferase family specifically localized to the acrosome of mammalian spermatids. *Glycobiology, 12*(11), 771-783.

Wiseman, R. L., Zhang, Y. H., Lee, K. P. K., Harding, H. P., Haynes, C. M., Price, J., . . . Ron, D. (2010). Flavonol Activation Defines an Unanticipated Ligand-Binding Site in the Kinase-RNase Domain of IRE1. *Molecular Cell, 38*(2), 291-304. doi: 10.1016/j.molcel.2010.04.001

Witters, P., Cassiman, D., & Morava, E. (2017). Nutritional Therapies in Congenital Disorders of Glycosylation (CDG). *Nutrients, 9*(11). doi: Artn 1222

10.3390/Nu9111222
Wolf, A. S., & Grayhack, E. J. (2015). Asc1, homolog of human RACK1, prevents frameshifting in yeast by ribosomes stalled at CGA codon repeats. *Rna, 21*(5), 935-945. doi: 10.1261/rna.049080.114
Xu, C., Bailly-Maitre, B., & Reed, J. C. (2005). Endoplasmic reticulum stress: cell life and death decisions. *J Clin Invest, 115*(10), 2656-2664. doi: 10.1172/JCI26373
Xu, C., & Ng, D. T. (2015). Glycosylation-directed quality control of protein folding. *Nat Rev Mol Cell Biol, 16*(12), 742-752. doi: 10.1038/nrm4073
Xu, C., & Ng, D. T. (2015). *O*-mannosylation: The other glycan player of ER quality control. *Semin Cell Dev Biol, 41*, 129-134. doi: 10.1016/j.semcdb.2015.01.014
Xu, C., Wang, S., Thibault, G., & Ng, D. T. (2013). Futile protein folding cycles in the ER are terminated by the unfolded protein *O*-mannosylation pathway. *Science, 340*(6135), 978-981. doi: 10.1126/science.1234055
Xu, W. M., & Beutler, E. (1994). The Characterization of Gene-Mutations for Human Glucose Phosphate Isomerase Deficiency Associated with Chronic Hemolytic-Anemia. *Journal of Clinical Investigation, 94*(6), 2326-2329. doi: Doi 10.1172/Jci117597
Zakrzewska, A., Palamarczyk, G., Krotkiewski, H., Zdebska, E., Saloheimo, M., Penttila, M., & Kruszewska, J. S. (2003). Overexpression of the gene encoding GTP:mannose-1-phosphate guanyltransferase, mpg1, increases cellular GDP-mannose levels and protein mannosylation in Trichoderma reesei. *Appl Environ Microbiol, 69*(8), 4383-4389. doi: 10.1128/aem.69.8.4383-4389.2003
Zatorska, E., Gal, L., Schmitt, J., Bausewein, D., Schuldiner, M., & Strahl, S. (2017). Cellular Consequences of Diminished Protein *O*-Mannosyltransferase Activity in Baker's Yeast. *International Journal of Molecular Sciences, 18*(6). doi: Artn 1226 10.3390/Ijms18061226
Zhang, S., Xu, C. C., Larrimore, K. E., & Ng, D. T. W. (2017). Slp1-Emp65: A Guardian Factor that Protects Folding Polypeptides from Promiscuous Degradation. *Cell, 171*(2), 346-+. doi: 10.1016/j.cell.2017.08.036
Zielinska, D. F., Gnad, F., Schropp, K., Wisniewski, J. R., & Mann, M. (2012). Mapping *N*-Glycosylation Sites across Seven Evolutionarily Distant Species Reveals a Divergent Substrate Proteome Despite a Common Core Machinery. *Mol Cell, 46*(4), 542-548. doi: 10.1016/j.molcel.2012.04.031

ACKNOWLEDGMENTS

I would like to start by expressing my gratitude to the AG Strahl within the Center for organismal Studies (COS) of Heidelberg. First, to Prof. Sabine Strahl, for giving me the chance of being part of her lab; for her dedication, her understanding and her decisive support in terms of endless discussions and inspirational input throughout the lights and shadows of this project. Second, to my colleagues: Dr. Sina Noor, Dr. Ricardo Carvalho, Dr. Christina Hölscher, Dr. Harden Rieger, Dr. Natalia Rinis and Dr. Antonija Grbavac for creating a great and deeply collaborative working atmosphere. To Anke Metschies for all her personal support and for being the best technician that the yeast lab could ever have. To Karin Dallmeier, for her optimism and regular assistance in all those bureaucratic issues in which my language and solving skills were really limited. To my former crew of Ph.D. students: Dr. Markus Bartels, Dr. Ewa Zatorksa and (soon Dr.) Patrick Neubert simply for being friends, rather than just colleagues; I possibly could not have circumvented certain obstacles without their backing. To the former members of the AG Strahl: Dr. Martin Loibl, Dr. Mark Lommel, Dr. Jakob Engel and Dr. Daniela Bausewein for her mentoring and guidance during the first years. I would also like to warmly mention the bachelor students that carried out their research under my supervision: Karen Schriever and Sven Klassa. For their motivation and resilience towards the, not always simple, projects they took part of.

I would also like to thank the members of my thesis advisory committee Dr. Sebastian Schuck and Prof. Matthias Mayer for all the time they invested in giving me helpful feedback on my progress. To the HBIGS graduate school for offering administrative support and valuable complementary scientific formation; and to the Center for organismal studies (COS) and the Zentrum für Molekulare Biologie der Universität Heidelberg (ZMBH) members and facilities that made my life easier. I am grateful to our collaborators, the group of Prof. Maya Schuldiner, Prof. Michael Knopp and Prof. Bern Bukau and Dr. Günter Kramer for their commitment and feedback.

Last but not least, I would like to include all those people that stood by my side all these long years, some of them *in situ*: special mention to my Rohrbacher family with whom I had the honor of sharing my time here, Tribubu and the American/Spanish crew for all the music and the nice non-scientific times; some others, from the distance: my old home friends for being a constant reminder of what one leaves in standby; and most important my father, mother and brother for holding me up unconditionally, this work is also theirs.

Heidelberg, 6th of August of 2019